Retrieving leaf and canopy characteristics from their radiative properties using physically based models : from laboratory to satellite observations

Jingyi Jiang

THÈSE

Présentée par

Jingyi Jiang

Pour obtenir le titre de

DOCTEUR DE L'UNIVERSITE D'AVIGNON ET DES PAYS DE VAUCLUSE

Spécialité : Télédétection de la Végétation

Retrieving leaf and canopy characteristics from their radiative properties using physically based models: from laboratory to satellite observations

Date de soutenance: 18 Juin 2019

Composition du jury:

Mathias Disney	UCL, Royaume-Uni	Rapporteur
Stéphane Jacquemoud	Paris Diderot University, France	Rapporteur
Jean Philippe Gastellu-Etchegorry	CESBIO, France	Examinateur
Aleixandre Verger Ten	CREAF, Espagne	Examinateur
Marie Weiss	INRA-EMMAH, France	Co-directeur de thèse
Frédéric Baret	INRA-EMMAH, France	Directeur de thèse

Table of content

1. Introduction

Global demand for agricultural crops is increasing and may continue for the next decades with the increase of global population and per-capita demand due to rising living standards (Mauser et al. 2015). A 100-110% increase in global crop demand is forecasted from 2005 to 2050 (Tilman et al. 2011). However, with the backdrop of climate change, the frequency of extreme weather is rising which causes marked damage to crops and threatens local to global food security (Lesk et al. 2016; Nelson et al. 2016). Therefore, more efforts should be made to meet the increasing global crop demand with minimal environmental impacts.

1.1 Nitrogen fertilization problem

During the past decades, the use of Nitrogen as fertilizer is intensified and results in the incensement of the grain production (FAO 2017). Indeed, since the early 1960s, the use of N fertilizers has grown approximately sevenfold (Figure 1 (Lu and Tian 2017)) . As a matter of fact, N is one of the most important factors determining biomass production in ecosystems (Le Maire et al. 2008). However, the significant improvement of the profitability of agriculture by using nitrogen fertilization is at the expense of a degradation of our environment. Nowadays, 30–80% of N applied to farmland is lost to surface, ground-waters and atmosphere (Bednarek et al. 2014; Van Grinsven et al. 2014). Therefore, the optimization of crop cultivation and rates of N fertilizers application should be balanced at field scale according to the crop needs. Providing sufficient nitrogen for the particular environmental conditions and genotype have several economic and environmental benefits, including the reduction of the water and atmospheric pollution (Goffart et al. 2008), the increase of yield and quality of the crop, the evolvement of the cropping systems toward a sustainable agriculture (Spiertz 2009).

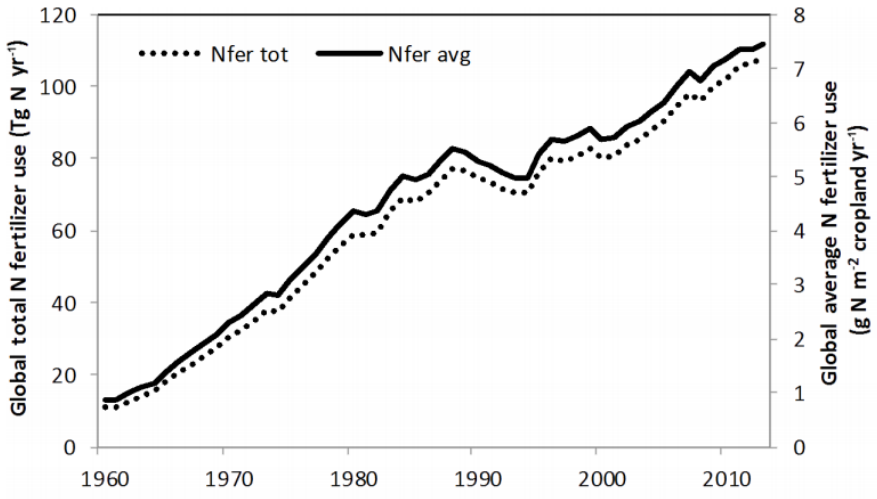

Figure 1 Temporal patterns of global nitrogen (N) fertilizer use in terms of total amount (tot) and average rate on per unit of cropland area (avg) per year (Lu and Tian 2017).

Compared with destructive sampling, non-destructive approaches based on optical measurements provide an efficient way to estimate N content and have been widely used in precision farming and phenotyping to optimize genotypes (Scharf et al. 2002). At field level, unmanned aerial vehicle (UAV) and satellite observations can provide real time monitoring of the spatial variation of the N status along the growing season (Beeri et al. 2005; Pölönen et al. 2013). To achieve this goal, several methods have been developed in the literature: N content can be directly estimated from regression relationships with vegetation indices (Feng et al. 2016; Kusnierek and Korsaeth 2015) or it can be indirectly retrieved by establishing relationships with canopy or leaf chlorophyll content that can either be estimated from vegetation indices or radiative transfer model inversion. Indeed, many studies have demonstrated the strong correlation between leaf chlorophyll content (C_{ab}) and leaf nitrogen content (N%) (Cartelat et al. 2005; Schlemmer et al. 2013), as well as the relationship between canopy

nitrogen content (QN) and Canopy Chlorophyll Content (CCC) which is defined as the product between C_{ab} and the Green Area Index (GAI: the green elements of the canopy) (Baret et al. 2007; Houles et al. 2007). Spectral features of chlorophyll in visible and near-infrared (NIR) are usually used as indicators of N content (Feng et al. 2016; Kusnierek and Korsaeth 2015). In addition, methods based on chlorophyll fluorescence emission ratio are also widely applied to crop N status monitoring (Schächtl et al. 2005; Tremblay et al. 2012). However, this thesis will not deal with fluorescence methods since there is no satellite mission today compatible with the spatial resolution required for precision farming or phenotyping application (Drusch et al. 2017).

1.2 Estimation of leaf and canopy characteristics: from leaf measurements to satellite data

When dealing with nitrogen content, C_{ab}, CCC and GAI are among the most important biophysical variables since they also drive the radiative transfer within the canopy, which makes them accessible in a non-destructive way. Chlorophyll is the major plant pigments in photosynthesis. It is not only applied as an indirect estimation of N status but also closely related to plant stress and senescence. Since chlorophyll is the main plant component determining the reflectance in the visible and red-edge region of the spectrum, optical measurements are relevant to provide information for estimation of leaf and canopy chlorophyll content (Gitelson et al. 2002). Similarly to the Leaf Area Index (LAI), defined as half the total developed area of leaves per unit horizontal ground area (Chen and Black 1992), (Baret et al. 2010; Duveiller et al. 2011) proposed to consider GAI that refers to the surface of all the canopy green elements, including the green leaves, stems and other organs. Indeed, all the green elements contribute to the reflectance observations, making GAI better accessible from remote sensing imagery than LAI.

To estimate biophysical variables from leaf and canopy level, both empirical vegetation index (VI) methods based on the combination of leaf or canopy reflectance in few bands and physically based methods based on the physical process within leaf or canopy structure have been developed. Retrieval algorithms used to estimate leaf and canopy variables from laboratory to satellite observations can be split into two main categories (Baret and Buis 2008): (1) radiometric data-driven approaches (Figure 2, left) like Look-Up-Tables (LUT) (Duan et al. 2014; González-Sanpedro et al. 2008) and iterative optimization methods (Lauvernet et al. 2008). They are based on finding the best match between the measured reflectance (transmittance) and those simulated from radiative transfer model (RT model) or stored within a database from experimental observations. (2) Regression methods (Figure 2, right) such as linear or polynomial multiple regression (Liu et al. 2012; Nguy-Robertson et al. 2012), or machine learning based ones such as Neural Networks (Li et al. 2015; Weiss et al. 2002), Random Forests Regression (Breiman 2001), Support Vector Machine (Durbha et al. 2007) and Gaussian Process Regression (Verrelst et al. 2012). The calibration or training database can be generated either using simulations from RT model or experimental measurements.

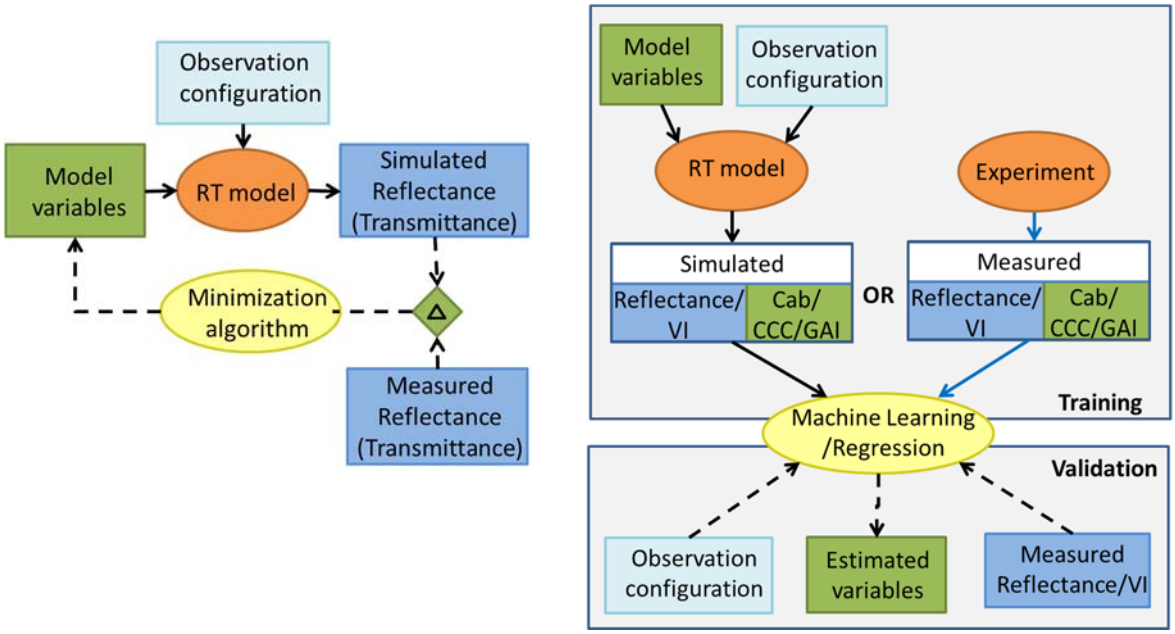

Figure 2 Two main retrieval methods to estimate leaf and canopy variables from laboratory to satellite observations. Left: radiometric data driven approach, Right: variable driven approach.

1.2.1 Methods to estimate the chlorophyll content at the leaf level

At the leaf level, leaf spectra are usually measured at the laboratory from hyperspectral sensors (Féret et al. 2011). Then, based on these measurements, methods including both empirical and physically based modeling approaches have been developed to estimate the leaf chlorophyll content (C_{ab}).

1.2.1.1 Empirical methods

Vis are combinations of spectral bands that capture some absorption characteristics of a given biochemical content. Empirical methods with VIs are widely used with ratios of reflectance at wavelengths that are sensitive to leaf chlorophyll (Croft and Chen 2017). The main types of indices are derived from three forms: simple ratio (SR), normalized difference (ND), modified versions of SR and ND and indices using reflectance derivatives (Le Maire et al. 2004). Several comprehensive reviews have investigated the range of vegetation indexes for determining chlorophyll content (Croft et al. 2014; Le Maire et al. 2004). Table 1 provides a selection of typical vegetation indices for estimating C_{ab}.

However, some limitations still exist when the VI relationship is calibrated over a given training dataset and is then applied to different species or contrasted environmental conditions such as variation in soil background or in the illumination levels in relation to the position of the leaf within the canopy (Lymburner et al. 2000; Wang et al. 2011). In addition, when considering phenotyping applications, quantifying the differences expected between genotypes grown under similar conditions is more challenging. The differences between genotypes in pigment, water and dry matter contents are generally limited. In these conditions, a significant part of the variation in leaf optical properties is also due to variations in the leaf structure, the distribution of pigments in the leaf volume as well as surface features. This affects the relationships between vegetation indices and chlorophyll content while a physically based model of leaf optical properties should allow to explicitly account for these potentially confounding effects. Furthermore, new genotypes grown under given environmental conditions may have characteristics not well represented in the VI-relationship training database, making the biochemical content estimation uncertain.

Table 1 Examples of vegetation indices for estimating C_{ab}.

Index	Name	Equation	Reference
CI_{green}	Gitelson ratio green	$\frac{R800}{R550} - 1$	(Gitelson et al. 2003)
$CI_{red\text{-}edge}$	Gitelson ratio red edge	$\frac{R800}{R710} - 1$	(Gitelson et al. 2003)
NDVI	Normalized difference VI	$\frac{R800 - R680}{R800 + R680}$	(Rouse Jr et al. 1974)
$NDVI_{re}$	Normalized difference VI – red edge	$\frac{R750 - R705}{R750 + R705}$	(Gitelson and Merzlyak 1994)
PRI	Photochemical Reflectance Index	$\frac{R531 - R570}{R531 + R570}$	(Sims and Gamon 2002)
SIPI	Structure insensitive pigment index	$\frac{R800 - R455}{R800 - R680}$	(Penuelas et al. 1995)

1.2.1.2 Physically based Methods

Physically based modeling approaches are developed to understand the relationship between leaf optical properties and leaf biochemical. According to the differences in leaf structure assumption and calculation algorithm, it can be categorized into five classes (Jacquemoud and Ustin 2001; Jacquemoud and Ustin 2008) :

- ***Plate models*** assume the leaf as a stack of one or several absorbing plates with rough surfaces giving rise to isotropic diffusion (Allen et al. 1969).
- ***N-flux models***, derived from the Kubelka-Munk theory, consider the leaf as a slab of absorbing and diffusing material (Allen and Richardson 1968; Yamada and Fujimura 1991).
- ***Radiative transfer Equation,*** where the leaf is considered as a random medium with a spatially varying permittivity. The variations of the electric field are described using the Maxwell theory (Ganapol et al. 1998).
- ***Stochastic models,*** where the leaf is divided into independent tissues and the radiative transfer is simulated by a Markov chain (Maier et al. 1999; Tucker and Garratt 1977).
- ***Ray-tracing models*** simulate the photon transport within the leaf and calculate the optical properties for bifacial leaves with detailed description of the leaf structure (Baranoski 2006; Dorigo et al. 2007; Ustin et al. 2001).

As a typical plate model, PROSPECT is one of the most widely used leaf RT models (Feret et al. 2008; Fourty et al. 1996; Jacquemoud and Baret 1990; Jacquemoud et al. 2009). It allows simulating leaf optical properties from a limited set of state variables and has been successfully applied to retrieve leaf biochemical composition from leaf reflectance and transmittance (Jacquemoud et al. 2009; Le Maire et al. 2004; Zarco-Tejada et al. 2004). Several versions of the PROSPECT model are available. They mostly differ by the number of chlorophyllian pigments considered, the spectral variation of the specific absorption coefficient and of the refractive index that controls the scattering processes in the leaf. However, because of the homogeneous assumptions of plate models, the simulated reflectance and transmittance of bifacial leaves from PROSPECT model are always the same, which contradicts some observations of leaf optical properties on both faces (Baldini et al. 1997; Stuckens et al. 2009b).

1.2.2 Methods to estimate the chlorophyll content and GAI from satellite data

At the canopy level, satellite data carried out at different scales allows detailed and frequent observations of the vegetation canopy. The monitoring of vegetation through remote sensing techniques has been applied in domains such as agriculture, ecology and climate change (Atzberger 2013; Wang et al. 2010) since it provides a non-intrusive and cost effective way of monitoring the spatial variations of the plant status. Only since recently, the high spatial and temporal resolution of systems made satellite remote sensing suitable for agricultural monitoring at the field and intra-field levels. The SENTINEL-2 constellation has the advantages of a short revisiting time (5 days revisit cycle) and decametric spatial resolution (10 – 60m) (Drusch et al. 2012). It can generate geo-information at local, regional, national and global scales near real-time with free-access. Some new approaches and applications in agriculture fields have been applied with SENTINEL-2 observations (Bontemps et al. 2015; Clevers et al. 2017; Clevers and Gitelson 2013).

In the same way as the for the leaf level, methods to estimate biophysical variables from remote sensing data can be classified in empirical methods based on regression between the variables and VIs or reflectance, and physically based RT models inversion (Baret and Buis 2008; Verrelst et al. 2012).

1.2.2.1 Empirical methods

For empirical methods, additionally to the VIs developed at leaf level for chlorophyll estimation (Table 1), some indices (e.g. OSAVI, TVI and MTVI2) were specifically designed at the canopy level, showing different sensitivities to leaf chlorophyll, canopy structure (and thus GAI), soil background and atmospheric condition (Bannari et al. 1995; Baret and Guyot 1991; Henrich et al. 2009). Even though different empirical VIs have been applied to provide accurate estimation of GAI or chlorophyll based on established statistical relationships with field measurements (Broge and Leblanc 2001; Broge and Mortensen 2002; Liu et al. 2012), they are limited by the cultivar, location and time with local calibration and the small number of bands concurrently used (generally 2–3) (Thenkabail 2015). But for very high spatial resolution observations obtained from unmanned aerial vehicles (UAV), empirical models were proved to overperform PROSAIL inversion by focusing on green pixels solely to estimate leaf chlorophyll content (Jay et al. 2018).

1.2.2.2 Physically based methods

Physically based RT models describe the physical processes governing the interaction of light with the canopy elements, and allows taking explicitly into account the information on the observational configuration (Delloye et al. 2018; Strahler 1997; Verrelst et al. 2012). Therefore, it is often preferred for its better transferability, robustness, and flexibility.

- ***Turbid medium assumption: 1D models***

One-dimensional radiative transfer models (1D RTM) assume the canopy as a horizontally infinite turbid or discrete scatters medium (Figure 3A). 1D RTMs such as PROSAIL (Jacquemoud et al. 2009) or ACRM (Kuusk and Nilson 2001) require only a small number of input variables and are computationally very efficient. They approximate the canopy as a turbid medium where leaves are considered as infinitely small particles randomly distributed in the canopy volume. 1D RTMs are well adapted to situations where the amount of information on the target is limited. This is the case for kilometric resolution observations where the generally mixed nature of pixels and their unknown composition makes the problem difficult to be properly solved. Indeed, 1D RTMs provide “apparent” values of the biophysical variables that have been proven to be very useful over regional to global scales applications (Camacho et al. 2013; Delloye et al. 2018; Xiao et al. 2015). At high spatial resolution, 1D-RTMs are applicable to canopy structures close to the turbid medium assumption, e.g. showing little canopy aggregation including row structure. However, this assumption is often not realistic at higher spatial resolutions going from satellite decametric through metric and sub-metric images recorded on-board unmanned Aerial Vehicles (UAVs) (Duan et al. 2014; Verger et al. 2014) or ground vehicles (Comar et al. 2012). In this case, a more realistic description of the canopy structure

is required to get more accurate simulations of the RT models (Ross 2012) and therefore improve the variable retrieval performances.

- ***Hybrid models***

Apart from the simple 1D turbid medium description, several types of RT models have been developed with an enhanced realism at the expense of increasing complexity (Goel 1988). Hybrid models such as GEOSAIL (Huemmrich 2001) or the hybrid GORT model (Li and Strahler 1985)(Li and Strahler 1985) combine the geometric optics of large scale canopy structure with the principles of radiative transfer for volume scattering within each geometric structure (e.g. protrusion represented by cylinders, ellipsoids, cones), allowing the inclusion of some clumping at the canopy scale (Figure 3b). However, an inherent loss of information results from the assumption that averaging canopy structural properties and averaging the scattering behaviour of the canopy (Disney et al. 2000). Therefore, the development of 3D radiative transfer models (3D RTM) based on a realistic and detailed description of the canopy structure are highly desired.

- ***More realistic description of the canopy structure: 3D models***

3D RTMs are developed to simulate the light propagation within canopies by combining an explicit 3D description of the plant and stand architecture with the optical properties of the different canopy elements (Figure 3C and 3D). Commonly used 3D RTMs are based either on radiosity or ray tracing methods. Radiosity methods rely on a 'view factor' matrix built to represent the scattering between one surface and every other surfaces within a scene. The view factor is then used in an iterative manner to solve the radiative transfer between all surfaces (Cohen and Wallace 2012). Since the radiosity method is a global algorithm, reflectance from multi view angles can be calculated at once. However, for complex scenes, it is time-consuming due to a high number of scattering primitives. Examples of radiosity-based methods include RGM (Qin and Gerstl 2000) and RAPID (Huang et al. 2013) which integrates explicit porous objects over arbitrary canopies to accelerate the computation time in complex landscapes. The ray tracing method is based on a sampling of photon trajectories within the scene (Disney et al. 2000). It traces the path of light in an image plane and simulates the effects of its encounters with other vegetation or ground elements. Because of its efficiency and scalability, many approaches are implemented with the Monte Carlo ray tracing method such as Flight (North 1996) where the scene is described with the geometric primitives and volume-averaged parameters, Raytran (Govaerts and Verstraete 1998) or DART (Gastellu-Etchegorry et al. 2015; Gastellu-Etchegorry et al. 2004) which is based on the exact kernel and discrete ordinate approach.

Several open source 3D ray tracing render engines were developed concurrently for computer graphics applications, including LuxCoreRender (LuxCoreRender 2018), MITSUBA (Jakob 2014) and Pov-ray (Persistence of Vision Raytracer) (POV-team 2013). LuxCoreRender and MITSUBA are developed based on the PBRT (Pharr et al. 2016) which is a physically based unbiased ray tracer, while Pov-ray is built from the non-physically based render engine where empirical shading algorithm is used (Casa and Jones 2005). Because of their flexibility and performances, these computer graphics tools are gradually used by the remote sensing community (Casa and Jones 2005; Coubard et al. 2011; Stuckens et al. 2009a).

However, in addition to the higher complexity of the canopy structure description and the associated increase in the number of required parameters, running a simulation is computationally intensive. Method like model emulation techniques (Gómez-Dans et al. 2016; Verrelst et al. 2017) is proposed based on machine learning techniques to bypass the computational burden. However, Training such emulators is thus computationally more expensive and requires a higher number of simulations to represent properly the variability induced by leaf biochemical composition, wavelength and soil properties.The generation of large LUTs or training datasets to retrieve canopy attributes from a set of reflectances measured in a given observational configuration requires a lot of time. As a matter of fact, the reflectance should be simulated in all the considered directions and wavebands, for a high number of canopy architectures, composed of different elements with given optical properties (leaf,

stem, ears, green, yellow,…) and soil background. The computation time as well as the accurate 3D characterization of the canopy remains one of the principal limitations when inverting realistic 3D RTMs.

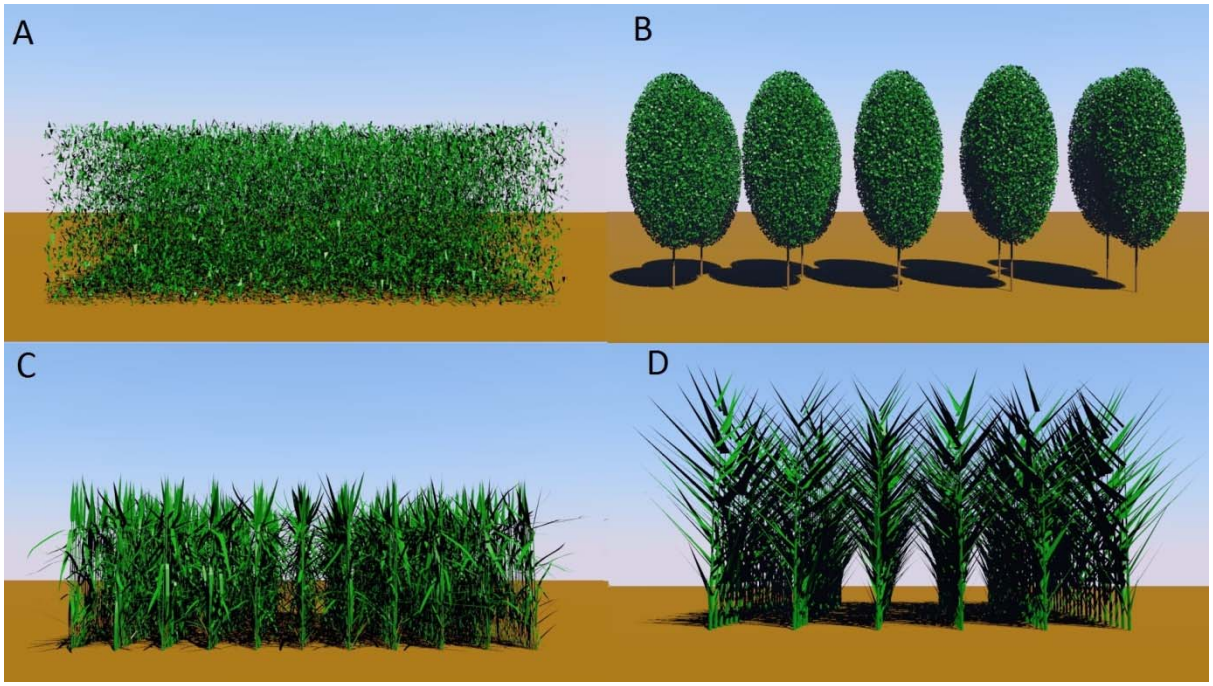

Figure 3 Examples of (A) 1D model (B) GORT model and 3D model of (C) wheat canopy and (D) maize canopy (simulated by LuxCoreRender).

1.3 Study objective and outlook

In the context of crop nitrogen monitoring for smart agriculture and field phenotyping applications, remote sensing appears as an efficient tool to characterize the vegetation status. Although some retrieval methods relying on the inversion of physically based models have already been developed both at the laboratory and satellite observation levels, the accuracy of estimation is still limited by computing capacities or by the use of flexible but rather simple models. These latter are based on an oversimplification of the leaf and canopy structure that induces biases in the estimation of the crop state variables of interest (Stuckens et al. 2009a). The objective of this work is thus to propose and evaluate an efficient, accurate and robust method to retrieve leaf and canopy characteristics from close and remote sensing observations. This method relies on RT models with realistic descriptions of the leaf and canopy structures.

The study is divided in two main parts corresponding to the two considered levels of observation (Figure 4):

- The first part focuses on ***the leaf level***. We first evaluate the ability of the different versions of the PROSPECT model to estimate biochemical variables like chlorophyll, water and dry matter contents using an optimization inversion method. Our results highlight a bias for chlorophyll estimation that we attribute to the fact that the specific absorption coefficients of the PROSPECT model are calibrated over a large range of species characterized by two distinct mesophyll structures: the palisade mesophyll contains most of the chlorophyll, while the spongy mesophyll is characterized by a small amount of chlorophyll and more air space with a high level of scattering. We thus propose to develop the FASPECT model that explicitly describes the two kinds of mesophyll layers. Therefore, we built a four-layer model of the leaf and recalibrated the corresponding specific absorption coefficients of the main absorbing materials. We validate the FASPECT model against eight measured datasets.

- The second part focuses on ***the canopy level***. We first select the physically based and unbiased rendering engine, LuxCoreRender (LuxCoreRender 2018), to compute the radiative transfer using a realistic 3D description of canopy structure. We first evaluate LuxCoreRender against the state of the art 3D models using the RAMI online model checker (Widlowski et al. 2008). Because of the significant time required to render one scene, we propose a simple approach to describe the dependency of canopy reflectance from the wavelength, leaf and soil properties. This allows to considerably speed-up the simulation capacity and run LuxCoreRender to build a training database from a large range of simulations. We then develop a machine learning inversion algorithm to retrieve the main canopy state variables (e.g GAI, C_{ab} and CCC) from a set of SENTINEL2 canopy reflectance. We consider two types of crops (wheat and maize) and compare the 3D approach (so called "crop specific") to the turbid medium assumption (so called "generic"), based either on simulations or on measurements.

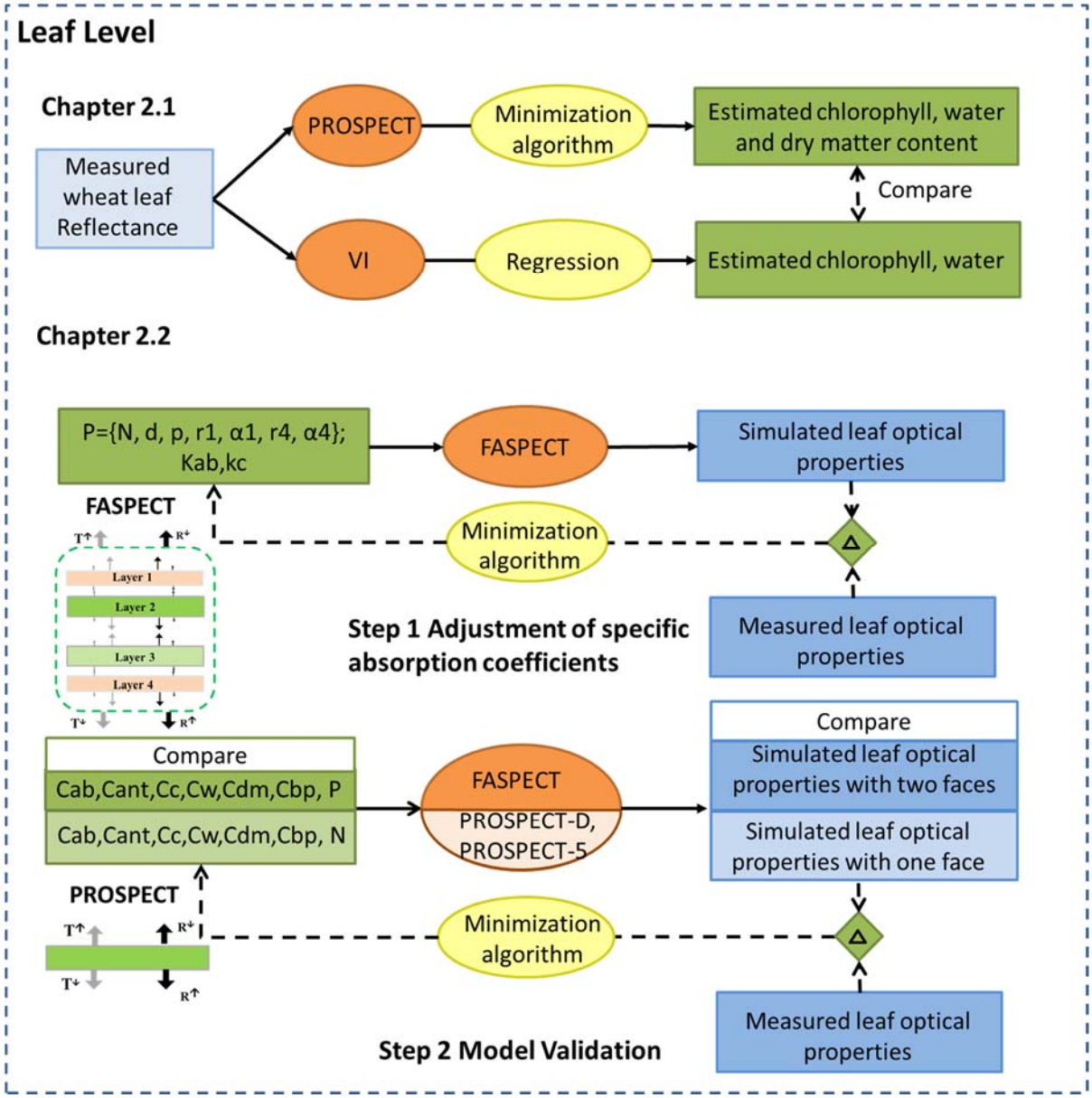

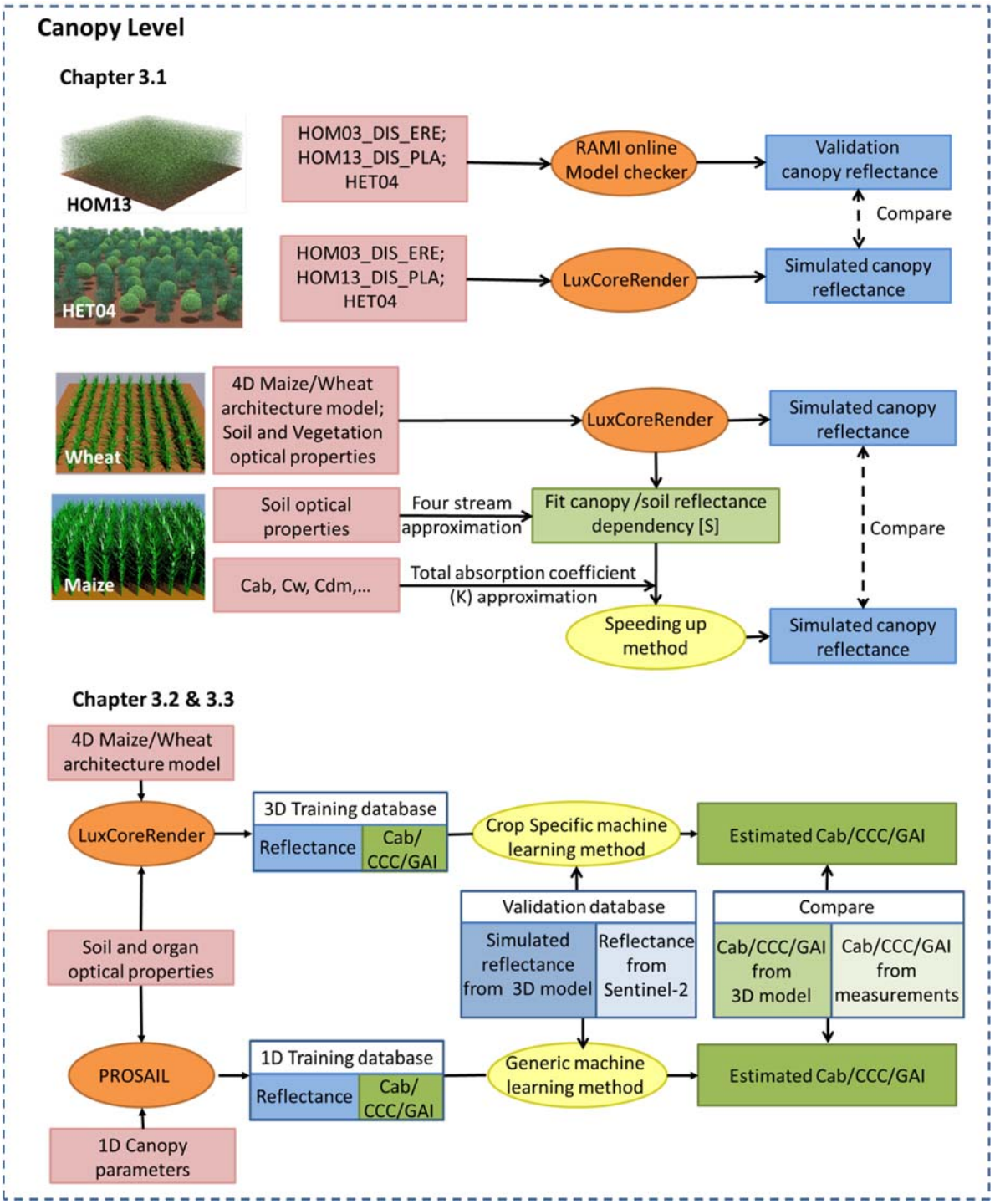

Figure 4 Flow chart of the study.

Reference

Allen, W.A., Gausman, H.W., Richardson, A.J., & Thomas, J.R. (1969). Interaction of isotropic light with a compact plant leaf. *JOSA, 59*, 1376-1379

Allen, W.A., & Richardson, A.J. (1968). Interaction of light with a plant canopy. *JOSA, 58*, 1023-1028

Atzberger, C. (2013). Advances in remote sensing of agriculture: Context description, existing operational monitoring systems and major information needs. *Remote Sensing, 5*, 949-981

Baldini, E., Facini, O., Nerozzi, F., Rossi, F., & Rotondi, A. (1997). Leaf characteristics and optical properties of different woody species. *Trees, 12*, 73-81
Bannari, A., Morin, D., Bonn, F., & Huete, A. (1995). A review of vegetation indices. *Remote Sensing Reviews, 13*, 95-120
Baranoski, G.V. (2006). Modeling the interaction of infrared radiation (750 to 2500 nm) with bifacial and unifacial plant leaves. *Remote Sensing of Environment, 100*, 335-347
Baret, F., & Buis, S. (2008). Estimating canopy characteristics from remote sensing observations: Review of methods and associated problems. *Advances in land remote Sensing* (pp. 173-201): Springer
Baret, F., De Solan, B., Lopez-Lozano, R., Ma, K., & Weiss, M. (2010). GAI estimates of row crops from downward looking digital photos taken perpendicular to rows at 57.5 zenith angle: Theoretical considerations based on 3D architecture models and application to wheat crops. *Agricultural and Forest meteorology, 150*, 1393-1401
Baret, F., & Guyot, G. (1991). Potentials and limits of vegetation indices for LAI and APAR assessment. *Remote Sensing of Environment, 35*, 161-173
Baret, F., Houles, V., & Guérif, M. (2007). Quantification of plant stress using remote sensing observations and crop models: the case of nitrogen management. *Journal of Experimental Botany, 58*, 869-880
Bednarek, A., Szklarek, S., & Zalewski, M. (2014). Nitrogen pollution removal from areas of intensive farming—comparison of various denitrification biotechnologies. *Ecohydrology & Hydrobiology, 14*, 132-141
Beeri, O., Phillips, R., Carson, P., & Liebig, M. (2005). Alternate satellite models for estimation of sugar beet residue nitrogen credit. *Agriculture, Ecosystems & Environment, 107*, 21-35
Bontemps, S., Arias, M., Cara, C., Dedieu, G., Guzzonato, E., Hagolle, O., Inglada, J., Matton, N., Morin, D., & Popescu, R. (2015). Building a data set over 12 globally distributed sites to support the development of agriculture monitoring applications with Sentinel-2. *Remote Sensing, 7*, 16062-16090
Breiman, L. (2001). Random forests. *Machine learning, 45*, 5-32
Broge, N.H., & Leblanc, E. (2001). Comparing prediction power and stability of broadband and hyperspectral vegetation indices for estimation of green leaf area index and canopy chlorophyll density. *Remote Sensing of Environment, 76*, 156-172
Broge, N.H., & Mortensen, J.V. (2002). Deriving green crop area index and canopy chlorophyll density of winter wheat from spectral reflectance data. *Remote Sensing of Environment, 81*, 45-57
Camacho, F., Cernicharo, J., Lacaze, R., Baret, F., & Weiss, M. (2013). GEOV1: LAI, FAPAR essential climate variables and FCOVER global time series capitalizing over existing products. Part 2: Validation and intercomparison with reference products. *Remote Sensing of Environment, 137*, 310-329
Cartelat, A., Cerovic, Z., Goulas, Y., Meyer, S., Lelarge, C., Prioul, J.-L., Barbottin, A., Jeuffroy, M.-H., Gate, P., & Agati, G. (2005). Optically assessed contents of leaf polyphenolics and chlorophyll as indicators of nitrogen deficiency in wheat (Triticum aestivum L.). *Field Crops Research, 91*, 35-49
Casa, R., & Jones, H.G. (2005). LAI retrieval from multiangular image classification and inversion of a ray tracing model. *Remote Sensing of Environment, 98*, 414-428
Chen, J.M., & Black, T. (1992). Defining leaf area index for non‐flat leaves. *Plant, Cell & Environment, 15*, 421-429
Clevers, J., Kooistra, L., & Van Den Brande, M. (2017). Using Sentinel-2 data for retrieving LAI and leaf and canopy chlorophyll content of a potato crop. *Remote Sensing, 9*, 405
Clevers, J.G., & Gitelson, A.A. (2013). Remote estimation of crop and grass chlorophyll and nitrogen content using red-edge bands on Sentinel-2 and-3. *International Journal of Applied Earth Observation and Geoinformation, 23*, 344-351
Cohen, M.F., & Wallace, J.R. (2012). *Radiosity and realistic image synthesis*. Elsevier

Comar, A., Burger, P., De Solan, B., Baret, F., Daumard, F., & Hanocq, J.-F. (2012). A semi-automatic system for high throughput phenotyping wheat cultivars in-field conditions: description and first results. *Functional Plant Biology, 39*, 914-924
Coubard, F., Brédif, M., Paparoditis, N., & Briottet, X. (2011). Reflectance estimation from urban terrestrial images: Validation of a symbolic ray-tracing method on synthetic data. *International Archives of the Photogrammetry, Romote Sensing and Spatial Information Sciences, 38*, 3
Croft, H., & Chen, J. (2017). Leaf pigment content. In: Elsevier Canada
Croft, H., Chen, J., & Zhang, Y. (2014). The applicability of empirical vegetation indices for determining leaf chlorophyll content over different leaf and canopy structures. *Ecological Complexity, 17*, 119-130
Delloye, C., Weiss, M., & Defourny, P. (2018). Retrieval of the canopy chlorophyll content from Sentinel-2 spectral bands to estimate nitrogen uptake in intensive winter wheat cropping systems. *Remote Sensing of Environment, 216*, 245-261
Disney, M., Lewis, P., & North, P. (2000). Monte Carlo ray tracing in optical canopy reflectance modelling. *Remote Sensing Reviews, 18*, 163-196
Dorigo, W.A., Zurita-Milla, R., de Wit, A.J., Brazile, J., Singh, R., & Schaepman, M.E. (2007). A review on reflective remote sensing and data assimilation techniques for enhanced agroecosystem modeling. *International Journal of Applied Earth Observation and Geoinformation, 9*, 165-193
Drusch, M., Del Bello, U., Carlier, S., Colin, O., Fernandez, V., Gascon, F., Hoersch, B., Isola, C., Laberinti, P., & Martimort, P. (2012). Sentinel-2: ESA's optical high-resolution mission for GMES operational services. *Remote Sensing of Environment, 120*, 25-36
Drusch, M., Moreno, J., Del Bello, U., Franco, R., Goulas, Y., Huth, A., Kraft, S., Middleton, E.M., Miglietta, F., & Mohammed, G. (2017). The fluorescence explorer mission concept—ESA's Earth explorer 8. *IEEE transactions on Geoscience and Remote Sensing, 55*, 1273-1284
Duan, S.-B., Li, Z.-L., Wu, H., Tang, B.-H., Ma, L., Zhao, E., & Li, C. (2014). Inversion of the PROSAIL model to estimate leaf area index of maize, potato, and sunflower fields from unmanned aerial vehicle hyperspectral data. *International Journal of Applied Earth Observation and Geoinformation, 26*, 12-20
Durbha, S.S., King, R.L., & Younan, N.H. (2007). Support vector machines regression for retrieval of leaf area index from multiangle imaging spectroradiometer. *Remote Sensing of Environment, 107*, 348-361
Duveiller, G., Weiss, M., Baret, F., & Defourny, P. (2011). Retrieving wheat Green Area Index during the growing season from optical time series measurements based on neural network radiative transfer inversion. *Remote Sensing of Environment, 115*, 887-896
FAO (2017). World fertilizer trends and outlook to 2020. In. Rome: Food and Agriculture Organization
Feng, W., Zhang, H.-Y., Zhang, Y.-S., Qi, S.-L., Heng, Y.-R., Guo, B.-B., Ma, D.-Y., & Guo, T.-C. (2016). Remote detection of canopy leaf nitrogen concentration in winter wheat by using water resistance vegetation indices from in-situ hyperspectral data. *Field Crops Research, 198*, 238-246
Feret, J.-B., François, C., Asner, G.P., Gitelson, A.A., Martin, R.E., Bidel, L.P.R., Ustin, S.L., le Maire, G., & Jacquemoud, S. (2008). PROSPECT-4 and 5: Advances in the leaf optical properties model separating photosynthetic pigments. *Remote Sensing of Environment, 112*, 3030-3043
Féret, J.-B., François, C., Gitelson, A., Asner, G.P., Barry, K.M., Panigada, C., Richardson, A.D., & Jacquemoud, S. (2011). Optimizing spectral indices and chemometric analysis of leaf chemical properties using radiative transfer modeling. *Remote Sensing of Environment, 115*, 2742-2750
Fourty, T., Baret, F., Jacquemoud, S., Schmuck, G., & Verdebout, J. (1996). Leaf optical properties with explicit description of its biochemical composition : direct and inverse problems. *Remote Sensing of Environment, 56*, 104-117
Ganapol, B.D., Johnson, L.F., Hammer, P.D., Hlavka, C.A., & Peterson, D.L. (1998). LEAFMOD: A New Within-Leaf Radiative Transfer Model. *Remote Sensing of Environment, 63*, 182-193

Gastellu-Etchegorry, J.-P., Yin, T., Lauret, N., Cajgfinger, T., Gregoire, T., Grau, E., Feret, J.-B., Lopes, M., Guilleux, J., & Dedieu, G. (2015). Discrete Anisotropic Radiative Transfer (DART 5) for modeling airborne and satellite spectroradiometer and LIDAR acquisitions of natural and urban landscapes. *Remote Sensing, 7*, 1667-1701
Gastellu-Etchegorry, J., Martin, E., & Gascon, F. (2004). DART: a 3D model for simulating satellite images and studying surface radiation budget. *International Journal of Remote Sensing, 25*, 73-96
Gitelson, A., & Merzlyak, M.N. (1994). Spectral reflectance changes associated with autumn senescence of Aesculus hippocastanum L. and Acer platanoides L. leaves. Spectral features and relation to chlorophyll estimation. *Journal of Plant Physiology, 143*, 286-292
Gitelson, A.A., Gritz, Y., & Merzlyak, M.N. (2003). Relationships between leaf chlorophyll content and spectral reflectance and algorithms for non-destructive chlorophyll assessment in higher plant leaves. *Journal of Plant Physiology, 160*, 271-282
Gitelson, A.A., Zur, Y., Chivkunova, O.B., & Merzlyak, M.N. (2002). Assessing Carotenoid Content in Plant Leaves with Reflectance Spectroscopy¶. *Photochemistry and Photobiology, 75*, 272-281
Goel, N.S. (1988). Models of vegetation canopy reflectance and their use in estimation of biophysical parameters from reflectance data. *Remote Sensing Reviews, 4*, 1-212
Goffart, J., Olivier, M., & Frankinet, M. (2008). Potato crop nitrogen status assessment to improve N fertilization management and efficiency: past–present–future. *Potato research, 51*, 355-383
Gómez-Dans, J.L., Lewis, P.E., & Disney, M. (2016). Efficient emulation of radiative transfer codes using Gaussian processes and application to land surface parameter inferences. *Remote Sensing, 8*, 119
González-Sanpedro, M., Le Toan, T., Moreno, J., Kergoat, L., & Rubio, E. (2008). Seasonal variations of leaf area index of agricultural fields retrieved from Landsat data. *Remote Sensing of Environment, 112*, 810-824
Govaerts, Y.M., & Verstraete, M.M. (1998). Raytran: A Monte Carlo ray-tracing model to compute light scattering in three-dimensional heterogeneous media. *IEEE transactions on Geoscience and Remote Sensing, 36*, 493-505
Henrich, V., Götze, E., Jung, A., Sandow, C., Thürkow, D., & Gläßer, C. (2009). Development of an Online indices-database: motivation, concept and implementation. *EARSeL proceedings, EARSeL, Tel Aviv*
Houles, V., Guerif, M., & Mary, B. (2007). Elaboration of a nitrogen nutrition indicator for winter wheat based on leaf area index and chlorophyll content for making nitrogen recommendations. *European Journal of Agronomy, 27*, 1-11
Huang, H., Qin, W., & Liu, Q. (2013). RAPID: A radiosity applicable to porous individual objects for directional reflectance over complex vegetated scenes. *Remote Sensing of Environment, 132*, 221-237
Huemmrich, K. (2001). The GeoSail model: a simple addition to the SAIL model to describe discontinuous canopy reflectance. *Remote Sensing of Environment, 75*, 423-431
Jacquemoud, S., & Baret, F. (1990). PROSPECT : A model of leaf optical properties spectra. *Remote Sensing of Environment, 34*, 75-91
Jacquemoud, S., & Ustin, S.L. (2001). Leaf optical properties: A state of the art. In, *8th International Symposium of Physical Measurements & Signatures in Remote Sensing* (pp. 223-332): CNES, Aussois France
Jacquemoud, S., & Ustin, S.L. (2008). Modeling leaf optical properties. In, *Photobiological Sciences Online*
Jacquemoud, S., Verhoef, W., Baret, F., Bacour, C., Zarco-Tejada, P.J., Asner, G.P., François, C., & Ustin, S.L. (2009). PROSPECT + SAIL models: A review of use for vegetation characterization. *Remote Sensing of Environment, 113*, S56-S66
Jakob, W. (2014). Mitsuba Documentation Version 0.5.0. https://www.mitsuba-renderer.org/

Jay, S., Baret, F., Dutartre, D., Malatesta, G., Héno, S., Comar, A., Weiss, M., & Maupas, F. (2018). Exploiting the centimeter resolution of UAV multispectral imagery to improve remote-sensing estimates of canopy structure and biochemistry in sugar beet crops. *Remote Sensing of Environment*
Kusnierek, K., & Korsaeth, A. (2015). Simultaneous identification of spring wheat nitrogen and water status using visible and near infrared spectra and powered partial least squares regression. *Computers and Electronics in Agriculture, 117*, 200-213
Kuusk, A., & Nilson, T. (2001). Testing directional properties of a forest reflectance model. *Journal of Geophysical Research: Atmospheres, 106*, 12011-12021
Lauvernet, C., Baret, F., Hascoët, L., Buis, S., & Le Dimet, F.-X. (2008). Multitemporal-patch ensemble inversion of coupled surface–atmosphere radiative transfer models for land surface characterization. *Remote Sensing of Environment, 112*, 851-861
Le Maire, G., Francois, C., & Dufrene, E. (2004). Towards universal broad leaf chlorophyll indices using PROSPECT simulated database and hyperspectral reflectance measurements. *Remote Sensing of Environment, 89*, 1-28
Le Maire, G., François, C., Soudani, K., Berveiller, D., Pontailler, J.-Y., Bréda, N., Genet, H., Davi, H., & Dufrêne, E. (2008). Calibration and validation of hyperspectral indices for the estimation of broadleaved forest leaf chlorophyll content, leaf mass per area, leaf area index and leaf canopy biomass. *Remote Sensing of Environment, 112*, 3846-3864
Lesk, C., Rowhani, P., & Ramankutty, N. (2016). Influence of extreme weather disasters on global crop production. *Nature, 529*, 84
Li, W., Weiss, M., Waldner, F., Defourny, P., Demarez, V., Morin, D., Hagolle, O., & Baret, F. (2015). A generic algorithm to estimate LAI, FAPAR and FCOVER variables from SPOT4_HRVIR and landsat sensors: evaluation of the consistency and comparison with ground measurements. *Remote Sensing, 7*, 15494-15516
Li, X., & Strahler, A.H. (1985). Geometric-optical modeling of a conifer forest canopy. *IEEE transactions on Geoscience and Remote Sensing*, 705-721
Liu, J., Pattey, E., & Jégo, G. (2012). Assessment of vegetation indices for regional crop green LAI estimation from Landsat images over multiple growing seasons. *Remote Sensing of Environment, 123*, 347-358
Lu, C., & Tian, H. (2017). Global nitrogen and phosphorus fertilizer use for agriculture production in the past half century: shifted hot spots and nutrient imbalance. *Earth System Science Data, 9*, 181-192
LuxCoreRender (2018). LuxCoreRender Wiki. https://wiki.luxcorerender.org/LuxCoreRender_Wiki. In
Lymburner, L., Beggs, P.J., & Jacobson, R. (2000). Estimation of canopy-average surface specific leaf area using Landsat TM data. *Photogrammetric Engineering and Remote Sensing, 66*, 183-191
Maier, S.W., Lüdeker, W., & Günther, K.P. (1999). SLOP: A Revised Version of the Stochastic Model for Leaf Optical Properties. *Remote Sensing of Environment, 68*, 273-280
Mauser, W., Klepper, G., Zabel, F., Delzeit, R., Hank, T., Putzenlechner, B., & Calzadilla, A. (2015). Global biomass production potentials exceed expected future demand without the need for cropland expansion. *Nature communications, 6*, 8946
Nelson, M.C., Ingram, S.E., Dugmore, A.J., Streeter, R., Peeples, M.A., McGovern, T.H., Hegmon, M., Arneborg, J., Kintigh, K.W., & Brewington, S. (2016). Climate challenges, vulnerabilities, and food security. *Proceedings of the National Academy of Sciences, 113*, 298-303
Nguy-Robertson, A., Gitelson, A., Peng, Y., Viña, A., Arkebauer, T., & Rundquist, D. (2012). Green leaf area index estimation in maize and soybean: Combining vegetation indices to achieve maximal sensitivity. *Agronomy Journal, 104*, 1336-1347
North, P.R. (1996). Three-dimensional forest light interaction model using a Monte Carlo method. *IEEE transactions on Geoscience and Remote Sensing, 34*, 946-956
Penuelas, J., Baret, F., & Filella, I. (1995). Semi-empirical indices to assess carotenoids/chlorophyll a ratio from leaf spectral reflectance. *Photosynthetica, 31*, 221-230

Pharr, M., Jakob, W., & Humphreys, G. (2016). *Physically based rendering: From theory to implementation*. Morgan Kaufmann
Pölönen, I., Saari, H., Kaivosoja, J., Honkavaara, E., & Pesonen, L. (2013). Hyperspectral imaging based biomass and nitrogen content estimations from light-weight UAV. In, *Remote Sensing for Agriculture, Ecosystems, and Hydrology XV* (p. 88870J): International Society for Optics and Photonics
POV-team (2013). Introduction to POV-Ray for POV-Ray version 3.7.http://www.povray.org
Qin, W., & Gerstl, S.A. (2000). 3D scene modeling of semidesert vegetation cover and its radiation regime. *Remote Sensing of Environment, 74*, 145-162
Ross, J. (2012). *The radiation regime and architecture of plant stands*. Springer Science & Business Media
Rouse Jr, J.W., Haas, R., Schell, J., & Deering, D. (1974). Monitoring vegetation systems in the Great Plains with ERTS
Schächtl, J., Huber, G., Maidl, F.-X., Sticksel, E., Schulz, J., & Haschberger, P. (2005). Laser-induced chlorophyll fluorescence measurements for detecting the nitrogen status of wheat (Triticum aestivum L.) canopies. *Precision agriculture, 6*, 143-156
Scharf, P., Schmidt, J., Kitchen, N., Sudduth, K., Hong, S., Lory, J., & Davis, J. (2002). Remote sensing for nitrogen management. *Journal of soil and water conservation, 57*, 518-524
Schlemmer, M., Gitelson, A., Schepers, J., Ferguson, R., Peng, Y., Shanahan, J., & Rundquist, D. (2013). Remote estimation of nitrogen and chlorophyll contents in maize at leaf and canopy levels. *International Journal of Applied Earth Observation and Geoinformation, 25*, 47-54
Sims, D.A., & Gamon, J.A. (2002). Relationships between leaf pigment content and spectral reflectance across a wide range of species, leaf structures and developmental stages. *Remote Sensing of Environment, 81*, 337-354
Spiertz, J. (2009). Nitrogen, sustainable agriculture and food security: a review. *Sustainable Agriculture* (pp. 635-651): Springer
Strahler, A.H. (1997). Vegetation canopy reflectance modeling—Recent developments and remote sensing perspectives. *Remote Sensing Reviews, 15*, 179-194
Stuckens, J., Somers, B., Delalieux, S., Verstraeten, W., & Coppin, P. (2009a). The impact of common assumptions on canopy radiative transfer simulations: A case study in Citrus orchards. *Journal of Quantitative Spectroscopy and Radiative Transfer, 110*, 1-21
Stuckens, J., Verstraeten, W.W., Delalieux, S., Swennen, R., & Coppin, P. (2009b). A dorsiventral leaf radiative transfer model: Development, validation and improved model inversion techniques. *Remote Sensing of Environment, 113*, 2560-2573
Thenkabail, P.S. (2015). *Land resources monitoring, modeling, and mapping with remote sensing*. CRC Press
Tilman, D., Balzer, C., Hill, J., & Befort, B.L. (2011). Global food demand and the sustainable intensification of agriculture. *Proceedings of the National Academy of Sciences, 108*, 20260-20264
Tremblay, N., Wang, Z., & Cerovic, Z.G. (2012). Sensing crop nitrogen status with fluorescence indicators. A review. *Agronomy for sustainable development, 32*, 451-464
Tucker, C.J., & Garratt, M.W. (1977). Leaf optical system modeled as a stochastic process. *Applied Optics, 16*, 635-642
Ustin, S., Jacquemoud, S., & Govaerts, Y. (2001). Simulation of photon transport in a three‐dimensional leaf: implications for photosynthesis. *Plant, Cell & Environment, 24*, 1095-1103
Van Grinsven, H., Spiertz, J., Westhoek, H., Bouwman, A., & Erisman, J. (2014). Nitrogen use and food production in European regions from a global perspective. *The Journal of Agricultural Science, 152*, 9-19
Verger, A., Vigneau, N., Chéron, C., Gilliot, J.-M., Comar, A., & Baret, F. (2014). Green area index from an unmanned aerial system over wheat and rapeseed crops. *Remote Sensing of Environment, 152*, 654-664

Verrelst, J., Muñoz, J., Alonso, L., Delegido, J., Rivera, J.P., Camps-Valls, G., & Moreno, J. (2012). Machine learning regression algorithms for biophysical parameter retrieval: Opportunities for Sentinel-2 and-3. *Remote Sensing of Environment, 118*, 127-139
Verrelst, J., Rivera Caicedo, J.P., Muñoz-Marí, J., Camps-Valls, G., & Moreno, J. (2017). SCOPE-based emulators for fast generation of synthetic canopy reflectance and sun-induced fluorescence Spectra. *Remote Sensing, 9*, 927
Wang, K., Franklin, S.E., Guo, X., & Cattet, M. (2010). Remote sensing of ecology, biodiversity and conservation: a review from the perspective of remote sensing specialists. *Sensors, 10*, 9647-9667
Wang, L., Qu, J.J., Hao, X., & Hunt, E.R. (2011). Estimating dry matter content from spectral reflectance for green leaves of different species. *International Journal of Remote Sensing, 32*, 7097-7109
Weiss, M., Baret, F., Leroy, M., Hautecoeur, O., Bacour, C., Prevol, L., & Bruguier, N. (2002). Validation of neural net techniques to estimate canopy biophysical variables from remote sensing data. *Agronomie-Sciences des Productions Vegetales et de l'Environnement, 22*, 547-554
Widlowski, J.-L., Robustelli, M., Disney, M., Gastellu-Etchegorry, J.-P., Lavergne, T., Lewis, P., North, P., Pinty, B., Thompson, R., & Verstraete, M. (2008). The RAMI On-line Model Checker (ROMC): A web-based benchmarking facility for canopy reflectance models. *Remote Sensing of Environment, 112*, 1144-1150
Xiao, Z., Liang, S., Sun, R., Wang, J., & Jiang, B. (2015). Estimating the fraction of absorbed photosynthetically active radiation from the MODIS data based GLASS leaf area index product. *Remote Sensing of Environment, 171*, 105-117
Yamada, N., & Fujimura, S. (1991). Nondestructive measurement of chlorophyll pigment content in plant leaves from three-color reflectance and transmittance. *Applied Optics, 30*, 3964-3973
Zarco-Tejada, P.J., Miller, J.R., Harron, J., Hu, B., Noland, T.L., Goel, N., Mohammed, G.H., & Sampson, P. (2004). Needle chlorophyll content estimation through model inversion using hyperspectral data from boreal conifer forest canopies. *Remote Sensing of Environment, 89*, 189-199

2 Estimating leaf biochemical content from laboratory spectral measurements

Leaf biochemical content corresponds to traits related to the plant state and its functioning in relation to photosynthesis, respiration and transpiration. The main leaf absorbers including chlorophyll, carotenoid, water and dry matter contents show strong and specific absorption features, which impacts the leaf reflectance and transmittance spectra. It is therefore possible to estimate the content of these constituents from laboratory spectral measurements. In this chapter, we first evaluated the performances of the several versions of the PROSPECT model against Vis to estimate leaf biochemical content from leaf reflectance measurements. Since a number of plant species have distinct optical properties between the upper and lower leaf faces, which are neglected in PROSPECT, we developed and validated FASPECT to take into account the differences between the two faces. This chapter is thus split into 2 main sections that correspond to journal articles:

- ***Article 1: Estimation of leaf traits from reflectance measurements: comparison between methods based on vegetation indices and several versions of the PROSPECT model*** (published in *Plant Methods)*. The study is based on an experiment conducted over six wheat cultivars grown under several nitrogen levels and sowing densities. Leaf reflectance spectra in the 450–2250 nm domain were acquired at two growing stages, concurrently with destructive measurements of chlorophyll, carotenoid, water and dry matter contents. Estimation performances were compared between several versions of PROSPECT model and those obtained using empirical relationships with vegetation indices (VI). Results show that PROSPECT model inversion and empirical VI approach provide similar retrieval performances and are useful methods to estimate leaf biochemical composition from spectral measurements. However, for PROSPECT models, the dry matter content is not very well estimated and significant bias was observed for chlorophyllian pigments estimates.

- ***Article 2: Optical properties differences between upper and lower leaf faces: measurements, and development of the FASPECT model***
  In this article, we propose the FASPECT model that considers the leaf as a stack of four-layers. The upper and lower epidermis layers are characterized by distinct wavelength-independent reflectivity and the leaf mesophyll is assumed to be made of a palisade and a spongy parenchyma layers with two proportional parameters to describe the distribution of pigments and leaf structure. Therefore, six additional parameters are required to describe the differences in leaf optical properties between upper and lower faces as compared to the PROSPECT model which describes the homogeneous case. Because of the concentrated chlorophyll in palisade mesophyll, the specific absorption coefficients of chlorophyll and carotenoids are recalibrated. Validation was done against eight datasets.
  Results show that FASPECT simulates accurately the reflectance and transmittance of the two faces and over-performs the PROSPECT models for single face spectra. In the inverse mode, significant improvements are observed for the estimation of dry matter content as compared to PROSPECT. We thus demonstrate that FASPECT is efficient and could be used in 3D canopy radiative transfer models to simulate canopy reflectance more accurately, especially for plants with significant differences in leaf optical property between faces.

2.1 The current limits of the PROSPECT model to estimate leaf biochemical content

Jiang *et al. Plant Methods (2018) 14:23*
https://doi.org/10.1186/s13007-018-0291-x

Plant Methods

RESEARCH

Open Access

Estimation of leaf traits from reflectance measurements: comparison between methods based on vegetation indices and several versions of the PROSPECT model

Jingyi Jiang[1*], Alexis Comar[2], Philippe Burger[3], Pierre Bancal[4], Marie Weiss[1] and Frédéric Baret[1]

Abstract

Background: Leaf biochemical composition corresponds to traits related to the plant state and its functioning. This study puts the emphasis on the main leaf absorbers: chlorophyll a and b (C_{ab}), carotenoids (C_c), water (C_w) and dry mater (C_m) contents. Two main approaches were used to estimate [C_{ab}, C_c, C_w, C_m] in a non-destructive way using spectral measurements. The first one consists in building empirical relationships from experimental datasets using either the raw reflectances or their combination into vegetation indices (VI). The second one relies on the inversion of physically based models of leaf optical properties. Although the first approach is commonly used, the calibration of the empirical relationships is generally conducted over a limited dataset. Consequently, poor predictions may be observed when applying them on cases that are not represented in the training dataset, i.e. when dealing with different species, genotypes or under contrasted environmental conditions. The retrieval performances of the selected VIs were thus compared to the ones of four PROSPECT model versions based on reflectance data acquired at two phenological stages, over six wheat genotypes grown under three different nitrogen fertilizations and two sowing density modalities. Leaf reflectance was measured in the lab with a spectrophotometer equipped with an integrating sphere, the leaf being placed in front of a white Teflon background to increase the sensitivity to leaf biochemical composition. Destructive measurements of [C_{ab}, C_c, C_w, C_m] were performed concurrently.

Results: The destructive measurements demonstrated that the carotenoid, C_c, and chlorophyll, C_{ab}, contents were strongly correlated ($r^2 = 0.91$). The sum of C_{ab} and C_c, i.e. the total chlorophyllian pigment content, C_{abc}, was therefore used in this study. When inverting the PROSPECT model, accounting for the brown pigment content, C_{bp}, was necessary when leaves started to senesce. The values of C_{abc} and C_w were well estimated ($r^2 = 0.81$ and $r^2 = 0.88$ respectively) while the dry matter content, C_m, was poorly estimated ($r^2 = 0.00$). Retrieval of C_w from PROSPECT versions was only slightly biased, while substantial overestimation of C_{abc} was observed. The ranking between estimated values of C_{abc} and C_w from the several PROSPECT versions and that derived using the VIs were similar to the ranking observed over the destructively measured values of C_{abc} and C_w.

Conclusions: PROSPECT model inversion and empirical VI approach provide similar retrieval performances and are useful methods to estimate leaf biochemical composition from spectral measurements. However, the PROSPECT model inversion gives potential access to additional traits on surface reflectivity and leaf internal structure. This study suggests that non-destructive estimation of leaf chlorophyll and water contents is a relevant method to provide leaf traits with relatively high throughput.

*Correspondence: jingyi.jiang@inra.fr
[1] EMMAH UMR 1114, INRA, UAPV, 84914 Avignon, France
Full list of author information is available at the end of the article

Keywords: Chlorophyll content, Carotenoid content, Water content, Dry matter content, Radiative transfer model, Reflectance, Transmittance, Leaf, Wheat, Phenotyping

Background

Plant phenotyping was recognized as one of the major bottleneck in the genetic improvement of crops [1]. It is currently a rapidly growing research domain that follows the continuous technical advances of sensors, robotics and computer systems for data processing. It relies on non-destructive and high-throughput measurements used to assess functional traits repeatedly throughout the growing season [2]. Plant phenotyping is completed at three main scales [3]: (1) the plot scale, i.e. a collection of plants mostly sampled in field conditions, (2) the plant scale generally measured under controlled conditions in the greenhouse, and (3) the organ scale, i.e. an element of the plant (leaf, stem, reproductive or storage organs) that can be sampled either in the field or under controlled conditions. For phenotyping purposes, the leaf biochemical composition provides valuable information on the plant state regarding some key processes such as photosynthesis, respiration and transpiration. The close relationship between chlorophyll and carotenoid pigments and nitrogen status of crops was indeed investigated by several studies [4–10] and depends on crop phenological stages as well on the leaf light environment [11–14]. Variation of the leaf relative water content (water mass per unit leaf mass) is related to the water stress experienced by the plant [15] or indicates the senescence level [16]. Green leaves show generally small deviations of the relative water content to keep the leaf turgescent while being compatible with biochemical processes [17]. The dry matter content corresponds to the leaf mass per area. It is related to photosynthesis and respiration processes [18–20]. It also controls the transformation of the mass of assimilates produced and allocated to the leaf into a leaf area increment within many crop models [21–23].

Chlorophyll, carotenoid, water and dry matter contents show strong and specific absorption features, which impact the leaf reflectance and transmittance spectra [24]. It is therefore possible to estimate the content of these constituents from the measurement of leaf optical properties [25–27]. Indeed, the actual quantity that drives light reflectance and transmittance is the content (mass of constituent per unit leaf area) rather than the concentration (mass of constituent per unit leaf dry mass): the biochemical content governs the effective path length of light through the leaf and controls thus the leaf reflectance and transmittance through scattering and absorption processes.

The estimation of the leaf chlorophyll and carotenoid content from optical measurements [28, 29] became very popular with the rise of precision farming focusing on nitrogen applications [13]. Empirical relationships between leaf water content and leaf optical properties have also been calibrated over experimental datasets and were demonstrated to be efficient [30–34]. Fewer studies reported attempts to estimate dry matter content from reflectance measurements [26, 35, 36]. These studies are generally reporting results obtained over a wide range of contents due either to interspecific differences or to contrasted environmental conditions such as variation in salinity or in the illumination levels in relation to the position of the leaf in the canopy [35, 36]. However, quantifying the differences expected between genotypes grown under similar conditions is more challenging: the differences between genotypes in pigment, water and dry matter contents are generally limited. In these conditions, a significant part of the variation in leaf optical properties is also due to variations in the leaf mesophyll structure, the distribution of pigments in the leaf volume as well as surface features. This affects the relationships between vegetation indices and chlorophyll content while a physically based model of leaf optical properties should allow to explicitly account for these potentially confounding effects. Furthermore, new genotypes grown under given environmental conditions may have characteristics not well represented in the VI-relationship training database, making the biochemical content estimation uncertain. A recent review of models of leaf optical properties [37] distinguishes three main approaches based either on radiative transfer [38–41], on stochastic processes [42, 43], or on ray tracing [44, 45]. PROSPECT is one of the most widely used leaf radiative transfer models [24, 41, 46, 47]. It has been successfully applied to retrieve leaf biochemical composition from reflectance and/or transmittance measurements [26, 46, 48, 49]. Several versions of the PROSPECT model are available. They mostly differ by the increasing detail in the pigments used and the associated values of the specific absorption coefficients, water and dry matter, as well as by the value of the refractive index controlling the scattering processes in the leaf.

The objective of this study was to evaluate the performances of the several versions of the PROSPECT model to estimate leaf chlorophyll, C_{ab}, carotenoid, C_c, water, C_w, and dry matter, C_m, contents from leaf reflectance measurements in the context of phenotyping experiments.

Performances were compared to those obtained using empirical relationships with vegetation indices. The study is based on an experiment conducted over six wheat cultivars grown under several nitrogen levels and sowing densities. Leaf reflectance spectra in the 450–2250 nm domain were acquired at two growing stages, concurrently with destructive measurements of chlorophyll, carotenoid, water and dry matter contents. Attention was paid both to the accuracy and precision of the biochemical content estimates as well as to the ranking capacity necessary to identify differences between genotypes.

Methods

The biological material

The experiment took place near Toulouse at the INRA centre "Auzeville Tolosane" (43°33′N, 1°28′E) in France over a site presenting deep and homogenous soil conditions. The wheat plants from which the leaves were collected were grown in field conditions described in [2]. The crop was sown in October 2011 and harvested in June 2012. Three factors were taken into account in the experimental design which resulted into 36 modalities: six cultivars (four winter wheat: Apache, Caphorn, Soissons and Hysun (hybrid); two durum wheat: Isildur and Biensur), two sowing densities and three nitrogen levels.

The measurements

Leaves were collected in April 2012 at the "two nodes" stage and in June 2012 during grain filling. All the 36 modalities were sampled in April, while only 26 of them were collected in June. For each of the resulting 62 samples, six top leaves were randomly collected. Three of them were used for the destructive measurements of dry matter and water content and the remaining three for destructive measurements of chlorophyll and carotenoid. Reflectance measurements were conducted for each of the six leaves used for destructive measurements. All data for destructive and spectral measurements are provided in Additional file 1.

Destructive measurements

The area (S) of each leaf was first measured by scanning each sample and processing the resulting image with the SCANAREA software [40]. Then, the three leaves used for the destructive measurements of C_m and C_w were weighed before (M_{fresh}), and after (M_{dry}) drying them out at 80 °C in an oven during 2 days. The dry matter (C_m in mg/cm^2) and water contents (C_w in mg/cm^2) were then computed using the following equations:

$$C_m = \frac{M_{dry}}{S} \quad (1)$$

$$C_w = \frac{M_{fresh} - M_{dry}}{S} \quad (2)$$

The three leaves used for C_{ab} and C_c leaves were lyophilized and stored in the dark at − 20 °C after measuring their area. The mass of Chlorophyll a and b and carotenoid were then estimated according to [50] by extracting the pigments in acetone and measuring the optical density of the solution. The corresponding content was computed using the measured area of each leaf.

Spectral measurements

The optical properties of the 372 leaves were acquired using an ASD Fieldspec-3 spectroradiometer (Analytical Spectral Devices Inc., Boulder, Colorado, USA) equipped with an integrating sphere Li-Cor 1800-12 (LI-COR Inc., Lincoln, NE). Data were sampled at intervals of 1.4 nm (350–1050 nm) and 2 nm (1000–2500 nm) with a spectral resolution of 3 nm for the region 350–1000 nm and 10 nm for the region 1000–2500 nm [51]. The direction of the incoming light was almost normal to the leaf sample while the bare fiber of the spectroradiometer viewed the integrating sphere wall under a 25° field of view (Fig. 1). The original Li-Cor lamp system of the integrating sphere was replaced by a lamp connected to a stabilized power supply. The original infrared filter was removed to increase the light available in this domain where the spectrophotometer has a lower sensitivity than in the shorter wavelengths. A Teflon white panel was used as the background of the leaf as proposed by [49] to increase the optical path in the leaf, thus enhancing the absorption features. Another Teflon white panel was used as a secondary reference to compute the directional-hemispherical reflectance factor (DHRF) of the leaf-white background system. The absolute $DHRF_{ref}$ of the secondary Teflon white reference was calibrated against a spectralon primary reference panel [52].

Three spectrophotometer measurements were completed for each of the six leaves sampled per date, cultivar

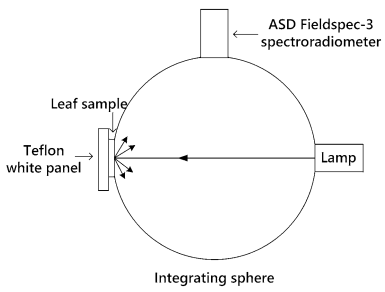

Fig. 1 The experimental setup for leaf reflectance measurement with Teflon white panel

and modality. The average ($S_{leaf}(\lambda)$) of the resulting 18 individual spectra was computed and then transformed into the corresponding DHRF ($DHRF_{leaf}(\lambda)$) according to Eq. (3):

$$DHRF_{leaf}(\lambda) = \frac{2S_{leaf}(\lambda)}{\left(S_{ref\_bef}(\lambda) + S_{ref\_aft}(\lambda)\right)} DHRF_{ref}(\lambda) \quad (3)$$

where $S_{ref\_bef}(\lambda)$ and $S_{ref\_aft}(\lambda)$ are the spectra of the secondary Teflon reference completed before and after the series of the 18 leaf spectrophotometer measurements. The reflectance of the white background was measured systematically just after the $S_{ref\_aft}(\lambda)$ measurements to account for possible changes of its properties due to the contact with the leaf.

The vegetation indices

A vegetation index is a combination of spectral bands that captures some absorption characteristics of a given biochemical content. Several of them have been proposed in the literature, mainly to assess water [33], and chlorophyll and carotenoid contents [48, 53, 54]. However, their associated performances are still a matter of discussion when the calibration and validation datasets differ in acquisition conditions, crop state and/or soil background [55, 56]. Two VIs (Dx4 and CIre) were selected among the most popular ones for chlorophyll content estimates (Table 1): Dx4 was developed for the Dualex Scientific+™ instrument (Force-A, Orsay, France) to estimate chlorophyll content from the transmittance in the red-edge (T_{710}) and the near infrared (T_{850}) [29]. CIre is the ratio between the reflectance in the near infrared ($R_{760-800}$) and the red-edge ($R_{690-710}$) [28, 57]. For water content, two popular indices were selected: SRw [31] is the ratio between reflectance in the short wave infrared (R_{1300}; R_{1450}) and NDw [27] is a normalized difference of bands in the short wave infrared (R_{1062}, R_{1393}). Since all the selected VIs are designed to enhance the absorption features of chlorophyllian pigments or water for leaf transmittance (Dx4) or reflectance over a black background (other VIs), they are also expected to work similarly for leaf optical properties measured over a white background. Simple linear functions were considered to empirically relate the biochemical contents and Dx4, CIre and SRw. A second order polynomial function was used to relate NDw and C_w. A leave-one-out method was used to quantify the performances of the empirical calibration using the r^2 (squared Pearson correlation coefficient) and RMSE (root mean square error) between the estimated and measured biochemical contents.

Table 1 Definition of the selected vegetation indices

Variables	VIs	Formula	References
C_{abc}	Dx4	$\frac{T_{850}}{T_{710}} - 1$	[29]
	CIre	$\frac{R_{760-800}}{R_{690-710}} - 1$	[28, 57]
C_w	SRw	$\frac{R_{1300}}{R_{1450}}$	[31]
	NDw	$\frac{R_{1062}-R_{1393}}{R_{1062}+R_{1393}}$	[27]

Inversion of the PROSPECT model

PROSPECT versions

The PROSPECT model [41] extended to multiple layers (plates) the (single) plate model from Allen [58] using the Stokes system of equations [59]. The mesophyll structure parameter, N, characterizes the number of homogenous elementary layers that constitute the leaf. Each elementary layer is described by the refractive index of the leaf material, n, and by an absorption coefficient computed as the sum of the specific absorption coefficients of each constituent weighted by their corresponding content. Several versions of the PROSPECT model have been proposed in the literature. They differ mainly by the specific absorption coefficients and refractive index. The original version was first updated based on a dataset of 58 leaves representing a broad range of species over which the specific absorption coefficients were recalibrated [26]. This resulted into PROSPECT version 3 (P3) [24, 41]. More recently, new values of the specific absorption coefficients and refractive index were proposed by [46] based on a larger set of leaf reflectance and transmittance measurements. It resulted into PROSPECT version 4 (P4) where chlorophyll and carotenoids were pooled together, and PROSPECT version 5 (P5) where chlorophyll and carotenoids were described separately. Finally, PROSPECT-D was proposed by [60], where anthocyanins were described explicitly in addition to chlorophyll a and b and carotenoids. Besides, the refractive index was also recalibrated. Finally, the contribution of the brown pigment content (C_{bp}) to leaf absorption can be added to each of the 4 PROSPECT versions, leading to P3b, P4b, P5b and PDb versions (Table 2). Brown pigments correspond to polyphenols that appear during leaf senescence [46].

Adaptation of PROSPECT to the measurement configuration

The reflectance measurements were achieved with the leaf placed over a white Teflon background to enhance the sensitivity to the leaf biochemical composition by increasing the optical path in the leaf [49]. PROSPECT simulates the directional hemispherical reflectance

Table 2 Description of the different PROSPECT model versions considered in this study

Version name	PROSPECT 3		PROSPECT 4		PROSPECT 5		PROSPECT D	
Chlorophyllian pigment separation	C_{abc}		C_{abc}		C_{ab} and C_c		C_{ab}, C_c and C_{Anth}	
References	[26]		[46]		[46]		[60]	
Brown pigments	$C_{bp} = 0$	C_{bp}	$C_{bp} = 0$	C_{bp}	$C_{bp} = 0$	C_{bp}	$C_{bp} = 0$	C_{bp}
Abbreviated name	P3	P3b	P4	P4b	P5	P5b	PD	PDb

Fig. 2 Leaf model to measure reflectance over a white background: the reflectance and transmittance values of each layer are indicated.R_{surf} is the surface reflectivity for both upper and lower leaf surfaces (independent of wavelength), $R_{leaf}(\lambda)$ and $T_{leaf}(\lambda)$ are the leaf reflectance and transmittance simulated by PROSPECT, assuming no reflectivity at the top and the bottom of the leaf volume. R_{wb} is the reflectance of the Teflon white background. All the reflectance and transmittance terms are bi-hemispherical except the upper and lower leaf surface reflectivity is directional-hemispherical

(R_{leaf}) and transmittance (T_{leaf}) of the leaf from the knowledge of the chlorophyll, carotenoid, water and dry matter contents, as well as brown pigments and the mesophyll structure parameter, N [41, 46]. In this study, the computation of the surface reflectivity was approximated by using the parameter R_{surf} conversely to the original PROSPECT version where the 'α' solid angle was used to mimic the leaf surface roughness. This allows to get a wider range of variability of surface reflectivity in agreement with observations [61]. R_{surf} was assumed to be independent from wavelength since the refractive index is very little spectrally dependent in the 350–2500 nm domain [61, 62]. Because wheat presents only small differences between the upper and lower surface features, R_{surf} was assumed to be the same for both faces. Indeed, the possible small differences between the two faces have a marginal impact on leaf characteristics estimates since the value of the illuminated face will mainly control the optical properties of the system. Figure 2 showed the representation of the system of layers used to compute leaf reflectance when the leaf was placed over the white Teflon background. The leaf volume layer was characterized by the reflectance and transmittance simulated by PROSPECT assuming no reflectivity at the top and the bottom, while the leaf upper and lower epidermis layers were characterized by R_{surf} with no absorption.

The system described in Fig. 2 was solved in three steps. First the reflectance of the lower leaf surface over the white Teflon background, R^{wb}_{surf}, was computed as:

$$R^{wb}_{surf}(\lambda) = R_{surf} + \frac{R_{wb}(\lambda)\left(1 - R_{surf}\right)^2}{1 - R_{surf}R_{wb}(\lambda)} \quad (4)$$

where R_{surf} is the reflectivity of the lower surface, assuming that the transmissivity of the interface is $1 - R_{surf}$ and there is no absorption at the leaf surface. $R_{wb}(\lambda)$ is the hemispherical reflectance of the Teflon white background. The reflectance at the bottom of the upper epidermis, $R^{wb}_{bue}(\lambda)$, was then computed as:

$$R^{wb}_{bue}(\lambda) = R_{leaf}(\lambda) + \frac{R^{wb}_{surf}(\lambda)T_{leaf}(\lambda)^2}{1 - R_{leaf}(\lambda)R^{wb}_{surf}(\lambda)} \quad (5)$$

where $R_{leaf}(\lambda)$ is the leaf volume reflectance computed from the PROSPECT model for which the reflectivity of the surface of the leaf volume is set to 0; $T_{leaf}(\lambda)$ is the corresponding leaf volume transmittance. Note that Eq. (5) assumes that the properties of the leaf are the same on both faces and that the directional hemispherical reflectance and transmittance are equal to the bi-hemispherical corresponding quantities. Then, the reflectance of the leaf over the white background was computed using the upper surface reflectivity which was assumed to be identical to the lower surface:

$$R^{wb}_{leaf}(\lambda) = R_{surf}(\lambda) + \frac{R^{wb}_{bue}(\lambda)\left(1 - R_{surf}(\lambda)\right)^2}{\left(1 - R_{surf}(\lambda)R^{wb}_{bue}(\lambda)\right)} \quad (6)$$

Finally, since the incident light on the leaf may directly illuminate the white background in case of small leaves, an additional parameter, f_{wb}, was introduced to describe this situation. f_{wb} is the fraction of white Teflon background illuminated directly by the light source. The corresponding reflectance of the system was finally written as:

$$R(\lambda) = R_{wb}(\lambda).f_{wb} + \left(1 - f_{wb}\right).R^{wb}_{leaf}(\lambda) \quad (7)$$

Fitting the white background PROSPECT model variables

An iterative minimization of the cost function, $J(V)$ (Eq. 8), was applied to estimate the model variables, V, where $V=[C_{abc}, C_w, C_m, N, R_{surf}, f_{wb}]$ for P3 and P4, $V=[C_{ab}, C_c, C_w, C_m, N, R_{surf}, f_{wb}]$ for P5 and $V=[C_{ab}, C_c, C_{Anth}, C_w, C_m, N, R_{surf}, f_{wb}]$ for PD. The brown pigments C_{bp} were also considered as an additional variable for each of the four models (P3b, P4b, P5b, PDb).

The cost function $J(V)$ computed the distance between the PROSPECT simulated reflectance spectrum and the actual measurements over the 18 acquisitions performed on each date, cultivar and modality:

$$J(V)=\sqrt{\frac{1}{1800}\sum_{\lambda=400}^{\lambda=2200}\left(R^{wb*}_{prospect}(\lambda)-R^{wb}_{leaf}(\lambda)\right)^2} \quad (8)$$

The original 300–2500 nm spectral range of the ASD spectroradiometer was restricted to the 400–2200 nm domain because (1) the PROSPECT model was calibrated only for wavelengths higher than 400 nm and (2) the signal was dominated by noise for wavelengths longer than 2200 nm. Furthermore, the 400–2200 nm spectral domain contains a significant part of all the spectral features of the biochemical components considered in this study.

The interior point minimization algorithm [63] was used to minimize $J(P)$ by keeping the variables within their bounds (Table 3). Three initial guesses (Table 3) were used to avoid the algorithm to be trapped in a local minimum. The estimated biochemical contents were then computed as the mean value over the three optimization results. Fortunately, in most situations the three initial guesses were providing almost the same solution.

Results

Relationships between biochemical contents

The relationships between C_{ab}, C_c, C_w and C_m were first investigated over the destructive measurements which were considered as the reference. Note that C_{bp} was not measured since polyphenols are difficult to extract.

The results showed that dry matter content was independent from the content of the other constituents with r^2 lower than 0.02 (Fig. 3). Chlorophyll and, in a lesser extent, carotenoid contents were correlated to water content (r^2 larger than 0.2 significant at $\alpha=5\%$) since a loss of water is concomitant with a loss of chlorophyll and carotenoid pigments for the senescing leaves (Fig. 3). The strongest correlation was observed between chlorophyll and carotenoid pigments ($r^2=0.91$ with a ratio of C_{ab}/C_c5, when the offset is neglected Fig. 3), which was consistent with the results from [54] and [41]. However, while these studies found an offset of 5 µg/cm^2 in this relationship over a large range of species, we observed a lower offset for the carotenoid content (≈1 µg/cm^2) when all the chlorophyll had disappeared. Considering this strong relationship between chlorophyll and carotenoid contents, we did not consider them separately in the following of the study.

PROSPECT spectra simulation performances

The performances of the inversion were first evaluated by considering the agreement between the simulated and the measured reflectance spectra. Figure 4 shows an example of a measured and simulated leaf reflectance spectrum, as well as the several terms used in Eqs. (4–7). The reflectance was simulated using the estimated values of the variables V after minimizing the cost function $J(V)$ (Eq. 8). This result showed that the reflectance spectra simulated using the retrieved PROSPECT model variables closely matched the measurements. Indeed, when considering the whole dataset, the average RMSE between the measured and estimated spectra over all the samples and the different PROSPECT versions was 0.013 (Fig. 5). PD and PDb provided the lowest RMSE. The observed outliers corresponded to senescent leaves for which absorption features cannot be properly modeled with the present PROSPECT model versions.

Table 3 Initial guesses and bounding limits required to perform the fitting of the PROSPECT models

Variables	C_c (µg/cm^2)	C_{ab} (µg/cm^2)	C_{abc} (µg/cm^2)	C_{Anth} (µg/cm^2)	C_m (mg/cm^2)	C_w (mg/cm^2)	C_{bp}	N	R_{surf}	f_{wb}
Initial guess										
1	10	50	60	5	12	5	0.01	1.4	0.05	0.01
2	5	20	20	1	8	1.5	0.2	2	0.1	0.2
3	50	80	90	10	40	18	0.001	1.1	0.01	0.1
Bounds										
Min	0	0	0	0	1	1	0	1.01	0	0.0
Max	80	140	140	20	50	30	1	3.5	0.5	1.0

List of the three initial guesses and bounding limits used to minimize the cost function for each variable. Min and Max are the minimum and maximum bounding values of each variable

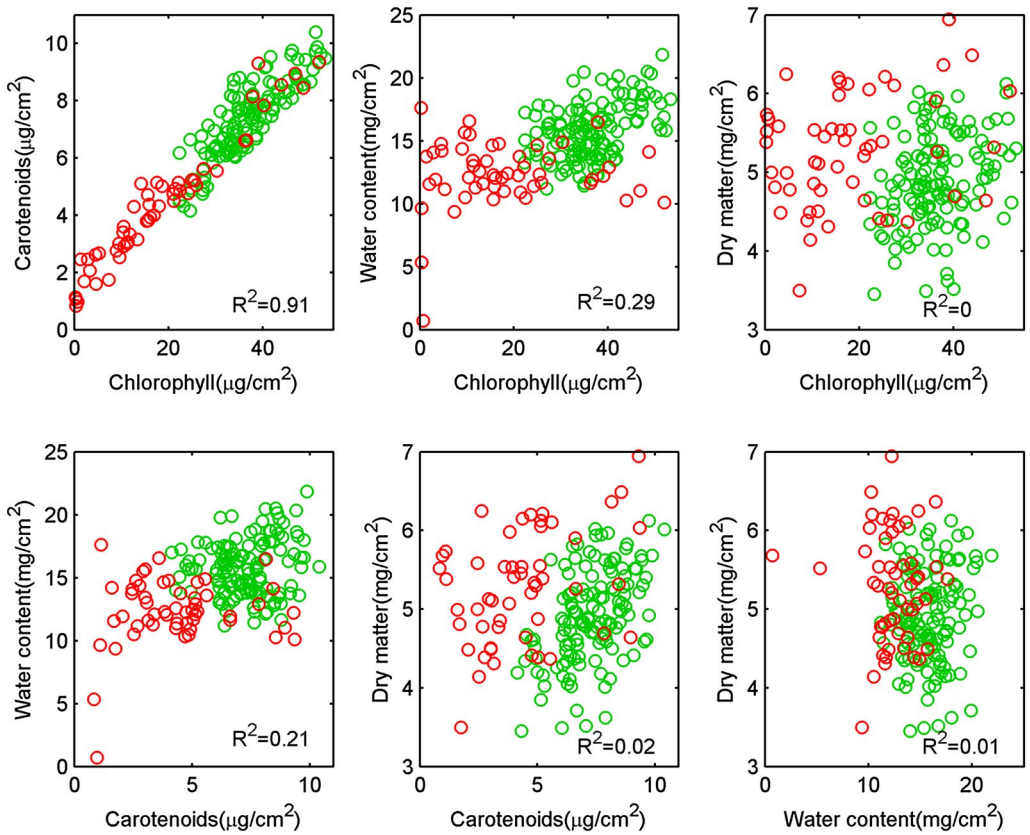

Fig. 3 Relationships between the four biochemical leaf traits from destructive measurements. Green and red points correspond to measurements achieved at two nodes (April) and grain filling (June) stages respectively. The squared Pearson correlation coefficient (r^2) of each relationship is indicated

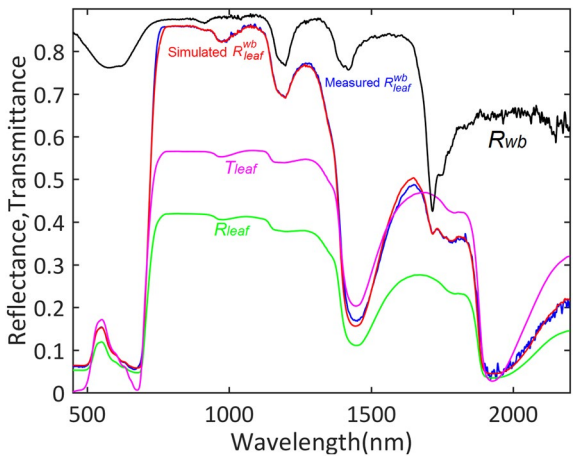

Fig. 4 Example of a measured leaf spectrum (red) and a corresponding PROSPECT simulation (blue). The reflectance (R_{leaf} and T_{leaf}) and transmittance of the leaf volume are shown in green and magenta respectively. The reflectance computed at the top of the leaf volume (R_{wb}) considering measurements over a Teflon white background is shown in black

Performances for biochemical composition estimation

The values of the retrieved C_{ab}, C_c, C_{abc}, C_w and C_m were compared to the destructive measurements. Results (Table 4) showed that when combining these pigments into chlorophyllian pigments, C_{abc} estimates were strongly correlated with the destructive measurements for all the PROSPECT versions (r^2 between 0.59 and 0.79). The addition of brown pigments (P3b, P4b, P5b and PDb) provided more accurate estimation of C_{abc} (r^2 between 0.79 and 0.81), particularly for the June measurements after the beginning of the senescence (Fig. 6). When correcting the chlorophyll systematic overestimation by a linear fit (Fig. A, dashed line), the RMSE values varied from 6 to 9 μg/cm^2. However, part of the scattering might also be attributed to uncertainties in the destructive measurements of chlorophyllian pigments used as a reference, estimated to be around 10%, i.e. 3 μg/cm^2.

Leaf water content was very well estimated regardless of the PROSPECT version (Table 4). However, a small bias was systematically observed ($1.13 \leq \text{slope} \leq 1.24$).

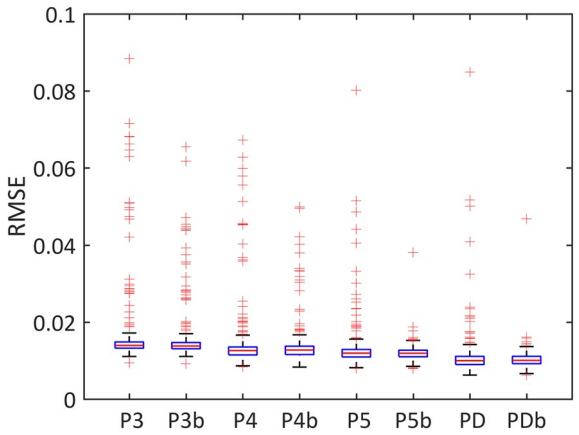

Fig. 5 Box plot of RMSE between the measured and simulated reflectance using the 8 PROSPECT versions (P3:PROSPECT 3, P3b: PROSPECT 3 considering the brown pigment content, P4:PROSPECT 4, P4b: PROSPECT 4 considering the brown pigment content, P5:PROSPECT 5, P5b: PROSPECT 5 considering the brown pigment content, PD: PROSPECT D, PDb: PROSPECT D considering the brown pigment content)

The estimation of the dry matter content showed very poor performances, with a $r^2 = 0.00$, a significant bias (between 2.18 and 2.88 mg/cm^2) and RMSE values after bias correction around 1.8 mg/cm^2.

The mean value of the retrieved N parameter (mesophyll structure) differed according to the four PROSPECT versions: N < 1.5 for P3, P3b, PD and PDb while N > 1.6 for P4, P4b, P5 and P5b. This behavior was partly linked to some compensation effects between R_{surf} and f_{wb} during the model inversion process. The surface component of the leaf reflectance, R_{surf}, also varied between the PROSPECT versions. It was found to be 0.05 with P3 and P3b which was in better agreement with the literature [2, 64], as compared to the other PROSPECT versions ($R_{surf} = 0.01$). Estimates of f_{wb} using P4, P4b, P5, and P5b, were higher ($f_{wb} \approx 0.07$) than for P3, P3b, PD and PDb ($f_{wb} \approx 0.03$).

Comparison between C_{abc} and C_w estimates from PROSPECT and vegetation indices

The comparison was first based on the Spearman correlation coefficient that offered the advantage to be independent from possible bias and little sensitive to the non-linearity between the biochemical contents and the VIs considered in this study. The Spearman correlation coefficient quantifies the consistency of the ranking between the biochemical content measurements used as reference and those estimated from non-destructive techniques. The ranking capacity of phenotyping techniques, i.e. the relative values of traits rather than their absolute values, is indeed probably the first property required by the breeders.

The total chlorophyllian pigment content was here considered since it was difficult to estimate independently the chlorophyll a and b from the carotenoids (Table 5). Furthermore, C_{ab} and C_c were strongly correlated (Fig. 3). The PROSPECT versions using the brown pigments were considered here because of their better performances.

Results (Table 5) showed that, after bias correction, the performances of C_{abc} estimation were good for all the versions of PROSPECT and similar to the ones of Dx4. They were slightly degraded for CIre ($\rho = 0.78$; RMSE Corr = 7.08) as compared to PROSPECT and Dx4 estimates ($\rho > 0.8$; RMSE Corr = 6.63).

Performances for water content estimation were very good, especially when considering the Spearman correlation coefficient, which was higher than for C_{abc}. The four versions of the PROSPECT model provided similar results after bias correction (Table 5). However, NDw slightly improved the estimation of water content both for ρ and RMSE.

Discussion

Accuracy of the PROSPECT versions to simulate reflectance spectra

The performances (RMSE) in terms of the full spectrum reconstruction were decreasing from the first (P3) to the last (PD) version of PROSPECT (Fig. 5). These results did not match the model performances for biochemical content estimation (Table 4) because of three main reasons: (1) there were possible compensations between the several specific absorption coefficients during the PROSPECT calibration process. (2) A bias in the specific absorption coefficient results in a bias in the biochemical content estimates. (3) there might also be compensations between some parameter estimates during the PROSPECT model inversion implemented in this study.

The inclusion of the brown pigments helped decreasing the number of outliers for all the model versions (Fig. 5), particularly for the June measurements when senescence was observed (results not shown). The spectral variations of the RMSE between measured and simulated reflectance clearly showed the advantage of including the brown pigments to get more accurate and precise reflectance simulations in the 400–1000 nm domain (Fig. 7a, b). Between 1000 nm and 2200 nm (Fig. 7b, d), the effect of the brown pigments was negligible as expected since they do not absorb in these longer wavelengths.

Closer inspection (Fig. 7c) showed that P3b and P4b versions that did not account for the carotenoids showed larger RMSE values in the 400–570 nm domain. In the red edge (700–780 nm), all the PROSPECT versions showed artefacts as compared to the measurements, while the RMSE was much lower for P3b than for the other versions. The separation of anthocyanin from chlorophyllian

Table 4 Performances of the inversion process over the 372 sampled leaves

Variables	Metrics	P3	P3b	P4	P4b	P5	P5b	PD	PDb
C_{abc} (µg/cm^2)	r^2	0.65	*0.81*	0.59	0.79	0.63	0.80	0.79	0.80
	RMSE	30.92	27.66	19.90	*10.93*	25.85	19.21	25.33	22.72
	RMSE Corr	8.70	*6.51*	9.88	6.67	8.94	6.66	6.83	6.67
	Slope	1.67	1.63	1.35	*1.18*	1.54	1.41	1.57	1.50
	Bias	− 27.70	− 25.09	− 14.99	*− 8.11*	− 23.29	− 17.56	− 23.22	− 20.69
C_{ab} (µg/cm^2)	r^2	–	–	–	–	0.81	*0.82*	0.81	*0.82*
	RMSE					24.60	18.71	19.39	*17.29*
	RMSE Corr					5.60	*5.29*	5.52	5.45
	Slope					1.67	1.50	1.52	*1.45*
	Bias					− 22.38	− 16.78	− 17.52	*− 15.39*
C_c (µg/cm^2)	r^2					0.16	0.04	*0.48*	0.45
	RMSE					9.00	*3.91*	6.18	5.75
	RMSE Corr	–	–	–	–	5.63	3.42	*1.56*	1.58
	slope					0.88	*0.99*	1.80	1.74
	Bias					− 0.91	*− 0.78*	− 5.70	− 5.30
C_w (mg/cm^2)	r^2	*0.88*	0.87	0.85	0.85	0.86	0.86	0.85	0.85
	RMSE	*2.35*	2.87	3.75	3.91	3.65	3.79	2.47	2.67
	RMSE Corr	1.06	1.13	1.06	1.07	*1.03*	1.04	1.08	1.09
	Slope	*1.13*	1.17	1.23	1.24	1.23	1.24	1.14	1.16
	Bias	*− 1.96*	− 2.47	− 3.54	− 3.68	− 3.48	− 3.59	− 2.14	− 2.34
C_m (mg/cm^2)	r^2	0.00	0.00	0.00	0.00	0.00	0.00	0.00	0.00
	RMSE	*2.45*	2.82	2.82	3.07	2.83	3.06	2.59	2.87
	RMSE Corr	*1.67*	1.80	1.80	1.90	1.80	1.89	1.75	1.84
	slope	*0.56*	0.47	0.47	0.42	0.47	0.42	0.53	0.46
	Bias	*2.18*	2.60	2.61	2.88	2.62	2.88	2.33	2.65
N	Mean	1.45	1.47	1.64	1.63	1.64	1.62	1.43	1.41
R_{surf}	Mean	0.05	0.05	0.01	0.01	0.01	0.01	0.01	0.01
f_{wb}	Mean	0.01	0.02	0.07	0.07	0.07	0.07	0.04	0.04

The estimation performances of C_{abc}, C_{ab}, C_c, C_w and C_{dm} were quantified using the squared Pearson correlation coefficient (r^2) and the RMSE computed between the measured and estimated biochemical contents over the 186 available data. The RMSE Corr was computed when correcting for possible systematic deviations using a linear model characterized by a slope as observed in Fig. 6. Bias value was the difference between the mean measured and mean estimated biochemical contents. The numbers in italic indicate the best result for each biochemical content and model version

pigments in PDb further decreased the RMSE between 500 to 600 nm where anthocyanin absorbs light. PDb that describes the biochemical content of more pigments than the other versions showed therefore the best agreement with the measured reflectance spectra.

In the 1000–2200 nm domain, P3 and P3b showed significant RMSE peaks on the lower wavelength shoulders of the main water absorption features at 1150, 1400 and 1900 nm although it performed best at 1300 and 1600 nm. P4, P4b, P5 and P5b showed similar RMSE peaks around the water absorption features.

Comparison between PROSPECT versions for C_{abc}, C_w and C_m estimates

Taking into account the presence of brown pigments significantly improved the performances of all the PROSPECT model versions to estimate C_{ab} and C_{abc}, resulting in r^2 values between 0.79 and 0.81 instead of 0.59 and 0.79 when brown pigments are not considered (Table 4). In the following, the discussion will therefore concentrate on the PROSPECT versions that include the brown pigments.

When distinguishing between chlorophyll and carotenoids using the P5b and PDb versions, the estimated chlorophyll content was strongly correlated with the destructive measurements with similar performances as those observed when chlorophyll and carotenoids were pooled together (Table 4). Conversely, carotenoids were poorly estimated although PDb performed much better than P5b. A clear separation was observed between the April measurements corresponding to the greener leaves with more chlorophyllian pigments and the June

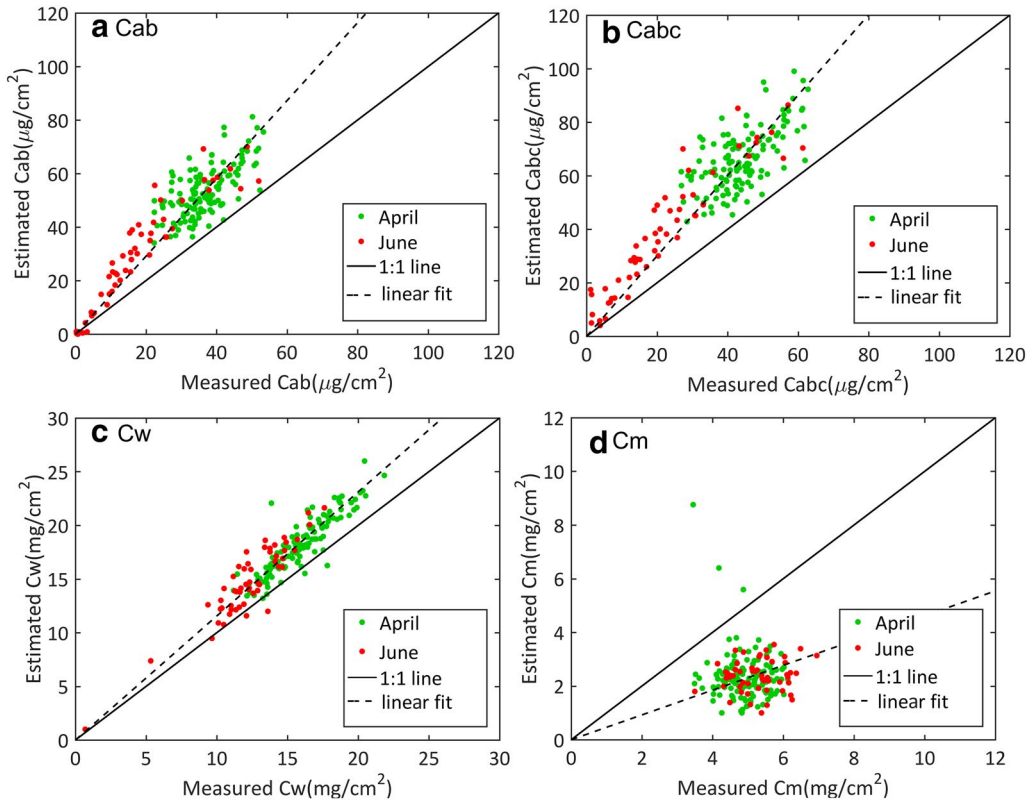

Fig. 6 Scatter plots between measured and estimated biochemical contents from PROSPECT PDb (PROSPECT D considering the brown pigment content). The solid line corresponds to the 1:1 line. **a** Chlorophyll and carotenoid content (C_{abc}); **b** chlorophyll content (C_{ab}); **c** water content (C_w); **d** dry matter content (C_m). The dashed line is the best linear fit corrected from the offset. Green and red points correspond to measurements achieved at two nodes (April) and grain filling (June) stages respectively

Table 5 Comparison between destructive measurements of C_{abc} and C_w and PROSPECT or vegetation indices estimates

Variables	Metrics	PROSPECT				VIs			
		P3b	P4b	P5b	PDb	Dx4	CIre	SRw	NDw
C_{abc} (μg/cm²)	ρ	0.81	0.80	*0.82*	0.80	0.80	0.78	–	–
	r^2	*0.81*	0.79	0.80	0.80	0.80	0.77	–	–
	RMSE Corr	*6.54*	6.72	6.70	6.71	6.63	7.08	–	–
C_w (mg/cm²)	ρ	0.93	0.93	0.92	0.91	–	–	0.89	*0.94*
	r^2	0.87	0.85	0.86	0.85	–	–	0.80	*0.88*
	RMSE Corr	1.14	1.08	*1.05*	1.11	–	–	1.28	1.29

The estimation performances from the four PROSPECT versions (including brown pigments) and vegetation indices against destructive measurements: spearman correlation coefficient (ρ), squared Pearson correlation coefficient (r^2) and RMSE Corr as provided in Table 4. RMSE Corr for VIs was computed from the fitted empirical model between the biochemical contents and the VIs: linear functions for Dx4, CIre and SRw, a second order polynomial function for NDw. The numbers in italic indicate the best result for each biochemical content

measurements with overall lower values for all the PROSPECT versions (illustrated for PDb in Fig. 6a, b). Although PDb accounts for the anthocyanin pigments (C_{anth}), the corresponding estimates were very low with $C_{anth} < 0.5$ μg/cm² (Fig. 8) while larger values (0.5 μg/cm² $< C_{anth} <$ 5 μg/cm²) were observed for the senescent leaves when the carotenoid (and thus chlorophyll) content was very low. For senescent leaves, the estimated anthocyanin content appeared to be correlated with the estimated carotenoid (and chlorophyll) pigment content (Fig. 8) although such a correlation was not reported from measured contents in previous studies [65]. This

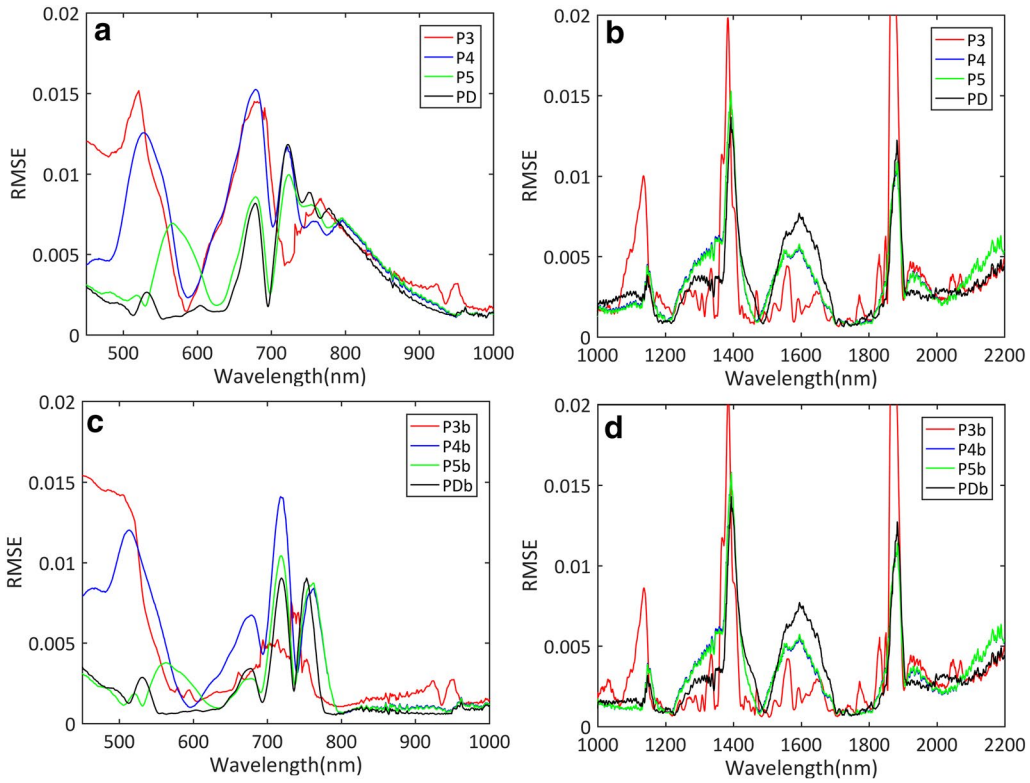

Fig. 7 Spectral variation of RMSE between measured and PROSPECT-simulated reflectance. **a** RMSE for the 400–1000 nm domain without brown pigments; **b** RMSE for the 1000–2200 nm domain without brown pigments; **c** RMSE for the 400–1000 nm domain with brown pigments; **d** RMSE for the 1000–2200 nm domain with brown pigments. Different versions of PROSPECT are presented

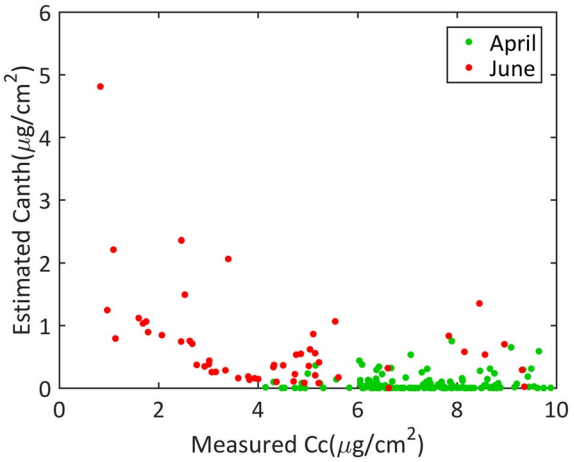

Fig. 8 Scatter plots between estimated anthocyanins and measured carotenoid from PROSPECT PDb (PROSPECT D considering the brown pigment content). Green and red points correspond to measurements achieved at two nodes (April) and grain filling (June) stages respectively

may be due to possible compensations between brown pigment, carotenoid and chlorophyll contents during the PROSPECT inversion process. In any case, results showed that accounting for the anthocyanin pigments for wheat leaves was not mandatory since these pigments were generally present only in very small quantities and anthocyanins present relatively weak absorption features. Thus, it appeared more efficient to estimate the content of pooled chlorophyllian pigments, C_{abc}, without considering the anthocyanin for wheat leaves. Furthermore, after bias correction all the PROSPECT versions performed similarly for C_{abc} estimation in wheat leaves (Tables 4, 5).

However, absolute estimates of C_{ab} and C_{abc} from the PROSPECT model were significantly biased when compared to destructive measurements. Indeed, the specific absorption coefficients of the PROSPECT models were calibrated over a large range of species, including dicotyledonous and monocotyledonous leaves. The structure of dicotyledonous leaves is characterized by a

well-developed spongy mesophyll that increases the average optical path while monocotyledonous leaves such as wheat have only a palisadic parenchyma where chloroplasts are concentrated [37]. Therefore, the values of the PROSPECT specific absorption coefficient calibrated over a large range of species might not represent accurately the actual individual values for each species. The distribution of the chlorophyllian pigments (e.g. pigment clumping) may also explain the different bias observed (Fig. 8) for yellow (June) and green leaves (April). For high values of chlorophyll content, e.g. green leaves, chlorophyll is concentrated within the chloroplasts and the chloroplasts themselves are organized in a clumped way in the cells. Conversely, the distribution of chlorophyllian pigments within yellow leaves is more uniform. As the specific absorption coefficients of PROSPECT were calibrated mostly over medium to high values of chlorophyll content, the estimated C_{abc} for yellow leaves led to overestimate the chlorophyll content due to the lower reflectance value expected for uniform pigment distribution as compared to a clumped situation.

All the PROSPECT versions provided very precise estimates of leaf water content (Tables 4, 5). This is mainly explained by the strong and specific absorption features of water. Conversely to what was observed for the chlorophyllian pigments, including the brown pigments did not improve the fitting process: actually, brown pigments are mainly absorbing in the visible domain where water shows only marginal absorption features. The bias observed between estimated and measured values of C_w, although significant, was much lower than that observed previously for C_{abc}. Some differences were noticed between PROSPECT versions, with P3 providing the lowest bias (Table 4). The smaller bias observed for C_w as compared to that of C_{abc} is mainly explained by the more even distribution of water within the leaf volume as compared to chlorophyll. Furthermore, the relative rRMSE (=6%) obtained after bias correction was much lower than the one observed for C_{abc} (rRMSE=20%). This may be explained by the errors associated to the destructive measurements. For water content, the measurements were relatively accurate and precise because only few simple steps are required: measurements of the area and the fresh and dry weights. Conversely, the accuracy and precision associated to pigment content were expected to be degraded because of the several additional steps needed (leaf storage in the cold, extraction in a solution, spectrophotometer calibration…). Nevertheless, errors were also associated to the reflectance measurements, including the stability of the light source and that of the spectrophotometer, the characterization of the white references and the spectrophotometer calibration. Additional investigation should thus be conducted to quantify the repeatability of the destructive measurements as compared to the proposed method based on reflectance measurements. Furthermore, the interest of using a white background should also be investigated.

Table 6 Minimum, maximum of observed dry matter content, corresponding RMSE and relative RMSE (rRMSE) values of estimates from PROSPECT model inversion as reported in previous studies

Data set	Reference	PROSPECT versions	Reflectance/transmittance	Species	Min (mg/cm^2)	Max (mg/cm^2)	RMSE (mg/cm^2)	rRMSE
Baret and Fourty (1997)	[26]	P3	Reflectance + transmittance	Temperate species and crops	2.2	8.3	1.4–1.6	0.23–0.26
Feret et al. (2008): LOPEX (Hosgood et al. 1994)	[46, 66]	P4, P5	Reflectance + transmittance	Temperate	1.7	15.2	3.5	0.26
				Temperate	1.7	33.1	2.6	0.08
ANGERS (Feret 2008)				Tropical	6.4	22.9	4.9	0.30
HAWAII (Feret 2008)								
Feret et al. (2011)	[27]	P5	Reflectance + (transmittance)**	Temperate and Tropical	0.8	33.1	3.1	0.09
Li and Wang (2011)	[67]	P4	Reflectance	Temperate species	2.6	11.9	2.7*	0.29
Ali et al. (2016)	[68]	P4	Reflectance + transmittance	Broadleaf	3.4	13.6	3.7*	0.36
				Conifer	1.1	29.1	8.6*	0.31
Present study		P3, P4, P5, PD	Reflectance	Wheat	4.0	6.0	2.5–3.1	1.25–1.55

* Indicates that better performances were obtained by modified PROSPECT model inversion methods

** Transmittance was not available for part of the data

All the PROSPECT versions showed no correlation between the estimated C_m and the corresponding destructive measurements with a systematic underestimation. However, the RMSE values were of the same order as those reported in previous studies generally conducted over larger range of C_m values based on a similar inversion process (Table 6). However, the relative RMSE (rRMSE) was larger than for the other studies [26, 27, 46, 66–68]. Those latter, conversely to the present study, consider a large range of species where broadleaf and coniferous trees were often mixed with herbaceous plants. Therefore, the poor correlation observed was mainly explained by the very small variability of C_m measured in this wheat experiment. Existing modified PROSPECT inversion methods that include the design of a specific merit function for C_m [67] or the use of prior information [55, 68] and provided improved results over mixed trees could also be tested for C_m estimation in wheat experiment in the future.

Comparison between VI and PROSPECT based methods for C_{abc} and C_w estimates

The ranking capacity between cultivars appeared to be very similar using either the VI or the PROSPECT based methods. It should be noticed that ranking did not require any calibration for VIs or bias correction for PROSPECT model inversion. However, in the context of phenotyping, the ranking between genotypes is not always sufficient. Estimates of the absolute values of the biochemical contents will allow using crop models to access functional traits. The results showed that biases were observed for estimates from PROSPECT inversion. This problem could be solved properly at least in two different ways: (1) by recalibrating the specific absorption coefficients for wheat leaves; (2) by changing the formalism of PROSPECT and including heterogeneous distribution of absorbers in the leaf. This will require a recalibration of the specific absorption coefficients over a large range of leaf types. Because of the limited amount of data available, as well as the fact that the only measured optical property was the reflectance over a white background, we did not perform a recalibration of the PROSPECT specific absorption coefficients. Therefore, a simple empirical recalibration of the raw estimates of PROSPECT using the destructive measurements was proposed. Results show that the performances of the vegetation indices were comparable to those of PROSPECT after this bias correction (Table 5). However, the PROSPECT model had the capacity to account for the effect of variation in the leaf surface and leaf mesophyll structure. Even though the relationship between C_m and the leaf mesophyll structure was reported in previous studies [41, 69] when considering mixed species including both monocotyledons and dicotyledons, this relationship might not be so strong for a single species like wheat. Therefore, this may be important in the context of phenotyping experiments where new genotypes with particular surface or mesophyll features may be encountered.

Conclusion

The ability of the PROSPECT model and vegetation indices to estimate wheat leaf biochemical content was evaluated. Reflectance measurements were collected over detached leaves using a spectrophotometer equipped with an integrating sphere. Leaves were put over a white Teflon background to enhance the absorption features and the PROSPECT model was adapted to account for this specific measurement configuration. Estimates from the inversion of several PROSPECT model versions were compared with destructive measurements. The considered versions differed by the explicit description of the absorption of some pigments (chlorophyll ab, carotenoid, anthocyanin, brown pigments) and the dataset used to calibrate the corresponding specific absorption coefficients and the refractive index. Results demonstrated that all the PROSPECT versions provided reasonable estimates of water and chlorophyll contents when the brown pigment content was used as an additional variable. This was particularly important when considering senescing leaves. Consideration of the anthocyanin did not offer major interest since wheat leaves did not show high values of anthocyanin content. The separation between chlorophyll and carotenoid contents did not bring significant improvement since they are strongly correlated. Consequently, the pooled chlorophyllian pigments (chlorophyll + carotenoids) should be used as a leaf trait. However, significant bias was observed for chlorophyllian pigments, probably due to the non-even distribution of chlorophyll in the leaf volume as well as some possible clumping of the chlorophyll pigments. Water content was estimated with a smaller bias, in relation to the more even distribution of the water in the leaf volume. In contrast with most of other studies involving the PROSPECT model applied to a large mix of species, this study concentrated on a single species. This highlights the limits of a generic formalism and calibration of the current PROSPECT models. Further investigations should therefore focus on a better description of the chlorophyll distribution in the leaf volume to account for differences between species. Furthermore, the bias and discrepancies observed in this study might be also partly explained by the measurement uncertainties associated to reflectance and biochemical contents.

PROSPECT estimates of chlorophyllian pigments and water contents were compared with empirical relationships based on vegetation indices. Results showed very

similar performances in terms of ranking as well as in terms of RMSE after bias correction for PROSPECT model estimates. Although VIs provided a very simple and straightforward method for biochemical content estimates, PROSPECT model inversion offered the advantage to explicitly account for genotypic differences in leaf surface features, R_{surf} and mesophyll structure (N). However, these two additional variables should be more deeply investigated to evaluate their interest as potential new traits. Indeed, R_{surf} could allow characterizing the glaucosity observed between genotypes and conditions through the differences in leaf 'color' due to leaf surface features.

Finally, this study indicates that non-destructive methods may provide similar or better precision of chlorophyllian pigments and water contents as compared to classical destructive measurements [29]. However, the repeatability of these traits should be more formally compared over a large phenotyping dataset. The currently limited throughput of the indirect methods based on leaf reflectance achieved in the lab may be replaced in the close future by the development of new imaging techniques achieved at the canopy level as suggested by [70].

Additional file

Additional file 1. Contains the experimental dataset used in this study e.g. the measured wheat leaf reflectance over the white background and the corresponding chlorophyll a and b, carotenoid, dry matter and water contents. The EXCEL file includes 4 sheets. The first sheet is the description of the dataset. The sheet 'reflectance_Chl' includes the leaf reflectance over the white background measured from 400 mm to 2200 mm for 186 wheat leaves and the corresponding chlorophyll a and b and carotenoid content measured destructively. The sheet 'reflectance_Cw_Cm' is the leaf reflectance over the white background measured from 350 mm to 2500 mm for 186 wheat leaves and the corresponding water and dry matter contents from destructive measurements. Sheet 'reflectance of white background' describes the reflectance of the white background.

Abbreviations

B_{max}: maximum bound; B_{min}: minimum bound; C_{ab}: chlorophyll a and b content (µg/cm^2); C_c: carotenoid content (µg/cm^2); C_{abc}: chlorophyll and carotenoid content (µg/cm^2). $C_{abc} = C_{ab} + C_c$; C_{Anth}: anthocyanin content (µg/cm^2); C_m: dry matter content (mg/cm^2); C_w: water content (mg/cm^2); C_{bp}: brown pigment content (no unit); N: mesophyll structure index (no unit); R_{surf}: reflectivity of the leaf surface (no unit); J: cost function (no unit); f_{wb}: fraction of background illuminated by the incident light in the integrating sphere (no unit); R_{leaf}: reflectance of the leaf (over black background) (no unit); T_{leaf}: transmittance of the leaf (no unit); R^{wb}_{leaf}: reflectance of the leaf over the white background (no unit); R^{wb}_{val}: reflectance of the leaf without the epidermis over the white background (no unit); R_{wb}: reflectance of the white background (no unit); M_{fresh}: leaf fresh weight (g); M_{fresh}: leaf dry weight (g); S: leaf area (cm^2); $DHRF$: directional hemispherical reflectance (no unit); n: refractive index (no unit); RMSE: root mean square error.

Author's contributions

AC and FB designed the experiment. AC, FB, PB and PB participated to the measurements. AC and JJ processed the data. JJ, AC, FB and MW wrote the manuscript that was reviewed by PB and PB. All authors read and approved the final manuscript.

Author details

[1] EMMAH UMR 1114, INRA, UAPV, 84914 Avignon, France. [2] HIPHEN, Avignon, France. [3] AGIR UMR 1248, INRA, Toulouse, France. [4] UMR ECOSYS, INRA, Grignon, France.

Acknowledgements

We would like to thank all the INRA technicians involved in the experiment. INRA experimental unit UE 802 took care of the trial. Anaïs Bioche Msc student within INRA UMR AGIR did most of the leaf measurements together with P. Burger.

Competing interests

The authors declare that they have no competing interests.

Availability of data and methods

The datasets supporting the conclusions of this article are included within the article and its additional files.

Consent for publication

All authors read and approved the final manuscript.

Ethics approval and consent to participate

Not applicable.

Funding

This study was part of the BELCAM project funded by BELSPO (Belgium) and the PHENOME project (ANR-11-INBS-012) funded by the "Programme d'investissement d'Avenir". The grant of the principal author was funded by the Chinese Scholarship Council. The work was mostly completed within the UMT-CAPTE funded by the French ministry of Agriculture.

Publisher's Note

Received: 20 September 2017 Accepted: 13 March 2018
Published online: 20 March 2018

References

1. Furbank RT, Tester M. Phenomics—technologies to relieve the phenotyping bottleneck. Trends Plant Sci. 2011;16(12):635–44.
2. Comar A, Burger P, De Solan B, Baret F, Daumard F, Hanocq J-F. A semi-automatic system for high throughput phenotyping wheat cultivars in-field conditions: description and first results. Funct Plant Biol. 2012;39(11):914–24.
3. Walter A, Studer B, Kölliker R. Advanced phenotyping offers opportunities for improved breeding of forage and turf species. Ann Bot. 2012;110(6):1271–9.
4. Blackmer TM, Schepers JS, Varvel GE, Meyer GE. Analysis of aerial photography for nitrogen stress within corn fields. Agron J. 1996;88(5):729–33.
5. Cartelat A, Cerovic Z, Goulas Y, Meyer S, Lelarge C, Prioul J-L, Barbottin A, Jeuffroy M-H, Gate P, Agati G. Optically assessed contents of leaf polyphenolics and chlorophyll as indicators of nitrogen deficiency in wheat (*Triticum aestivum* L.). Field Crops Res. 2005;91(1):35–49.
6. Debaeke P, Rouet P, Justes E. Relationship between the normalized SPAD index and the nitrogen nutrition index: application to durum wheat. J Plant Nutr. 2006;29(1):75–92.
7. Ercoli L, Mariotti M, Masoni A, Massantini F. Relationship between nitrogen and chlorophyll content and spectral properties in maize leaves. Eur J Agron. 1993;2(2):113–7.
8. Follett R, Follett R, Halvorson A. Use of a chlorophyll meter to evaluate the nitrogen status of dryland winter wheat. Commun Soil Sci Plant Anal. 1992;23(7–8):687–97.
9. Fox R, Piekielek W, Macneal K. Using a chlorophyll meter to predict nitrogen fertilizer needs of winter wheat. Commun Soil Sci Plant Anal. 1994;25(3–4):171–81.

10. Houles V, Guerif M, Mary B. Elaboration of a nitrogen nutrition indicator for winter wheat based on leaf area index and chlorophyll content for making nitrogen recommendations. Eur J Agron. 2007;27(1):1–11.
11. Seemann JR, Sharkey TD, Wang J, Osmond CB. Environmental effects on photosynthesis, nitrogen-use efficiency, and metabolite pools in leaves of sun and shade plants. Plant Physiol. 1987;84(3):796–802.
12. Evans J, Poorter H. Photosynthetic acclimation of plants to growth irradiance: the relative importance of specific leaf area and nitrogen partitioning in maximizing carbon gain. Plant Cell Environ. 2001;24(8):755–67.
13. Muñoz-Huerta RF, Guevara-Gonzalez RG, Contreras-Medina LM, Torres-Pacheco I, Prado-Olivarez J, Ocampo-Velazquez RV. A review of methods for sensing the nitrogen status in plants: advantages, disadvantages and recent advances. Sensors. 2013;13(8):10823–43.
14. Shadchina T, Dmitrieva V. Leaf chlorophyll content as a possible diagnostic mean for the evaluation of plant nitrogen uptake from the soil. J Plant Nutr. 1995;18(7):1427–37.
15. Penuelas J, Fillela I, Biel C, Serrano L, Savé R. The reflectance at the 950–970 nm region as an indicator of plant water status. Int J Remote Sens. 1993;14(10):1887–905.
16. Tahara M, Carver BF, Johnson RC, Smith EL. Relationship between relative water content during reproductive development and winter wheat grain yield. Euphytica. 1990;49(3):255–62.
17. Vile D, Garnier É, Shipley B, Laurent G, Navas M-L, Roumet C, Lavorel S, Díaz S, Hodgson JG, Lloret F, Midgley GF, Poorter H, Rutherford MC, Wilson PJ, Wright IJ. Specific leaf area and dry matter content estimate thickness in laminar leaves. Ann Bot. 2005;96(6):1129–36.
18. Teng S, Qian Q, Zeng D, Kunihiro Y, Fujimoto K, Huang D, Zhu L. QTL analysis of leaf photosynthetic rate and related physiological traits in rice (*Oryza sativa* L.). Euphytica. 2004;135(1):1–7.
19. Echarte L, Rothstein S, Tollenaar M. The response of leaf photosynthesis and dry matter accumulation to nitrogen supply in an older and a newer maize hybrid. Crop Sci. 2008;48(2):656–65.
20. Ntanos D, Koutroubas S. Dry matter and N accumulation and translocation for Indica and Japonica rice under Mediterranean conditions. Field Crops Res. 2002;74(1):93–101.
21. Ellsworth DS, Reich PB. Canopy structure and vertical patterns of photosynthesis and related leaf traits in a deciduous forest. Oecologia. 1993;96(2):169–78.
22. Neales TF, Incoll L. The control of leaf photosynthesis rate by the level of assimilate concentration in the leaf: a review of the hypothesis. Bot Rev. 1968;34(2):107–25.
23. Hoogenboom G, Jones J, Boote K. Modeling growth, development, and yield of grain legumes using SOYGRO, PNUTGRO, and BEANGRO: a review. Trans ASAE. 1992;35(6):2043–56.
24. Fourty T, Baret F, Jacquemoud S, Schmuck G, Verdebout J. Leaf optical properties with explicit description of its biochemical composition: direct and inverse problems. Remote Sens Environ. 1996;56:104–17.
25. Yoder BJ, Pettigrew-Crosby RE. Predicting nitrogen and chlorophyll content and concentration from reflectance spectra (400–2500 nm) at leaf and canopy scales. Remote Sens Environ. 1995;53:199–211.
26. Baret F, Fourty T. Estimation of leaf water content and specific leaf weight from reflectance and transmittance measurements. Agronomie. 1997;17(9–10):455–64.
27. Féret J-B, François C, Gitelson A, Asner GP, Barry KM, Panigada C, Richardson AD, Jacquemoud S. Optimizing spectral indices and chemometric analysis of leaf chemical properties using radiative transfer modeling. Remote Sens Environ. 2011;115(10):2742–50.
28. Gitelson AA, Gritz Y, Merzlyak MN. Relationships between leaf chlorophyll content and spectral reflectance and algorithms for non-destructive chlorophyll assessment in higher plant leaves. J Plant Physiol. 2003;160(3):271–82.
29. Cerovic ZG, Masdoumier G, Ghozlen NB, Latouche G. A new optical leaf-clip meter for simultaneous non-destructive assessment of leaf chlorophyll and epidermal flavonoids. Physiol Plant. 2012;146(3):251–60.
30. Hunt ER, Rock BN. Detection of changes in leaf water content using near and middle-infrared reflectances. Remote Sens Environ. 1989;30:43–54.
31. Seelig HD, Hoehn A, Stodieck LS, Klaus DM, Adams Iii WW, Emery WJ. Relations of remote sensing leaf water indices to leaf water thickness in cowpea, bean, and sugarbeet plants. Remote Sens Environ. 2008;112(2):445–55.
32. Danson F, Steven M, Malthus T, Clark J. High-spectral resolution data for determining leaf water content. Int J Remote Sens. 1992;13(3):461–70.
33. Ceccato P, Flasse S, Tarantola S, Jacquemoud S, Grégoire J-M. Detecting vegetation leaf water content using reflectance in the optical domain. Remote Sens Environ. 2001;77(1):22–33.
34. Ullah S, Skidmore AK, Groen TA, Schlerf M. Evaluation of three proposed indices for the retrieval of leaf water content from the mid-wave infrared (2–6 µm) spectra. Agric For Meteorol. 2013;171:65–71.
35. Lymburner L, Beggs PJ, Jacobson R. Estimation of canopy-average surface specific leaf area using Landsat TM data. Photogram Eng Remote Sens. 2000;66(2):183–91.
36. Wang L, Qu JJ, Hao X, Hunt ER. Estimating dry matter content from spectral reflectance for green leaves of different species. Int J Remote Sens. 2011;32(22):7097–109.
37. Jacquemoud S,Ustin SL. Modeling leaf optical properties. Photobiological Sciences Online 2008. http://photobiology.info/Jacq_Ustin.html.
38. Dawson TP, Curran PJ, Plummer SE. LIBERTY—modeling the effects of leaf biochemical concentration on reflectance spectra. Remote Sens Environ. 1998;65(1):50–60.
39. Fukshansky L, Fukshansky-Kazarinova N, Remisowsky AMV. Estimation of optical parameters in a living tissue by solving the inverse problem of the multiflux radiative transfer. Appl Opt. 1991;30(22):3145–53.
40. Ganapol BD, Johnson LF, Hammer PD, Hlavka CA, Peterson DL. LEAFMOD: a new within-leaf radiative transfer model. Remote Sens Environ. 1998;63(2):182–93.
41. Jacquemoud S, Baret F. PROSPECT: a model of leaf optical properties spectra. Remote Sens Environ. 1990;34:75–91.
42. Maier SW, Lüdeker W, Günther KP. SLOP: a revised version of the stochastic model for leaf optical properties. Remote Sens Environ. 1999;68(3):273–80.
43. Tucker CJ, Garratt MW. Leaf optical system modeled as a stochastic process. Appl Opt. 1977;16(3):635–42.
44. Baranoski GV,Rokne JG. An algorithmic reflectance and transmittance model for plant tissue. In: Conference of the European Association for Computer Graphics EUROGRAPHICS'97. 1997. Budapest.
45. Ustin SL, Jacquemoud S, Govaerts Y. Simulation of photon transport in a three-dimensional leaf: implications for photosynthesis. Plant Cell Environ. 2001;24(10):1095–103.
46. Feret J-B, François C, Asner GP, Gitelson AA, Martin RE, Bidel LPR, Ustin SL, le Maire G, Jacquemoud S. PROSPECT-4 and 5: advances in the leaf optical properties model separating photosynthetic pigments. Remote Sens Environ. 2008;112(6):3030–43.
47. Jacquemoud S, Verhoef W, Baret F, Bacour C, Zarco-Tejada PJ, Asner GP, François C, Ustin SL. PROSPECT + SAIL models: a review of use for vegetation characterization. Remote Sens Environ. 2009;113(Supplement 1):S56–66.
48. le Maire G, François C, Dufrêne E. Towards universal broad leaf chlorophyll indices using PROSPECT simulated database and hyperspectral reflectance measurements. Remote Sens Environ. 2004;89(1):1–28.
49. Stuckens J, Verstraeten WW, Delalieux S, Swennen R, Coppin P. A dorsiventral leaf radiative transfer model: development, validation and improved model inversion techniques. Remote Sens Environ. 2009;113(12):2560–73.
50. Lichtenthaler HK, Wellburn AR. Determinations of total carotenoids and chlorophylls a and b of leaf extracts in different solvents. Biochem Soc Trans. 1983;11(5):591–2.
51. Hatchell DC, ASD Technical guide. 1999, Analytical Spectral Devices Inc. p. 140.
52. Höpe A, Hauer K-O. Three-dimensional appearance characterization of diffuse standard reflection materials. Metrologia. 2010;47(3):295.
53. Gitelson AA, Vina A, Ciganda V, Rundquist DC, Arkebauer TJ. Remote estimation of canopy chlorophyll content in crops. Geophys Res Lett. 2005;32(8):1–4.
54. Gitelson AA, Zur Y, Chivkunova OB, Merzlyak MN. Assessing carotenoid content in plant leaves with reflectance spectroscopy. Photochem Photobiol. 2002;75(3):272–81.
55. Shiklomanov AN, Dietze MC, Viskari T, Townsend PA, Serbin SP. Quantifying the influences of spectral resolution on uncertainty in leaf trait estimates through a Bayesian approach to RTM inversion. Remote Sens Environ. 2016;183:226–38.

56. Le Maire G, François C, Soudani K, Berveiller D, Pontailler J-Y, Bréda N, Genet H, Davi H, Dufrêne E. Calibration and validation of hyperspectral indices for the estimation of broadleaved forest leaf chlorophyll content, leaf mass per area, leaf area index and leaf canopy biomass. Remote Sens Environ. 2008;112(10):3846–64.
57. Gitelson AA, Keydan GP, Merzlyak MN. Three-band model for noninvasive estimation of chlorophyll, carotenoids, and anthocyanin contents in higher plant leaves. Geophys Res Lett. 2006;33(11):1–5.
58. Allen WA, Gausman HW, Richardson AJ, Thomas JR. Interaction of isotropic light with a compact plant leaf. J Opt Soc Am. 1969;59(10):1376–9.
59. Stokes GG. On the intensity of the light reflected from or transmitted through a pile of plates. Proc R Soc Lond. 1862;11:545–56.
60. Féret J-B, Gitelson A, Noble S, Jacquemoud S. PROSPECT-D: towards modeling leaf optical properties through a complete lifecycle. Remote Sens Environ. 2017;193:204–15.
61. Comar A, Baret F, Viénot F, Yan L, De Solan B. Wheat leaf bidirectional reflectance measurements: description and quantification of the volume, specular and hot-spot scattering features. Remote Sens Environ. 2012;121:26–35.
62. Saunderson J. Calculation of the color of pigmented plastics. JOSA. 1942;32(12):727–36.
63. Byrd RH, Gilbert JC, Nocedal J. A trust region method based on interior point techniques for nonlinear programming. Math Program. 2000;89(1):149–85.
64. Comar A, Baret F, Obein G, Simonot L, Meneveaux D, Viénot F, De Solan B. ACT: a leaf BRDF model taking into account the azimuthal anisotropy of monocotyledonous leaf surface. Remote Sens Environ. 2014;143:112–21.
65. Asner GP, Martin RE, Ford AJ, Metcalfe DJ, Liddell MJ. Leaf chemical and spectral diversity in Australian tropical forests. Ecol Appl. 2009;19(1):236–53.
66. Hosgood B, Jacquemoud S, Andreoli G, Verdebout J, Pedrini A,Schmuck G. The JRC leaf optical properties experiment (LOPEX'93). Eur. Commiss., Directorate—General XIII, Telecommun, Inf, Market and Exploitation of Res., L-2920, Belgium, CL-NA-16095-EN-C. 1994.
67. Li P, Wang Q. Retrieval of leaf biochemical parameters using PROSPECT inversion: a new approach for alleviating ill-posed problems. IEEE Trans Geosci Remote Sens. 2011;49(7):2499–506.
68. Ali AM, Darvishzadeh R, Skidmore AK, van Duren I, Heiden U, Heurich M. Estimating leaf functional traits by inversion of PROSPECT: assessing leaf dry matter content and specific leaf area in mixed mountainous forest. Int J Appl Earth Obs Geoinf. 2016;45:66–76.
69. Dechant B, Cuntz M, Vohland M, Schulz E, Doktor D. Estimation of photosynthesis traits from leaf reflectance spectra: correlation to nitrogen content as the dominant mechanism. Remote Sens Environ. 2017;196:279–92.
70. Jay S, Gorretta N, Morel J, Maupas F, Bendoula R, Rabatel G, Dutartre D, Comar A, Baret F. Estimating leaf chlorophyll content in sugar beet canopies using millimeter-to centimeter-scale reflectance imagery. Remote Sens Environ. 2017;198:173–86.

2.2 Improving the PROSPECT model to retrieve leaf biochemical content

FASPECT: a model of leaf optical properties accounting for the differences between upper and lower faces

Jingyi Jiang, Alexis Comar, Marie Weiss, Samuel Buis & Frederic Baret

ABSTRACT:

A number of plant species have distinct optical properties between upper and lower leaf faces, which are a fact that has been neglected in most leaf and canopy radiative transfer models. It is assumed that differences between faces are attributed to a non-homogeneous distribution of absorbing and scattering materials within the leaf as well as particular surface features of both epidermises. In this paper, the FASPECT model which is based on a leaf four-layer system was proposed. The upper and lower epidermis layers are characterized by distinct wavelength-independent reflectivity. Leaf mesophyll is assumed to be made of a palisade and a spongy parenchyma layers with two proportional parameters to describe the distribution of pigments and leaf structure. Six additional parameters are required to describe the differences in leaf optical properties between upper and lower faces as compared to the PROSPECT model which describes the homogeneous case. Because of the concentrated chlorophyll in palisade mesophyll, the SACs of chlorophyll and carotenoids are recalibrated. Validation was done with eight datasets. Results show that reflectance and transmittance from one face is enough for biochemical content estimation. Even though marginal improvements are achieved for estimation of pigments and water content, significant improvements are observed for estimation of dry matter content. For spectrum estimation, the FASPECT model simulates accurately the reflectance and transmittance of the two faces and overperforms PROSPECT models for single face measurements. Therefore, the FASPECT model would be efficient to simulate leaf optical properties with two faces and can be applied with 3D canopy radiative transfer model to simulate canopy reflectance precisely.

KEY WORDS: leaf radiative transfer model, reflectance, transmittance, chlorophyll, dry matter content,

1 Introduction

The monitoring of vegetation by remote sensing techniques at different scales has been applied to agriculture, ecology and climate change (Wang et al. 2010; Atzberger 2013). Vegetation radiative transfer models are very useful for exploiting remote sensing observations and transform the signal collected onboard a satellite into structural or biochemical vegetation characteristics. Modeling the radiative transfer at the canopy level requires a description of leaf optical properties (Croft and Chen 2017). Leaves are often represented as lambertian surfaces with the same reflectance and transmittance properties for both faces. However, a number of species show differences in scattering properties between the two faces as reported by (Grant et al., 1987; Woolley, 1971)(Baldini et al. 1997; Stuckens et al. 2009b). As a matter of facts, leaves ensure a number of functions under a wide range of environmental conditions and have therefore developed adaptations leading to differentiations between faces. (Stuckens et al. 2009a) demonstrated that bifacial or dorsiventral leaves with contrasted optical properties between both faces induce significant effect on the canopy reflectance.

Leaf optical properties models simulate leaf reflectance and transmittance from a limited set of state variables describing the content of absorbing materials such as chlorophyll, water or dry matter, and the scattering occurring at the interfaces between materials with different refraction index values. Several modeling approaches have been proposed (Jacquemoud and Ustin 2001) including ray-tracing models, stochastic models, N-flux models and plate models. A very detailed description of leaf features could be implemented using ray-tracing models (Ustin et al. 2001; Baranoski 2006). However, these models are difficult to use because of the complexity of the description of the leaf structure and content, as well as because of the computation time required for the simulations (Dorigo et al. 2007). The SLOP (Stochastic model for Leaf Optical Properties) model (Maier et al. 1999) described the radiative transfer process as a stochastic process with Markov chain. Although it offers potentials to account for the differences between both sides of the leaf, its current implementation with simple assumptions on leaf internal structure and the lack of proper epidermis layer prevent from simulating differences of reflectance or transmittance between both faces. N-flux models (Allen and Richardson 1968) allows considering several layers within the leaf. (Yamada and Fujimura 1991) developed a leaf radiative transfer model based on the Kubelka-Munk theory {Kubelka, 1931 #1354}. This approach is computationally efficient and allows to potentially simulate differences between both lea faces. However, most efforts have been dedicated to the plate model approach. Plate models treat the leaf as one or several absorbing plates with rough surfaces giving rise to isotropic diffusion (Allen et al. 1969). The PROPSECT model (Jacquemoud and Baret 1990) is one of the most widely used plate model that has been successfully applied to retrieve leaf biochemical composition from leaf reflectance and transmittance (Le Maire et al. 2004; Zarco-Tejada et al. 2004; Jacquemoud et al. 2009) (Stuckens et al. 2009b) {Jiang, 2018 #6469}. A series of improved versions were proposed. PROSPECT-4 and 5 (Feret et al. 2008) separated carotenoids from chlorophyllian pigments and recalibrated the specific absorption coefficients describing the spectral features of the main light absorbers in the leaf. More recently, PROSPECT-D (Féret et al. 2017) added anthocyanins and showed better performances in both reflectance and transmittance simulations and pigment content estimation. However, no emphasis was put on the differences between leaf faces before (Stuckens et al. 2009b) who developed the DLM (Dorsiventral Leaf Model). DLM is based on the plate model approach with possible non uniform distribution of the absorbing materials and reflectivity of the epidermis that may differ between the two faces.

This study aims at documenting and modeling the possible differences between the optical properties both leaf faces. Reflectance and transmittance measurements were performed over a few leaf samples to quantify the possible differences between faces. FASPECT, an evolution of the PROSPECT model is proposed to explicitly account for the inhomogeneity in the leaf structure and simulate the corresponding differences in leaf optical properties between faces. The specific absorption coefficients of chlorophyll and carotenoids were then recalibrated. Finally, the performance of FASPECT model was evaluated over several independent datasets. Both the accuracy of pigment estimation and differences between simulated and measured optical properties were compared with PROSPECT-5 and PROSPECT-D.

2 Measurements

2.1 Available datasets

Eight datasets available from several researchers were used as the calibration and validation dataset (Table 2). For LOPEX and ANGER, different plant species are included with leaf reflectance and transmittance for one face ranging from 400 nm to 2500 nm. As it was reported by (Feret et al. 2008) that there is a question about the accuracy of the pigment content in LOPEX, the accuracy of the estimated chlorophyll and carotenoid contents should be considered. For VIRGINIA, MAPLE, HAZEL, DOGWOOD1 and DOGWOOD2, each dataset has single specie with measured pigment contents. Except DOGWOOD2 which only has reflectance for one face, VIRGINIA, MAPLE, HAZEL and DOGWOOD1 contain both reflectance and transmittance measurements for one face in visible bands. Details of experiment protocol of optical properties measurements and determination of pigment contents can be found in (Hosgood et al. 1994; Gitelson et al. 2006; Feret et al. 2008; Merzlyak et al. 2008; Gitelson et al. 2009). To apply those datasets which have optical properties for one face to FASPECT model, the reflectance and transmittance were assumed to be measured from the upper face considering the usual observation habit. For Avignon, the reflectance and transmittance for both faces were measured with 10 species according to methods described in Section2.

Table 2. Description of available datasets.

		LOPEX*,[1]	ANGER*,[2]	VIRGINIA[3,4]	MAPLE[3,4]	HAZEL[3,4]	DOG-WOOD1[3,4]	DOG-WOOD2[5]	Avignon
Number of species		50	2003	1	1	1	1	1	10
Number of samples		64	308	81	48	13	20	51	50
Spectral range (nm)		400-2450	400-2450	400-800	400-780	400-800	440-796	400-1000	400-2200
Optical properties		R&T for one face	R&T for one face	R&T for one face	R&T for one face	R&T for one face	R&T for one face	R for one face	R&T for two faces
C_{ab} (µg/cm-2)	Min	1.36	0.78	0.09	0.14	22.69	0.07	1.53	-
	Max	98.80	106.70	53.76	32.98	34.62	15.03	39.81	-
	Mean	47.28	34.41	11.05	7.43	26.37	4.53	23.77	-
C_c (µg/cm-2)	Min	3.45	0.00	0.15	1.82	-	0.42	1.73	-
	Max	28.35	25.28	12.27	10.4	-	5.71	10.76	-
	Mean	10.31	8.84	2.98	5.25	-	2.96	5.39	-
C_{ant} (µg/cm-2)	Min	-	-	0.00	1.12	0.25	0.40	1.07	-
	Max	-	-	37.50	21.66	13.61	15.49	30.23	-
	Mean	-	-	8.63	8.75	7.13	6.88	12.71	-
C_w (g/cm-2)	Min	0.0046	0.0044	-	-	-	-	-	-
	Max	0.0450	0.0340	-	-	-	-	-	-
	Mean	0.0114	0.0116	-	-	-	-	-	-
C_m (g/cm-2)	Min	0.0019	0.0017	-	-	-	-	-	-
	Max	0.0137	0.0331	-	-	-	-	-	-
	Mean	0.0054	0.0052	-	-	-	-	-	-

*LOPEX and ANGERS datasets are downloaded from http://opticleaf.ipgp.fr/index.php?page=database.

[1](Hosgood et al. 1994); [2](Feret et al. 2008); [3](Merzlyak et al. 2008); [4](Gitelson et al. 2009); [5](Gitelson et al. 2006)

2.2 Additional measurements of reflectance and transmittance of both faces

Measurements were made over ten species of plants to represent different optical properties of leaves between upper and lower faces: Fig tree (Ficus Carica), Laurel tree (Laurus Nobilis), Olive tree (Olea Europaea), Lime tree (Tilia Europea), Lemon tree (Citrus Limon), Persimmon tree (Diospyros Kaki), Giant Cane (Arundo Donax), White poplar tree (Populus Alba), Common grape vine (Vitis Vinifera) and Apple tree (Malus Domestica). For each species, five leaves were selected with similar visual aspects. Reflectance and transmittance were measured at three distinct locations over each leaf, avoiding the larger veins. The ASD Fieldspec spectroradiometer was used with a Li-Cor 1800-12 integrating sphere to obtain directional-hemispherical reflectance and transmittance values. The spectroradiometer sampled the 400 to 2200 nm spectral domains with 1-nm steps and a spectral resolution around 10 nm. The original Li-Cor lamp system of the integrating sphere was replaced by a lamp powered with a large battery ensuring steady electric power input. The infrared filter placed in front of the original light source was removed as well. The incoming light was almost normal to the leaf sample both for reflectance and transmittance measurements, while the bare fiber of the ASD spectroradiometer (25° field of view) viewed the integrating sphere wall and was perpendicularly to the sample. To reduce possible stray-light, the experiment was conducted in a darkroom. Lab calibrated Teflon reference surface was used to get absolute directional hemispherical reflectance values of the sample from the absolute reflectance and transmittance of the Teflon (R_{ref} and T_{ref}). To avoid possible changing of the signal over time, the signal values of reflectance and transmittance of the references were acquired before (SR_{ref_bef} and ST_{ref_bef}) and after (SR_{ref_aft} and ST_{ref_aft}) measurements of each leaf. Therefore, the reflectance R_i and transmittance T_i of the leaf sample *i* were calculated as:

$$R_i(\lambda) = R_{ref}(\lambda)\frac{2*SR_i(\lambda)}{SR_{ref\_bef}(\lambda)+SR_{ref\_bef}(\lambda)} \text{ and } T_i(\lambda) = T_{ref}(\lambda)\frac{2*ST_i(\lambda)}{ST_{ref\_aft}(\lambda)+ST_{ref\_aft}(\lambda)} \quad (1)$$

where SR_i and ST_i are the averaged signal values of reflectance and transmittance for each leaf *i*. Uncertainties were characterized by the averaged RMSE values for each leaf. For the whole wavelength, the uncertainties of reflectance (RMSE≈0.01) are comparatively smaller than that of the transmittance (RMSE≈0.02), which mainly came from different measurement locations (Figure 5).

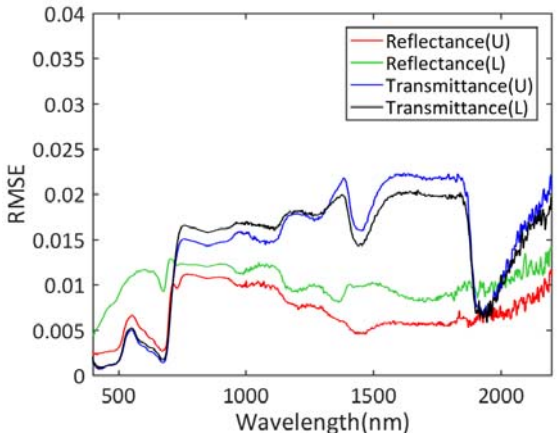

Figure 5. Uncertainties of measured reflectance and transmittance for both faces (U: upper face; L: lower face).

Differences between upper and lower faces show regularities across the ten species (Figure 6). In the visible domain (400 - 750 nm), pigments including chlorophyll, carotenoids and anthocyanins are main absorbing materials. For most species, reflectance from the upper face is smaller than that from the lower face, while transmittance is almost the same from both faces. Therefore, more light

is absorbed when it incomes from the upper face. Conversely, in near infrared (NIR; 750 - 1400 nm), reflectance from the upper faces is larger and transmittance is smaller than those from the lower face. For the whole bands (400 - 2200 nm), light incidents from the upper face always result in larger absorptance compared with that from the lower face. This might represent a double advantage for plants: when photosynthesis is limited by the amount of incoming light, the upper side facing the sun will better trap light. Conversely, in case of excess radiation such as under water stress, plants may reorient their leaves with the lower side facing the sun to reduce the amount radiation (Pastenes et al. 2004; Liu et al. 2007).

However, the discrepancies among species exist, especially for differences in reflectance. Figure 6A shows that relatively large differences of reflectance between faces (0.2 – 0.4 in visible and short-wave infrared (SWIR; 1400 – 2200 nm)) are observed in Lime Tree (covered with fine hairs), White poplar tree and Olive tree (whitish on the lower face), while for the rest seven species, smaller differences (< 0.1) are exhibited.

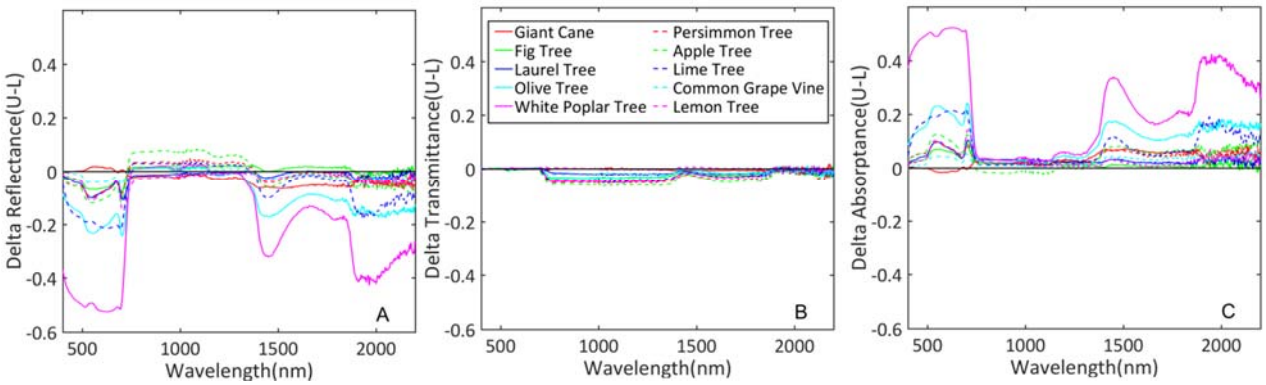

Figure 6. Differences between the upper and lower faces of in (A) reflectance, (B) transmittance and (C) absorptance of 10 species (U: upper face; L: lower face).

3 Modeling

3.1 Leaf described as a four-layer system

A typical dicot leaf is made up of the palisade and spongy mesophyll tissue layers, bounded by two epidermis layers (Figure 7). The epidermis is a single layer of colorless cells with few chloroplasts. Palisade mesophyll is elongated perpendicular to the leaf surface and is arranged into one or a few densely packed layers which contain most of chloroplasts(Govaerts et al. 1996). The spongy mesophyll is made up of irregularly shaped cells and large intercellular air spaces, which facilitate gases circulation inside the leaf. Because of the small amount of absorbing material and much air space in the spongy mesophyll, a large proportion of light coming from the palisade mesophyll is scattered back and is absorbed by chloroplasts within the palisade mesophyll (Raven et al. 2005). This is consistence with measurement results (Figure 6) that absorptance from the upper face is larger than that from the lower face.

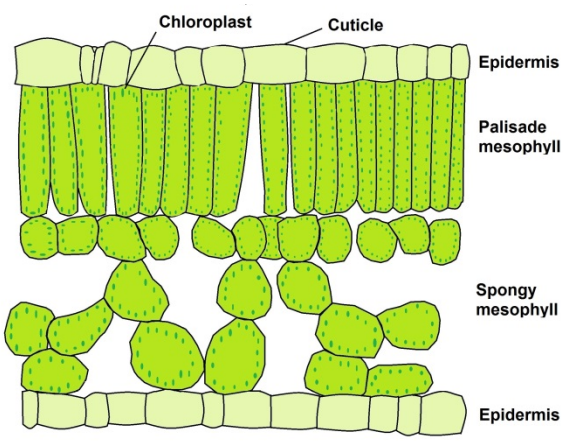

Figure 7. Schematic Structure of a typical dicotyledon leaf.

According to Figure 7, the radiate transfer scheme in the four-layer system of a typical leaf is abstracted (Figure 8): the upper layer is made of the upper epidermis (Layer 1) and the palisade mesophyll (Layer 2) and the lower layer is made of the spongy mesophyll (Layer 3) and the lower epidermis (Layer 4). Subscripts ($_1$, $_2$, $_3$ and $_4$) are layer numbers. The arrows ($^{\uparrow}$ and $^{\downarrow}$) indicate the directions of the incident flux. Small letters (r and t) correspond to reflectance and transmittance of each layer, while capital letters are for fluxes created by the multiple layers. Specifically, $R_{12}^{\downarrow}$, $R_{12}^{\uparrow}$, $T_{12}^{\downarrow}$and $T_{12}^{\uparrow}$ are noted as the reflectance and transmittance for the combination of Layer 1 and Layer 1. $R_{34}^{\downarrow}$, $R_{34}^{\uparrow}$, $T_{34}^{\downarrow}$and $T_{34}^{\uparrow}$ represent fluxes from combination of Layer 3 and Layer 4. R and T are the total fluxes of the leaf.

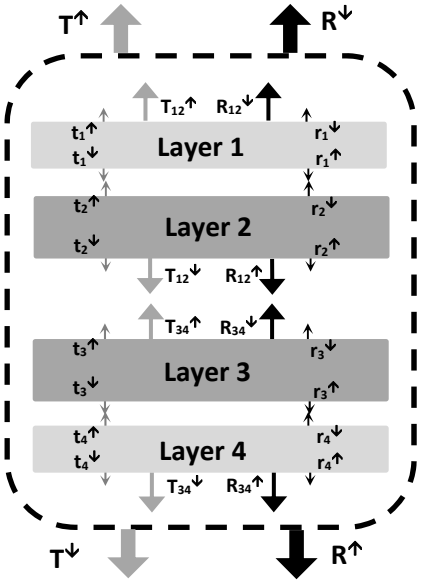

Figure 8. The scheme used to describe the fluxes in a four-layer system.

Reflectance of the upper layer ($R_{12}^{\downarrow}$ and $R_{12}^{\uparrow}$) and lower layer ($R_{34}^{\downarrow}$ and $R_{34}^{\uparrow}$) with two directions of incident fluxes can be written as:

$$R_{12}^{\downarrow} = r_1^{\downarrow} + \frac{r_2^{\downarrow} t_1^{\downarrow} t_1^{\uparrow}}{1 - r_2^{\downarrow} r_1^{\uparrow}} \text{ and } R_{12}^{\uparrow} = r_2^{\uparrow} + \frac{r_1^{\uparrow} t_2^{\downarrow} t_2^{\uparrow}}{1 - r_2^{\downarrow} r_1^{\uparrow}} \quad (1)$$

$$R_{34}^{\downarrow} = r_3^{\downarrow} + \frac{r_4^{\downarrow} t_3^{\downarrow} t_3^{\uparrow}}{1 - r_4^{\downarrow} r_3^{\uparrow}} \text{ and } R_{34}^{\uparrow} = r_4^{\uparrow} + \frac{r_3^{\uparrow} t_4^{\downarrow} t_4^{\uparrow}}{1 - r_4^{\downarrow} r_3^{\uparrow}}$$

(2)

Similarly, transmittance of the upper layer ($T_{12}^{\downarrow}$ and $T_{12}^{\uparrow}$) and lower layer ($T_{34}^{\downarrow}$ and $T_{34}^{\uparrow}$) from two directions become:

$$T_{12}^{\downarrow} = \frac{t_1^{\downarrow} t_2^{\downarrow}}{1 - r_2^{\downarrow} r_1^{\uparrow}} \text{ and } T_{12}^{\uparrow} = \frac{t_1^{\uparrow} t_2^{\uparrow}}{1 - r_2^{\downarrow} r_1^{\uparrow}}$$

(3)

$$T_{34}^{\downarrow} = \frac{t_3^{\downarrow} t_4^{\downarrow}}{1 - r_4^{\downarrow} r_3^{\uparrow}} \text{ and } T_{34}^{\uparrow} = \frac{t_3^{\uparrow} t_4^{\uparrow}}{1 - r_4^{\downarrow} r_3^{\uparrow}}$$

(4)

Finally, the total reflectance and transmittance for the four layer system noted $R^{\downarrow}$, $T^{\downarrow}$ for upper face and $R^{\uparrow}$, $T^{\uparrow}$ for lower face are given by:

$$R^{\downarrow} = R_{12}^{\downarrow} + \frac{R_{34}^{\downarrow} T_{12}^{\downarrow} T_{12}^{\uparrow}}{1 - R_{34}^{\downarrow} R_{12}^{\uparrow}} \text{ and } R^{\uparrow} = R_{34}^{\uparrow} + \frac{R_{12}^{\uparrow} T_{34}^{\downarrow} T_{34}^{\uparrow}}{1 - R_{34}^{\downarrow} R_{12}^{\uparrow}}$$

(5)

$$T^{\downarrow} = \frac{T_{12}^{\downarrow} T_{34}^{\downarrow}}{1 - R_{34}^{\downarrow} R_{12}^{\uparrow}} \text{ and } T^{\uparrow} = \frac{T_{12}^{\uparrow} T_{34}^{\uparrow}}{1 - R_{34}^{\downarrow} R_{12}^{\uparrow}}$$

(6)

In the visible domain, the absorption of radiation is very strong because the first layer contains most of the chlorophyll. Since the transmittance is comparatively small and similar for both faces (Figure 6B), the reflectance of two faces can be approximated as the reflectance of the upper layer ($R^{\downarrow} \approx R_{12}^{\downarrow}$) and the reflectance of the lower layer ($R^{\uparrow} \approx R_{34}^{\uparrow}$). Because of the higher chlorophyll content of the upper layer, its reflectance is smaller than that of the lower layer ($R_{12}^{\downarrow} < R_{34}^{\uparrow}$). So the reflectance of the upper face is expected to be smaller than that of the lower face ($R^{\downarrow} < R^{\uparrow}$).

In NIR, the differences between transmittance of two faces become more obvious. As a matter of fact, in our experiment, the incident radiation is collimated along the leaf normal while the directionality of leaf reflectance is mainly composed with a specular and a lambertian scattering components (Bousquet et al. 2005). More specifically, the transmittance of the first layer with incident flux from up to down, $T_{12}^{\downarrow}$, is mostly affected by the incoming collimated light source. Conversely, the transmittance in the opposite direction, $T_{12}^{\uparrow}$, is mainly subjected to a diffuse incoming flux generated by multiple scattering occurring within the leaf volume. Because of the reduced specular contribution and longer path length compared with the collimated incoming light, $T_{12}^{\uparrow}$ is smaller than $T_{12}^{\downarrow}$.Therefore, the ratio between these two transmittances would be greater than 1 ($\gamma_{12} = T_{12}^{\downarrow} / T_{12}^{\uparrow} > 1$) and the same applies to the lower layer ($\gamma_{34} = T_{34}^{\uparrow} / T_{34}^{\downarrow} > 1$). The difference between the transmittance of two faces (Δ_T) can be written as (from equation 4):

$$\Delta T = T^{\downarrow} - T^{\uparrow} = \frac{T_{12}^{\downarrow} T_{34}^{\downarrow}}{1 - R_{34}^{\downarrow} R_{12}^{\uparrow}} \left(1 - \frac{\gamma_{12}}{\gamma_{34}}\right)$$

(7)

According to the measurements, transmittance of the upper face is larger than that of the lower face ($\Delta_T < 0$, $\boldsymbol{\gamma_{34} < \gamma_{12}}$). So the difference between transmittance for different incoming fluxes (the normal collimated and diffuse) of the upper layer ($\boldsymbol{T_{12}^{\downarrow}}$ and $\boldsymbol{T_{12}^{\uparrow}}$), is larger than that of the lower layer ($\boldsymbol{T_{34}^{\uparrow}}$ and $\boldsymbol{T_{34}^{\downarrow}}$). This is probably because the structure of palisade parenchyma keeps the incoming collimated light normal to the leaf surface, while the spongy parenchyma would enhance light scattering for both collimated and diffuse lights.

3.2 Development of the FASPECT model

In original PROSPECT model, only one layer of the leaf was considered and the radiative transfer process within the leaf was ignored. This allowed little flexibility to describe particular surface features and would result in some bias for the simulation of leaf optical properties. Based on the

built system of leaf (Figure 8), the FASPECT model is proposed to consider the leaf as four layers. Radiative transfer terms of each layer are showed in Table 3.

In FASPECT, epidermis layers are assumed to be very thin with negligible absorption, so transmittance of epidermis can be described by 1 minus the corresponded reflectance. As it was explained in Section 3.1, $t_1^{\downarrow}$ from the incoming collimated light is larger than $t_1^{\uparrow}$ from the multiple scattered lights within the leaf, so $r_1^{\downarrow}$ is smaller than $r_1^{\uparrow}$ and the ratio between two reflectance of upper epidermis would be smaller than 1 ($\alpha_1 = r_1^{\downarrow} / r_1^{\uparrow} < 1$). Similarly, $r_4^{\uparrow}$ is smaller than $r_4^{\downarrow}$, so $\alpha_2 = r_4^{\uparrow} / r_4^{\downarrow} < 1$. According to several converging observations(Jacquemoud and Baret 1990; Bousquet et al. 2005), the wavelength dependency of the refraction index was assumed negligible in the 400-2500 nm spectral domain. Therefore, epidermis reflectivity was considered independent on wavelength.

The leaf structure parameter (N) is sum of the structure parameter of palisade mesophyll (N_2) and spongy mesophyll (N_3). The parameter $p = N_2 / N$ is used to characterize the gradient between two mesophyll layers. In original PROSPECT model, p was set to be 0.5 for all kinds of leaves. Even though the proportion of palisade and spongy parenchyma is comparatively average, p should be slightly smaller than 0.5 for leaves with well-developed spongy mesophyll or around 0.5 for monocotyledonous leaves.

The total absorption coefficient (K) is the sum of the pigment contents multiply by the corresponding SACs. For chlorophyll and carotenoids, they are manly existed in palisade mesophyll and spongy mesophyll. The distribution of them is computed using parameter d, which represents the ratio between chlorophyll or carotenoids content in palisade mesophyll (C_{ab2} or C_{c2}) and the total chlorophyll content (C_{ab} or C_c). So the chlorophyll or carotenoids content in spongy mesophyll (C_{ab3} or C_{c3}) can be computed as $C_{ab} \cdot (1-d)$ or $C_c \cdot (1-d)$. In previous versions, chlorophyll was assumed to be uniform distributed within the leaf ($d = 0.5$). However, since palisade mesophyll contains most of chloroplasts, d should ranges from 0.5 to 1. For water and dry matter contents, they are assumed to be distributed proportionally as the distribution of N in mesophyll layers. So water or dry matter content in palisade mesophyll (C_{w2} or C_{m2}) are computed as $p \cdot C_w$ or $p \cdot C_m$ and those in spongy mesophyll (C_{w3} or C_{m3}) are computed as $(1-p) \cdot C_w$ or $(1-p) \cdot C_m$.

As compared to previous versions of PROSPECT model, the description of differences between faces is achieved at the expense of 6 additional parameters that do not vary with wavelength: d, p, r_1, α_1, r_4 and α_4.

Table 3. Radiative transfer terms of four layers in the FASPECT model.

Layer	Name	Contents of absorbing materials				Leaf structure parameter	[Reflectance, Transmittance]
		Chlorophyll	Carotenoids	Water	Dry matter		
1	Upper epidermis	0	0	0	0	-	$[r_1^{\downarrow}, t_1^{\downarrow}]=[r_1^{\downarrow}, 1\text{-}r_1^{\downarrow}]$ $[r_1^{\uparrow}, t_1^{\uparrow}]=[r_1^{\uparrow}, 1\text{-}r_1^{\uparrow}]$ $\alpha_1 = r_1^{\downarrow}/\, r_1^{\uparrow}$
2	Palisade mesophyll	$C_{ab}\cdot d$	$C_c\cdot d$	$C_w\cdot p$	$C_m\cdot p$	$N_2=N\cdot$p	$[r_2^{\downarrow}, t_2^{\downarrow}, r_2^{\uparrow}, t_2^{\uparrow}]$ = PROSPECT (n, N_2, K_2)
3	Spongy mesophyll	$C_{ab}\cdot(1\text{-}d)$	$C_c\cdot(1\text{-}d)$	$C_w\cdot(1\text{-}p)$	$C_m\cdot(1\text{-}p)$	$N_3=N\cdot(1\text{-}p)$	$[r_3^{\downarrow}, t_3^{\downarrow}, r_3^{\uparrow}, t_3^{\uparrow}]$ = PROSPECT (n, N_3, K_3)
4	Lower epidermis	0	0	0	0	-	$[r_4^{\downarrow}, t_4^{\downarrow}]=[r_4^{\downarrow}, 1\text{-}r_4^{\downarrow}]$ $[r_4^{\uparrow}, t_4^{\uparrow}]=[r_4^{\uparrow}, 1\text{-}r_4^{\uparrow}]$ $\alpha_4 = r_4^{\downarrow}/\, r_4^{\uparrow}$

C_{ab}, C_c, C_w and C_m are contents of chlorophyll, carotenoids, water and dry matter. N is the leaf structure parameter. d is the ratio between C_{ab} (C_c) in palisade mesophyll and total C_{ab} (C_c). p is the ratio between N (C_w / C_m) of the palisade mesophyll and the total N (C_w / C_m). n is the refractive index. K is the total absorption coefficient. r and t are reflectance and transmittance of each layer. Subscripts ($_1$, $_2$, $_3$ and $_4$) represent layer numbers. The arrows ($^{\uparrow}$ and $^{\downarrow}$) are the directions of the incident flux.

3.3 Model calibration

3.3.1 Selection of calibration dataset

Different from PROSPECT model which assumes biochemical contents are homogenous distributed within the leaf, the FASPECT model treats each variable proportionally distributed in different layer. So it is necessary to recalibrate the SACs of biochemical variables. As explained in Section 3.2, the distribution of chlorophyll and carotenoids are more centered in palisade mesophyll while the distribution of water and dry matter content within leaf is comparatively homogenous. Therefore, the SACs of chlorophyll and carotenoids should be recalibrated and the SACs of water and dry matter content are kept the same as PROPSECT-5. For anthocyanin, since it is distributed in different leaf cell layers for different species, phylogeny and environmental conditions (Lee 2002), it is difficult to determine its distribution with one or two parameters. As simplification, anthocyanin is assumed to be evenly distributed and the SAC was from PROSPECT-D. According to the comparison from (Féret et al. 2017), the refractive index from PROSPECT-3 which was computed from an albino maize leaf provided the best performance, while the refractive index from PROSPECT-5 would induce artifices in leaf optical properties because of the strong spectral variation. So the refractive index from PROSPECT-3 is applied to FASPECT model.

Therefore, the calibration dataset should include both the measured reflectance and transmittance ranging from 400 nm to 2400 nm and the measured biochemical variables including pigment contents (chlorophyll, carotenoid and anthocyanin), water and dry matter contents. Considering the accuracy problem from LOPEX (Feret et al. 2008), the ANGER dataset which meets those criterions is chosen as the calibration dataset. ANGER was also used to calibrate PROSPECT-4, PROSPECT -5 and PROSPECT –D. It includes leaves with different states like albino or etiolated leaves which play a vital role to eliminate the strong correlation between chlorophyll and carotenoid in mature leaves (Feret et al. 2008). From (Féret et al. 2017), the anthocyanin contents (C_{ant}) of each sample from ANGER were estimated using spectral index with good accuracy when C_{ant} < 11 µg/cm^{-2}, so the estimated C_{ant} was also included and samples with low C_{ant} (< 5 µg/cm^{-2}) were kept to reduce the influence from estimated anthocyanin. To eliminate redundancy of calibration dataset, samples with little impact on calibrated SACs of chlorophyll and carotenoids were removed. Finally, totally 120 samples from ANGER were selected as the calibration dataset and the remaining (188 samples) were used as the validation dataset. It is notice that only optical properties from one face were available in ANGER, so all reflectance and transmittance used to adjust SACs in the next section were considered as optical properties from upper face.

3.3.2 Adjustment of specific absorption coefficients

As calibration algorithm proposed in (Feret et al. 2008), the calibration of SACs was conducted using iteration optimization methods with two-steps. Firstly, the structure parameter *N* was determined with three selected bands in NIR where absorption was smaller. Then, each SAC was calibrated wavelength by wavelength with the whole calibration dataset. However, in FASPECT model, six additional parameters which are independent with wavelength are added. So, more bands covering the whole wavelength are needed to define wavelength invariant parameters.

For the first step, different combinations of bands were traversed to fit the spectral curve using smoothing spline function from Matlab2016. The sum of the root-mean-square error (RMSE) between measured and simulated spectrum from calibration dataset were used to evaluate the fitting results. In this way, 30 most representative bands were selected from 400 nm to 2450 nm with the curve fitting methods (Figure 9).

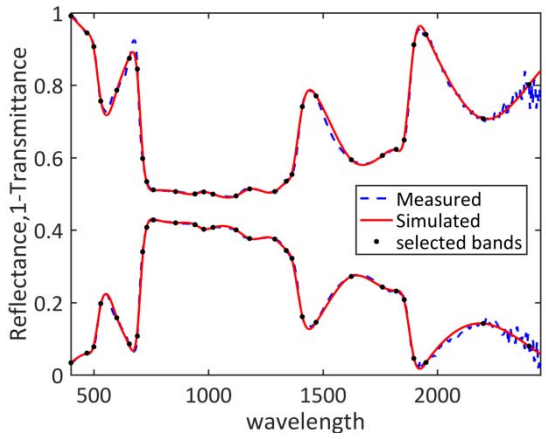

Figure 9. 30 representative bands from 400 nm to 2450 nm. The blue dotted lines are measured reflectance and transmittance of one leaf from ANGER. The black dots are 30 selected bands. The red solid lines are simulated reflectance and transmittance with selected bands using smoothing spline method.

Then parameters P_j={N_j, d_j, p_j, r_{1j}, α_{1j}, r_{4j} , α_{4j} } of the leaf j which are invariant with wavelength and SACs of chlorophyll ($K_{ab}(\lambda)$) and carotenoid ($K_c(\lambda)$) of 30 selected bands were estimated on the basis of the iterative optimization:

$$J\left(K_i(\lambda_n), P_j\right) = \sum_{n=1}^{30} \sum_{j=1}^{num=120} (R_{mes,j}(\lambda_n) - R_{mod,j}(k(\lambda_n), P_j))^2 + (T_{mes,j}(\lambda_n) - T_{mod,j}(k(\lambda_n), P_j))^2 \quad (9)$$

where

$$k(\lambda_n) = (\sum_i K_i(\lambda_n) * C_{i,j})/N_j \quad (10)$$

$R_{mes,j}(\lambda_n)$ and $T_{mes,j}(\lambda_n)$ are measured reflectance and transmittance at wavelength λ_n of leaf j. $R_{mod,j}(\lambda_n)$ and $T_{mod,j}(\lambda_n)$ are simulated reflectance and transmittance of upper face from FASPECT model. *num* is the number of samples from calibration dataset. $k(\lambda_n)$ is the total absorption coefficient at wavelength λ_n. K_i is the SAC of constituent i. $C_{i,j}$ is the concentration of constituent i of leaf j. N_j is the corresponding leaf structure parameter

Secondly, with the calculated P_j of each leaf, $K_{ab}(\lambda)$ and $K_c(\lambda)$ were calibrated with the inversion of FAPSECT model using all the samples from calibration dataset at each wavelength. The cost function J was minimized:

$$J(K_i(\lambda)) = \sum_{j=1}^{num=120} (R_{mes,j}(\lambda) - R_{mod,j}(k(\lambda), P_j))^2 + (T_{mes,j}(\lambda) - T_{mod,j}(k(\lambda), P_j))^2 \quad (11)$$

3.4 Model validation

The model inversion was performed through adjusting input variables P= {N, d, p, r_1, α_1, r_4, α_4} and the concentration of each constituent C_i so that simulations matched observations by minimizing the following cost function:

$$J(P, C_i) = \sum_{face} \sum_{\lambda_{min}}^{\lambda_{max}} (R_{mes,face}(\lambda) - R_{mod,face}(P, C_i)^2 + (T_{mes,face}(\lambda) - T_{mod,face}(P, C_i))^2 \quad (12)$$

where *face* represent upper and lower faces. C_i corresponds to C_{ab}, C_c, C_{ant}, C_w and C_m. The inversions utilized the fmincon function from Matlab2016.

To test whether FASPECT model could generate accurate estimation of biochemical composition when only reflectance and transmittance from one face is available, 100 simulated cases with different combinations of biochemical contents and corresponding reflectance and transmittances from two faces were generated from FASPECT model. To make the simulations more realistic, 2% uncertainties were added to simulated optical properties as errors from measurements. As comparison, both optical properties from two faces and optical properties from single face were applied for model inversion to estimate biochemical contents. Then, the FASPECT model was evaluated over all available datasets except samples used for calibration. The procedure was repeated with PROPSPECT-5 and PROSPECT-D using the same cost function (Equation (12)) as comparison. The estimates were validated from both spectrum simulation and biochemical content estimation. RMSE was used to compute the differences between measured and estimated biochemical contents or difference between measured and estimated spectrum at each wavelength.

4 Results and discussion

4.1 Adjusted specific absorption coefficients

The adjusted SACs of chlorophylls and carotenoids were showed in Figure 10. As comparison, results from PROSPECT-5 and PROSPECT-D were also demonstrated. Compared with PROSPECT-5, the tendency of SACs from FASPECT are more close to that from PROSPECT-D. For wavelength from 400 nm to 500 nm, the SACs of chlorophylls and carotenoids from FASPECT are slightly higher than PROSPCT-D and the SAC of chlorophylls is a bit lower than that from PROSPCT-D at wavelength around 680 nm. This difference is possibly introduced by the adding parameters *d* and *p* which describe the different distribution of pigments and structure variation.

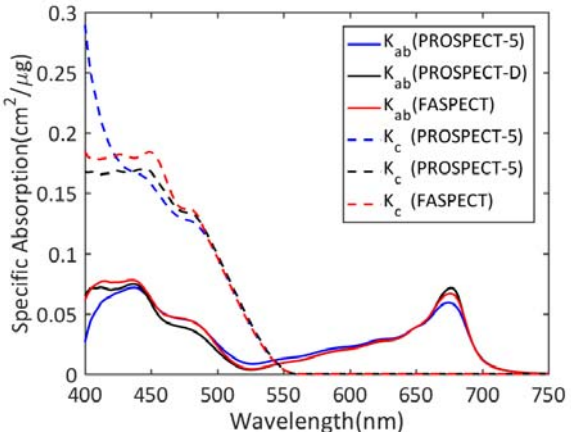

Figure 10. Specific absorption coefficients of chlorophylls (solid line) and carotenoids (dashed line) from PROSPECT-5 (blue), PROSPECT-D (black) and FASPECT (red).

4.2 Validation of model performance

4.2.1 Estimation of leaf pigments

Results to validate the ability of model inversion with two faces or single face are compared in Table 4.When reflectance and transmittance from upper or lower face are used, similar RMSE are observed compared with results estimated from reflectance and transmittance with two faces. Therefore, optical properties from single face are enough for biochemical content estimation. When only reflectance or transmittance from upper face is available, results estimated from transmittance performs much better than that from reflectance. This is might because the transmittance contains more information with light goes through the leaf interior, while the reflectance from one side is not sufficient to get accurate estimation for model inversion.

Table 4. RMSE of estimation of pigments, water and dry matter content using optical properties from two faces or single face with simulated dataset.

	R+T (UP+DOWN)	R+T(UP)	R+T(DOWN)	R(UP)	T(UP)
C_{ab} (µg/cm-2)	0.29	0.24	0.35	3.77	0.55
C_c (µg/cm-2)	0.51	0.46	0.24	3.84	0.20
C_{ant} (µg/cm-2)	0.11	0.13	0.17	2.60	0.11
C_w (g/cm-2)	0.0001	0.0001	0.0001	0.0002	0.0001
C_m (g/cm-2)	0.0003	0.0003	0.0003	0.0003	0.0003

R and T correspond to the reflectance and transmittance of the leaf. UP and DOWN indicate the reflectance or transmittance is coming from the upper and lower faces of the leaf.

Inversions from PROSPECT-5, PROSPECT-D and FASPECT are compared using RMSE between measured and estimated pigments, water and dry matter content (Table 5). For C_{ab} and C_c, similar results from PROSPECT-D and FASPECT are showed in RMSE and scatter plots between measured and estimate results (Figure 11 A and B)), while bias from PROSPECT-5 are comparatively larger. For ANGER and VIRGINIA, parts of the validation data were used as calibration datasets for PROPSECT-D. For C_{ant}, slight reduce of RMSE is got especially for DOGWOOD-2 when only reflectance is available (Figure 11C). The estimation of water content is always accurate from PROPSECT-5, PROSPECT-D and FASPRCT models. For C_m, significant improvement is achieved where estimates are more centred around 1:1 line (Figure 11E). This is possibly because of the adding of p which could better describe the distribution of leaf structure and the adding of parameters describing epidermis optical properties (r_1, α_1, r_4, and α_4) to improve the spectrum simulation in SWIR.

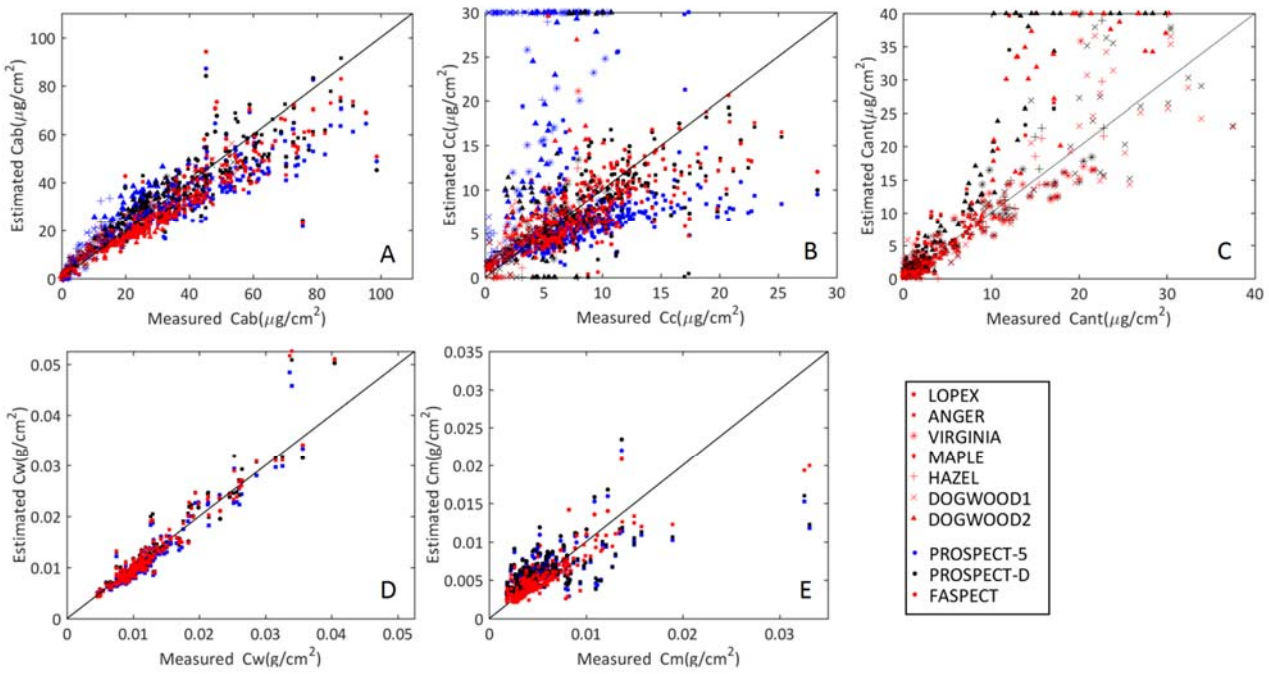

Figure 11 Comparison between measured and estimated (A) chlorophyll (B) carotenoids (C) anthocyanins (D) water content and (E) dry matter estimated from PROSPECT-5 (blue), PROSPECT-D (black) and FASPECT (red) on seven validate datasets.

Table 5. RMSE of estimation of pigments, water and dry matter content using PROSPECT-5, PROSPECT-D and FASPECT inversion with validation datasets. The bold font is the lowest values.

		LOPEX	ANGER	VIRGINIA	MAPLE	HAZEL	DOGWOOD1	DOGWOOD2
C_{ab} (µg/cm-2)	PROSPECT-5	14.17	11.29	3.63	3.99	5.89	7.12	8.52
	PROSPECT-D	**13.93**	**7.94**	**2.58**	3.19	**2.28**	4.06	6.31
	FASPECT	14.82	8.93	2.71	**3.07**	2.89	**3.48**	**5.01**
C_c (µg/cm-2)	PROSPECT-5	4.54	6.6	15.82	14.06	-	17.65	16.59
	PROSPECT-D	3.97	3.83	**1.21**	**2.26**	-	2.11	10.87
	FASPECT	**3.91**	**3.60**	1.68	2.76	-	**1.89**	**5.53**
C_{ant} (µg/cm-2)	PROSPECT-5	-	-	-	-	-	-	-
	PROSPECT-D	-	3.22	4.61	3.68	2.87	4.17	14.49
	FASPECT	-	**3.17**	**4.09**	**3.40**	**1.94**	**2.51**	**10.71**
C_w (g/cm-2)	PROSPECT-5	0.0055	**0.0021**	-	-	-	-	-
	PROSPECT-D	**0.0017**	0.0025	-	-	-	-	-
	FASPECT	**0.0017**	0.0024	-	-	-	-	-
C_m (g/cm-2)	PROSPECT-5	0.0025	0.0030	-	-	-	-	-
	PROSPECT-D	0.0028	0.0029	-	-	-	-	-
	FASPECT	**0.0018**	**0.0020**	-	-	-	-	-

4.2.2 Spectrum reconstruction

To compare the accuracy of reconstructed spectrum from PROSPECT-5, PROSPECT-D and FASPECT, spectral RMSE between measured and estimated results from validation datasets were computed for the whole wavelength (Figure 12). In visible domain, PROSPECT-5 provides the highest RMSE in both reflectance and transmittance, while FASPECT is slightly lower than PROSPECT-D with RMSE ranging from 0.005 to 0.015. In NIR, spectral RMSE from FASPECT shows the lowest value for most bands from 800 nm to 1400 nm. For wavelength from 1400 nm to 2000 nm, RMSE from PROSPECT-5 is lower than the other two versions in transmittance. This is possibly due to the refractive index used in PROSPECT-5 which was calibrated with ANGER dataset. When it is applied with the same dataset, lower spectral RMSE would be got with strong spectral variations. For Avignon dataset, optical properties from both sides were estimated at the same time with FASPECT model (

Figure 13). The spectral RMSE is around 0.02 except the reflectance from lower face. When three species, White poplar tree, Olive tree and Lime Tree, which have larger differences between faces are excluded, the spectral RMSE of the reflectance from lower face reduced especially from 400 to 500 nm (green dotted line in

Figure 13). To validate if errors were introduced from the FASPECT model, reflectance and transmittance from the lower face of White poplar tree were also simulated with PROSPECT-D

(Figure 14). But larger differences are demonstrated in simulated results compared with those from FASPECT. Therefore, errors might come from the description of lower epidermis which are whitish or hairy and have a certain thickness with some absorptance. In general, FASPECT model can simulate the reflectance and transmittance of the two faces accurately and shows better performance compared with other models for single face measurements.

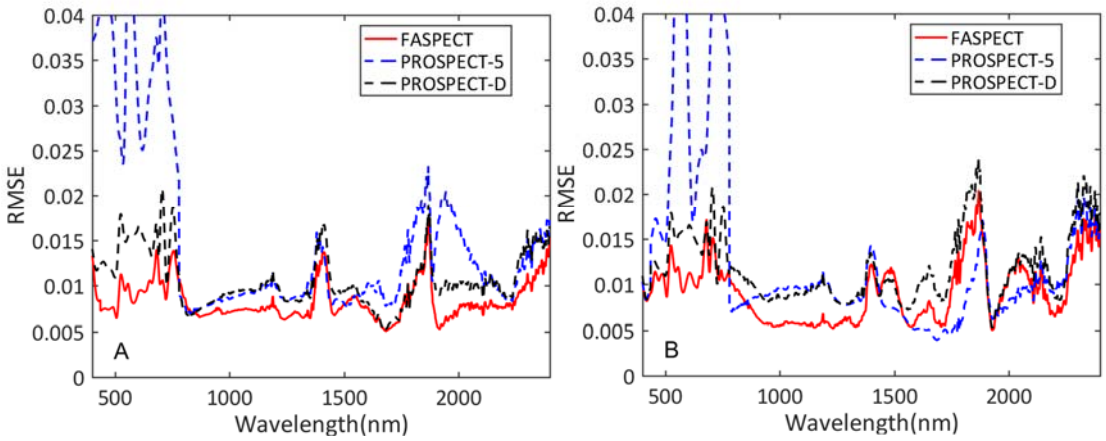

Figure 12 Spectral RMSE between measured and estimated (A) reflectance and (B) transmittance inverted from PROSPECT-5, PROSPECT-D and FASPECT for the validation dataset.

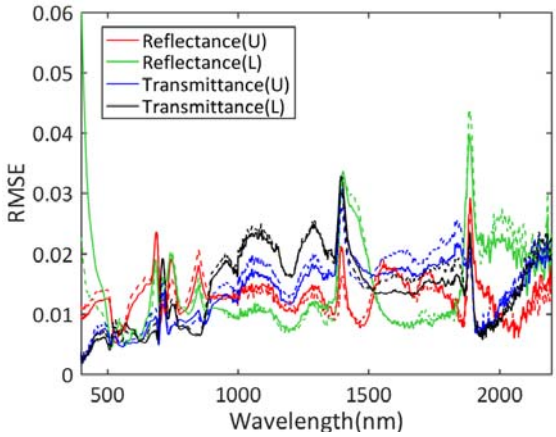

Figure 13 Spectral RMSE between measured and estimated reflectance and transmittance with two faces (U: upper face, L: lower face) inverted from FASPECT for Avignon dataset. Solid lines are spectral RMSE from 10 species. Dashed lines represent spectral RMSE from 7 species (White poplar tree, Olive tree and Lime Tree are excluded).

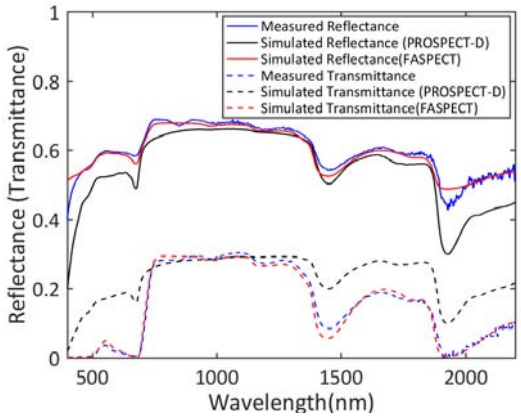

Figure 14 Measured and simulated reflectance and transmittance from the lower face of White poplar tree using PROSPECT-D and FASPECT.

4.3 Sensitivity analysis

A global sensitivity analysis was conducted to better understand the role of each input variable of FASPECT on leaf reflectance and transmittance of both faces. The global sensitivity analysis can quantify the importance of inputs through allowing all inputs to concurrently sample their range of variation (Saltelli et al. 2000) and has been proved to be efficient and robust when applied on vegetation radiative transfer models (Gu et al. 2016; Zhou et al. 2018). Here, the Extended Fourier Amplitude Sensitivity Test (EFAST) method (Saltelli et al. 1999) was used to compute the total sensitivity index which describes the impact of each variable and the interactions between input variables on model output. 12 input variables (C_{ab}, C_c, C_{ant}, C_w, C_m, N, d, p, r_1, α_1, r_4, and α_4) with independent uniform distribution laws over the widest possible range of values (Table 6) were included in the analysis. Consider the computational efficiency and the robustness of the method, 12000 samples were selected to generate the model output and the total sensitivity index of each variable was computed wavelength by wavelength.

Table 6. Ranges of input variables for the sensitivity analysis.

Input	C_{ab}	C_c	C_{ant}	C_w	C_m	N	d	p	r_1	α_1	r_4	α_4
Units	µg/cm2	µg/cm2	µg/cm2	g/cm2	g/cm2	-	-	-	-	-	-	-
Min	0	0	0	0	0.001	1	0	0.5	0.001	0.001	0.001	0.001
Max	140	50	50	0.06	0.05	3.5	0.5	1	0.1	1	0.1	1

To show the sensitivity more clearly, results are normalized to 0-1 through divided by the sum of sensitivity from all parameters at each wavelength. The sensitivity of each parameter for differences between upper and lower faces is investigated in Figure 15. Results show that parameters describing epidermis optical properties (r_1, α_1, r_4, and α_4) play an important role for reflectance and transmittance anisotropy in whole bands. More sensitivity is observed from lower epidermis compared with that from upper side. Even though r_1, α_1, r_4, and α_4 are the only four variables

inducing differences in optical properties between faces based on the assumptions embedded in FASPECT, structure parameters and the amount of absorbing materials would also have significant effects for differences between the two faces. For structure parameter (*N*), sensitivity exists in all the wavelengths. But for parameters describing chlorophyll distribution (*d*) and structure variation (*p*), obviously sensitivity is observed in the visible domain where chlorophyll inhomogeneity is expressed. Chlorophyllian pigments present larger effects in visible bands, while water and dry matter express significant influence in NIR and SWIR.

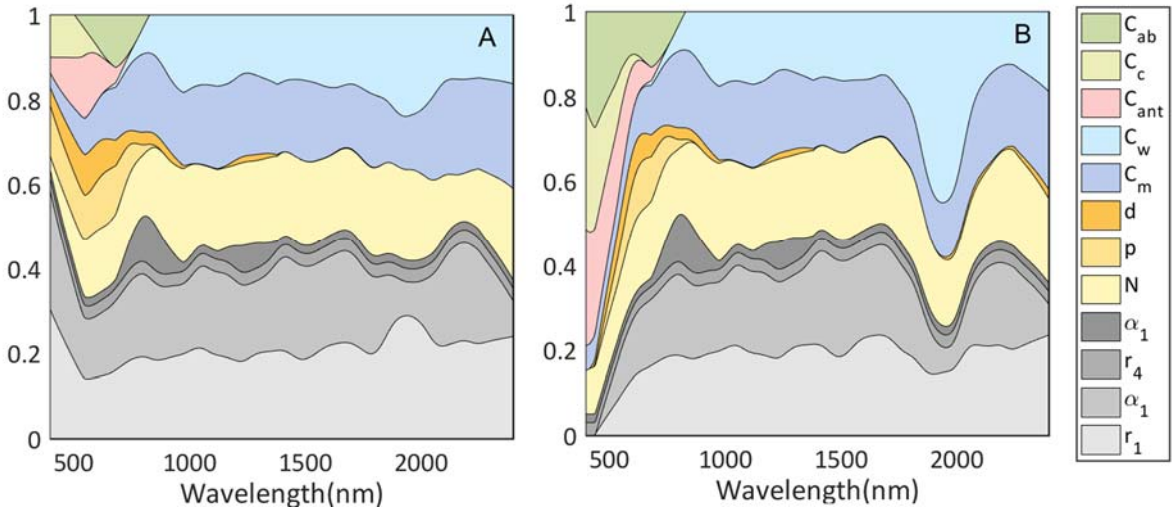

Figure 15 Normalized total sensitivity indices for differences in (A) reflectance and (B) transmittance between two faces of leaf as simulated by the FASPECT model. The area with different colors represents the normalized total sensitivity index of each input variable.

5 Conclusion

In this study, a model named FASPECT which is based on a four-layer system of leaf was proposed to describe the differences in leaf optical properties between upper and lower faces. Two epidermis layers are simulated with reflectance and transmittance which are assumed to be constant with wavelength. The palisade and spongy parenchyma are characterized by two proportional parameters to describe the distribution of structure parameter, water, dry matter and chlorophyllian contents within the two internal layers. The radiative transfer process in two parenchyma layers is simulated with PROSPECT model. Because of the concentrated chlorophyll in palisade mesophyll, the SACs of chlorophyll and carotenoids are recalibrated. The new model was validated with a series of database. For pigment estimation, it provides similar performance as compared with PROSPECT-D. For dry matter content, the estimation from FASPECT model is more accurate than previous versions of PROSPECT model. At the same time, FASPECT model can provide comparatively accurate simulation of reflectance and transmittance from two faces. And more precise simulation of reflectance and transmittance from one face is also got with lower RMSE compared with PROSPECT-5 and PROSPECT-D for most bands. The validation results shows that the new model provide a more accurate way to simulate leaf optical properties from two faces. The improvements of dry matter estimation can be applied in fields like the estimation of biomass or conservation of nutrients of leaves. A global sensitivity analysis of the FASPECT model demonstrates the role of biochemical contents, structure parameters and optical properties of epidermis on differences of reflectance and transmittance between faces. Among the six additional parameters used in FASPECT, parameters which characterize pigments and structure distributions within the leaf show more importance in

the visible domain, while epidermis reflectivity affects the whole spectral domain. For further application, the FASPECT model can be applied with 3D canopy radiative transfer model to better simulate the reflectance of canopy when add the contribution of the lower side of leaves. Then, it can be applied with satellite images with high resolution or proxy remote sensing images to estimate leaf and canopy state variables more precisely.

References

Allen, W.A., & Richardson, A.J. (1968). Interaction of light with a plant canopy. *JOSA, 58*, 1023-1028

Allen, W.A., Gausman, H.W., Richardson, A.J., & Thomas, J.R. (1969). Interaction of isotropic light with a compact plant leaf. *JOSA, 59*, 1376-1379

Jacquemoud, S., & Baret, F. (1990). PROSPECT : A model of leaf optical properties spectra. *Remote Sensing of Environment, 34*, 75-91

Yamada, N., & Fujimura, S. (1991). Nondestructive measurement of chlorophyll pigment content in plant leaves from three-color reflectance and transmittance. *Applied Optics, 30*, 3964-3973

Hosgood, B., Jacquemoud, S., Andreoli, G., Verdebout, J., Pedrini, A., & Schmuck, G. (1994). The JRC leaf optical properties experiment (LOPEX'93). *Eur. Commiss., Directorate—General XIII, Telecommun, Inf, Market and Exploitation of Res., L-2920, Belgium, CL-NA-16095-EN-C*

Govaerts, Y.M., Jacquemoud, S., Verstraete, M.M., & Ustin, S.L. (1996). Three-dimensional radiation transfer modeling in a dicotyledon leaf. *Applied Optics, 35*, 6585-6598

Baldini, E., Facini, O., Nerozzi, F., Rossi, F., & Rotondi, A. (1997). Leaf characteristics and optical properties of different woody species. *Trees, 12*, 73-81

Maier, S., Lüdeker, W., & Günther, K. (1999). SLOP: A revised version of the stochastic model for leaf optical properties. *Remote Sensing of Environment, 68*, 273-280

Saltelli, A., Tarantola, S., & Chan, K.-S. (1999). A quantitative model-independent method for global sensitivity analysis of model output. *Technometrics, 41*, 39-56

Saltelli, A., Chan, K., & Scott, E.M. (2000). *Sensitivity analysis*. Wiley New York

Jacquemoud, S., & Ustin, S.L. (2001). Leaf optical properties: A state of the art. In, *8th International Symposium of Physical Measurements & Signatures in Remote Sensing* (pp. 223-332): CNES, Aussois France

Ustin, S., Jacquemoud, S., & Govaerts, Y. (2001). Simulation of photon transport in a three‐dimensional leaf: implications for photosynthesis. *Plant, Cell & Environment, 24*, 1095-1103

Lee, D.W. (2002). Anthocyanins in leaves: distribution, phylogeny and development

Le Maire, G., Francois, C., & Dufrene, E. (2004). Towards universal broad leaf chlorophyll indices using PROSPECT simulated database and hyperspectral reflectance measurements. *Remote Sensing of Environment, 89*, 1-28

Pastenes, C., Pimentel, P., & Lillo, J. (2004). Leaf movements and photoinhibition in relation to water stress in field-grown beans. *Journal of Experimental Botany, 56*, 425-433

Zarco-Tejada, P.J., Miller, J.R., Harron, J., Hu, B., Noland, T.L., Goel, N., Mohammed, G.H., & Sampson, P. (2004). Needle chlorophyll content estimation through model inversion using hyperspectral data from boreal conifer forest canopies. *Remote Sensing of Environment, 89*, 189-199

Bousquet, L., Lachérade, S., Jacquemoud, S., & Moya, I. (2005). Leaf BRDF measurements and model for specular and diffuse components differentiation. *Remote Sensing of Environment, 98*, 201-211

Raven, P.H., Evert, R.F., & Eichhorn, S.E. (2005). *Biology of plants*. Macmillan

Baranoski, G.V. (2006). Modeling the interaction of infrared radiation (750 to 2500 nm) with bifacial and unifacial plant leaves. *Remote Sensing of Environment, 100*, 335-347

Gitelson, A.A., Keydan, G.P., & Merzlyak, M.N. (2006). Three-band model for noninvasive estimation of chlorophyll, carotenoids, and anthocyanin contents in higher plant leaves. *Geophysical Research Letters, 33*, 1-5

Dorigo, W.A., Zurita-Milla, R., de Wit, A.J., Brazile, J., Singh, R., & Schaepman, M.E. (2007). A review on reflective remote sensing and data assimilation techniques for enhanced agroecosystem modeling. *International Journal of Applied Earth Observation and Geoinformation, 9*, 165-193

Liu, C.C., Welham, C.V., Zhang, X.Q., & Wang, R.Q. (2007). Leaflet movement of Robinia pseudoacacia in response to a changing light environment. *Journal of Integrative Plant Biology, 49*, 419-424

Ratto, M., Young, P.C., Romanowicz, R., Pappenberger, F., Saltelli, A., & Pagano, A. (2007). Uncertainty, sensitivity analysis and the role of data based mechanistic modeling in hydrology. *Hydrology and Earth System Sciences, 11*, 1249-1266

Feret, J.-B., François, C., Asner, G.P., Gitelson, A.A., Martin, R.E., Bidel, L.P.R., Ustin, S.L., le Maire, G., & Jacquemoud, S. (2008). PROSPECT-4 and 5: Advances in the leaf optical properties model separating photosynthetic pigments. *Remote Sensing of Environment, 112*, 3030-3043

Merzlyak, M.N., Chivkunova, O.B., Solovchenko, A.E., & Naqvi, K.R. (2008). Light absorption by anthocyanins in juvenile, stressed, and senescing leaves. *Journal of Experimental Botany, 59*, 3903-3911

Gitelson, A.A., Chivkunova, O.B., & Merzlyak, M.N. (2009). Nondestructive estimation of anthocyanins and chlorophylls in anthocyanic leaves. *American Journal of Botany, 96*, 1861-1868

Jacquemoud, S., Verhoef, W., Baret, F., Bacour, C., Zarco-Tejada, P.J., Asner, G.P., François, C., & Ustin, S.L. (2009). PROSPECT + SAIL models: A review of use for vegetation characterization. *Remote Sensing of Environment, 113*, S56-S66

Stuckens, J., Somers, B., Delalieux, S., Verstraeten, W., & Coppin, P. (2009a). The impact of common assumptions on canopy radiative transfer simulations: A case study in Citrus orchards. *Journal of Quantitative Spectroscopy and Radiative Transfer, 110*, 1-21

Stuckens, J., Verstraeten, W.W., Delalieux, S., Swennen, R., & Coppin, P. (2009b). A dorsiventral leaf radiative transfer model: Development, validation and improved model inversion techniques. *Remote Sensing of Environment, 113*, 2560-2573

Wang, K., Franklin, S.E., Guo, X., & Cattet, M. (2010). Remote sensing of ecology, biodiversity and conservation: a review from the perspective of remote sensing specialists. *Sensors, 10*, 9647-9667

Atzberger, C. (2013). Advances in remote sensing of agriculture: Context description, existing operational monitoring systems and major information needs. *Remote Sensing, 5*, 949-981

Gu, C., Du, H., Mao, F., Han, N., Zhou, G., Xu, X., Sun, S., & Gao, G. (2016). Global sensitivity analysis of PROSAIL model parameters when simulating Moso bamboo forest canopy reflectance. *International Journal of Remote Sensing, 37*, 5270-5286

Croft, H., & Chen, J. (2017). Leaf Pigment Content. In

Féret, J.-B., Gitelson, A., Noble, S., & Jacquemoud, S. (2017). PROSPECT-D: Towards modeling leaf optical properties through a complete lifecycle. *Remote Sensing of Environment, 193*, 204-215

Zhou, G., Ma, Z., Sathyendranath, S., Platt, T., Jiang, C., & Sun, K. (2018). Canopy Reflectance Modeling of Aquatic Vegetation for Algorithm Development: Global Sensitivity Analysis. *Remote Sensing, 10*, 837

2.3 Conclusion of the chapter

In this chapter, we compared the ability of both empirically and physically based methods to estimate leaf traits from laboratory spectral measurements. Then, we proposed a new optical properties model, named FASPECT, which takes into account some differences between the leaf upper and lower faces.

We first evaluated the ability of the main PROSPECT model versions and vegetation indices to estimate wheat leaf biochemical content. Results demonstrate that all the PROSPECT versions provide reasonable estimates of water and chlorophyll contents, especially when the brown pigment content is taken into account. However, significant bias is observed for chlorophyllian pigments, probably due to the non-even distribution of chlorophyll in the leaf volume as well as some possible clumping of the chlorophyll pigments. In contrast with most of other studies involving the PROSPECT model applied to a large mix of species, this study concentrates only on different wheat cultivars. This highlights the limits of a generic formalism and calibration of the current PROSPECT models. Further investigations should therefore focus on a better description of the chlorophyll distribution in the leaf volume to account for differences between species. Compared with empirical relationships based on vegetation indices, very similar performances in terms of ranking as well as in terms of RMSE after bias correction for PROSPECT model estimates are observed. Although VIs provide a very simple and straightforward method for biochemical content estimates ,PROSPECT model inversion offers the advantage to explicitly account for genotypic differences in leaf surface features, e.g. leaf surface reflectivity and mesophyll structure. It therefore appears that non-destructive methods may provide similar or even better accuracy of chlorophyllian pigments and water contents as compared to classical destructive measurements.

Following these conclusions, we proposed the FASPECT model to describe the leaf structure more realistically by focusing on the difference between the upper and lower faces, and the chlorophyll distribution within the leaf. We therefore considered the leaf as a four-layer system. The two epidermis layers are lambertian and characterized by their reflectance and transmittance spectra. Then, two proportional parameters are used to describe the distribution of the structure parameter and leaf biochemical constituents (chlorophyll, water and dry matter) between the two internal layers that represent the palisade and spongy parenchyma. The radiative transfer process in the two parenchyma layers is simulated with PROSPECT model. We first re-calibrated the specific absorption coefficients of chlorophyll and carotenoids for FASPECT to take into consideration the assumption that the chlorophyll is concentrated in the palisade mesophyll. Then, we validated FASPECT using eight databases. First, we showed that FASPECT provides accurate simulations of reflectance and transmittance of the two leaf faces. Furthermore, the FASPECT reflectance and transmittance simulation of the upper leaf face is better than PROSPECT-5 and PROSPECT-D for most of the spectrum. When used in the inverse mode, while for chlorophyllian pigment content estimation, FASPECT provides similar performance as PROSPECT-D, the use of FASPECT significantly improves the estimation of the dry matter content. Therefore, FASPECT can now be used in canopy radiative transfer modelling to better account for leaves showing high differences between the two faces.

3 Estimates of canopy characteristics from satellite data

The green area index (GAI) and the chlorophyll content at leaf (C_{ab}) and canopy (CCC) levels are among the most important biophysical variables since they both relate to the canopy photosynthetic potential and to the amount of electromagnetic radiation reflected into space which make them accessible from satellite data. Chlorophyll content is not only applied as an indirect estimation of N states but also closely relate to plant stress and senescence.In the past decades, the retrieval of these variables from remote sensing data to generate operational products at high spatial resolution (e.g. lower than decametric) was mainly based on VI-empirical relationships or 1D Radiative Transfer Model (1D RTM) inversion. While the use of VI is sensitive to the calibration database used to establish the empirical relationship, 1D RTM inversion appear and generic more robust but they rely on a very simple description of the canopy structure (e.g. turbid assumption), which may not be sufficient to properly describe the canopy. Thanks to the recent advances in computation performances, it is now possible to invert 3D RTMs to improve the accuracy of biophysical variation estimation. The objective of this chapter is thus to improve canopy characteristics estimation from satellite data by taking into account the 3D structure of the canopy.

We first evaluated the ability of the LuxCorerender engine to properly simulate the radiative transfer model in the canopy based on a 3D description of the vegetation structure. Then, to allow the development of inversion method, we proposed a speeding up method to simulate canopy reflectance of a given canopy by considering 3D simulations of a limited number of soil and leaf properties. Based on simulations, we then compared the ability of three estimation methods (VIs, 1D RTM and 3D RTM) to assess different quantities related to the leaf and plant surface, including the green area index, the plant area index, and the leaf area index for different canopy structures corresponding to wheat and maize. Finally, we compared the estimation of effective GAI, C_{ab}, and CCC from 1D RTM (generic algorithm) and 3D RTM (crop specific algorithm) inversion in wheat and maize using both 3D simulations and SENTINEL2 observations. This chapter is therefore split into 3 main sections that correspond to the following articles:

- ***Article 1: Speeding up 3D radiative transfer simulations: a physically based approximation of canopy reflectance dependency on wavelength, leaf biochemical composition and soil reflectance.*** The article has been submitted in *Remote Sensing of Environment*. The objective of this article is to propose an accurate and physically based approximation to speed-up 3DRTM radiative transfer simulations. This method allows to simulate the reflectance in a given acquisition configuration for any wavelength, leaf biochemical composition and soil background reflectance from a limited number of 3D radiative transfer model simulations. The four stream approximation is firstly applied to describe the interactions between the soil background and the vegetation layers using two or three terms. Then, the dependency of each of these terms to wavelength and leaf properties is described using the leaf total absorption coefficient. For a given canopy structure and observation configuration, only 12 to 18 reference simulations are required to simulate the corresponding reflectances for any wavelength, soil background or leaf optical properties. Very good accuracy is achieved when compared with the reference dataset generated from 3D RTM.

- ***Article 2: The importance of LAI definition when deriving it from reflectance observations.*** In this study, we evaluate the ability of 1D and 3D RTM inversion to estimate different quantities related to the leaf area index LAI, e.g. the plant area index PAI (that includes both green and yellow plant elements), the green area index GAI (that includes only green plant elements), and the effective green area index. Based on 3D mock-ups of maize and wheat, we computed these quantities and simulated the canopy reflectance using the 3DRTM.Conditions including different phenological stages, leaf optical properties, soil reflectance, canopy structures and sun angles were thus considered. Different inversion methods including VIs, 1D RTM PROSAIL and 3D RTM LuxCoreRender are compared. Results show that effective GAI is best estimated from remote sensing observations according to inversion results from 3D RTM. Inversion results from 3D model are more

accurate compared with VIs and PROSAIL model. We then investigate the impact of the sun position on the inversion results and found that the 3D model estimation is less sensitive to the sun position, especially in the row direction, where the turbid assumption of the 1D model is not valid.

- ***Article 3: Optimal learning for GAI and chlorophyll estimation from 1D and 3D radiative transfer model inversion: the case of wheat and maize crops observed by Sentinel2.***
  The objective of this study is to compare the estimation of GAI and chlorophyll at leaf and canopy level from 1D and 3D RTM inversion with Sentinel-2 observations. Two crops, wheat and maize, with different phenological stages are tested. Both 1D PROSAIL and 3D specific model are selected to build the learning database. NN are used as the inversion method to train the learning database. Results show that 3D model provides more accurate estimation of GAI and CCC for both wheat and maize compared with 1D RTM. The inclusion of bands in red-edge and SWIR region improve the estimation of GAI and the utilization of bands in red-edge region is important for chlorophyll estimation.

3.1 LuxCoreRender: validation and solutions to speedup simulations

Speeding up 3D radiative transfer simulations: a physically based approximation of canopy reflectance dependency on wavelength, leaf biochemical composition and soil reflectance

Jingyi Jiang[a], Marie Weiss[a], Shouyang Liu[a,b], Nadia Rochdi[c], Frédéric Baret[a]

[a] EMMAH UMR 1114, INRA, UAPV, 84914 Avignon, France
[b] LEPSE, Université Montpellier, INRA, Montpellier SupAgro, 34060 Montpellier, France
[c] Alberta Terrestrial Imaging Centre and Department of Geography, University of Lethbridge, 4401 University Drive W., Lethbridge, Alberta T1K 3M4, Canada

Abstract

A physically based approach is proposed to describe the dependency of canopy reflectance from the wavelength, leaf and soil properties. The four stream approximation is first applied to describe the interaction between the soil background and the vegetation layers. This leads to the calibration of three terms for a given canopy structure, observation configuration and leaf properties. This number can be reduced to two by using a linear approximation which shows a slight degradation when the multiple scattering contribution is significant. The dependency of each of the two or three terms to wavelength and leaf properties is described using the leaf total absorption coefficient. Our approach requires only 12 (linear approximation) to 18 (four stream approximation) simulations of a reference model to describe the full canopy reflectance dependency to wavelength, leaf and soil properties. The approach was evaluated against reference canopy reflectance simulations using the ray tracing LuxCoreRender model. LuxCoreRender was first validated against reference radiative transfer models. The reference dataset corresponds to range of detailed 3D maize canopies showing variation of leaf and background properties under different view and sun directions in a set of wavebands. Results demonstrate that our approach provides accurate description of the dependency of canopy reflectance to wavelength, leaf and soil properties with RMSE = 0.0017 for the four stream approximation and RMSE = 0.0022 for the linear approximation. The proposed approach appears therefore computationally effective and well suited to generate a large number of canopy reflectance simulations with detailed 3D radiative transfer models that can be used to retrieve vegetation characteristics from remote sensing observations.

Keywords

Canopy reflectance; LuxCoreRender; 3D radiative transfer model; soil reflectance; leaf properties; wavelength

1 Introduction

Several methods have been developed to estimate biophysical variables from remote sensing data. They are either based on empirical regressions of different complexity up to machine learning algorithms applied to experimental data (Verrelst et al. 2012b), or on the inversion of physically based radiative transfer models (Baret and Buis 2008). The latter approach is generally preferred since it exploits our knowledge on the physical processes governing the interaction of light with the canopy elements, and allows taking explicitly into account the information on the observational configuration. Several inversion methods have been widely used including iterative optimization (Jacquemoud et al. 2000), Look-up-table (LUT) (Ganguly et al. 2012; Houborg et al. 2015) and machine learning (Li et al. 2015; Verrelst et al. 2012a). These algorithms require either simulations to be run very fast in the case of iterative optimization or to generate a large number of simulations to populate the LUT or the training database for machine learning approaches. 1D radiative transfer models require only a small number of input variables and are computationally very efficient. They approximate the canopy as a turbid medium where leaves are considered as infinitely small particles randomly distributed in the canopy volume. The 1D radiative transfer models are well adapted to situations where the amount of information on the target is limited. This is the case for kilometric resolution observations (Baret et al. 2013) where the generally mixed nature of pixels and their unknown composition makes the problem difficult to be properly solved. These simple 1D models provide apparent values of the biophysical variables that have been proven to be very useful over regional to global scales applications (Camacho et al. 2013; Delloye et al. 2018; Xiao et al. 2015). However, the increasing availability of frequent decametric resolution satellite images as well as sub-metric and sub-millimetric images recorded onboard unmanned Aerial Vehicles (UAVs) (Verger et al. 2014) or ground vehicles (Comar et al. 2012) require a more realistic description of the canopy structure to get more accurate simulations of the radiative transfer models (Ross 2012) and therefore improve the retrieval performances.

Apart from the simple 1D turbid medium description, several types of radiative transfer models (RTM) have been developed with an enhanced realism at the expense of increasing complexity (Goel 1988). Geometric optical models describe the canopy structure with simple protrusion objects such as cylinders, cones, spheres or ellipsoids distributed over a defined background surface. Hybrid models integrate geometric optical models with turbid medium models. These models define the canopy by a set of statistical properties represented by a distribution function or a simple average (Pinty and Verstraete 1998). However, an inherent loss of information results from these assumptions (Disney et al. 2000). 3D radiative transfer models based on a realistic and detailed description of the canopy structure are thus highly desired.

Several 3D RTMs have been proposed, either based on Monte Carlo ray tracing methods including Flight (North 1996) and Raytran (Govaerts and Verstraete 1998), or based on radiosity methods such as RGM (Qin and Gerstl 2000), or on the exact kernel and discrete ordinate approach as for DART (Gastellu-Etchegorry et al. 2004). These RTMs have been successfully used in the remote sensing community to simulate canopy reflectance (Bye et al. 2017; Gastellu-Etchegorry et al. 2015; Huang et al. 2013; Widlowski et al. 2015; Widlowski et al. 2008). Several open source 3D ray tracing render engines were developed concurrently for computer graphics applications. They include LuxCoreRender (LuxCoreRender 2018), MITSUBA (Jakob 2014) and Pov-ray (POV-team 2013). Because of their flexibility and performances, these computer graphics tools are gradually used by the remote sensing community (Casa and Jones 2005; Coubard et al. 2011; Stuckens et al. 2009). However, apart from the higher complexity of the canopy structure description and the associated increase in the number of required parameters, running a simulation is computationally intensive. The

generation of large LUTs or training datasets to retrieve canopy attributes from a set of reflectance measured in a given observational configuration takes a lot of time. This remains one of the principal limitations when inverting realistic 3D RTMs. As a matter of fact, the reflectance should be simulated in all the considered directions and wavebands. For better accuracy, the sensor spectral response should be taken into account to simulate the reflectance by simulating the reflectance over a large number of bands covering continuously the spectral band domain. Then, the reflectance values must be integrated by considering the spectral distribution of the incident light and the spectral sensitivity of each individual waveband of the sensor. Further, the simulations also require considering a large range of soil reflectance properties.

The objective of this study is to propose a method to accurately simulate canopy reflectance for any wavelength, leaf biochemical composition and soil reflectance from 3D simulations over a limited number of soil and leaf properties. It should therefore save a lot of time when populating a training database to calibrate a retrieval approach. It is based on the development of a metamodel from a limited reference set of canopy reflectance simulations. It is illustrated here using the LuxCoreRender ray tracing model (LuxCoreRender 2018) applied to detailed maize 3D architecture. A general description of the proposed method is first presented along with the LuxCoreRender implementation and the 3D maize architecture model. LuxCoreRender is then validated over reference canopy reflectance simulations. The several steps of the metamodel development and calibration are then presented, followed by an evaluation of the accuracy associated to the proposed method. Finally, the limits and potential applications of the method are discussed.

2 Methods

2.1 Overall presentation of the method

The proposed approach is based on two steps (Figure 16): (1) the calibration of the metamodel, and (2) its application to approximate canopy reflectance. In the first step, the metamodel is calibrated for a given canopy structure, Σ, and observation geometry, Ω. It is made of two nested sub-models. The first one describes the dependency of canopy reflectance to soil reflectance using a physically based approximation that requires few terms (called S) to be calibrated. The S calibration step requires using three reference soil reflectances corresponding to contrasted soils, including a black one. The second sub-model called F_S, describes the wavelength and leaf properties dependency of the previously calibrated S terms. It uses the leaf total absorption coefficient, K, as defined in the PROSPECT model (Jacquemoud et Baret, 1990) and assumes that the leaf mesophyll structure, N, is known and that the impact of the spectral variation of the refraction index, n, on leaf properties is marginal. This will be later discussed.

In the second step, for a given leaf biochemical composition, C_b, and wavelength, λ, the total absorption coefficient, K, is computed using the PROSPECT model and the known specific absorption coefficients of the leaf constituents $k_b(\lambda)$. The function F_S previously adjusted is used to compute each S term for the considered K value. Finally, canopy reflectance, R, is computed using the physically based approximation of canopy reflectance to soil properties that requires the S terms and the actual soil reflectance, r. A more detailed description of each step is provided in the following sections.

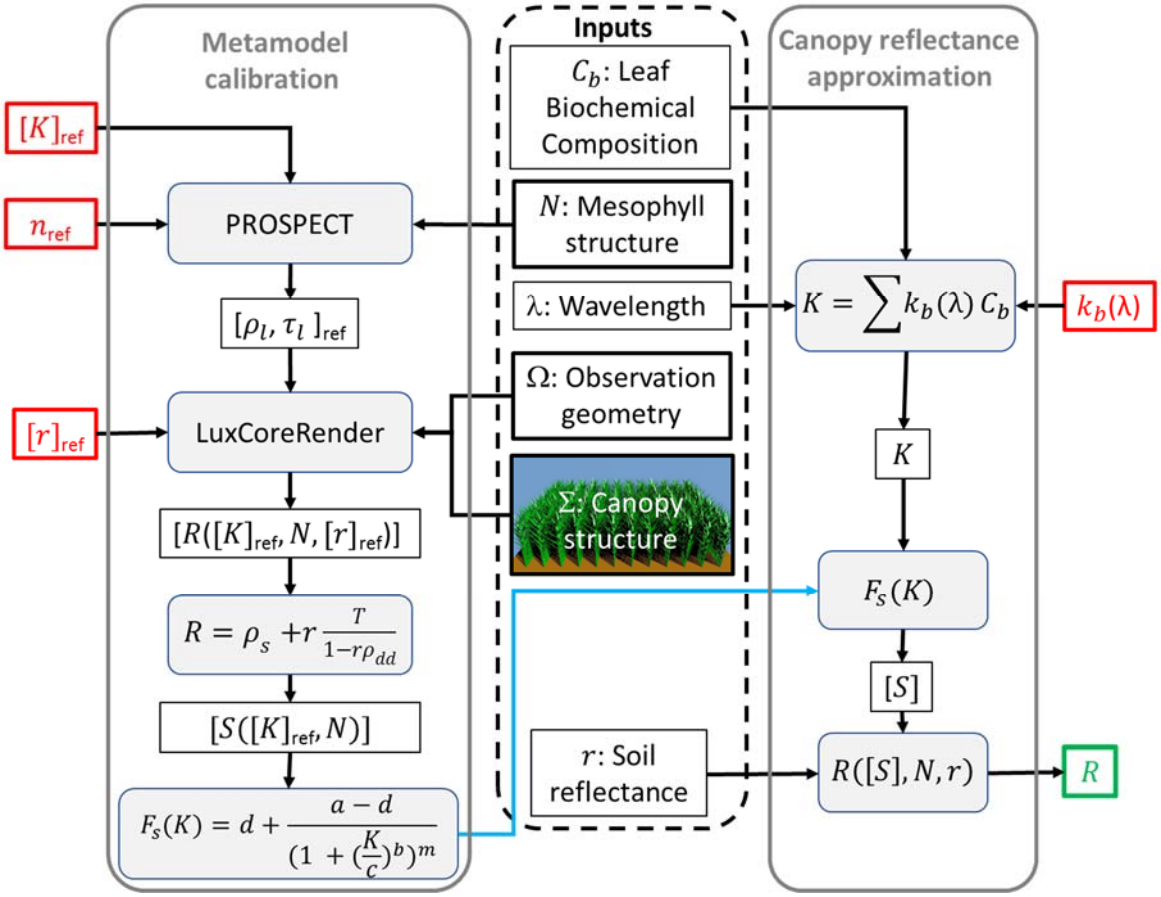

Figure 16. Flow diagram describing the proposed method. The two steps are identified by gray vertical unfilled rectangles with round corners. The output (*R*: canopy reflectance) is represented in green and the fixed inputs in red ($[K]_{ref}$: six reference values of the total leaf absorption coefficient *K*, n_{ref} : a single reference value of the leaf refraction index, $[r]_{ref}$: three reference values of soil reflectance, $k_b(\lambda)$: the specific absorption coefficients of the leaf constituents). The input canopy characteristics (C_b: leaf biochemical contents, *N*: the leaf mesophyll structure, λ: the wavelength, Ω: the observation configuration, Σ: the observation geometry, r: the actual soil reflectance of the canopy) are identified by a vertical rectangle with dashed black border. The several computation sub-steps are identified by gray horizontal rectangles with round corners and their output results by a smaller horizontal rectangle with black borders.

2.2 LuxCoreRender ray tracing model implementation

LuxCoreRender is a physically based and unbiased rendering engine. It is derived from the Physically Based Radiative Transfer project (Pharr et al. 2016) and is an open source software for ray tracing model simulations (Coubard et al. 2011). It computes the radiation fluxes according to physical equations describing the interaction between light and materials. It produces realistic images of photographic quality with a reasonable computation time (LuxCoreRender 2018).

The path tracing was selected as the ray-tracing integrator. The path tracing allows the path integrator to shoot rays from the camera into the scene and continues reflecting the ray off objects until it finds a light or the search is terminated (LuxCoreRender 2018). Even though it is usually slower than bidirectional or photon map integrator, it can provide unbiased simulation results. For each pixel, 128 rays were generated including direct and diffuse scattering. Leaves were assumed lambertian both for reflectance and transmittance. Stems had the same reflectance as the leaf but no transmission. The soil was set to be flat and lambertian. The scene illumination was simulated with only one directional light source.

A perspective camera was selected as the virtual camera with a 25° field of view (FOV) providing a 4.5m × 4.5 m when the camera is pointing the center of the scene from a 50 m distance. To avoid possible border effects, the scene was replicated 8 times around the central one. The simulated LuxCoreRender fluxes were then transformed into Bidirectional Reflectance Factors (BRF) by dividing them by the value simulated over a reference lambertian panel with BRF = 1.0 using the same illumination and observation configuration.

2.3 3D Maize architecture model

The 3D maize architecture model was developed by (López-Lozano et al. 2007). The development of the canopy is driven by the growing degree days. Five growth stages were simulated every 200 °Cd from the two leaves stage corresponding to 150 °Cd up to 950 °Cd corresponding to the start of male earing. The six parameters of the model (Table 7) were changed and resulted into 60 scenes simulated corresponding to typical maize canopies (Figure 17).

Table 7. Parameters of the 3D maize model used in this study.

Variable		Unit	Value
N_{max}	Maximum number of leaves per plant	-	18
S_{max}	Maximum leaf area per plant	m^2	0.5, 0.75
D	Plant density	plants/m^2	9
d_{rows}	Distance between rows	m	0.7, 0.8
H_{max}	Maximum plant height	m	2
Θ_{max}	Inclination of largest leaf	°	30, 45, 60
T	Stages expressed in thermal time	°Cd	150, 350, 550, 750, 950

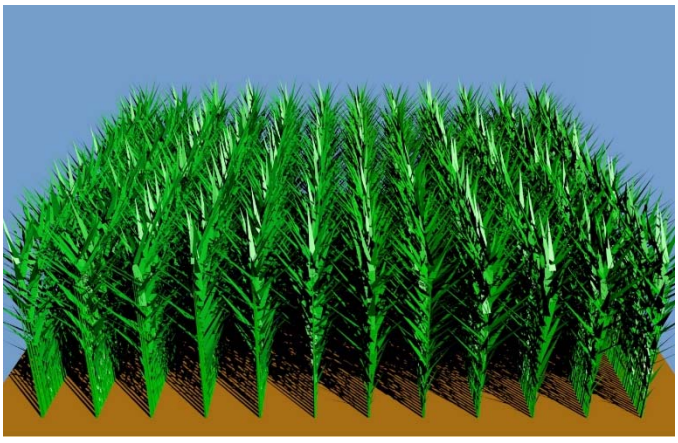

Figure 17. A typical 3D scene of maize canopy (N_{max}=18, S_{max} =0.75 m^2, D=8 plants/m^2, d_{rows} =0.7 m, H_{max}=2 m, Θ_{max}=45°, T=950 °Cd) simulated with LuxCoreRender.

3 Results

3.1 LuxCoreRender simulates accurately canopy reflectance

The RAMI Online Model Checker (ROMC) (Widlowski et al. 2008) provides a set of reference data designed to evaluate the performances of radiative transfer models. The reference data are composed of simulations generated by a set of validated RAMI models. Contrasted canopy types were selected with heterogeneous (HET04 in RAMI3) and homogeneous (HOM03 and HOM13 in RAMI3) architectures characterized by different leaf orientations and with different leaf optical properties. The reflectance of HOM13 was simulated in red band, while the reflectance of HET04 and HOM13 were in NIR band. For each case, the sun azimuth angle was set at 0°. Viewing directions were considered in both the principal and the perpendicular planes using a camera with orthographic projection and no geometric distortion. The heterogeneous canopy is composed of two elements with different optical properties.

Table 8. Main characteristics of the ROMC scenes used to evaluate LuxCoreRender. LAI stands for Leaf Area Index. SZA is the sun zenith angles. ρ_l and τ_l correspond to the reflectance and transmittance of the canopy elements. More details can be found in (Widlowski et al. 2008).

#	Type of canopy	LAI	ρ_l	τ_l	SZA
HOM03_DIS_ERE	Homogeneous; erectophile leaf distribution	3	0.50	0.44	20°
HOM13_DIS_PLA	Homogeneous; planophile leaf distribution	3	0.05	0.01	50°
HET04	spheres and cylinders, uniform leaf distribution	5	0.49/0.45	0.45/0.30	20°

Results show a very good agreement between LuxCoreRender and the ROMC reference data (Figure 18) with low root mean square error (RMSE≈0.0016). The model skill which is an integrated metrics describing how the model matches the reference data (Widlowski et al. 2008) was 98.3% and 99.6% respectively in the principal and perpendicular planes. It is therefore concluded that LuxCoreRender and the way it was implemented in this study reaches the same accuracy level as the state of the 3D-models involved in the RAMI exercise. It is thus able to provide accurate simulations of canopy reflectance across a large range of cases.

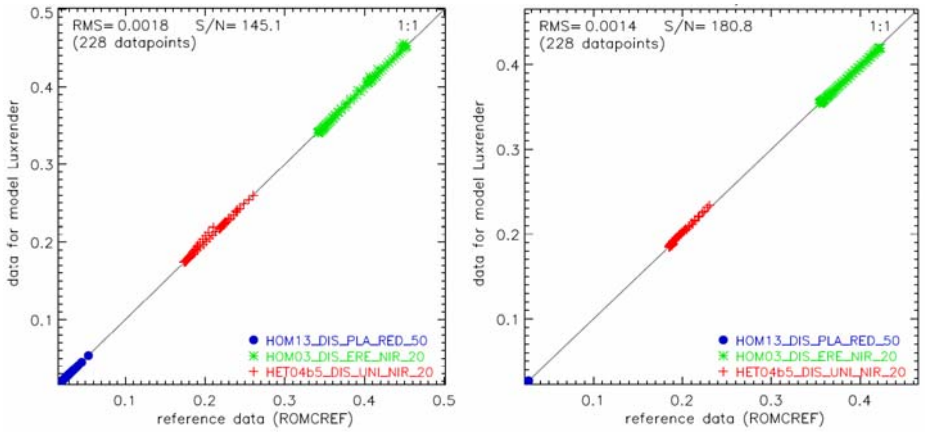

Figure 18. Comparison between LuxCoreRender reflectance simulations and ROMC (RAMI On-Line Model Checker) reference values. The three scenes presented in Table 8 are displayed: HOM03 (red), HOM13 (blue) and HET04 (green). Principal plane (left) and perpendicular plane (right). The black line corresponds to the 1:1 line.

3.2 Computation of the $\boldsymbol{S}$ term describing the dependency of canopy reflectance to soil reflectance.

3.2.1 The four stream approximation solves accurately the soil background problem

The four stream approximation (Suits 1972; Verhoef 1985) was used to describe the radiative coupling between the soil background and the vegetation layer. We thus assumed two directional fluxes in the source and observation directions and two diffuse fluxes in the upward and downward directions. Verhoef (1985) stated that in black-sky conditions (e.g. no diffuse illumination), the top-of-canopy BRF (R) is the sum of a purely bi-directional component (r_{so}) and a directional-hemispherical component (r_{sd}):

$$R = r_{so} + r_{sd} \tag{1}$$

with:

$$\begin{aligned} r_{so} &= \rho_{so} + \tau_{ss}\tau_{oo}r + \frac{(\tau_{ss}r+\tau_{sd}r)\tau_{do}+(\tau_{sd}+\tau_{ss}r\rho_{dd})r\tau_{oo}}{1-r\rho_{dd}} \\ r_{sd} &= \rho_{sd} + \frac{(\tau_{ss}r+\tau_{sd}r)\tau_{dd}}{1-r\rho_{dd}} \end{aligned} \tag{2}$$

where r refers to soil reflectance assumed lambertian, τ_{xy} and ρ_{xy} represent respectively the transmittance and the reflectance of the canopy layer. The incoming and outgoing directions are indicated respectively by subscripts $_x$ and $_y$ that can be either s (source direction), o (observation direction) or d (diffuse downward or upward directions). These notations are consistent with those used by (Verhoef 1985; Verhoef and Bach 2007). Equation (1) can be rewritten as:

$$\begin{aligned} R &= \rho_{so} + \rho_{sd} + \frac{\tau_{ss}\tau_{oo}r - \tau_{ss}\tau_{oo}r^2\rho_{dd} + (\tau_{ss}r+\tau_{sd}r)\tau_{do} + (\tau_{sd}+\tau_{ss}r\rho_{dd})r\tau_{oo} + (\tau_{ss}r+\tau_{sd}r)\tau_{dd}}{1-r\rho_{dd}} \\ &= \rho_{so} + \rho_{sd} + \frac{r(\tau_{ss}+\tau_{sd})(\tau_{oo}+\tau_{do}+\tau_{dd})}{1-r\rho_{dd}} = \rho_s + r\frac{T}{1-r\rho_{dd}} \end{aligned} \tag{3}$$

Where $\rho_s = \rho_{so} + \rho_{sd}$ and $T = (\tau_{ss} + \tau_{sd})(\tau_{oo} + \tau_{do} + \tau_{dd})$. The term ρ_s corresponds to the canopy reflectance simulated with a black soil:

$$r = r_0 = 0.0 \Rightarrow R_0 = \rho_s \tag{4}$$

The terms ρ_{dd} and T can be derived from the simulations of canopy reflectance, R_1 and R_2, corresponding to two additional contrasted soil reflectance, $r = r_1$ and $r = r_2$. The term ρ_{dd} can then be computed from equation (3) by applying it to r_1 and r_2:

$$\left.\begin{aligned} R_1 &= R_0 + r_1 \frac{T}{1-r_1\rho_{dd}} \\ R_2 &= R_0 + r_2 \frac{T}{1-r_2\rho_{dd}} \end{aligned}\right\} \Rightarrow \quad \rho_{dd} = \frac{\frac{(R_2-R_0)r_1}{(R_1-R_0)r_2}-1}{r_1\left(\frac{(R_2-R_0)}{(R_1-R_0)}-1\right)} \tag{5}$$

The term T is finally computed by replacing the value of ρ_{dd} from equation (4) into equation (3) applied to one of the previously used soil reflectance ($r_s = r_1, r_2$):

$$T = \frac{(R_2-R_0)(1-r_s\rho_{dd})}{r_s} \tag{6}$$

Therefore, the term S can be described as three terms $[S_{4s}] = [\rho_{dd}, \rho_s, T]$ from equation (3) depend on canopy structure and leaf optical properties. Furthermore, ρ_s and T also depend on the observational configuration defined by the view and illumination directions, while ρ_{dd} does not. The proposed solution to describe the dependency of canopy reflectance to soil reflectance needs therefore to be applied for a given combination of canopy structure, Σ, observational configuration, Ω, and leaf optical properties, $[\rho_l, \tau_l]$. For each combination $[\Sigma, \Omega, [\rho_l, \tau_l]]$, the terms $[S_{4s}]$ of equation (3) were computed according to equations (4) to (6) using three reference values of soil reflectance: $[r]_{ref} = [r_0, r_1, r_2]$ embracing the typical range of variation of soil reflectance.

The accuracy of the proposed approximation was evaluated over 60 scenes generated with the 3D maize model (Table 7) for nadir viewing and for 20° and 35° sun zenith angles in both the red [ρ_l(red) = 0.063; τ_l (red) = 0.018] and NIR bands [ρ_l(NIR) = 0.463; τ_l (NIR) = 0.522]. Canopy reflectance was simulated with LuxCoreRender for these 240 combinations $[\Sigma, \Omega, [\rho_l, \tau_l]]$ (60 scenes, two bands and two sun directions) for five soil reflectance values: $[r]$ = [0, 0.1, 0.2, 0.3, 0.4, 0.5] embracing the typical range of variation of soil reflectance in these bands. For each of the 240 $[\Sigma, \Omega, [\rho_l, \tau_l]]$ combinations, the terms $[S_{4s}] = [\rho_{dd}, \rho_s, T]$ were calibrated using equations (4) to (6) with $[r]_{ref}$ = [0, 0.1, 0.4]. Once $[\rho_{dd}, \rho_s, T]$ are calculated, canopy reflectance can be computed using equation (3) for any soil reflectance value. As validation, estimated results with $[r]$ = [0.2, 0.3, 0.5] were compared with LuxCoreRender canopy reflectance.

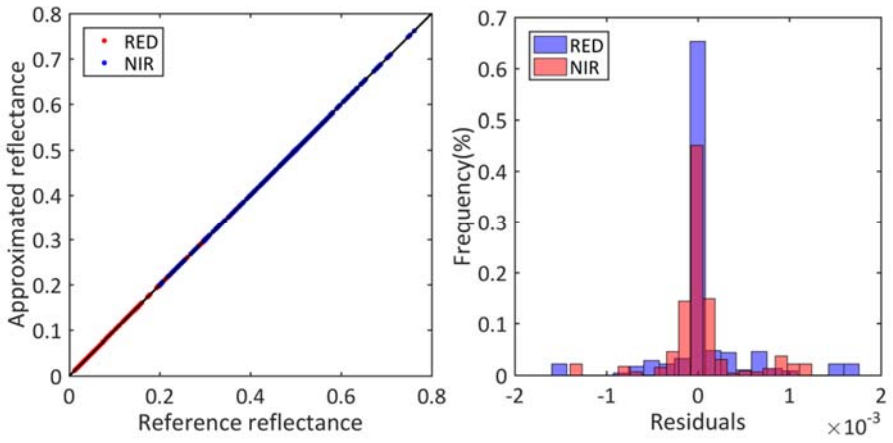

Figure 19. Left: scatterplot between the reference canopy reflectance simulated using LuxCoreRender and the corresponding one estimated using the four stream approximation (equation (3)) in red (red) and NIR (blue). The black solid line is the 1:1 line. Right: distribution of the residuals (difference between reference and approximated canopy reflectance) using the four stream approximation based on equation (3).

Results show that the proposed method provides very accurate approximations (RMSE≈0.0004 and r^2≈1) for the two bands and all the considered combinations (Figure 19. left). The distribution of the residuals between the reference LuxCoreRender simulated reflectance and the one estimated based on equations (3) to (6) is centered on 0.00 (Figure 19. right) with maximum absolute values of the residual smaller than 0.002. The four stream approximation was expected to be accurate for low values of soil reflectance since the soil contribution term $r\frac{T}{1-r\rho_{dd}}$ in equation (3) is negligible in these conditions. However, the four stream approximation is still valid even for r = 0.5, i.e. outside the domain of the method calibration (0.0 < r < 0.4). It is therefore an accurate way to estimate canopy reflectance for any soil background value using only three reference simulations corresponding to three soil reflectance values with $[r]_{ref}$= [0, 0.1, 0.4].

3.2.2 The linear approximation describes efficiently the dependency of canopy reflectance to soil properties

A further simplification can be introduced by neglecting the non-linear interaction term in equation (3), resulting into a linear approximation of the canopy reflectance that reduce the term S to $[S_{lin}] = [\rho_s, A]$:

$$R = \rho_s + rA \quad (7)$$

A can be computed analytically by deriving ρ_s from the black soil simulation (equation (4)) and simulating the canopy reflectance for one additional soil, r_s:

$$A = \frac{R_1 - R_0}{r_s} \quad (8)$$

Similarly to the four stream approximation, the terms $[S_{lin}]$ need to be computed for each combination of $[\Sigma, \Omega, [\rho_l, \tau_l]]$. The previous set of canopy reflectance simulations were thus used to evaluate the accuracy of this linear approximation: for each combination of $[\Sigma, \Omega, [\rho_l, \tau_l]]$, the terms $[S_{lin}]$ were computed using $[r]_{ref}$= [0, 0.4] and equations (4) and (8). Equation (7) was then applied to get the linear approximation of canopy reflectance for the soil properties used previously for the validation: $[r]$ = [0.2, 0.3, 0.5].

Results show that the linear approximation induces a slight degradation of the performances in the NIR (RMSE=0.0025, r^2=0.9994). This is due to a higher multiple scattering within the canopy due to higher leaf reflectance and transmittance values in that spectral domain (Figure 20). Detailed inspection of the distribution of the residuals shows that they are well centered on 0.0. However, the absolute value of the residuals can reach 0.008 in the NIR for medium values of vegetation development and high values of soil reflectance (r = 0.5). The linear approximation is therefore efficient in most of the cases although it requires only two LuxCoreRender simulations per $[\Sigma, \Omega, [\rho_l, \tau_l]]$ combinations to compute accurately the canopy reflectance for any soil background reflectance values.

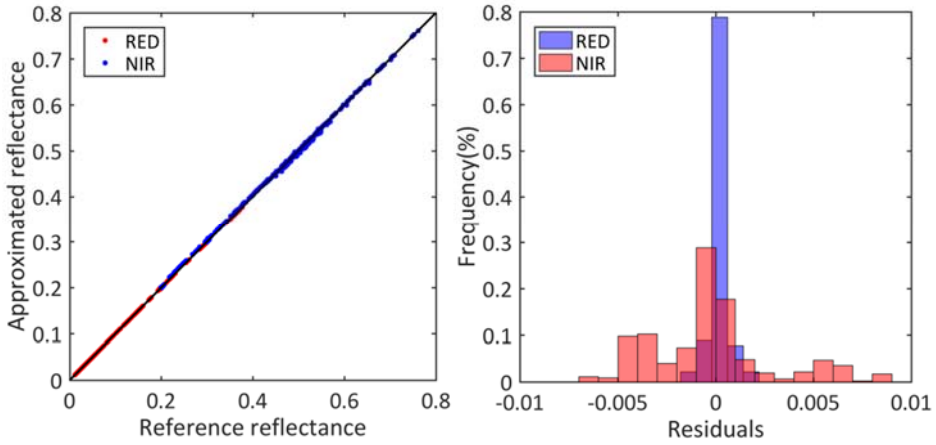

Figure 20. Left: scatterplot between the reference canopy reflectance simulated using LuxCoreRender and the corresponding one estimated using the linear approximation (equation (7)) in red (red) and NIR (blue). The black solid line is the 1:1 line. Right: distribution of the residuals (difference between reference and approximated canopy reflectance) using the linear approximation based on equation (7).

3.3 Dependency of the $\boldsymbol{S}$ terms to wavelength and leaf optical properties

3.3.1 Principles

Leaf optical properties depend on the surface features (Comar et al., 2012), the internal structure of the leaf mesophyll, the biochemical composition including the distribution of the constituents in the leaf volume, and the complex refraction index of these constituents (Baret et al. 1994). According to (Jacquemoud and Baret 1990), the real part of the refraction index, n, that drives the leaf scattering processes varies marginally for wavelengths belonging to the 400-2200 nm spectral domain. Therefore, the spectral variation of the leaf optical properties is mainly driven by the imaginary part of the refraction index that corresponds to the absorption coefficient. Consequently, neglecting the spectral variation of n allows to simulate leaf optical properties as a function of the total absorption coefficient, K, and the leaf mesophyll structure parameter, N (Fourty et al. 1996). The total absorption coefficient, K, is determined by the specific absorption coefficient of each biochemical constituent $k_b(\lambda)$ and the corresponding content C_b expressed in terms of mass per unit leaf area (Jacquemoud and Baret, 1990):

$$K = \sum k_b(\lambda) C_b \qquad (9)$$

For a given value of the leaf mesophyll structure parameter N, the refractive index n, the canopy structure Σ and the observational configuration Ω, the spectral variation of the three terms $[S_{4s}]=[\rho_{dd}, \rho_s, T]$ of the four stream solution identified in equation (3) or the two terms $[S_{lin}]=[\rho_s, \mathrm{A}]$ of the linear approximation in equation (7) can therefore be described by a smooth and monotonic function that depends on K (Baret et al. 1994). An empirical function, $F_S(K)$, can therefore be fitted to represent the dependency of each term $[S]$ of equations (3) or (7) to K for a given combination of $[\Sigma, \Omega, N, n]$.

3.3.2 Range of variation of $\boldsymbol{K}$ and impact of the spectral variation of the refraction index $\boldsymbol{n}$ on leaf properties

The range of variation of the total absorption coefficient, K, was computed for the 400 nm to 2200nm spectral domain based on the minimum and maximum values observed for $k_i(\lambda)$ from PROSPECT3 (Jiang et al., 2018) and the bounds of C_i values reported in the LOPEX dataset (Hosgood et al. 1995). Results show that K ranges from 0.0045 to 5.5.

The refractive index, n, varies slightly with the wavelength (Jacquemoud and Baret 1990). It ranges from 1.5 at 400 nm to 1.3 at 2200 nm. However, the impact of the spectral variation of n on leaf optical properties is generally marginal. This was verified using PROSPECT3 model simulations using a typical value of the leaf mesophyll structure parameter for maize crop, N = 1.5. Results show that the leaf reflectance is almost insensitive to variation of n, except for the very small values of the absorption coefficient (K < 0.4), when scattering processes are dominating (Figure 21A). Similar results are observed for transmittance, with however a larger impact for K < 2 (Figure 21B). In the following, we will consider that the refraction index is independent from the wavelength, with n_{ref}= 1.4 corresponding to the average value. The influence of this approximation on the computation of canopy reflectance will be further investigated in the next section. A set of K values approximately equally spaced in reflectance and transmittance were selected to represent the range of variation of leaf optical properties: $[K]_{ref}$ =[0.0045; 0.0509; 0.1909; 0.4626; 1.0951; 5.5000].

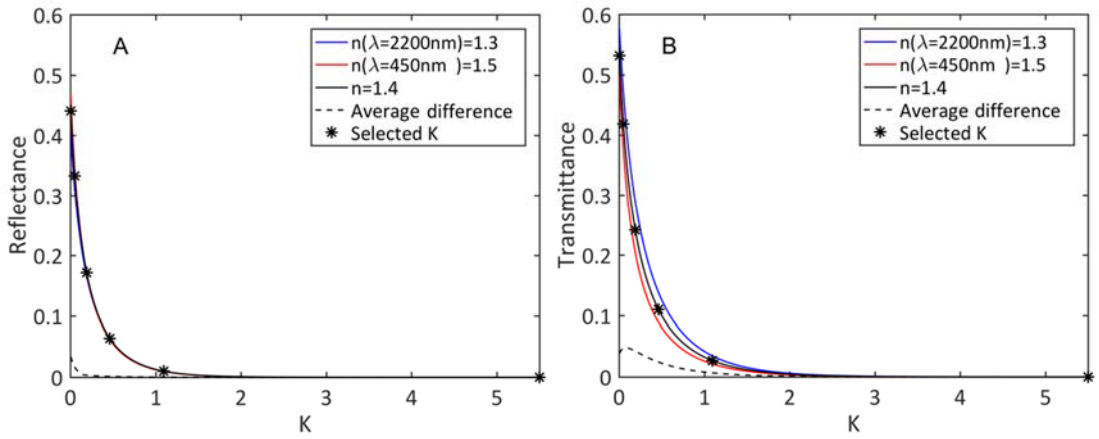

Figure 21. Relationship between the global absorption coefficient K and the refractive indexes n for leaf reflectance (left) and leaf transmittance (right). The black, blue and red lines correspond respectively to n = [1.3, 1.4, 1.5]. The dotted lines show the average absolute value of the difference between leaf reflectance or transmittance using n_{ref} = 1.4 (reference value) and n = 1.3 and 1.5. The asterisks correspond to the six values of $[K]_{ref}$ selected to describe the leaf reflectance and transmittance.

3.3.3 Calibration of function $\boldsymbol{F_S(K)}$ describing the dependency of the $\boldsymbol{S}$ terms to $\boldsymbol{K}$

For each canopy structure, observational configuration, mesophyll structure index, and refraction index, the dependency of the S terms to the K values can be approximated by a sigmoid function $F_S(K)$ fitted on the six previously selected K values:

$$F_S(K) = d + \frac{a-d}{(1+(\frac{K}{c})^b)^m} \quad (10)$$

Results show that the sigmoid functions described very well the variation of the S terms as a function of K, showing a RMSE value lower than 0.005 computed over data points that were not used for the

calibration (see the black dots in Figure 22). The S terms showed a smooth exponential decrease with K. The plateau is reached for $K > 0.5$ for ρ_{dd} and ρ_s, and for $K > 0.2$ for T and A (Figure 22). As expected, the S terms contributing to the reflectance value, ρ_{dd} and ρ_s, increase with LAI, while the other ones contributing to the transmittance, T and A, decrease with LAI.

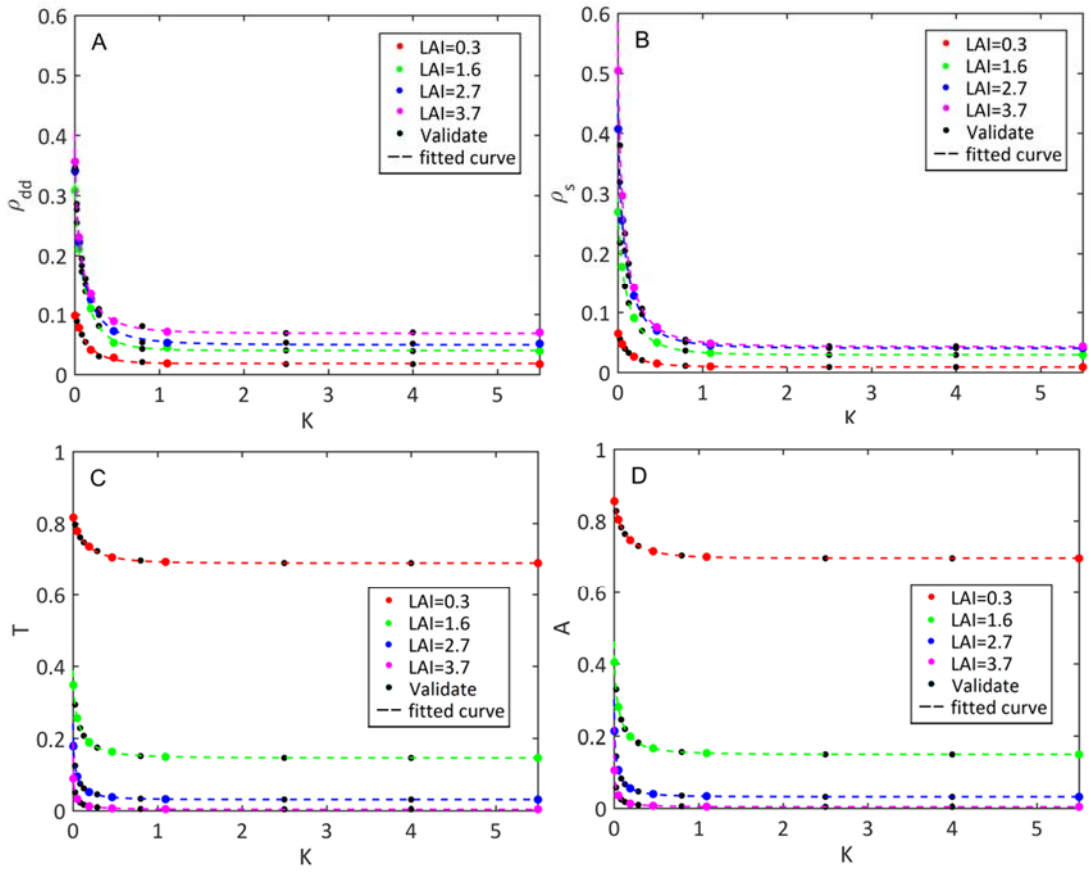

Figure 22. Relationship between the six selected global absorption coefficient K and the different S terms for several maize canopies (LAI = 0.3, 1.3, 2.7 and 3.7) using either the four stream approximation ([S_{4s}], A: ρ_{dd} , B: ρ_s, C: T) or the linear approximation ([S_{lin}], D: A). Dotted lines correspond to the fitted curves from $F_S(K)$ (equation (10)). The black dot corresponds to the validation points.

3.4 Very accurate approximation is obtained by calibrating the metamodel over 12 canopy reflectance simulations

The 60 canopy structure scenes described in Table 7 with two observational configurations (nadir viewing and SZA= [20°, 35°]) were used as validation cases. They were combined with the three soil properties proposed in Table 9 and the six leaf optical properties shown in Table 10. Finally, the canopy reflectance was computed in six bands of the SENTINEL 2 sensor (Drusch et al. 2012) (Table 9).

Table 9. Soil properties used to simulate canopy reflectance in six of the SENTINEL2 bands to validate the metamodel.

SENTINEL2 bands (nm)	450	560	665	705	740	865
Soil reflectance	0.067	0.106	0.140	0.152	0.163	0.191
	0.134	0.212	0.280	0.304	0.326	0.382
	0.201	0.318	0.420	0.456	0.489	0.573

Table 10. Leaf characteristics used for the PROSPECT model to simulate canopy reflectance to validate the metamodel.

N	Chlorophyll content ($\mu g.cm^{-2}$)	Water content ($g.cm^{-2}$)	Dry matter content ($g.cm^{-2}$)	Brown pigments content (-)
1.5	40	5	10	0.5
1.5	50	15	5	0.2
1.5	55	25	20	0.7
1.5	60	10	30	0.4
1.5	65	20	25	0.6
1.5	70	30	15	0.3

The 12960 (60 canopy structures x 2 observational configurations x 3 soil properties x 6 leaf characteristics x 6 bands) reference canopy reflectance were computed using LuxCoreRender and taking into account the spectral dependency of the refraction index, $n(\lambda)$. The metamodel was then calibrated on each of these 60 scenes for two observational configurations according to the scheme presented in Figure 16. The refraction index was set here to $n_{ref} = 1.4$ using $[r]_{ref}$ = [0.0, 0.1, 0.4] or $[r]_{ref}$ = [0.0, 0.4] respectively for the four stream and the linear approximations to compute the S terms using $[K]_{ref}$= [0.005, 0.040, 0.092, 0.177, 0.343, 1.096] to fit the functions $F_S(K)$.

Results show that the metamodel approximates with a very good accuracy the reference canopy reflectance simulations (Figure 23). The four stream approximation shows very little difference from the reference canopy reflectance, with RMSE=0.0017 (Figure 23A). Conversely, the linear approximation degrades slightly the agreement with the reference canopy reflectance particularly for canopy reflectance values larger than 0.3 (Figure 23B), corresponding mostly to the 740 nm and 865 nm bands and bright soils (r > 0.4) when the multiple scattering is relatively important, confirming our previous observations. More detailed inspection of the distribution of the residuals shows that the metamodel slightly overestimates the reference canopy reflectance showing a higher number of negative residuals especially for the linear approximation (Figure 24B). However, most negative residuals for the linear approximation are very small (< 0.005 for absolute value and < 4% for relative

value), while larger positive residuals are observed. These cases correspond to the higher values of leaf reflectance and transmittance as well as soil reflectance that enhance the multiple scattering. Nevertheless, the linear approximation provides an efficient solution with a reasonable accuracy: RMSE=0.0022.

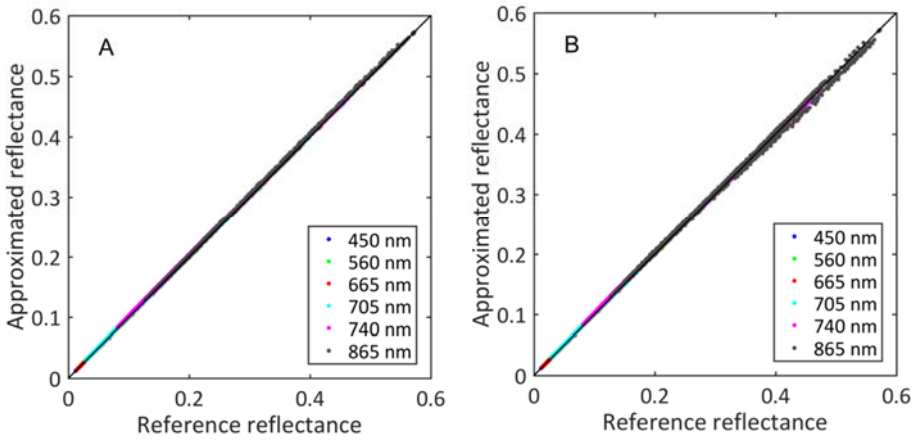

Figure 23. Comparison between the reference canopy reflectance simulated using LuxCoreRender and the approximated one using the metamodel. (A) Using the four stream approximation (B) Using the linear approximation.

A further analysis was conducted to evaluate the impact of assuming n_{ref} = 1.4 when approximating the canopy reflectance. For this purpose, the metamodel was calibrated according to the scheme presented in Figure 16, except that the refraction index was depending on wavelength ($n(\lambda)$) according to the values proposed in PROSPECT3. Results show that the slight overestimation of the metamodel is considerably reduced (Figure 24) when allowing the refraction index to vary with the wavelength. The accuracy of the metamodel is significantly improved both for the four stream (RMSE=0.0007) and the linear (RMSE=0.0018) approximations. The overestimation observed when assuming n_{ref} = 1.4 comes mostly from the fact that the six wavebands selected in this validation exercise are corresponding to values of 1.5 > n >1.43. When fixing $n_{ref} = 1.4$, leaf transmittance is overestimated (Figure 21B) which induces a slight overestimation of the simulated canopy reflectance. Therefore, the metamodel could be calibrated with a n value closer to that corresponding to the range of wavelengths considered.

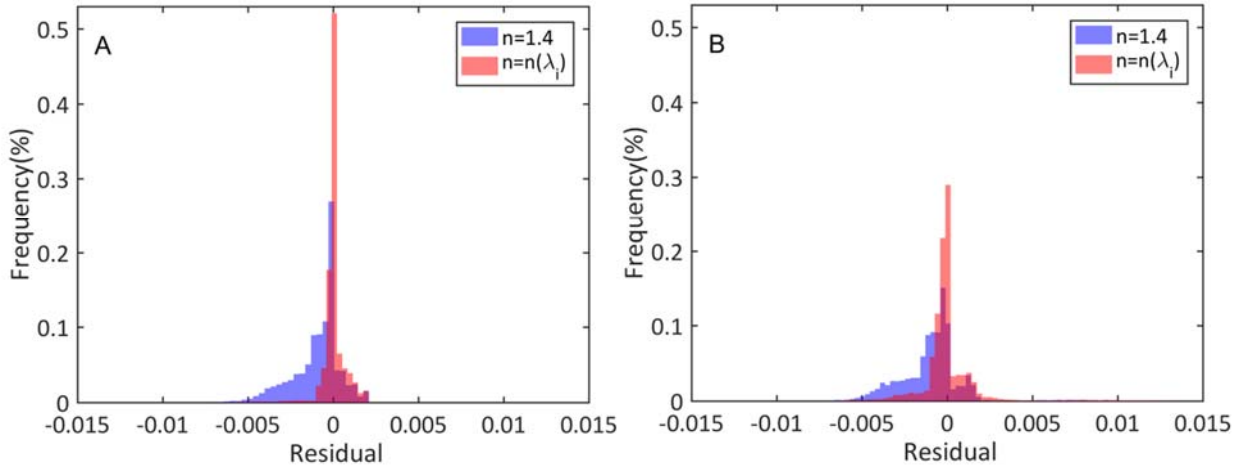

Figure 24. Distribution of the residuals (difference between reference and approximated canopy reflectance). (A) Using the four stream approximation (B) Using the linear approximation. Red: approximation using n_{ref} = 1.4. Blue: approximation using $n(\lambda)$.

4 Summary and perspectives

The LuxCoreRender physically based ray-tracing model was run to simulate reference canopy reflectance using a detailed 3D representation of canopy structure. LuxCoreRender was first validated against other reference radiative transfer models applied both to homogeneous and heterogeneous canopies in spectral domains where multiple scattering is small (red) or large (near infrared). Results show very good agreement between LuxCoreRender simulations and the reference values. This demonstrates that LuxCoreRender can be considered as a good reference radiative transfer model.

A scheme was then proposed to approximate the dependency of canopy reflectance to leaf properties, wavelength and soil reflectance. It is based on the separation between the influence of the canopy structure and observation configuration from that of the leaf and soil properties. This approach is similar to the 'spectral invariant' principles proposed by (Huang et al. 2007; Lewis and Disney 2007), although the photon recollision probability (Mõttus and Stenberg 2008; Wang et al. 2018) was not used in our study. The influence of the soil background on canopy reflectance was approximated using the four stream approximation that couples a soil background layer with a vegetation layer. The three terms used in this approximation require thus three reference simulations to be calibrated for a given canopy structure, observation configuration and leaf properties. Results show that the four stream approximation provides a good agreement with the reference values of canopy reflectance as computed with LuxCoreRender over a range of maize architecture observation configurations and leaf properties. A further simplification is proposed, requiring only two simulations of the reference model to calibrate the two terms used in the approximation. The multiple scattering between the soil and the vegetation layers is not explicitly considered in the linear approximation. It induces a slight underestimation of canopy reflectance in the red-edge and near infrared spectral domains with high soil reflectance. Nevertheless, the overall low RMSE=0.0039 demonstrates that this approximation is efficient.

The dependency of canopy reflectance from the leaf biochemical composition and wavelength was described by calibrating relationships between the total absorption coefficient K of the leaf and the two (linear approximation) or three terms (four stream approximation) needed to represent the soil

background effect. Because of the smoothness and monotony of these relationships, only six reference data points $[K]_{ref}$ are needed. The coefficients of these relationships are spectrally invariant since they only depend on canopy architecture and observation configuration. Using the total absorption coefficient, K, as proposed here offers the advantage to represent at the same time the dependency from the leaf biochemistry and wavelength. The refraction index, n, was set to an average value, n_{ref} = 1.4, over the 400-2200 nm domain because of its small spectral dependency. However, slight overestimation was observed in the test cases considered in this study and restricted to the 450-865 nm domain, where n > 1.4. In such conditions, the refraction index could be set to a fixed value more representative of the spectral domain considered. For the sake of simplicity, the leaf mesophyll structure index, N, was set to a fixed value. This is justified by its relatively small variability for a given species as well as the limited sensitivity of leaf reflectance and transmittance to small deviations of N around its mean value. However, it is possible to include N as an additional independent variable at the expense of additional reference model simulations to fit the more complex relationship between the leaf absorption coefficient and the two or three terms used to describe the dependency of canopy reflectance to soil background reflectance.

The proposed approach requires considering each combination of canopy structure and observation configuration. It was illustrated in this study for maize canopies using LuxCoreRender as a reference model while it is applicable to any canopy architecture and any reference radiative transfer model. However, we assumed that the vegetation layer is made of elements that can be described with the same total absorption coefficient K. In the case of canopies with several types of elements having different optical properties, the same approach could be used without any modification by focusing on the dependency of only one element type.

The method described in this study provides an efficient way to reduce the computation time required to generate large training datasets used to invert radiative transfer models and retrieve some canopy characteristics. This is of particular interest when using a large number of wavelengths such as for hyperspectral data, leaf biochemical composition and soil properties. Contrary to our approach that exploits the knowledge on the physical processes, model emulation techniques as proposed by (Gómez-Dans et al. 2016; Verrelst et al. 2017) are pure machine learning based techniques. Training such emulators is thus computationally more expensive and requires a higher number of simulations to represent properly the variability induced by leaf biochemical composition, wavelength and soil properties. However, both methods could be combined: model emulation could focus on the variability due to the canopy structure and observational configuration for the 12 (linear approximation) or 18 (four stream approximation) combinations of soil reflectance and total absorption coefficients K required by our approach. For each combination of canopy structure and observation configuration and a typical case with seven wavebands, four values of chlorophyll content and four values of soil background reflectance as used in (Verger et al. 2011) for LAI retrieval, 112 simulations with the reference 3D radiative transfer model would be necessary while only 12 simulations (linear approximation) are required with the linear approximation approach, leading to a nine-fold reduction of the computation time. The proposed approach appears therefore very efficient to generate large training datasets based on advanced radiative transfer models and realistic canopy architecture models.

Acknowledgements

This research was completed in the framework of the BELCAM project funded by the Belgian Science

Policy Office (BELSPO) in the STEREO II program.

Reference

(RAMI On-Line Model Checker). http://romc.jrc.ec.europa.eu/
Baret, F., & Buis, S. (2008). Estimating Canopy Characteristics from Remote Sensing Observations: Review of Methods and Associated Problems. In S. Liang (Ed.), *Advances in Land Remote Sensing* (pp. 173-201): Springer Netherlands
Baret, F., Vanderbilt, V.C., Steven, M.D., & Jacquemoud, S. (1994). Use of spectral analogy to evaluate canopy reflectance sensitivity to leaf optical properties. *Remote Sensing of Environment, 48*, 253-260
Baret, F., Weiss, M., Lacaze, R., Camacho, F., Makhmara, H., Pacholcyzk, P., & Smets, B. (2013). GEOV1: LAI and FAPAR essential climate variables and FCOVER global time series capitalizing over existing products. Part1: Principles of development and production. *Remote Sensing of Environment, 137*, 299-309
Bye, I., North, P., Los, S., Kljun, N., Rosette, J., Hopkinson, C., Chasmer, L., & Mahoney, C. (2017). Estimating forest canopy parameters from satellite waveform LiDAR by inversion of the FLIGHT three-dimensional radiative transfer model. *Remote Sensing of Environment, 188*, 177-189
Camacho, F., Cernicharo, J., Lacaze, R., Baret, F., & Weiss, M. (2013). GEOV1: LAI, FAPAR essential climate variables and FCOVER global time series capitalizing over existing products. Part 2: Validation and intercomparison with reference products. *Remote Sensing of Environment, 137*, 310-329
Casa, R., & Jones, H.G. (2005). LAI retrieval from multiangular image classification and inversion of a ray tracing model. *Remote Sensing of Environment, 98*, 414-428
Comar, A., Burger, P., de Solan, B., Baret, F., Daumard, F., & Hanocq, J.-F. (2012). A semi-automatic system for high throughput phenotyping wheat cultivars in-field conditions: description and first results. *Functional Plant Biology, 39*, 914-924
Coubard, F., Brédif, M., Paparoditis, N., & Briottet, X. (2011). Reflectance estimation from urban terrestrial images: Validation of a symbolic ray-tracing method on synthetic data. *International Archives of the Photogrammetry, Romote Sensing and Spatial Information Sciences, 38*, 3
Delloye, C., Weiss, M., & Defourny, P. (2018). Retrieval of the canopy chlorophyll content from Sentinel-2 spectral bands to estimate nitrogen uptake in intensive winter wheat cropping systems. *Remote Sensing of Environment, 216*, 245-261
Disney, M., Lewis, P., & North, P. (2000). Monte Carlo ray tracing in optical canopy reflectance modelling. *Remote Sensing Reviews, 18*, 163-196
Drusch, M., Del Bello, U., Carlier, S., Colin, O., Fernandez, V., Gascon, F., Hoersch, B., Isola, C., Laberinti, P., & Martimort, P. (2012). Sentinel-2: ESA's optical high-resolution mission for GMES operational services. *Remote Sensing of Environment, 120*, 25-36
Fourty, T., Baret, F., Jacquemoud, S., Schmuck, G., & Verdebout, J. (1996). Leaf optical properties with explicit description of its biochemical composition : direct and inverse problems. *Remote Sensing of Environment, 56*, 104-117
Ganguly, S., Nemani, R.R., Zhang, G., Hashimoto, H., Milesi, C., Michaelis, A., Wang, W., Votava, P., Samanta, A., & Melton, F. (2012). Generating global leaf area index from Landsat: Algorithm formulation and demonstration. *Remote Sensing of Environment, 122*, 185-202
Gastellu-Etchegorry, J.-P., Yin, T., Lauret, N., Cajgfinger, T., Gregoire, T., Grau, E., Feret, J.-B., Lopes, M., Guilleux, J., & Dedieu, G. (2015). Discrete Anisotropic Radiative Transfer (DART 5) for

modeling airborne and satellite spectroradiometer and LIDAR acquisitions of natural and urban landscapes. *Remote Sensing, 7*, 1667-1701
Gastellu-Etchegorry, J., Martin, E., & Gascon, F. (2004). DART: a 3D model for simulating satellite images and studying surface radiation budget. *International Journal of Remote Sensing, 25*, 73-96
Goel, N.S. (1988). Models of vegetation canopy reflectance and their use in estimation of biophysical parameters from reflectance data. *Remote Sensing Reviews, 4*, 1-212
Gómez-Dans, J.L., Lewis, P.E., & Disney, M. (2016). Efficient emulation of radiative transfer codes using Gaussian processes and application to land surface parameter inferences. *Remote Sensing, 8*, 119
Govaerts, Y.M., & Verstraete, M.M. (1998). Raytran: A Monte Carlo ray-tracing model to compute light scattering in three-dimensional heterogeneous media. *IEEE transactions on Geoscience and Remote Sensing, 36*, 493-505
Hosgood, B., Jacquemoud, S., Andreoli, G., Verdebout, J., Pedrini, G., & Schmuck, G. (1995). Leaf optical properties experiment 93 (LOPEX93). *Ispra Italy'European Commission, Joint Research Centre Institute of Remote Sensing Applications*
Houborg, R., McCabe, M., Cescatti, A., Gao, F., Schull, M., & Gitelson, A. (2015). Joint leaf chlorophyll content and leaf area index retrieval from Landsat data using a regularized model inversion system (REGFLEC). *Remote Sensing of Environment, 159*, 203-221
Huang, D., Knyazikhin, Y., Dickinson, R.E., Rautiainen, M., Stenberg, P., Disney, M., Lewis, P., Cescatti, A., Tian, Y., & Verhoef, W. (2007). Canopy spectral invariants for remote sensing and model applications. *Remote Sensing of Environment, 106*, 106-122
Huang, H., Qin, W., & Liu, Q. (2013). RAPID: A radiosity applicable to porous individual objects for directional reflectance over complex vegetated scenes. *Remote Sensing of Environment, 132*, 221-237
Jacquemoud, S., Bacour, C., Poilve, H., & Frangi, J.-P. (2000). Comparison of four radiative transfer models to simulate plant canopies reflectance: Direct and inverse mode. *Remote Sensing of Environment, 74*, 471-481
Jacquemoud, S., & Baret, F. (1990). PROSPECT : A model of leaf optical properties spectra. *Remote Sensing of Environment, 34*, 75-91
Jakob, W. (2014). Mitsuba Documentation Version 0.5.0. https://www.mitsuba-renderer.org/
Lewis, P., & Disney, M. (2007). Spectral invariants and scattering across multiple scales from within-leaf to canopy. *Remote Sensing of Environment, 109*, 196-206
Li, W., Weiss, M., Waldner, F., Defourny, P., Demarez, V., Morin, D., Hagolle, O., & Baret, F. (2015). A generic algorithm to estimate LAI, FAPAR and FCOVER variables from SPOT4_HRVIR and landsat sensors: evaluation of the consistency and comparison with ground measurements. *Remote Sensing, 7*, 15494-15516
López-Lozano, R., Baret, F., Chelle, M., Rochdi, N., & España, M. (2007). Sensitivity of gap fraction to maize architectural characteristics based on 4D model simulations. *Agricultural and Forest Meteorology, 143*, 217-229
LuxCoreRender (2018). LuxCoreRender Wiki. https://wiki.luxcorerender.org/LuxCoreRender_Wiki. In
Mõttus, M., & Stenberg, P. (2008). A simple parameterization of canopy reflectance using photon recollision probability. *Remote Sensing of Environment, 112*, 1545-1551
North, P.R. (1996). Three-dimensional forest light interaction model using a Monte Carlo method. *IEEE transactions on Geoscience and Remote Sensing, 34*, 946-956
Pharr, M., Jakob, W., & Humphreys, G. (2016). *Physically based rendering: From theory to implementation*. Morgan Kaufmann

Pinty, B., & Verstraete, M.M. (1998). Modeling the scattering of light by homogeneous vegetation in optical remote sensing. *Journal of the Atmospheric Sciences, 55*, 137-150
POV-team (2013). Introduction to POV-Ray for POV-Ray version 3.7.http://www.povray.org
Qin, W., & Gerstl, S.A. (2000). 3-D scene modeling of semidesert vegetation cover and its radiation regime. *Remote Sensing of Environment, 74*, 145-162
Ross, J. (2012). *The radiation regime and architecture of plant stands*. Springer Science & Business Media
Stuckens, J., Somers, B., Delalieux, S., Verstraeten, W., & Coppin, P. (2009). The impact of common assumptions on canopy radiative transfer simulations: A case study in Citrus orchards. *Journal of Quantitative Spectroscopy and Radiative Transfer, 110*, 1-21
Suits, J. (1972). Faraday and Kerr effects in magnetic compounds. *IEEE Transactions on Magnetics, 8*, 95-105
Verger, A., Baret, F., & Camacho, F. (2011). Optimal modalities for radiative transfer-neural network estimation of canopy biophysical characteristics: Evaluation over an agricultural area with CHRIS/PROBA observations. *Remote Sensing of Environment, 115*, 415-426
Verger, A., Vigneau, N., Chéron, C., Gilliot, J.-M., Comar, A., & Baret, F. (2014). Green area index from an unmanned aerial system over wheat and rapeseed crops. *Remote Sensing of Environment, 152*, 654-664
Verhoef, W. (1985). Earth observation modeling based on layer scattering matrices. *Remote Sensing of Environment, 17*, 165-178
Verhoef, W., & Bach, H. (2007). Coupled soil–leaf-canopy and atmosphere radiative transfer modeling to simulate hyperspectral multi-angular surface reflectance and TOA radiance data. *Remote Sensing of Environment, 109*, 166-182
Verrelst, J., Muñoz, J., Alonso, L., Delegido, J., Rivera, J.P., Camps-Valls, G., & Moreno, J. (2012a). Machine learning regression algorithms for biophysical parameter retrieval: Opportunities for Sentinel-2 and-3. *Remote Sensing of Environment, 118*, 127-139
Verrelst, J., Muñoz, J., Alonso, L., Delegido, J., Rivera, J.P., Camps-Valls, G., & Moreno, J. (2012b). Machine learning regression algorithms for biophysical parameter retrieval: Opportunities for Sentinel-2 and -3. *Remote Sensing of Environment, 118*, 127-139
Verrelst, J., Rivera Caicedo, J.P., Muñoz-Marí, J., Camps-Valls, G., & Moreno, J. (2017). SCOPE-based emulators for fast generation of synthetic canopy reflectance and sun-induced fluorescence Spectra. *Remote Sensing, 9*, 927
Wang, W., Nemani, R., Hashimoto, H., Ganguly, S., Huang, D., Knyazikhin, Y., Myneni, R., & Bala, G. (2018). An Interplay between Photons, Canopy Structure, and Recollision Probability: A Review of the Spectral Invariants Theory of 3D Canopy Radiative Transfer Processes. *Remote Sensing, 10*, 1805
Widlowski, J.-L., Mio, C., Disney, M., Adams, J., Andredakis, I., Atzberger, C., Brennan, J., Busetto, L., Chelle, M., Ceccherini, G., Colombo, R., Côté, J.-F., Eenmäe, A., Essery, R., Gastellu-Etchegorry, J.-P., Gobron, N., Grau, E., Haverd, V., Homolová, L., Huang, H., Hunt, L., Kobayashi, H., Koetz, B., Kuusk, A., Kuusk, J., Lang, M., Lewis, P.E., Lovell, J.L., Malenovský, Z., Meroni, M., Morsdorf, F., Mõttus, M., Ni-Meister, W., Pinty, B., Rautiainen, M., Schlerf, M., Somers, B., Stuckens, J., Verstraete, M.M., Yang, W., Zhao, F., & Zenone, T. (2015). The fourth phase of the radiative transfer model intercomparison (RAMI) exercise: Actual canopy scenarios and conformity testing. *Remote Sensing of Environment, 169*, 418-437
Widlowski, J.-L., Robustelli, M., Disney, M., Gastellu-Etchegorry, J.-P., Lavergne, T., Lewis, P., North, P., Pinty, B., Thompson, R., & Verstraete, M. (2008). The RAMI On-line Model Checker

(ROMC): A web-based benchmarking facility for canopy reflectance models. *Remote Sensing of Environment, 112*, 1144-1150
Xiao, Z., Liang, S., Sun, R., Wang, J., & Jiang, B. (2015). Estimating the fraction of absorbed photosynthetically active radiation from the MODIS data based GLASS leaf area index product. *Remote Sensing of Environment, 171*, 105-117

3.2 In-silico comparison between turbid medium and 3D realistic based radiative transfer models to estimate GAI of wheat and maize canopies: impact of leaf clumping

Effective GAI for crops is best estimated from reflectance observations as compared to GAI and LAI

Jingyi Jiang, Marie Weiss, Shouyang Liu, Fred Baret

Abstract

The definition of LAI is important when deriving it from reflectance observation for model application and validation. Canopy reflectance and the corresponding quantities of LAI, PAI, GAI and effective GAI are first calculated using 3D radiative transfer model (RTM) and 3D wheat and maize architecture models. Conditions including different phenological stages, leaf optical properties, soil reflectance, canopy structures and sun angles are all considered. Different inversion methods including vegetation indices, 1D RTM PROSAIL and 3D RTM LuxCoreRender are compared. Results show that effective GAI is best estimated from remote sensing observations according to inversion results from 3D RTM. Inversion results from 3D model are more accurate compared with VIs and PROSAIL model with RMSE = 0.33 for wheat and RMSE= 0.47 for maize. Different sun position will affect canopy reflectance of row crop and result in different performance of inversion. 3D model is less sensitive to sun angles, while 1D model is more affected when the angle between the sun light and the row angle is close to 0° because of the difference between turbid medium assumption and realistic canopies.

Highlights

- Canopy reflectance are simulated with 3D radiative transfer model
- Effective GAI is best estimated from remote sensing observations
- 3D model inversion provides the best estimation of effective GAI
- 3D model inversion results are insensitive to sun position

1 Introduction

Leaf area index (LAI) was defined by Chen and Black (1992) as half the total developed area of leaves per unit horizontal ground area. LAI is directly involved in the vegetation functioning an is therefore widely used in agriculture, ecology or global change domains. As leaves represent the main boundary between the plant and the atmosphere, it is a key variable used to evaluate the exchanges of energy, water and carbon (Fang and Liang 2008). It also both indicates the actual plant state and its potential growth (Gonsamo 2009). However, depending on the considered applications, several definitions of LAI should be used. LAI might be relevant when related to the aboveground biomass based on allometric approaches {Baret, 1989 #149} for a given species and development stage. Conversely, the rainfall interception efficiency of the canopy need to consider all the vegetation elements including leaves, stems or all other organs, either green or senescent (Domingo et al. 1998; Martello et al. 2015), leading to the definition of the Plant Area Index (PAI). For transpiration and photosynthesis, all the green parts that potentially exchange carbon and water mainly through the stomates need to be considered (Wang and Dickinson 2012), leading to the Green Area Index (GAI) definition. Furthermore, when considering the radiation interception efficiency, the spatial arrangement of green vegetation elements need to be considered because leaf clumping may reduce the interception efficiency by the mutual masking of elements, leading to the effective GAI definition. All the processes listed previously may be described within vegetation functioning models that need to be calibrated over measurements of state variables including LAI, GAI, effective GAI or PAI. A high degree of consistency is therefore required between the definition of the state variables used in the models and that of the corresponding measurements used to calibrate the models.

LAI can be mainly accessed through direct methods that consist in measuring the area of individual leaves for all the leaves present over a given ground area. Variants of the method selects only the green active parts of the leaves, leading to the Green Leaf Area Index (GLAI), or includes the area of all the other elements independently from their color leading to PAI or restricts to the green ones leading to GAI. However, these direct measurements methods are tedious and low-throughput and at least invasive but generally destructive which explains why indirect methods are widely used (Gower et al. 1999). Indirect methods are based on optical devices that document the canopy light regime or structure from 1D to 3D techniques. The 1D techniques are based on canopy transmittance measurements using either hemispherical light sensors {Leblanc, 2005 #4285} or directional ones (Brede et al., 2018). The LAI2000 instrument {Campbell, 1988 #246} can be considered as a 1.5 D since it measures canopy transmittance from 5 directions. All these 1D or 1.5D techniques are based on the same gap fraction theory (Jonckheere et al. 2004) with the sensors placed at the bottom of the canopy. They will be sensitive to the presence of all the elements above, either green or not, and will thus be proxy of the PAI (Norman and Campbell 1989). 2D techniques are based on cameras looking either at one specific directions {Baret, 2010 #6070} or using multiple directions from multiple images or from hemispherical images (Weiss et al. 2004). Images can be taken from the bottom of the canopy to get canopy transmittance and derive PAI estimates since it is difficult to separate the green from the non-green elements. Images can be also taken from the top of the canopy to get the green fraction (GF, the fraction of green pixels in an image) by identifying the green pixels from which the GAI will be estimated. 3D techniques have been also developed more recently using terrestrial laser scanners (Liu et al. 2017; Yan et al. 2019) or stereovision (Biskup et al. 2007). The resulting 3D point clouds are exploited to get the directional canopy transmittance and derive the corresponding PAI if no distinction is made between the green and non-green elements, or to get the directional green fraction leading to GAI estimates when the green points are identified. However, the transformation of the measured directional gap or green fraction into PAI or GAI is generally based on some assumptions on the canopy structure, particularly regarding leaf arrangement. One of the main assumption used considers leaves as randomly distributed within the canopy volume. A distinction is thus made between the true PAI or GAI and

the corresponding “effective” values that are derived from gap or green fraction measurements assuming that leaves are randomly distributed (Nilson 1999; Fang et al. 2018).

Similarly to indirect optical ground measurements, PAI and GAI can also be retrieved from reflectance observations using empirical or physically based methods. Empirical methods consist in calibrating relationships between a combination of reflectance in several wavebands and ground measured LAI. The most common method is the use of spectral vegetation indices (Richardson et al. 1992; Broge and Leblanc 2001; Broge and Mortensen 2002; Liu et al. 2012). However, machine learning techniques now allow to build more robust and accurate relationships providing that the data used to train the algorithms represents well the domain of application (Camacho et al, 2017). Conversely, physically based methods consist in inverting a Radiative Transfer Model (RTM) that simulates the actual physical processes involved in the photon transport within the canopy (Strahler 1997). Inversion techniques such as optimization (Jacquemoud et al. 2000), Look-Up-Tables (LUT) (González-Sanpedro et al. 2008; Duan et al. 2014) or machine learning (Weiss et al. 2002; Verrelst et al. 2012) are used to estimate the RTM input variables including PAI or GAI. The accuracy of such methods depends on the ability of the model to simulate realistically the reflectance of the targeted canopy given a description of the architecture of the canopy and the optical properties of its elements. 1D RTM such as PROSAIL {Jacquemoud, 2009 #4539} assume that the canopy is a horizontally homogeneous layer of randomly distributed leaves. Inverting 1D RTM has the advantage of being computationally efficient and characterized by a low number of inputs, which eases the setting of numerical experiments and constrains the possible ambiguities between variables during the inversion process (Baret and Buis 2008). However, several 3D radiative transfer models were developed to get more realistic simulations of canopy reflectance: they combine an explicit 3D description of the canopy architecture while accounting for the differences in optical properties of the several vegetation elements. However, the higher number of parameters and variables required and computer demanding simulations explains why 1D RTM are still mainly used within RTM inversion. Nevertheless, 3D RTMs such as FLIGHT (North 1996) based on Monte Carlo ray tracing methods or DART (Gastellu-Etchegorry et al. 2004) based on the discrete ordinate methods have already been used to retrieve canopy structure and biochemical variables from remote sensing data (Gascon et al. 2004; Malenovský et al. 2013; Banskota et al. 2015; Hernández-Clemente et al. 2017). Such 3D models are inverted using LUT or machine learning techniques. However, the large computation effort required to populate the LUT or the training dataset with these 3D RTMs simulations, combined with the larger number of variables required for a 3D description as compared to 1D RTMs explains why the space of canopy realizations is generally poorly sampled, resulting into possibly less robust PAI or GAI estimates.

The objective of this study is to evaluate the estimation performances of LAI, PAI, GAI and effective GAI when retrieved from top of canopy reflectance observations. We focused on wheat and maize at different phenological stages to get contrasted architectures. Realistic 3D wheat and maize scenes were generated and used to simulate the corresponding reflectance observations. Part of the simulations were considered as pseudo measurements used to evaluate the retrieval performances. The other part was used to populate a training dataset used to calibrate the RTM inversion method. We then compared the performances of several retrieval methods including vegetation indices (VIs), neural networks applied to 1D RTM PROSAIL (Jacquemoud et al. 2009) and 3D RTM LuxCoreRender (LuxCoreRender 2018) for LAI, PAI, GAI and effective GAI canopy variables.

2 Material and methods

2.1 The 3D crop architecture models

We selected two contrasted species: wheat with narrow and long leaves with small spacing between rows and plants, and maize with taller plants, larger leaves and stems and larger row and plant

spacing. While wheat canopies evolves from a clear row structure at early stages to a structure more similar to a turbid medium later in the vegetation cycle, maize canopy is characterized by a row structure at any phenological stage. Leaf inclination also varies differently during the growth cycle for these two species.

The 3D ADEL-Wheat model (Fournier et al. 2003) was selected to simulate the time course of the 3D architectural growth of wheat. It is an up-to-date model calibrated over a range of experimental conditions (Abichou et al. 2013). For maize, we used the 3D model created by López-Lozano et al (2007) where plants are described by simple geometric shapes (triangles for leaves and pyramids for stems), their growth being driven by thermal time. Even though this model does not account for leaf undulation and curvature, maize canopies are much better represented than when using a turbid medium model (Casa et al. 2010). As little knowledge is available on ear and flowers optical properties, both wheat and maize were simulated from emergence to the last stage before earing (wheat) or male flowering (maize). Therefore, for maize, as senescent leaves appear after male flowering, PAI and GAI will be equal, which is not the case for wheat. For both species, 810 canopies were generated according the variables listed in Table 11. The range of values considered for the input variables were derived from previous experiments (López-Lozano et al. 2007; Abichou et al. 2013; Liu et al. 2017). Each input variables was varied between the minimum and maximum values by a number of equal steps (Table 1). The corresponding LAI, PAI and GAI were calculated from the mock-ups for nine development stages evenly distributed within the 100 to 900°Cd for wheat, and from 150 to 950°Cd for maize. Since around 40% canopies have the GAI smaller than 1, 160 canopies with GAI<1 were randomly eliminated from the wheat and maize canopies. The distribution of GAI and average leaf angle (ALA) of simulated scenes are shown in

and examples of resulting scenes are provided in Figure 25.

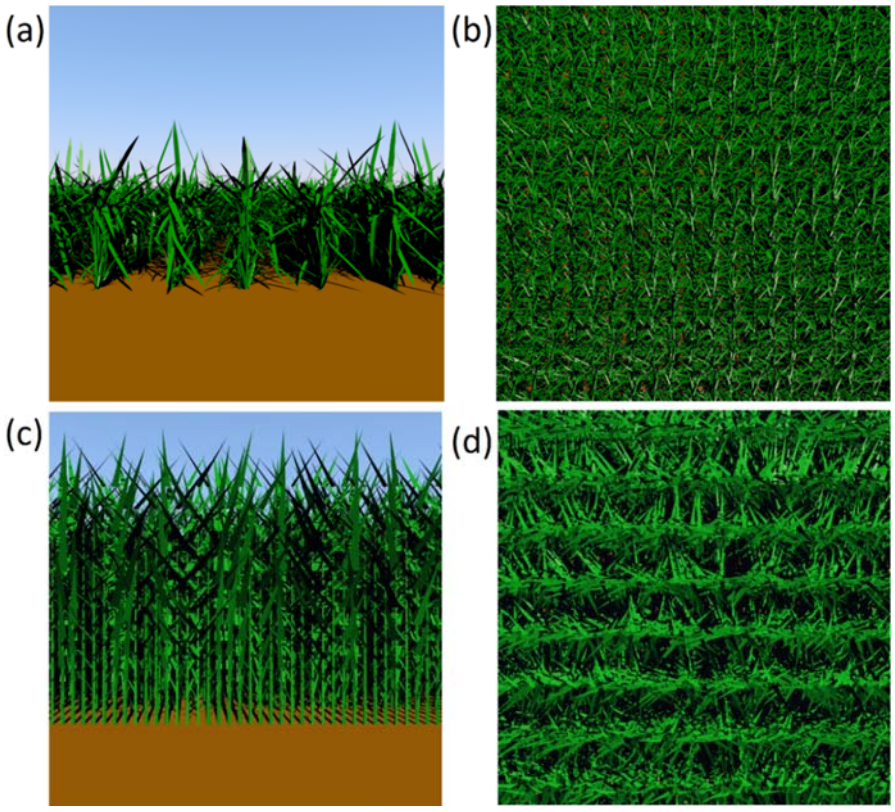

Figure 25 Typical 3D scenes of wheat ((a) front view; (b) top view) and maize ((c) front view; (d) top view) canopy simulated with ADEL-Wheat (LAI=2.26, GAI=2.34, effective GAI=2.15, PAI=2.56) and 3D maize models. (LAI=4.78, GAI=6.51, effective GAI=4.12, PAI=6.51)

Table 11 Parameters of ADEL-Wheat and 3D maize model used in this study.

	Variables		Unit	Min	Typical	Max	Steps
ADEL-Wheat	D	Plant density	plants/m^2	150	250	350	3
	N_{tiller}	Number of tillers per plant	-		3		1
	$N_{leaf.main}$	Number of leaves on the main stem	-		11		1
	TT_{phy}	Phyllochron	°Cd	80	100	120	3
	L_{lamina}	Length of lamina one	cm	8	12	16	3
	Ang_{shift}	Rotation of leaf basal inclination	°	-30	0	30	3
	Ang_{tiller}	Inclination of the base of the tiller	°		20		1
3D Maize Model	D	Plant density	plants/m^2		9 (typical 0.75???)		1
	d_{rows}	Distance between rows	m	0.6	0.7	0.8	3
	N_{max}	Maximum number of leaves per plant	-	18	20	22	3
	TT_{phy}	Phyllochron	°Cd		?		1
	S_{max}	Maximum leaf area per plant	m^2	0.5	0.75	0.7	3
	H_{max}	Maximum plant height	m		2		1
	Θ_{max}	Inclination of largest leaf	°	30	60	60	3

2.2 Reflectance simulations

2.2.1 LuxCoreRender ray tracing model

Canopy reflectance was simulated using the LuxCoreRender 3D render engine (LuxCoreRender 2018) based on 3D scenes generated by the crop architecture models. LuxCoreRender is an open source software derived from the PBRT project (Pharr et al. 2016; LuxCoreRender 2018). It has been validated using RAMI Online Model Checker (ROMC) (Widlowski et al. 2008) against a set of state-of-the-art models (Jiang et al, 2018).

We used the LuxCoreRender ray-tracing integrator with 1.36×10^3 samples of light and 16 path depths per pixel to guarantee the accuracy of the render of the simulated reflectance. Leaves were assumed lambertian and characterized by their reflectance and transmittance, while the stem is characterized by the same reflectance as the leaf with no transmittance. The soil was assumed flat and lambertian. The sun was the only light source with no adjacency contributions nor diffuse radiation. The scene was corresponding to a square of 4.5 m side to represent the average condition of the canopy. It was replicated three times to minimize possible border effects. The bidirectional reflectance factor was computed as the ratio of reflected photons in the view direction to those reflected by a perfect lambertian scatterer placed horizontally under the same illumination conditions.

2.2.2 Canopy reflectance simulations

Six wavelengths were selected to mimic Sentinel 2 bands in the visible and near infrared: 450 nm, 560 nm, 665 nm, 705 nm, 740 nm and 865 nm. Since reflectance simulation with LuxCoreRender is time consuming because of the ray-tracing process, we used the method proposed by Jiang et al (2018) to speed up the computations: for a given canopy structure and observational configuration, it allows to accurately compute canopy reflectance for any soil reflectance and any leaf properties (wavelength and biochemical composition) by simulating canopy reflectance for two contrasted backgrounds and six value of the absorption coefficient of the leaf that drives leaf reflectance and transmittance.

For each of the 650 scenes considered for each crop (Table 1), the camera was set at nadir (View Azimuth Angle (VAA) = 0° and View Zenith Angle (VZA) = 0°) while the sun position varied by considering eight Sun Zenith Angles (SZA) and four Sun Azimuth Angles (SAA) defined relatively to the row orientation (Table 2). Five typical soil spectra with a variability in soil brightness (B_s) were simulated to represent a large range of soil background. The leaf and stem optical properties were simulated using the PROSPECT3 model (Jacquemoud and Baret 1990; Baret and Fourty 1997) by considering the contents of four main absorbing element: chlorophyllian pigments (C_{abc}), dry matter (C_{dm}), water (C_w) and brown pigments (C_{bp}). Their distribution laws were defined similarly to (Li et al. 2015).

There were totally 37500 cases (Table 2) for each scene. To build learning database with mixed sun angles, one of the 20 geometry settings was randomly selected for each case. 70% of the 33750 cases with mixed geometry settings were selected as the learning database and the remaining of the whole cases was kept as the validation database.

Table 12 Distribution of input variables used to generate canopy reflectance with 3D simulations.

		Input variable	Minimum	Maximum	Mode	Std	Nb_Class	Law
	Observation geometry	VZA(°)	0					
		VAA(°)	0					
		SZA(°)	20, 35, 50, 65					
		SAA(°)	0, 25, 45, 67, 90					
Li et al, 2015 Jiang et al, 2018, Koetz et al, 2005	**Leaf optical properties**	Refractive Index n	1.4					
		Mesophyll, N	1.5					
		C_{ab}(µg.cm^{-2})	20	90	45	30	5	Gauss
		C_{dm}(g.cm^{-2})	0.003	0.011	0.005	0.005	5	Gauss
		C_w_Rel	0.6	0.85	0.75	0.08	5	Uniform
		C_{bp}	0.0	2.0	0.0	0.3	3	Gauss
	Soil background	B_s	0.5	3.5	1.2	2.0	5	Gauss

2.3 Effective GAI computation

This definition of the effective GAI should be consistent with what could be derived from indirect techniques at the ground level such as hemispherical images (Weiss et al. 2004).The effective GAI (GAI_{eff}) was therefore computed from Welles and Norman (1991) which corresponds to a close approximation of the Miller's formula (Miller 1967) that relates GAI to the directional green fraction, assuming that the leaves are randomly distributed in the canopy volume. The green fraction was simulated by LuxCoreRender for six view zenith angles spanning from 0° to 60° and averaged over all the azimuths.

2.4 1D PROSAIL simulations

The PROSAIL model (Baret et al. 1992) was generated from the combination of the leaf optical properties model PROSPECT (Jacquemoud and Baret 1990) and the SAIL (Scattering by Arbitrary Inclined Leaves) canopy reflectance model (Verhoef 1984) which assumes the canopy as a turbid medium, i.e. homogeneous infinitely extended horizontal layer of infinitely small leaves randomly distributed. A hotspot parameter was introduced by Kuusk et al. (1985) to account for the fact that leaves have finite dimensions. PROSAIL has been widely used to estimate canopy biophysical and structural variables for applications at different scales (Jacquemoud et al. 2009). PROSAIL was inverted by training Neural Networks as proposed by Li et al. (2015). This technique was applied to decametric resolution (Weiss et al. 2002) and exploited operationally to derive kilometric resolution (Baret et al. 2007) or decametric (Li et al. 2015; Delloye et al. 2018; Verrelst et al. 2018) biophysical products.

A dataset was first populated with PROSAIL model simulations using distribution of the input variables consistent with what was previously done with the 3D models (Table 2). The distribution of canopy structure variables (Table 13) were also consistent with those used previously for the 3D models (Figure to1). A total of 33750 cases were simulated for both wheat and maize with input variables and output reflectance. 70% of the whole cases were randomly selected as the 1D training database.

Table 13 Distribution of input variables used to generate the learning database with PROSAIL model. HOT is the hotspot parameter that partly controls the fact that leaves have finite dimensions and are not fully randomly distributed.

	Input variable	**Minimum**	**Maximum**	**Mean**	**Std**	**Class**	**Law**
Canopy structure	GAI	0.0	8.0	2.0	3.0	6	Gauss
	ALA (°)	30	70	45	30	3	Gauss
	hotspot	0.1	0.5	0.2	0.5	1	Gauss

2.5 Retrieval methods

2.5.1 VI based empirical retrieval

Many vegetation indices based on the combination of a few spectral bands have been developed to retrieve variables related to the plant photosynthetic activity, such as GAI, fAPAR, and chlorophyll content (Myneni et al. 1995). We selected three vegetation indices among those proposed in the literature (Henrich et al. 2009): the Normalized Difference Vegetation Index (NDVI) (Rouse Jr et al. 1974) which is the most widely used, the optimized Soil-Adjusted Vegetation Index (OSAVI) (Rondeaux et al. 1996) which was designed to minimize the effect from the soil background, and finally, the modified triangular vegetation index (MTVI2) which was found less sensitive to the

saturation effect and thus provides more accurate estimates of high GAI values while reducing the influence of the soil background (Haboudane et al. 2004).

$$NDVI = \frac{\rho_{NIR}-\rho_{red}}{\rho_{NIR}+\rho_{red}} (2)$$

$$OSAVI = \frac{\rho_{NIR}-\rho_{red}}{\rho_{NIR}+\rho_{red}+0.16} (3)$$

$$MTVI2 = 1.5\frac{1.2(\rho_{NIR}-\rho_{red})-2.5(\rho_{red}-\rho_{green})}{\sqrt{(2\rho_{NIR}+1)^2-(6\rho_{NIR}-5\sqrt{\rho_{red}})-0.5}} (4)$$

To relate VIs to different definitions of LAI, the modified version of Beer's Law describing VI as a function of the foliage amount F (Baret and Guyot, 1991) was selected:

$$VI = VI_\infty + (VI_g - VI_\infty)exp^{K_{VI}F} (5)$$

where F refers either to LAI, GAI, PAI or effective GAI. VI_∞ represents the VI value for very high density canopy ($F \rightarrow \infty$) and VI_g represents the VI value of bare soil ($F = 0$); K_{VI} is equivalent to the extinction coefficient in Beer's Law. Parameters $[VI_\infty,\ VI_g,\ K_{VI}]$ are fitted with the learning database generated from the 3D LuxCoreRender simulations using a robust regression.

2.5.2 Model inversion using neural networks

For both training database generated from 3D simulations and the PROSAIL model, a simple back-propagation neural networks (NN) with the same architecture as in Li et al. (2015) was selected. The inputs include the canopy reflectance in six bands and the geometrical configurations: the cosine of VZA, the cosine of SZA and the cosine of relative azimuth angle between VAA and SAA. The outputs are either LAI, PAI, GAI and effective GAI for the 3D model. For PROSAIL, the only outputs are the GAI that equals LAI (no other elements than the leaves), PAI (no senescent elements) and effective GAI (turbid medium assumption).

2.6 Performance metrics

As validation, the validation database generated from 3D simulation was used to evaluate the inversion results from NNs trained with 1D and 3D training database.The root mean square error (RMSE) and the coefficient of determination (R^2) are used to evaluate the agreement of the fit between the original VI value and the fitted one.

3 Results

3.1 Impact of canopy structure assumptions on reflectance

To put emphasis on the canopy structure, we simplified the simulations by assuming that the reflectance of canopy elements and soil background do not vary with time (Table 14). The camera was at nadir with SZA=45° and SAA=0°, 45° and 90°.

We then considered the presence or absence of stems and yellow leaves to evaluate the contribution of these organs to canopy reflectance. Using the ADEL-Wheat and the 3D maize architecture model, we found that the stem area is null for the early stages, e.g. during the development of the first leaves (thermal time less than 300°Cd), wheat stem area is in general smaller in proportion than for maize (Figure 26).

Table 14 Optical properties of the different parts of the plants and the soil in the red and NIR taken for the standard maize and wheat stands.

	Reflectance		Transmittance	
	Red	**NIR**	**Red**	**NIR**
Green leaf	0.063	0.463	0.018	0.522
Stem	0.063	0.463	0.000	0.000
Senescent leaf	0.347	0.474	0.287	0.432
Soil	0.140	0.191	-	-

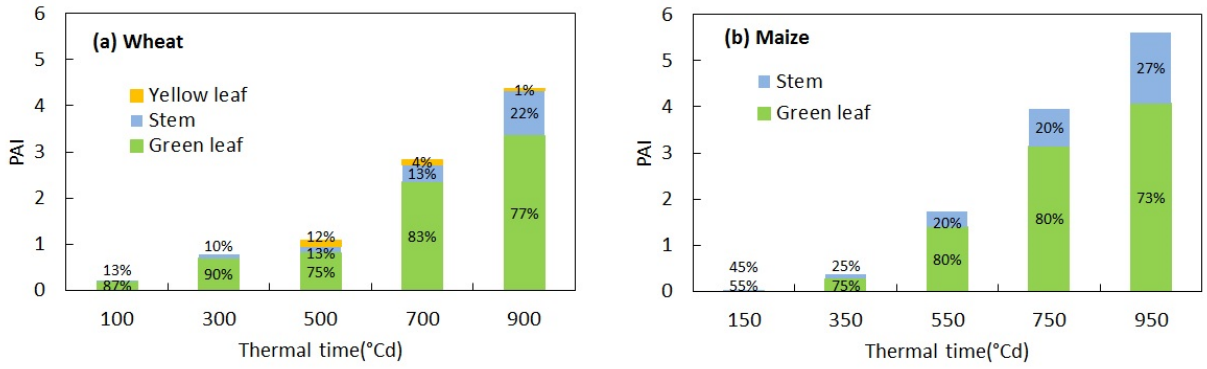

Figure 26 PAI and the proportion of green leaves (green), yellow leaves (yellow) and stems (blue) of typical (a) wheat and (b) maize canopies during the growing stages.

shows the LuxCoreRender simulated canopy reflectance by considering the presence of green stems or not in the red and NIR domains for the considered SAA values. Results showed that the stems had almost no influence on canopy reflectance in the red domain (Figure 27a and Figure 27c) especially when the soil contribution is the highest (SAA=0°). This is explained by the low value of leaf and stem reflectance and transmittance. Conversely, in the NIR domain, stems showed significant impact on canopy reflectance, particularly for the later stages when the contribution of stems to PAI increases (Figure 27b and Figure 27d). The decrease of canopy reflectance due to the stems is mainly explained by the strong stem absorption (null transmittance) that decreases the multiple scattering.

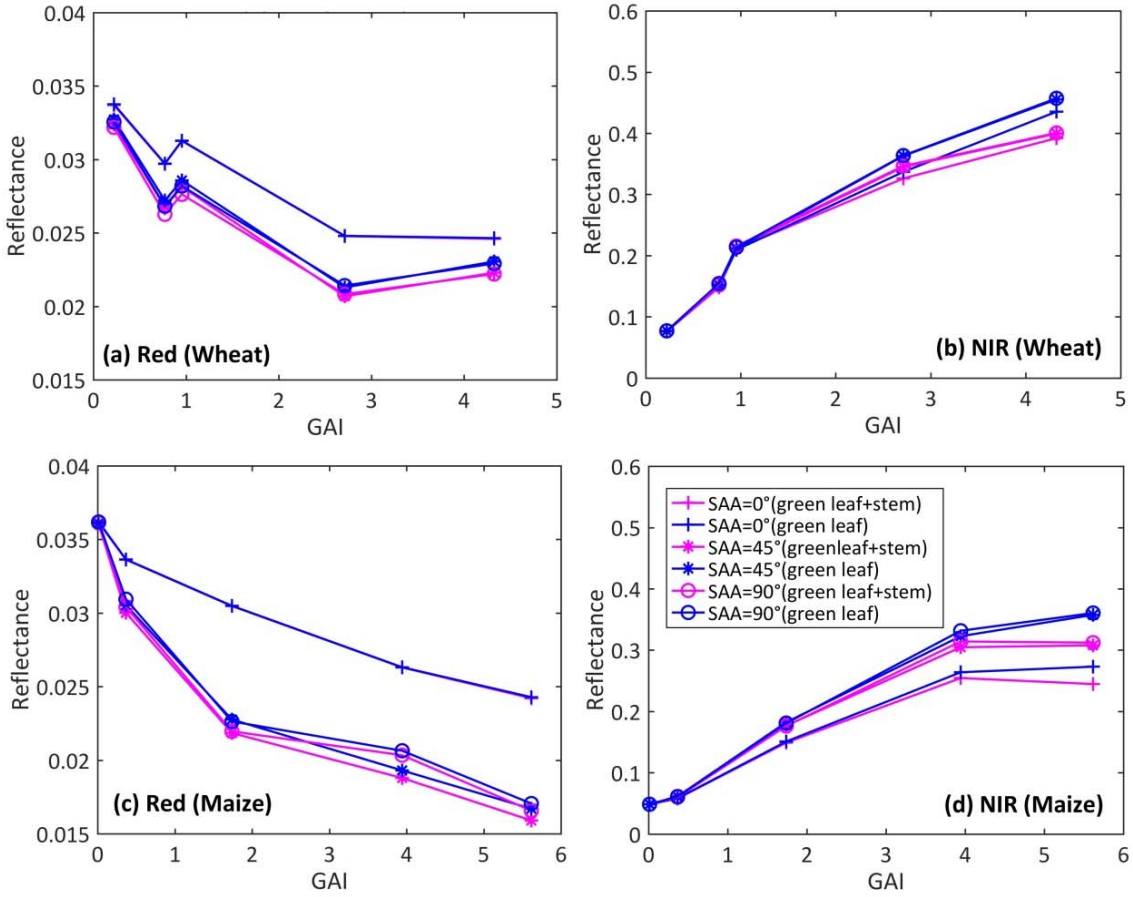

Figure 27 Comparison of canopy reflectance (3D structure) between canopy with leaves and stems (red) and canopy with only leaves (blue) in red and NIR. VZA = 0°, VAA = 0°, SZA = 45°, SAA = 0° (+), 45° (*) and 90° (◯). (a) wheat in red (b) wheat in NIR (c) maize in red (d) maize in NIR.

To perform a fair comparison between the turbid medium (e.g. 1D) assumption and the 3D crop architecture modelling, LuxCoreRender was used to simulate a turbid medium with the same canopy leaves and stems, but distributing them randomly in the canopy volume, while keeping their orientation. For both wheat and maize (Figure 28), the 1D reflectance is independent from the sun azimuthal position, while the 3D reflectance shows significant variations with sun azimuth, especially when the sun is parallel to the row direction (SZA=45°). In the NIR (Figure 28b and Figure 28d), the 1D reflectance is always higher than the 3D one. This is mainly due to a higher multiple scattering linked to a higher probability for a photon to interact with a leaf in the absence of clumping (Duthoit et al. 2008). Conversely, in the red domain (Figure 28a and Figure 28c) where the canopy reflectance is low, small differences are observed. The 1D reflectance is slightly smaller than the 3D one when the sun is in the row direction since there is a higher proportion of soil illuminated between the rows and soil reflectance is higher than that of the leaf. With the increasing of SAA, the 3D simulation in red decreases and is lower than 1D simulation, mostly because of the increasing fraction of shadowed soil and leaves seen. As expected, when canopy develops, the difference in reflectance between 1D and 3D assumptions increases for maize while remaining almost constant for wheat. This demonstrates that, conversely to maize, for the latest stages, the structure of the wheat canopy becomes closer to a turbid medium and the row effect is decreasing.

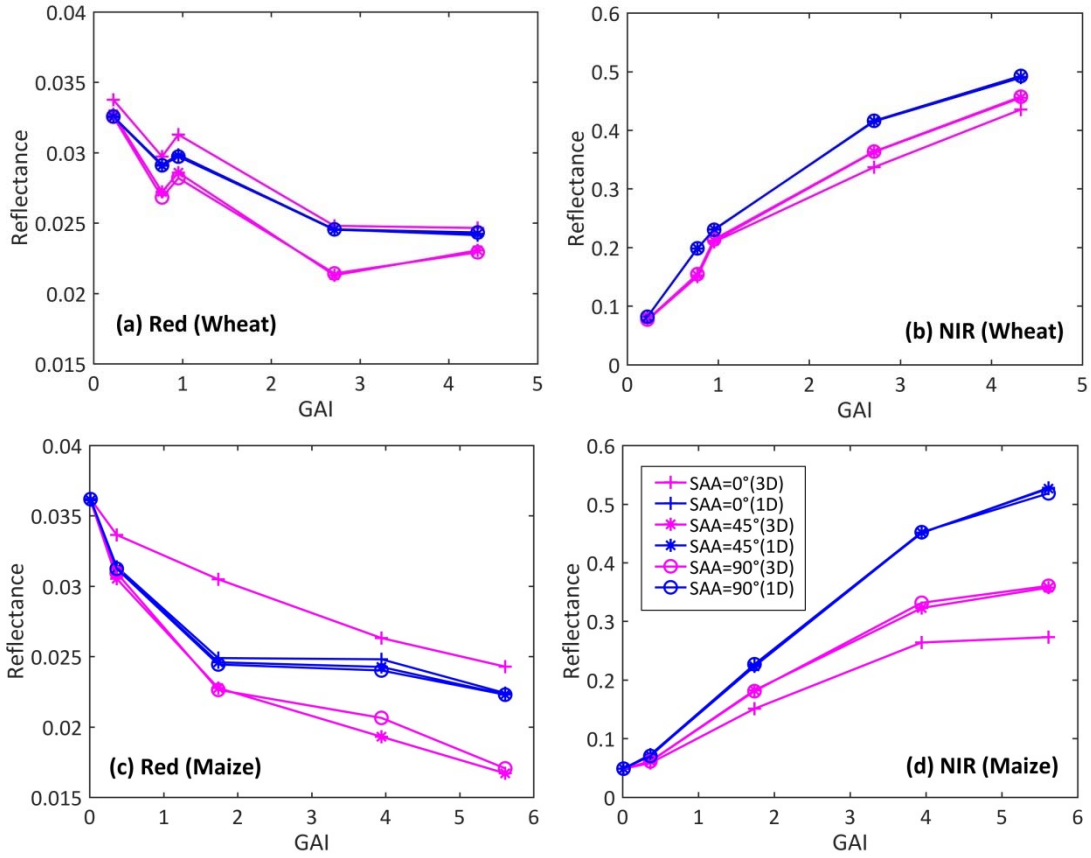

Figure 28 Comparison of canopy reflectance between turbid medium assumption (red) and 3D realistic structure (blue) in red (left) and NIR (right) for wheat (top) and maize (bottom). VZA = 0°, VAA = 0°, SZA = 45°, SAA = 0° (+), 45° (*) and 90° (◯).

3.2 Calibrating the relationships between VI and effective GAI

Based on Eq. 5, the relationship between VI and effective GAI are fitted using robust regression for each sun zenith and azimuth angles, or when using all the sun angles together. For both wheat and maize, the fixed sun angles improve the fitted results with higher R^2 for most sun angles (Table 15). More uncertainties are introduced with increasing SZA and decreasing of SAA. Performances for maize are more sensitive to the SZA than wheat canopies, which is explained by the more obvious row structure of maize. Even though both OSAVI and MTVI2 are reported with less sensitivity with soil backgrounds and canopy structure (Liu et al. 2012; Nguy-Robertson et al. 2012), OSAVI shows the similar R^2 as MTVI2 for wheat and better fitting accuracy for maize.

Table 15 The coefficient of determination (R^2) of robust regression between effective GAI and VIs (NDVI, OSAVI and MTVI2). VIs are calculated from reflectance with specific sun angle from learning database, or all the sun angles.

SZA / SAA		NDVI				OSAVI				MTVI2			
		20°	35°	50°	65°	20°	35°	50°	65°	20°	35°	50°	65°
Wheat	0°	0.87	0.87	0.87	0.86	0.96	0.96	0.96	0.96	0.96	0.96	0.96	0.96
	25°	0.87	0.88	0.86	0.76	0.96	0.97	0.96	0.93	0.96	0.96	0.96	0.94
	45°	0.88	0.88	0.83	0.73	0.97	0.97	0.96	0.91	0.97	0.97	0.96	0.93
	67°	0.88	0.87	0.82	0.73	0.97	0.97	0.95	0.90	0.97	0.97	0.96	0.93
	90°	0.88	0.87	0.82	0.73	0.97	0.97	0.95	0.90	0.97	0.97	0.96	0.93
	All angles	0.77				0.91				0.93			
Maize	0°	0.87	0.87	0.87	0.87	0.88	0.88	0.89	0.90	0.83	0.84	0.86	0.87
	25°	0.92	0.94	0.93	0.91	0.90	0.94	0.95	0.93	0.85	0.89	0.92	0.91
	45°	0.94	0.94	0.93	0.91	0.93	0.94	0.95	0.93	0.88	0.90	0.92	0.90
	67°	0.94	0.94	0.93	0.91	0.93	0.94	0.95	0.93	0.89	0.90	0.93	0.91
	90°	0.94	0.94	0.93	0.91	0.93	0.94	0.95	0.93	0.89	0.90	0.93	0.91
	All angles	0.84				0.87				0.82			

4 Discussion

4.1 Effective GAI is best estimated using 3D structure description

Estimation results based on 3D model inversion were calculated from NN trained over learning database simulated from 3D model and corresponded LAI, GAI, PAI and effective GAI. As validation, validation database was applied and results were evaluated in Figure 29 for wheat and Figure 30 for maize. Since no yellow leaves are considered in 3D maize model, only LAI and GAI are showed for maize canopy. When only green parts are considered (Figure 29b, RMSE = 0.51), the estimation based on canopy reflectance performs slightly better than adding yellow leaves (Figure 29c, RMSE = 0.53). This is consistent with **错误!未找到引用源。** where almost no contribution is found when yellow leaves are cantered at the bottom layer of canopy. Since GAI and PAI have larger range compared with LAI, adding stem area does not improve the estimation and result in the increase of RMSE (Figure 29c and Figure 30b). However, when plant clumping is considered, the estimation of effective GAI showed the best performance with the highest R^2 and the smallest RMSE (RMSE = 0.33, R^2 = 0.95 for wheat and RMSE = 0.47, R^2 = 0.90 for maize). Therefore, based on the canopy reflectance simulated from 3D crop architectures, effective GAI is more related to remote sensing observations.

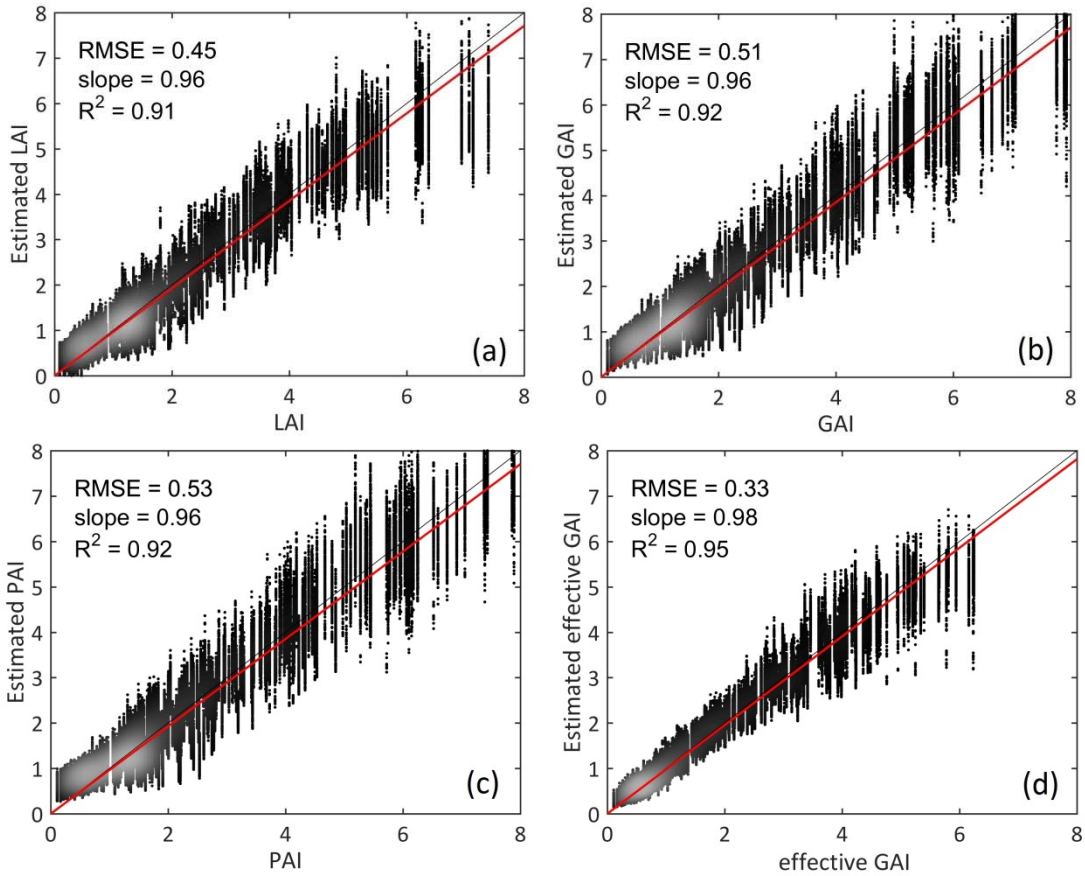

Figure 29 Scatter plots between estimated results from NN trained over 3D model simulations and (a) LAI (b) GAI (c) PAI and (d) effective GAI for wheat. The grey level intensity increases with the density of points. The black line corresponds to the 1:1 line. The red line is the best linear fit with no intercept.

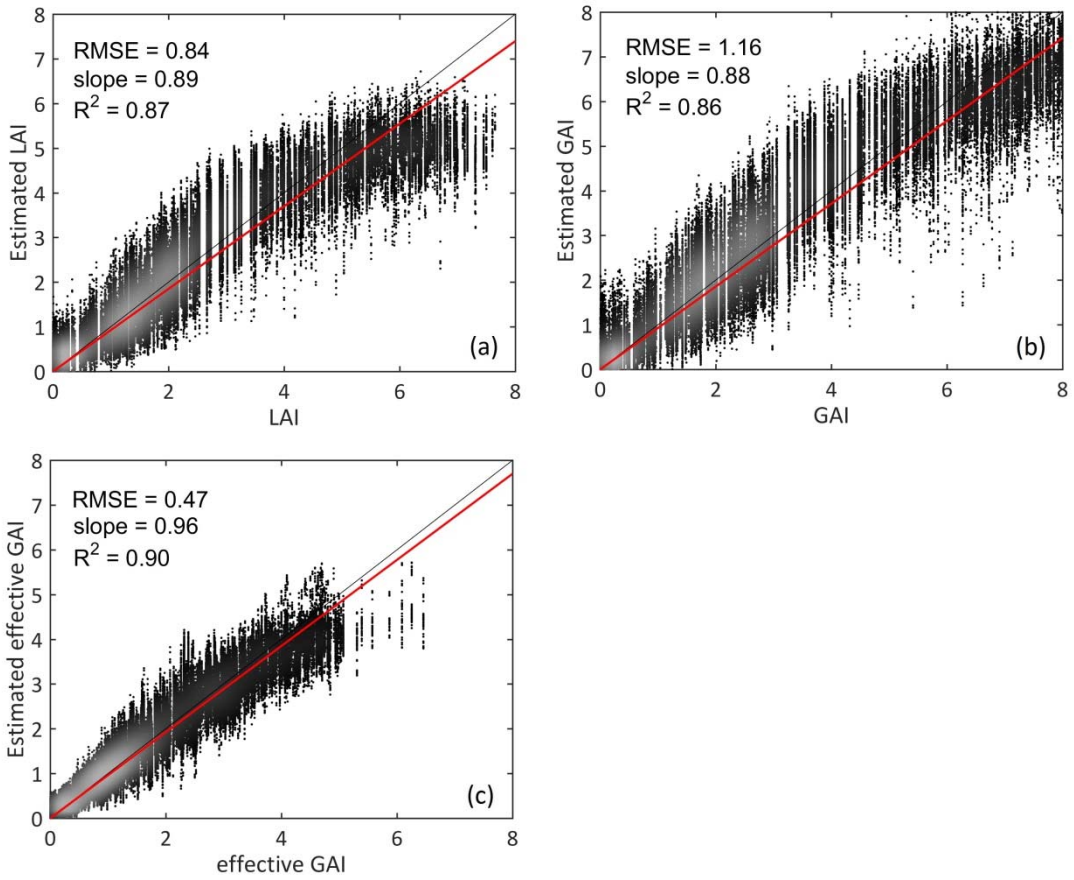

Figure 30 Scatter plots between estimated results from NN trained over 3D model simulations and (a) GAI (b) GAI and (c) effective GAI for maize. The grey level intensity increases with the density of points. The black line corresponds to the 1:1 line. The red line is the best linear fit with no intercept.

4.2 3D description improves estimates of effective GAI as compared to 1D structure description

Based on the NN trained by database from PROSAIL model, the estimated results from validation database were compared with effective GAI. For both wheat and maize, estimation results from 3D structure description (Figure 29d and Figure 30c) perform better than that from 1D structure description (Figure 31, RMSE = 0.64, R^2 = 0.86 for wheat and RMSE = 0.79, R^2 = 0.77 for maize) with higher R^2 and lower RMSE. Compared with estimated effective GAI from NN trained over 3D model, the underestimations were observed for both types when effective GAI were higher than 4. For effective GAI lower than 4, the estimated effective GAI from PROSAIL model show good agreements with effective GAI for wheat (Figure 31a), while comparatively more outliers appear for maize. Similar results are observed from (Duveiller et al. 2011) (Camacho et al, 2017) where training dataset is both simulated from PROSAIL model and are compared with measured effective GAI or derived ground GAI. Underestimation is observed for both wheat and maize when effective GAI is larger than 4. Reasons come from the hypothesis of 1D RTM where canopy is assumed to be homogeneous. Clumping is not taken into account for irregular distributed canopy and lead to GAI underestimation, especially for higher effective GAI values.

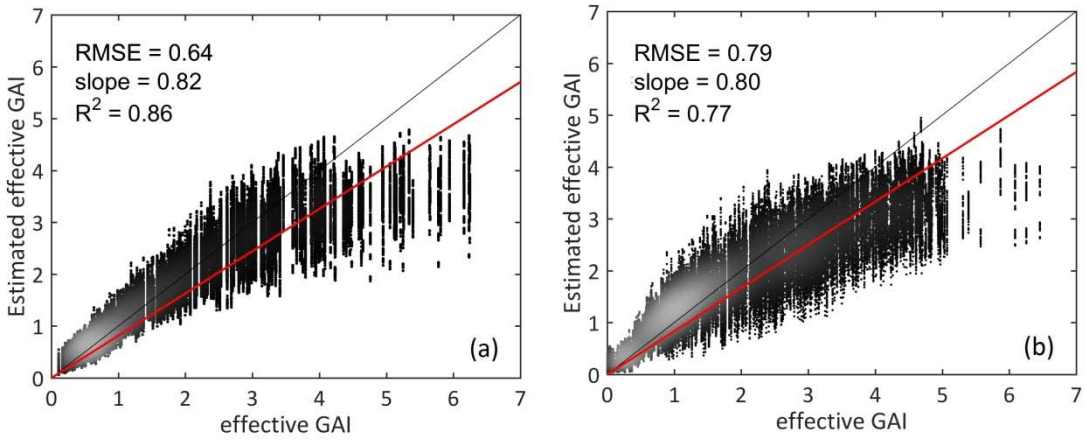

Figure 31 Scatter plots between estimated effective GAI from NN trained over PROSAIL model simulations and effective GAI for (a) wheat and (b) maize. The grey level intensity increases with the density of points. The black line corresponds to the 1:1 line. The red line is the best linear fit with no intercept.

4.3 Radiative transfer inversion performs better than using simple vegetation indices

Different VIs (regressed using canopy reflectance with mixed angle or fixed angle) were validated using the validation database from 3D simulations. The estimated effective GAI from VIs were compared with effective GAI (Table 16). VIs with fixed angle provide better estimation than VIs with mixed angles. For wheat, the estimation from MTVI2 is slightly better than OSAVI with RMSE = 0.96 and R^2 = 0.73 for mixed angle. For maize, OSAVI provides better estimation with smaller RMSE for mixed angle, while MTVI2 improves a little bit when fixed angle is applied. But compared with estimated results from radiative transfer inversion, simple VIs with fixed angle still have larger RMSE and smaller R^2. Even though different VIs showed good performance in previous studies (Liu et al. 2012; Kross et al. 2015; Corti et al. 2018), regression parameters as well as estimated accuracy are different when conditions like location, cultivar and phenological stages are changed. For simulated database in this study, larger ranges of optical properties, soil brightness and canopy structures were added. More changes of variables limit the application of simple VIs.

Table 16 Comparison between effective GAI and estimated effective GAI from VIs (NDVI, OSAVI and MTVI2), PROSAIL model and 3D model using the coefficient of determination (R^2) and the root mean square error (RMSE). Learning and validation database with mixed sun angles are applied.

	Wheat				**Maize**			
	RMSE		**R^2**		**RMSE**		**R^2**	
	Mixed angle	Fixed angle	Mixed angle	Fixed angle	Mixed angle	Fixed angle	Mixed angle	Fixed angle
NDVI	1.33	0.85	0.53	0.70	1.39	1.28	0.41	0.43
OSAVI	1.01	0.74	0.73	0.80	1.15	1.11	0.47	0.53
MTVI2	0.99	0.73	0.76	0.82	1.31	1.06	0.57	0.64
PROSAIL	0.64		0.86		0.79		0.77	
3D	0.33		0.95		0.47		0.91	

4.4 3D model inversion results are insensitive to sun position

The bidirectional reflectance distribution function (BRDF) of canopy reflectance is important to relate multi-angle remote sensing data to retrieve biophysical parameters (Liang and Strahler 1993). When the view angle is fixed at nadir, changing of sun position results in the variation of canopy reflectance with different proportion of the sunlit and shadowed regions in the row crops (Lord et al. 1988; Zhao et al. 2010).

For VIs, even though studies have proved that the influence of SZA on variability of VIs is relatively small especially for especially for later stages (Liu et al. 2012), it is significantly depends on SAA respect to row orientation. Take OSAVI of wheat canopy as an example, when sun direction is parallel to crop row, the VI-effective GAI relationship is quite independent from SZA (Figure 32a). But when sun direction is perpendicular to the row, larger variation is caused because of the larger changes of the proportion of sunlit and shadows areas. For different SZAs, the smaller it is, the less effect in canopy reflectance is caused by the row crop structure (Figure 32b).

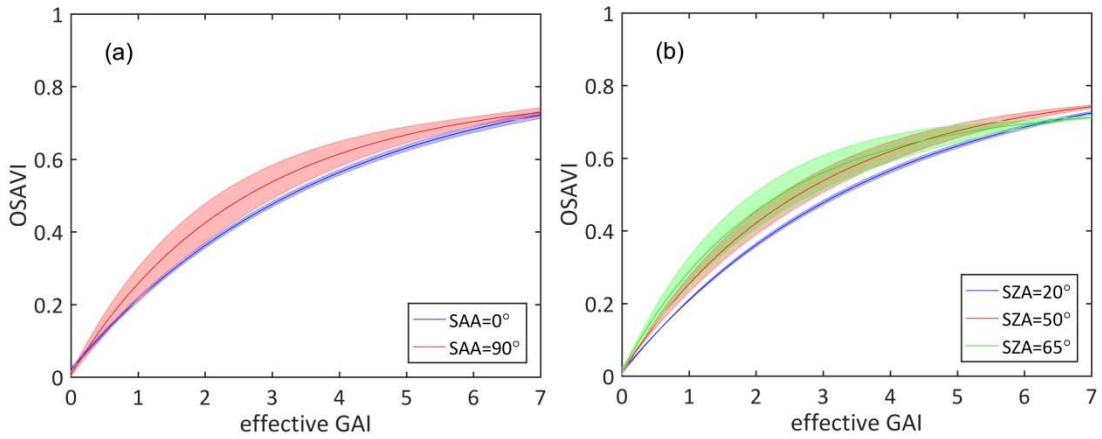

Figure 32 Mean value (solid line) and standard deviation (shadow face) of best-fit functions between (a)OSAVI and effective GAI with different SZAs (SZA = 20°, 35°, 50° and 65°) (b) OSAVI and effective GAI with different SAAs (SAA = 0°, 25°, 45°, 67° and 90°) from learning database for wheat.

For PROSAIL model, the BRDF effect is considered with input geometrical configurations and hot spot parameters. Nevertheless, the assumptions based on turbid medium distribution of leaves are different from row crops which show more clumped organization. Therefore, some sun positions will enhance this difference and result in the miscalculation of effective GAI values. RMSE between effective GAI and estimates from NN trained with PROSAIL and 3D simulations with specific sun angles are showed in Figure 33. For 3D simulations, inversion results are almost insensitive to sun position with RMSE around 0.3 for wheat and 0.4 for maize when SZA changing from 20° to 50° regardless of SAA. With the increasing area of shadowed leaves when SZA is quite large (SZA= 65°) or SAA is closer to 0°, some uncertainties are introduced because of the less observed radiation from leaves. For results from PROSAIL simulations, wheat canopy which is closer to ransom distribution of leaves shows less variation and higher accuracy compared with maize canopy. Even though errors would be introduced when SZA= 65° or SAA = 0°, results from PROSAIL model larger magnifies the result because of the increasing area of sunlit soil between rows leading to more obvious differences between turbid medium assumption and realistic canopies.

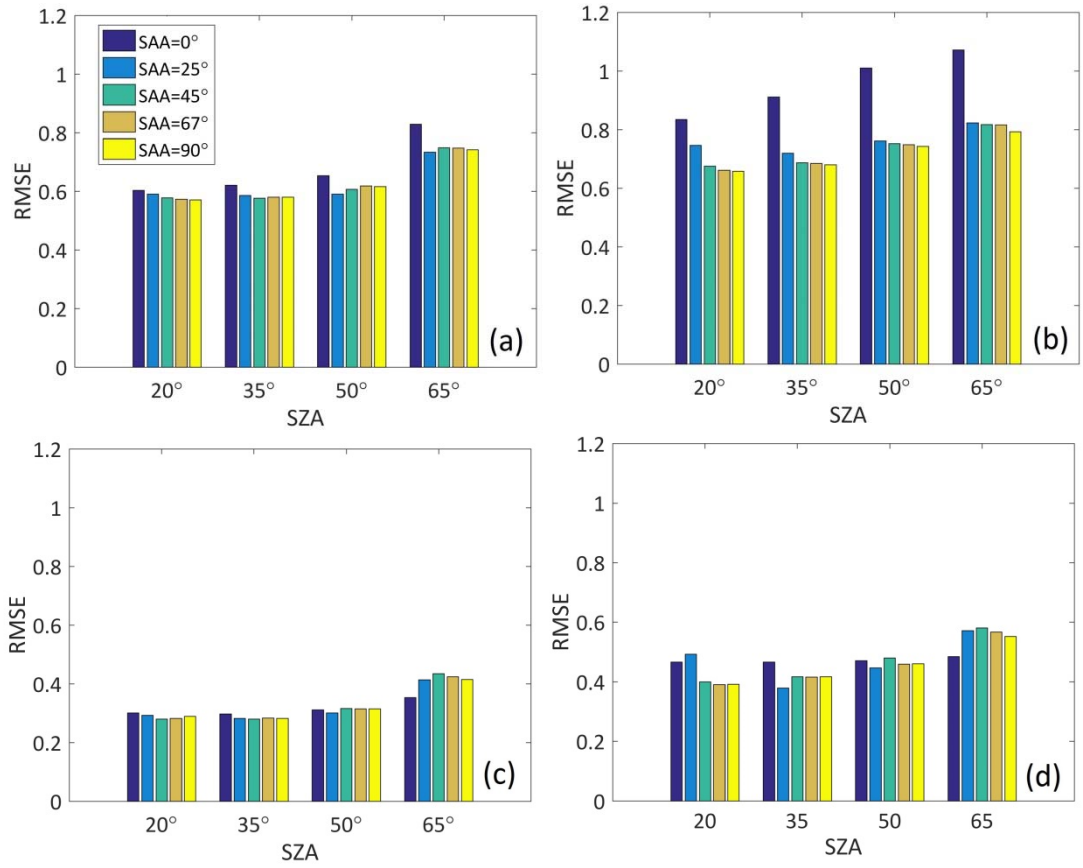

Figure 33 RMSE between effective GAI and estimated effective GAI from NN trained with (a,b) PROSAIL and (c,d) 3D datasets for (a,c) wheat and (b,d) maize. Results are validated using validation dataset with specific sun angle.

5 Conclusion

The definition of LAI retrieved from remote sensing observations was examined in this paper. Canopy reflectance of wheat and maize under different conditions was simulated at nadir with ray tracing model LuxCoreRender and 3D crop architecture models based on the 3D speed up method. LAI, GAI, PAI and effective GAI were computed according to different definitions. Totally 33750 cases were generated for each geometry setting and crop type.

Different canopy reflectance over different structure assumptions was first examined. For both wheat and maize, adding stems would decrease the reflectance because of the increase of absorption from stems, while adding yellow leaves before earring show almost no influence since most of them are located at bottom layer. Based on the NN, simulated canopy reflectance from 3D RTM was related to different definitions of LAI and effective GAI is best estimated with with the highest R^2 and the smallest RMSE (RMSE = 0.33, R^2 = 0.95 for wheat and RMSE = 0.47, R^2 = 0.90 for maize). Two other inversion methods (VIs and 1D RTM) were compared with results from 3D RTM. Three VIs (NDVI, OSAVI and MTVI2) were test and provided the worst performance compared with 1D and 3D RTM because canopy parameters with large changing ranges were considered. Based on the turbid medium assumption, the PROSAIL model which is a typical 1D RTM was applied for wheat and maize. However, limited by the turbid medium assumption of canopy structure, results from PROSAIL model showed comparatively larger RMSE compared with 3D RTM.

For row crops, sun-angle effects have been tested in different studies based on canopy reflectance measured in field experiments (Kollenkark et al. 1982; Shibayama and Wiegand 1985; Lord et al. 1988) or simulated with limited 3D architectures (Zhao et al. 2010). In this study, influence from different sun positions was examined in both canopy reflectance and inversion performance. Results showed that the parallel between sun light and row angle would result in more shadowed plants with the decreasing of canopy reflectance in red and the increasing in NIR, which consequently cause the worse inversion results because of the introduced uncertainties of plants. Generally speaking, 3D model is less sensitive to sun angles compared with the other two, while 1D model is more affected when the sun light is parallel to the row angle because of the difference between turbid medium assumption and realistic canopies.

This study indicates that the effective GAI shows better consistence with estimates from remote sensing images using empirical or physical methods. Estimated results from 3D model inversion are more accurate than VIs and 1D RTM. For future research, effective GAI from field measurements is more recommended to be compared with retrieved estimates from remote sensing methods and 3D model inversion is a good way to improve the estimation of canopy parameters.

References

Miller, J. (1967). A formula for average foliage density. *Australian Journal of Botany, 15*, 141-144

Rouse Jr, J.W., Haas, R., Schell, J., & Deering, D. (1974). Monitoring vegetation systems in the Great Plains with ERTS

Kollenkark, J., Vanderbilt, V., Daughtry, C., & Bauer, M. (1982). Influence of solar illumination angle on soybean canopy reflectance. *Applied Optics, 21*, 1179-1184

Goel, N.S., & Strebel, D.E. (1983). Inversion of vegetation canopy reflectance models for estimating agronomic variables. I. Problem definition and initial results using the Suits model. *Remote Sensing of Environment, 13*, 487-507

Verhoef, W. (1984). Light scattering by leaf layers with application to canopy reflectance modeling: the SAIL model. *Remote Sensing of Environment, 16*, 125-141

Shibayama, M., & Wiegand, C. (1985). View azimuth and zenith, and solar angle effects on wheat canopy reflectance. *Remote Sensing of Environment, 18*, 91-103

Lord, D., Desjardins, R.L., & Dubé, P.A. (1988). Sun-angle effects on the red and near infrared reflectances of five different crop canopies. *Canadian Journal of Remote Sensing, 14*, 46-55

Norman, J.M., & Campbell, G.S. (1989). Canopy structure. *Plant physiological ecology* (pp. 301-325): Springer

Jacquemoud, S., & Baret, F. (1990). PROSPECT : A model of leaf optical properties spectra. *Remote Sensing of Environment, 34*, 75-91

Baret, F., Jacquemoud, S., Guyot, G., & Leprieur, C. (1992). Modeled analysis of the biophysical nature of spectral shifts and comparison with information content of broad bands. *Remote Sensing of Environment, 41*, 133-142

Chen, J.M., & Black, T. (1992). Defining leaf area index for non‐flat leaves. *Plant, Cell & Environment, 15*, 421-429

Richardson, A., Wiegand, C., Wanjura, D., Dusek, D., & Steiner, J. (1992). Multisite analyses of spectral-biophysical data for sorghum. *Remote Sensing of Environment, 41*, 71-82

Liang, S., & Strahler, A.H. (1993). An analytic BRDF model of canopy radiative transfer and its inversion. *IEEE transactions on Geoscience and Remote Sensing, 31*, 1081-1092

Kuusk, A. (1994). A multispectral canopy reflectance model. *Remote Sensing of Environment, 50*, 75-82

Myneni, R.B., Hall, F.G., Sellers, P.J., & Marshak, A.L. (1995). The interpretation of spectral vegetation indexes. *IEEE transactions on Geoscience and Remote Sensing, 33*, 481-486

North, P.R. (1996). Three-dimensional forest light interaction model using a Monte Carlo method. *IEEE transactions on Geoscience and Remote Sensing, 34*, 946-956
Rondeaux, G., Steven, M., & Baret, F. (1996). Optimization of soil-adjusted vegetation indices. *Remote Sensing of Environment, 55*, 95-107
Baret, F., & Fourty, T. (1997). Estimation of leaf water content and specific leaf weight from reflectance and transmittance measurements. *Agronomie, 17*, 455-464
Strahler, A.H. (1997). Vegetation canopy reflectance modeling—Recent developments and remote sensing perspectives. *Remote Sensing Reviews, 15*, 179-194
Domingo, F., Sánchez, G., Moro, M., Brenner, A., & Puigdefábregas, J. (1998). Measurement and modelling of rainfall interception by three semi-arid canopies. *Agricultural and Forest meteorology, 91*, 275-292
Gower, S.T., Kucharik, C.J., & Norman, J.M. (1999). Direct and indirect estimation of leaf area index, fAPAR, and net primary production of terrestrial ecosystems. *Remote Sensing of Environment, 70*, 29-51
Nilson, T. (1999). Inversion of gap frequency data in forest stands. *Agricultural and Forest meteorology, 98*, 437-448
Jacquemoud, S., Bacour, C., Poilve, H., & Frangi, J.-P. (2000). Comparison of four radiative transfer models to simulate plant canopies reflectance: Direct and inverse mode. *Remote Sensing of Environment, 74*, 471-481
Broge, N.H., & Leblanc, E. (2001). Comparing prediction power and stability of broadband and hyperspectral vegetation indices for estimation of green leaf area index and canopy chlorophyll density. *Remote Sensing of Environment, 76*, 156-172
Broge, N.H., & Mortensen, J.V. (2002). Deriving green crop area index and canopy chlorophyll density of winter wheat from spectral reflectance data. *Remote Sensing of Environment, 81*, 45-57
Weiss, M., Baret, F., Leroy, M., Hautecoeur, O., Bacour, C., Prevol, L., & Bruguier, N. (2002). Validation of neural net techniques to estimate canopy biophysical variables from remote sensing data. *Agronomie-Sciences des Productions Vegetales et de l'Environnement, 22*, 547-554
Fournier, C., Andrieu, B., Ljutovac, S., & Saint-Jean, S. (2003). ADEL-wheat: a 3D architectural model of wheat development. In: Springer Verlag
Gascon, F., Gastellu-Etchegorry, J.-P., Lefevre-Fonollosa, M.-J., & Dufrene, E. (2004). Retrieval of forest biophysical variables by inverting a 3-D radiative transfer model and using high and very high resolution imagery. *International Journal of Remote Sensing, 25*, 5601-5616
Gastellu-Etchegorry, J., Martin, E., & Gascon, F. (2004). DART: a 3D model for simulating satellite images and studying surface radiation budget. *International Journal of Remote Sensing, 25*, 73-96
Haboudane, D., Miller, J.R., Pattey, E., Zarco-Tejada, P.J., & Strachan, I.B. (2004). Hyperspectral vegetation indices and novel algorithms for predicting green LAI of crop canopies: Modeling and validation in the context of precision agriculture. *Remote Sensing of Environment, 90*, 337-352
Jonckheere, I., Fleck, S., Nackaerts, K., Muys, B., Coppin, P., Weiss, M., & Baret, F. (2004). Review of methods for in situ leaf area index determination: Part I. Theories, sensors and hemispherical photography. *Agricultural and Forest meteorology, 121*, 19-35
Weiss, M., Baret, F., Smith, G., Jonckheere, I., & Coppin, P. (2004). Review of methods for in situ leaf area index (LAI) determination: Part II. Estimation of LAI, errors and sampling. *Agricultural and Forest meteorology, 121*, 37-53
Baret, F., Hagolle, O., Geiger, B., Bicheron, P., Miras, B., Huc, M., Berthelot, B., Niño, F., Weiss, M., & Samain, O. (2007). LAI, fAPAR and fCover CYCLOPES global products derived from VEGETATION: Part 1: Principles of the algorithm. *Remote Sensing of Environment, 110*, 275-286
Biskup, B., Scharr, H., Schurr, U., & Rascher, U. (2007). A stereo imaging system for measuring structural parameters of plant canopies. *Plant, Cell & Environment, 30*, 1299-1308
López-Lozano, R., Baret, F., Chelle, M., Rochdi, N., & Espana, M. (2007). Sensitivity of gap fraction to maize architectural characteristics based on 4D model simulations. *Agricultural and Forest meteorology, 143*, 217-229

Baret, F., & Buis, S. (2008). Estimating canopy characteristics from remote sensing observations: Review of methods and associated problems. *Advances in land remote Sensing* (pp. 173-201): Springer
Duthoit, S., Demarez, V., Gastellu-Etchegorry, J.-P., Martin, E., & Roujean, J.-L. (2008). Assessing the effects of the clumping phenomenon on BRDF of a maize crop based on 3D numerical scenes using DART model. *Agricultural and Forest meteorology, 148*, 1341-1352
Fang, H., & Liang, S. (2008). Leaf area index models
González-Sanpedro, M., Le Toan, T., Moreno, J., Kergoat, L., & Rubio, E. (2008). Seasonal variations of leaf area index of agricultural fields retrieved from Landsat data. *Remote Sensing of Environment, 112*, 810-824
Verrelst, J., Schaepman, M.E., Koetz, B., & Kneubühler, M. (2008). Angular sensitivity analysis of vegetation indices derived from CHRIS/PROBA data. *Remote Sensing of Environment, 112*, 2341-2353
Widlowski, J.-L., Robustelli, M., Disney, M., Gastellu-Etchegorry, J.-P., Lavergne, T., Lewis, P., North, P., Pinty, B., Thompson, R., & Verstraete, M. (2008). The RAMI On-line Model Checker (ROMC): A web-based benchmarking facility for canopy reflectance models. *Remote Sensing of Environment, 112*, 1144-1150
Gonsamo, A. (2009). *Remote sensing of leaf area index: enhanced retrieval from close-range and remotely sensed optical observations*. University of Helsinki, Department of Geography
Henrich, V., Götze, E., Jung, A., Sandow, C., Thürkow, D., & Gläßer, C. (2009). Development of an Online indices-database: motivation, concept and implementation. *EARSeL proceedings, EARSeL, Tel Aviv*
Jacquemoud, S., Verhoef, W., Baret, F., Bacour, C., Zarco-Tejada, P.J., Asner, G.P., François, C., & Ustin, S.L. (2009). PROSPECT + SAIL models: A review of use for vegetation characterization. *Remote Sensing of Environment, 113*, S56-S66
Casa, R., Baret, F., Buis, S., Lopez-Lozano, R., Pascucci, S., Palombo, A., & Jones, H.G. (2010). Estimation of maize canopy properties from remote sensing by inversion of 1-D and 4-D models. *Precision agriculture, 11*, 319-334
Zhao, F., Gu, X., Verhoef, W., Wang, Q., Yu, T., Liu, Q., Huang, H., Qin, W., Chen, L., & Zhao, H. (2010). A spectral directional reflectance model of row crops. *Remote Sensing of Environment, 114*, 265-285
Duveiller, G., Weiss, M., Baret, F., & Defourny, P. (2011). Retrieving wheat Green Area Index during the growing season from optical time series measurements based on neural network radiative transfer inversion. *Remote Sensing of Environment, 115*, 887-896
Liu, J., Pattey, E., & Jégo, G. (2012). Assessment of vegetation indices for regional crop green LAI estimation from Landsat images over multiple growing seasons. *Remote Sensing of Environment, 123*, 347-358
Nguy-Robertson, A., Gitelson, A., Peng, Y., Viña, A., Arkebauer, T., & Rundquist, D. (2012). Green leaf area index estimation in maize and soybean: Combining vegetation indices to achieve maximal sensitivity. *Agronomy Journal, 104*, 1336-1347
Verrelst, J., Muñoz, J., Alonso, L., Delegido, J., Rivera, J.P., Camps-Valls, G., & Moreno, J. (2012). Machine learning regression algorithms for biophysical parameter retrieval: Opportunities for Sentinel-2 and-3. *Remote Sensing of Environment, 118*, 127-139
Wang, K., & Dickinson, R.E. (2012). A review of global terrestrial evapotranspiration: Observation, modeling, climatology, and climatic variability. *Reviews of Geophysics, 50*
Abichou, M., Fournier, C., Dornbusch, T., Chambon, C., Baccar, R., Bertheloot, J., Vidal, T., Robert, C., Gouache, D., & Andrieu, B. (2013). Re-parametrisation of Adel-wheat allows reducing the experimental effort to simulate the 3D development of winter wheat. In, *7. International Conference on Functional Structure Plant Models* (p. np): Finnish Society of Forest Science
Malenovský, Z., Homolová, L., Zurita-Milla, R., Lukeš, P., Kaplan, V., Hanuš, J., Gastellu-Etchegorry, J.-P., & Schaepman, M.E. (2013). Retrieval of spruce leaf chlorophyll content from airborne image data using continuum removal and radiative transfer. *Remote Sensing of Environment, 131*, 85-102

Duan, S.-B., Li, Z.-L., Wu, H., Tang, B.-H., Ma, L., Zhao, E., & Li, C. (2014). Inversion of the PROSAIL model to estimate leaf area index of maize, potato, and sunflower fields from unmanned aerial vehicle hyperspectral data. *International Journal of Applied Earth Observation and Geoinformation, 26*, 12-20
Banskota, A., Serbin, S.P., Wynne, R.H., Thomas, V.A., Falkowski, M.J., Kayastha, N., Gastellu-Etchegorry, J.-P., & Townsend, P.A. (2015). An LUT-based inversion of DART model to estimate forest LAI from hyperspectral data. *IEEE Journal of Selected Topics in Applied Earth Observations and Remote Sensing, 8*, 3147-3160
Kross, A., McNairn, H., Lapen, D., Sunohara, M., & Champagne, C. (2015). Assessment of RapidEye vegetation indices for estimation of leaf area index and biomass in corn and soybean crops. *International Journal of Applied Earth Observation and Geoinformation, 34*, 235-248
Li, W., Weiss, M., Waldner, F., Defourny, P., Demarez, V., Morin, D., Hagolle, O., & Baret, F. (2015). A generic algorithm to estimate LAI, FAPAR and FCOVER variables from SPOT4_HRVIR and landsat sensors: evaluation of the consistency and comparison with ground measurements. *Remote Sensing, 7*, 15494-15516
Martello, M., Ferro, N., Bortolini, L., & Morari, F. (2015). Effect of incident rainfall redistribution by maize canopy on soil moisture at the crop row scale. *Water, 7*, 2254-2271
Pharr, M., Jakob, W., & Humphreys, G. (2016). *Physically based rendering: From theory to implementation*. Morgan Kaufmann
Hernández-Clemente, R., North, P., Hornero, A., & Zarco-Tejada, P. (2017). Assessing the effects of forest health on sun-induced chlorophyll fluorescence using the FluorFLIGHT 3-D radiative transfer model to account for forest structure. *Remote Sensing of Environment, 193*, 165-179
Liu, S., Baret, F., Abichou, M., Boudon, F., Thomas, S., Zhao, K., Fournier, C., Andrieu, B., Irfan, K., & Hemmerlé, M. (2017). Estimating wheat green area index from ground-based LiDAR measurement using a 3D canopy structure model. *Agricultural and Forest meteorology, 247*, 12-20
Corti, M., Cavalli, D., Cabassi, G., Gallina, P.M., & Bechini, L. (2018). Does remote and proximal optical sensing successfully estimate maize variables? A review. *European Journal of Agronomy, 99*, 37-50
Delloye, C., Weiss, M., & Defourny, P. (2018). Retrieval of the canopy chlorophyll content from Sentinel-2 spectral bands to estimate nitrogen uptake in intensive winter wheat cropping systems. *Remote Sensing of Environment, 216*, 245-261
Fang, H., Liu, W., Li, W., & Wei, S. (2018). Estimation of the directional and whole apparent clumping index (ACI) from indirect optical measurements. *ISPRS journal of photogrammetry and remote sensing, 144*, 1-13
LuxCoreRender (2018). LuxCoreRender Wiki. https://wiki.luxcorerender.org/LuxCoreRender_Wiki. In Verrelst, J., Malenovský, Z., Van der Tol, C., Camps-Valls, G., Gastellu-Etchegorry, J.-P., Lewis, P., North, P., & Moreno, J. (2018). Quantifying vegetation biophysical variables from imaging spectroscopy data: A review on retrieval methods. *Surveys in Geophysics*, 1-41
Yan, G., Hu, R., Luo, J., Weiss, M., Jiang, H., Mu, X., Xie, D., & Zhang, W. (2019). Review of indirect optical measurements of leaf area index: Recent advances, challenges, and perspectives. *Agricultural and Forest meteorology, 265*, 390-411

3.3 The use of 3D realistic models reduce the bias in GAI and chlorophyll estimates from satellite data: the case of wheat and maize crops under a wide range of conditions

Optimal learning for GAI and chlorophyll estimation from 1D and 3D radiative transfer model inversion: the case of wheat and maize crops observed by Sentinel2

Jingyi Jiang, Marie Weiss, Shouyang Liu, Kamran Irfan, Wenjuan Li, Cindy Delloye, Fred Baret

Abstract

The estimation of GAI and chlorophyll from 1D and 3D radiative transfer model inversion with neural network (NN) is compared in the case of wheat and maize. Training databases are first generated from 1D PROSAIL model and 3D specific model respectively. For 3D specific model, different phenological stages, leaf optical properties, soil reflectance, canopy structures and sun angles are included using a speeding up method. Based on the trained NN from 1D and 3D training databases, biophysical variables including green area index (GAI), leaf chlorophyll content (C_{ab}) and canopy chlorophyll content (CCC) are estimated using Sentinel-2 observations and compared with field measurements. Results show that 3D model provides more accurate estimation for most variables, with slight improvement for wheat (RMSE of GAI = 0.72, RMSE of C_{ab} = 9.6 µg/m^2 and RMSE of CCC = 43.39 µg/m^2) and larger improvement for maize (RMSE of GAI = 0.37 and RMSE of CCC = 51.49 µg/m^2). The inclusion of bands in red-edge and SWIR region improve the estimation of GAI and the utilization of bands in red-edge region is important for chlorophyll estimation.

Keywords

GAI, chlorophyll, 3D radiative transfer model, PROSAIL, inversion, neural network

1 Introduction

The green area index (GAI) and the chlorophyll content at leaf and canopy level are among most important biophysical variables since they both relate to the canopy photosynthetic potential and to the amount of electromagnetic radiation reflected into space which make them accessible from satellite data (Broge and Leblanc 2001). Different from leaf area index (LAI) which is defined as half the total developed area of leaves per unit horizontal ground area (Chen and Black 1992), GAI refers to the green elements with no differences between leaves, stems and reproductive organs (Baret et al. 2010). For reflectance observations, the retrieved variables using remote sensing imagery are proved to be more sensitive to the green elements (Duveiller et al. 2011). Leaf chlorophyll content (C_{ab}) is the major plant pigments in photosynthesis. It is not only applied as an indirect estimation of N states but also closely relate to plant stress and senescence (Croft and Chen 2017). Canopy chlorophyll content (CCC) is defined by the C_{ab} and GAI (Houles et al. 2007). Compared with C_{ab}, CCC which represents the optical path in the canopy where absorption by chlorophyll governs the radiometric signal is proved to be more suited for canopy nitrogen content (Baret et al. 2007b; Delloye et al. 2018; Zhou et al. 2016).

Methods to estimate GAI, C_{ab} and CCC from remote sensing data include empirical methods based on empirical regression or machine learning techniques to relate the variables and vegetation indexes, and physically based radiative transfer models (RTM) inversions (Baret and Buis 2008; Verrelst et al. 2012). Even though studies have proved that empirical methods can provide more accurate estimation of canopy variables (Jay et al. 2017; Liu et al. 2012), they are limited by the cultivar, location and time with local calibration. Physically based RTMs are developed according to the physical processes involve in the photon transport within vegetation canopies (Verger et al. 2011). 1D radiative transfer models (1D RTM) like PROSAIL model (Jacquemoud et al. 2009) and kuusk model (Kuusk 1994) are built based on the turbid medium assumption. Combined with different inversions techniques (e.g. optimization, Look-Up-Tables (LUT) and machine learning methods), they are inverted to estimate canopy variables with the advantage of being computational efficient regardless of plant types. However, because of the simplified assumption on canopy structure, errors are introduced for more clumped conditions. Different 3D radiative transfer models (3D RTM) like FLIGHT (North 1996), DART (Gastellu-Etchegorry et al. 2004) and open source renders (e.g. PBRT (Stuckens et al. 2009) and POV-Ray (POV-team 2013)) have been developed to provide more accurate simulation of canopy reflectance with precise description of canopy structure. According to the speeding up method of 3D simulation (Jiang et al. 2019b), canopy reflectance can be simulated by considering only a limited number of soil and leaf properties for the given observation geometry. A learning and validation database of wheat and maize composed of large numbers of canopy reflectance simulations have been generated with detailed 3D RTM (Jiang et al. 2019a), which provide the possibility to retrieve biophysical variables from remote sensing observations.

As one of the machine learning methods, Neural Networks (NN) are intensively used to estimate biophysical variables with simulated learning database from RTM based on remote sensing observations from medium to decametric resolutions (Baret et al. 2007a; Delloye et al. 2018; Verrelst et al. 2018; Weiss et al. 2002). The estimation performances of NN highly rely on the training database, the architecture and the training process to learn the internal relationships between the inputs and the corresponding outputs (Bacour et al. 2006; Kimes et al. 1998). When multiple variables are estimated, some studies trained a single network with several outputs considering the additional physical constraint among variables (Bacour et al. 2006; Baret et al. 2007a;

Schlerf and Atzberger 2006), while the others prefer to define and train the networks independently for each variable with the statement that concurrent estimation of several variables with a single network would lead to poorer performance (Baret et al. 2013; Li et al. 2015; Verger et al. 2011). However, no studies compare the influence from single or multiple networks specifically.

The European Sentinel-2 Mission (S2) with decametric resolution and high revisit capability could provide continuity to monitoring services over global terrestrial surfaces (Van der Meer et al. 2014). S2 includes three new bands in red-edge region (centered at 705, 740 and 783 nm) which has been proved to improve the inversion of biophysical variables (Clevers and Gitelson 2013; Delegido et al. 2011). Different band combinations have been tested with machine learning algorithms (Delloye et al. 2018; Verrelst et al. 2012; Verrelst et al. 2013). Results show that the estimation of GAI and chlorophyll would benefit a lot from bands in the red-edge in different degrees, while adding bands in SWIR cause low gain in accuracy for both variables.

The objective of this study is to compare the estimation of GAI and chlorophyll at leaf and canopy level from 1D and 3D RTM inversion with S2 observations. Two crops, wheat and maize, with different phenological stages are included. Both 1D PROSAIL and 3D specific model are used to build the learning database. NN are selected as the inversion method to train the learning database. For different biophysical variables, estimated results from NN with single or multiple outputs are firstly compared. Then the better one is applied with 1D and 3D RTM to compare the inversion results with field measurements using reflectance from Sentinal-2. Influence from different bands setting of Sentinal-2 are also tested. Finally, performance of RTMs with NN in the case of wheat and maize crops are concluded.

2 Materials and Methods

2.1 Ground reference measurements

The Produits Pour Sentinel-2 (P2S2) Project provides an extensive calibration and validation dataset over a large range of crops observed under contrasted growth conditions at several phenological stages. Measurements from P2S2 were applied as the ground reference in this study. Four data acquisition sites are located in France (Camargue, Toulouse, Boigneville) and Belgium (Gembloux). Totally 43 Elementary Sampling Units (ESUs) of wheat (from February to April, 2018) and 45 ESUs of maize (from May to August, 2018) with ground measurements of GAI and C_{ab} before earring were selected as the validation dataset (Table 17).

Table 17 Characteristics of selected ESUs over four measurement sites from P2S2 Project.

Site	Lat (°)	Lon (°)	Crop type	Measurement date (2018)	Nb. ESUs
Camargue, France	43.6	4.5	wheat	21/02- 27/03	9
			maize	13/06– 03/08	20
Toulouse, France	43.4	1.2	wheat	27/02– 02/05	10
Boigneville, France	48.3	2.4	wheat	26/01– 02/05	12
			maize	27/06	10
Gembloux, Belgium	50.6	4.7	wheat	14/03– 16/05	12
			maize	22/05- 27/06	15

The sampling protocol of measurements following the recommendations from the Committee on Earth Observation Systems Land Product Validation group (CEOS-LPV) (Fernandes et al. 2014). An ESU corresponds to a 15m × 15m area in a homogeneous part of field with 30 meters far from the field borders. The centre coordinates of the ESU is geo-located with a GPS within an accuracy of few meters. For each ESU,

three sub-samples (2m × *d*m, *d* varied with the crop row spacing) along the row direction were used to capture the possible variability (Figure 34).

In each subsample, five Digital Hemispherical Photography (DHP) downward looking acquisitions are performed along a diagonal transect to represent the possible row effect. The resulting 15 images were processed together using CAN-EYE software version 6.4.95 (https://www6.paca.inra.fr/can-eye) to estimate the GAI at the ESU level. The output effective GAI from CAN-EYE was used to compare with the estimation results from satellite observations because it has been proved that effective GAI is better linked with remote sensing observations regardless of the inversion methods (Jiang, 2019). In this paper, 'GAI' was used to represent 'effective GAI' in the following estimations and comparisons.

The chlorophyll was measured using SPAD measurements (Minolta 1989) with a minimum of 15 leaves randomly located at the top of the canopy per subsample. Based on the consensus equation from Gerovic et al. (2012), the SPAD readings were transformed into surface-based specific units of chlorophyll (µg/cm^2):

$$\text{Chlorophyll} = (99*\text{SPAD})/(144-\text{SPAD}) \quad (1)$$

For each ESU, 45 values of chlorophyll were averaged as C_{ab}. The CCC of was calculated from the measured GAI from DHPs multiplied by the averaged C_{ab} from SPAD.

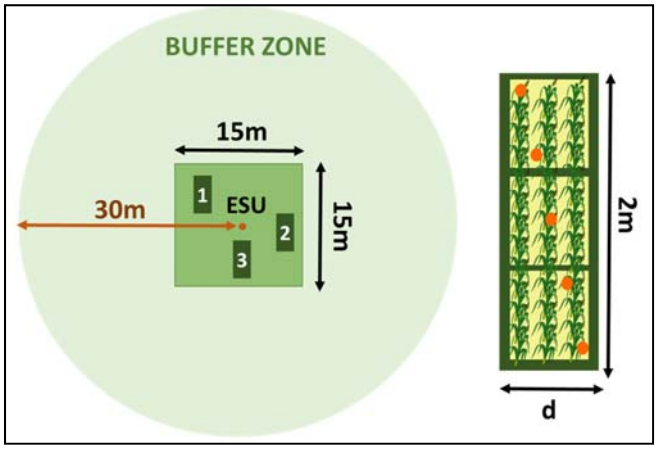

Figure 34 Spatial Sampling within an ESU. On the left, the circle represents the buffer zone with 30m radius centered on the ESU. The 15m x15 m ESU includes three sub-samples where measurements are taken as illustrated on the right. The orange circles represent the position of the DHP camera for GAI estimates.

2.2 Sentinel-2 data

Sentinel-2 is an Earth observation mission operated by European Space Agency (ESA) (Drusch et al. 2012). This mission consists of two satellites Sentinel-2A (S2A) launched on 23 June 2015 and Sentinel-2B (S2B) launched on 7 March 2017. They follow a sun-synchronous orbit with altitude of 786 km and an overpass time at 10:30am UTC. The combination of two satellites offer a nominal revisit with a period of 5-day. S2 provides data over 13 spectral bands, ranging from visible spectrum to short-wave infrared spectra. In this study, three 10m bands (B3: 560nm, B4: 665nm, B8: 842nm) and six 20m bands (B5: 705 nm, B6: 740 nm, B7: 783 nm, B8a: 865 nm, B11: 1610 nm and B12: 2190 nm) were applied to retrieve GAI, C_{ab} and CCC. To make it consistent, the S2 10m bands were aggregated at 20m resolution.

On all P2S2 sites, cloud free S2A and S2B multi-spectral instrument (MSI) Level-2A images on closet dates of ground measurements (maximum 7 days difference) were downloaded from Theia Land data center (https://theia.cnes.fr). These surface reflectance images were generated based on cloud detection and atmospheric correction algorithm MAJA (Rouquié et al. 2017). The accuracy of MAJA

algorithm on cloud detection and aerosol estimation has been well validated in several studies (Baetens et al. 2019; Sola et al. 2018). The pixels contaminated by the clouds/cloud shadow or flagged as snow were not used in this study. Average value of the 3 by 3 pixels region was calculated as representative of each site. View zenith angle, view azimuth angle and sun positions of each image were also extracted from the metadata file of S2.

2.3 Radiative transfer models

2.3.1 1D model

The widely used PROSAIL model (Jacquemoud et al. 2009)was selected as 1D radiative transfer model in this study. It couples the PROSPECT leaf optical properties model (Jacquemoud and Baret 1990) and the SAIL canopy reflectance model(Verhoef 1984). Based on the turbid medium assumptions, the PROSAIL model assumes the canopy to be homogenous regardless of species. The canopy structure is defied with variables including GAI, average leaf angle (ALA) and hot spot parameter (HOT) from SAIL mode. The leaf optical properties are simulated based on the leaf structure parameter and combinations of leaf biophysical variables with corresponding absorption coefficients.

2.3.2 3D model

2.3.2.1 The 3D architecture model

To show different crop architectures, two contrasted species were selected: wheat which is closer to the turbid medium assumption, while maize keeps the row structure at different phenological stages. The 3D ADEL-Wheat model (Fournier et al. 2003) and the 3D maize model created by López-Lozano et al (2007) were utilized to simulate 3D wheat and maize respectively with same setting of canopy variables as (Jiang et al. 2019a). For both wheat and maize, totally 650 scenes were generated and selected to represent the distribution of canopy architectures.

2.3.2.2 LuxCoreRender simulation

LuxCoreRender (LuxCoreRender 2018) which is developed based on open source render engine PBRT (Pharr et al. 2016) was selected as the ray tracing model to simulate canopy reflectance with 3D crop architecture model. It has been validated using RAMI Online Model Checker (ROMC) (Jiang et al. 2019b; Widlowski et al. 2008). Basic settings of the render engine and optical properties were defined in Table 18. Canopy reflectance with different wavelength, leaf and soil properties were computed based on the limited numbers of simulations from reference mode and the extension method proposed in Jiang et al.(2019b). The 3D canopy mock-up was replicated at least three times larger than the spot size to avoid boundary effects. The canopy reflectance was computed through rendering results divided by the value computed for a lambertian reflector under the same conditions. To compute the effective GAI of each scene, the gap fraction was calculated with the image from the nadir viewing camera (field of view = 120°) based on Miller's formula (Miller 1967).

Table 18 Basic settings of LuxCoreRender and optical properties of the canopy.

Name		properties
Render engine		Tiled path, 25 depth per pixel
Light source		Sun with no environment effect
Camera		Field of view: 10°, Height: 10 m, Spot size: 1.7 × 1.7 m^2
Optical properties	Leaf	Lambertian with reflectance and transmittance
	Stem	Lambertian with reflectance
	Soil	Lambertian with reflectance

2.4 Radiative transfer model inversion

2.4.1 Training database

With PROSAIL and 3D specific model, two training database were built based on variables from Table 19. Descriptions of the ranges and distribution law of each variable as well as constraints on the co-distributions between variables were defined according to Weiss and Baret (2016). To make two training database comparable, distribution of leaf optical properties were kept the same and seven typical soil reflectance spectrums multiplied by different soil brightness were applied for two models. For 3D model, the refraction index (n) and mesophyll structure (N) were fixed according to 3D speed up method (Jiang et al. 2019b). For different canopy structures, different GAI, ALA and HOT were included in PROSAIL model for both wheat and maize, while different 3D wheat and maize architectures were generated according Section 2.3.2. For PROSAIL model, the maximum GAI was set to 15 to solve the saturation problem existed for high GAI value (Delloye et al. 2018). Considering the effect of sun direction in row crop, each 3D scene was simulated with four sun zenith angles (SZA) and five sun azimuth angles (SAA) with camera at nadir place (view zenith angle (VZA) and view azimuth angle (VAA) are 0°). Here SAA is defined as the relative azimuth angle between sun and crop row.

To make it consistent as S2, the simulated reflectance from both PROSAIL and 3D model were both spectrally integrated to represent actual S2 bands according to the spectral response function of the sensor. For PROSAIL model, totally 33750 cases were simulated with input canopy variables and output reflectance corresponding to 9 selected S2 bands. For 3D model with each crop specie and geometry setting, the same number of cases was also generated with the same output bands.

Table 19 Variables to build training database with PROSAIL and 3D model. The standard deviation (Std), mode, minimum and maximum values are used to describe the distribution law. Nb. Class is the number of classes of the variable.

			Input variable	Min	Max	Mode	Std	Nb. Class	Law
1D RTM		**Canopy structure**	GAI	0.0	15.0	2.0	3.0	6	Gauss
			ALA (°)	30	70	45	30	3	Gauss
			HOT	0.1	0.5	0.2	0.5	1	Gauss
	3D RTM	**Soil background**	B_s	0.5	3.5	1.2	2.0	5	Gauss
		Leaf optical properties	Cab(µg.cm^{-2})	20	90	45	30	5	Gauss
			C_{dm}(g.cm^{-2})	0.003	0.011	0.005	0.005	5	Gauss
			C_w_Rel	0.6	0.85	0.75	0.08	5	Uniform
			C_{bp}	0.0	2.0	0.0	0.3	3	Gauss
			Mesophyll, N	1.2	1.8	1.5	0.3	3	Gauss
				3D:N=1.5					
			Refractive Index n	1D : n=n(λ) ; 3D :n=1.4					
		Observation geometry	VZA(°)	0					
			VAA(°)	0					
			SZA(°)	20, 35, 50, 65					
			SAA(°)	0, 25, 45, 67, 90					

2.4.2 Neural networks

Based on the training database generated from PROSAIL and 3D model, a back-propagation artificial neural network (ANN) was applied to retrieve three biophysical variables: GAI, C_{ab} and CCC. According to implementations from Li et al. (2015), the architecture of ANN include three layers: one input layer with normalized input data, one hidden layer of five neurons with sigmoid transfer functions and one output layer of a linear neuron. Three networks were trained in parallel for the corresponding variable. To compare the performance between the single and multiple outputs from ANN, ANN with one output layer of three neurons (one neuron per variable to be estimated (Bacour et al. 2006)) was also tested. The number of neurons from hidden layer was increased to 10 to guarantee the simulation accuracy.

For each set of training database, 70% of the cases were randomly selected to train the NN and the remaining was used to evaluate the theoretical performances. To assess the influence from different combinations of S2 bands, three band settings were applied as the inputs: (1) bands with 10m resolution: B3, B4 and B8 (2) bands with red-edge: B3, B4, B5, B6, B7 and B8a (3) bands with red-edge and SWIR: B3, B4, B5, B6, B7, B8a, B11 and B12. For PROSAIL model, variables of input layer include the reflectance in different band sets and the geometrical configurations (the cosine of VZA, SZA and relative angle between VAA and SAA). For 3D model, NNs were trained for each geometrical configuration and the input layer was composed of reflectance in different band sets from the corresponding training database. The accuracy of the inversion was evaluated with several statistical criteria including the coefficient of determination (R^2), Root Mean Square Error (RMSE), Relative Root Mean Square Error (RRMSE) and Bias which are calculated as follows:

$$RMSE = \sqrt{\frac{\sum_{i=1}^{N}(E_i - M_i)^2}{N}} \quad (2)$$

$$RRMSE = \mathrm{RMSE}/\overline{M} \quad (3)$$

$$Bias = \frac{\sum_{i=1}^{N}(E_i - M_i)}{N} \quad (4)$$

where E is the estimate value, M is the measured value, $\overline{M}$ is the mean of measured results and N is the number of measurements.

3 Results and discussion

3.1 Estimating single or multiple variables concurrently?

Based on the training and validation database simulated from 1D and 3D model, the theoretical performances of three specific NN with single output and one NN with three outputs using eight bands (B3, B4, B5, B6, B7, B8a, B11 and B12) are compared using RMSE between the estimated and validation GAI, C_{ab} and CCC. For 1D PROSAIL model (Figure 35), specific NN with single output provide quite similar performance as the NN with multiple outputs. For 3D wheat (Figure 36) and 3D maize (Figure 37) model, even though lower RMSE and less scattering points are showed for both NN with single and multiple outputs, NN trained with single variable has higher theoretical accuracy for all variables. Although Bacour et al. (2006) proposed that using a NN with multiple outputs allows imposing an additional physical constraint to the inverse problem as the variables are not independent, errors might be introduced to other variables at the same time which increase uncertainties of the simulation when one variable is misestimated from the single NN. Similar conclusion was also stated from Verger et al. (2011) where NN with single output would lead to poorer performance when estimate LAI, FCOVER and FAPAR from NN trained with PROSAIL training database. Therefore, the specific NN with single output is more recommended when multiple variables are estimated especially for 3D model inversion.

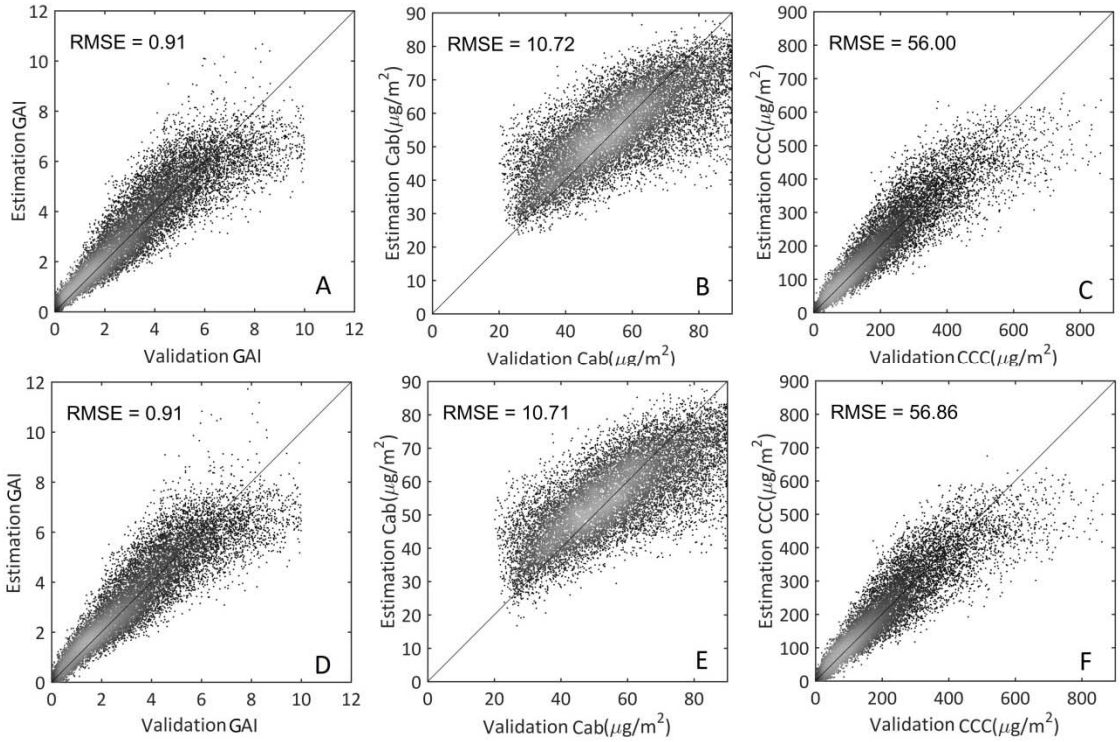

Figure 35 The theoretical performances of the NN over the simulated dataset from 1D PROSAIL model. A, B and C are validation results of GAI, C_{ab} and CCC from three NNs with single output; D, E and F are validation results from one NN with multiple outputs. The grey level intensity increases with the density of points. The black solid line is the 1:1 line.

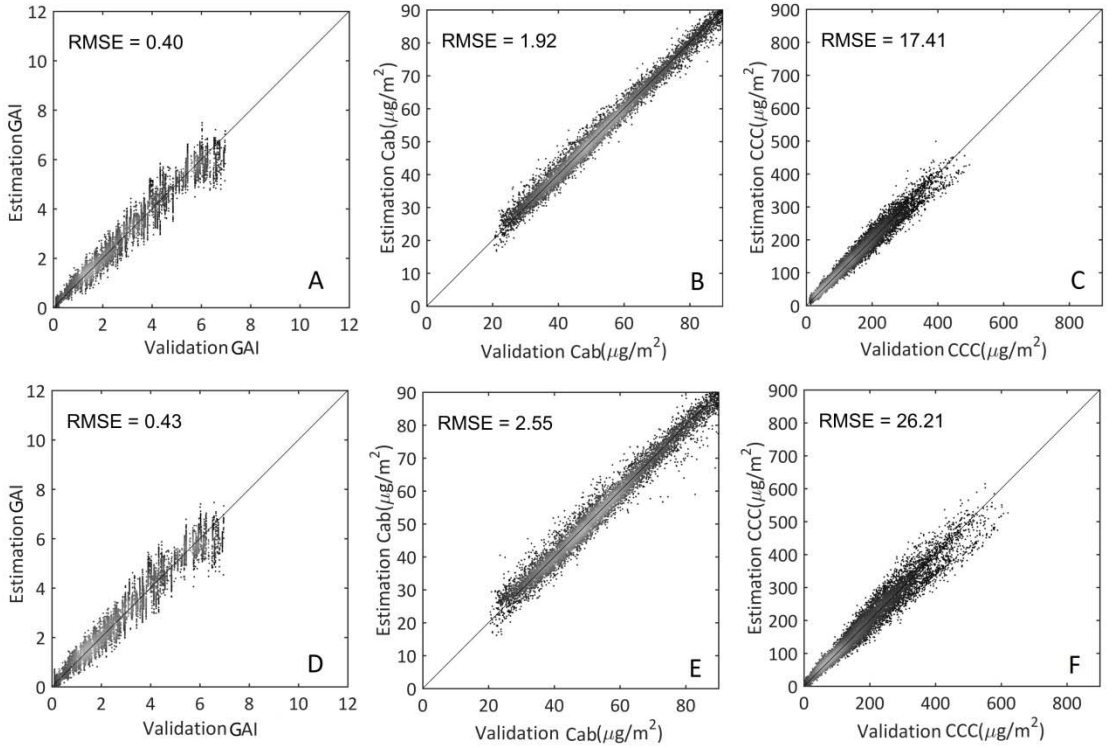

Figure 36 Simulated performances of the NN over the simulated dataset from 3D wheat model. A, B and C are validation results of GAI, C_{ab} and CCC from three NNs with single output; D, E and F are

validation results from one NN with multiple outputs. The grey level intensity increases with the density of points. The black solid line is the 1:1 line.

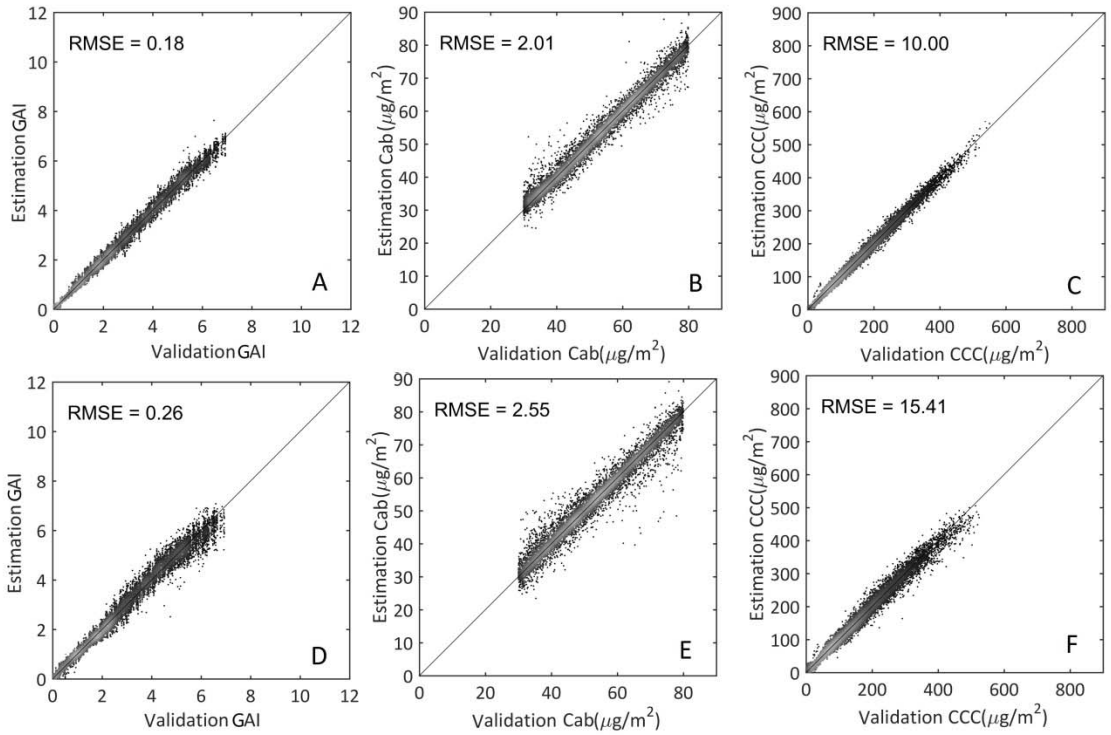

Figure 37 Simulated performances of the NN over the simulated dataset from 3D maize model. A, B and C are validation results of GAI, C_{ab} and CCC from three NNs with single output; D, E and F are validation results from one NN with multiple outputs. The grey level intensity increases with the density of points. The black solid line is the 1:1 line.

3.2 3D model improves GAI and chlorophyll estimation

To compare the performance of inversion between 1D PROSAIL model and 3D wheat and maize model, biophysical variables GAI, C_{ab} and CCC are retrieved using S2 with eight spectral bands (B3, B4, B5, B6, B7, B8a, B11 and B12) based on the NNs from 1D or 3D training database. As it was mentioned in the last section, the specific NN with single output is applied.

For 1D PROSAIL model, estimated GAI corresponds well to the field measurements (Figure 38A and 5C, RMSE = 0.75 and R^2 = 0.75 for wheat and RMSE = 0.72 and R^2 = 0.87 for maize). For maize, slight overestimation occurs when GAI is larger than 2 (Bias = 0.46). C_{ab} retrieval using NN shows a systematic overestimation for both wheat (Figure 38B, RMSE = 11.29 µg/m^2 and Bias = 5.9 µg/m^2) and maize (Figure 38E, RMSE = 16.99 µg/m^2 and Bias = 16.17 µg/m^2), although correction of SPAD has been applied according to Eq. (1). To avoid ambiguities between GAI and C_{ab} from inversion, CCC is directly estimated from NN. Some scattering is observed for wheat (Figure 38C, RMSE = 56.83 µg/m^2), while overestimation still exist for maize CCC estimation (Figure 38F, RMSE = 81.87 µg/m^2).

When 3D specific wheat and maize model are applied, the overall inversion results show an improvement for each variable except C_{ab} of maize. Less scattering and little bias is achieved with smaller RMSE for both wheat and maize. For GAI and CCC, even though estimation of wheat is improved (Figure 39A and 6C, RMSE = 0.72 for GAI and RMSE = 51.14 µg/m^2 for CCC), more increase of performance is got from maize (RMSE of GAI decreasing from 0.72 to 0.37 and RMSE of CCC

decreasing from 81.887 to 51.49). This is mainly because the wheat canopy is more similar as turbid medium assumption from 1D model where leaves are assumed to be randomly distributed, while the maize canopy is more discrete as row crops and show larger difference from 1D model. For C_{ab} of wheat, estimation result shows lower RMSE and reduced bias (Figure 39B, RMSE = 10.11 µg/m^2 and Bias = 0.4 µg/m^2). But for C_{ab} of maize, worse performance is got with increased RMSE and decreased R^2 (Figure 39E, RMSE = 17.44 µg/m^2 and R^2 = 0.5). Reasons for the failed estimation of maize C_{ab} is might from the wrong setting of maize optical properties. More experiments with 3D simulation of maize canopy are still undergoing to solve this problem.

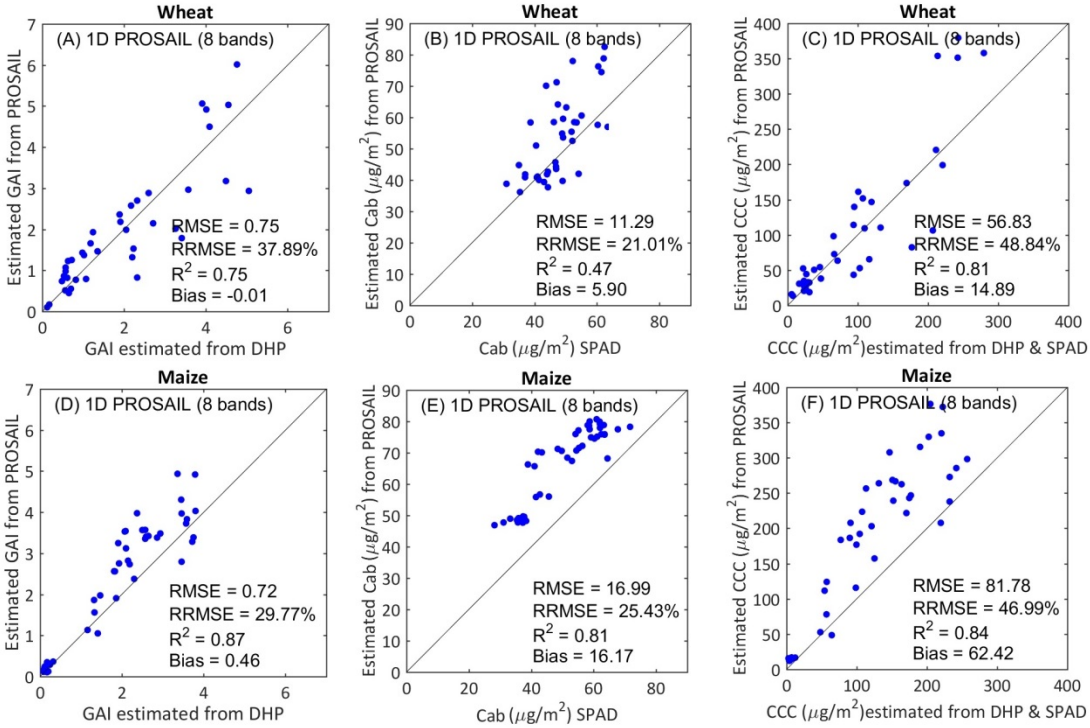

Figure 38 Accuracy of the GAI, C_{ab} and CCC retrieved from S2 images for the bands set (B3, B4, B5, B6, B7, B8a, B11 and B12) of wheat (A, B and C) and maize (D, E and F) using 1D PROSAIL model. The black solid line is the 1:1 line.

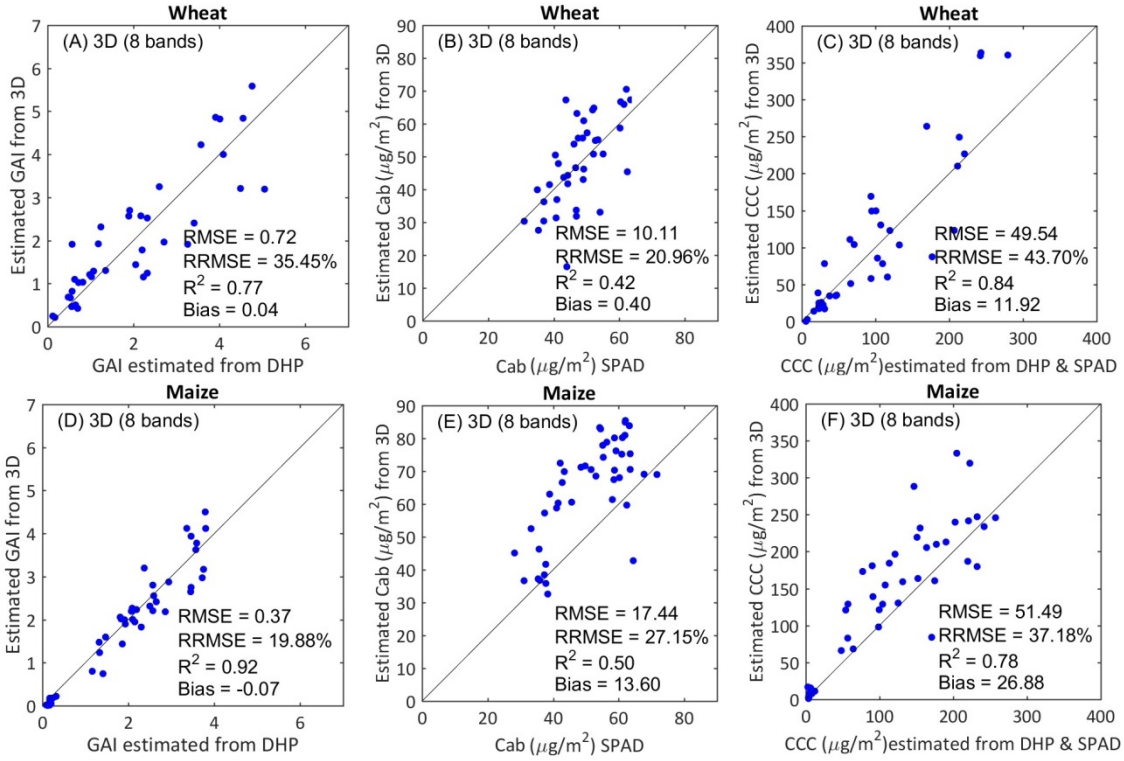

Figure 39 Accuracy of the GAI, C_{ab} and CCC retrieved from S2 images for the bands set (B3, B4, B5, B6, B7, B8a, B11 and B12) of wheat (A, B and C) and maize (D, E and F) using 3D wheat and maize model. The black solid line is the 1:1 line.

3.3 The band setting for 1D and 3D inversion

The retrieval performances of 1D and 3D inversion with 6 bands including red-edge (B3, B4, B5, B6, B7 and B8a) and 3 10m-resolution bands (B3, B4 and B8) were also presented.

For GAI estimation, increase performance is got with more bands added. For 3D model, RMSE of wheat increases from 0.72 to 0.81 and RMSE of maize increase from 0.37 to 0.69 from 3 to 8 bands. When six bands are applied, the overestimation of maize GAI is intensified for 1D inversion (Figure 40D, Bias = 0.69). When only 3 bands exist, the saturation is easier to reach when three bands are applied when GAI is larger than 4 (Figure 42A and 9D, Figure 43A and 10D). As it is stated by Segl et al. (2012), bands in SWIR are sensitive to soil spectral and red-edge bands show more links to vegetation biomass and GAI. In addition, bands in SWIR and red-edge are reported to be less disturbed by atmospheric perturbation. Therefore, the inclusion of SWIR and red-edge bands would increase the accuracy of estimation with more information added. Comparable results are got when compared with previous studies using PROSAIL model: Delloye et al. (2018) reached a RMSE = 0.72 (RRMSE = 27.2%) for wheat with 9 S2 bands (B3, B4, B5, B6, B7, B8, B8a, B11 and B12) and results with all 9 bands provide the best performance compared with other band settings. Veloso et al. (2012) got a RMSE = 0.51 (RRMSE = 31.2%) with mixed wheat, maize, sunflower and soybean with the combination of Formosat-2 and Spot satellites reflectance data. Simular overestimation of maize appeared when GAI ranged from 2 to 4.

The estimation of wheat C_{ab} is best estimated when six bands are applied (RMSE = 10.54 µg/m^2 and Bias = 5.78 µg/m^2 for 1D (Figure 40B) and RMSE = 9.6 µg/m^2 and Bias = 0.91 µg/m^2 for 3D (Figure 41B)). This can be explained by the excellent correlation between leaf chlorophyll and bands in red-

edge region (Segl et al. 2012). Similar results were also achieved from previous studies where C_{ab} was best estimated with extra bands in red-edge (Segl et al. 2012; Verrelst et al. 2012). However, as it was showed in other studies using 1D PROSAIL estimation with S2 reflectance (Delloye et al. 2018) or spectrodirectional measurements (Lunagaria and Patel 2018), overestimation always exists especially for C_{ab} larger than 50 µg/m^2. For 3D estimation, the overestimation is reduced with bias smaller than 1 µg/m^2 for different bands combination. For maize C_{ab}, the best estimation for 1D estimation is achieved with three 10m bands with less bias (Figure 42E, RMSE = 10.37 µg/m^2 and Bias = 8.01 µg/m^2), while errors still exist with 3D estimation with bad performance regardless of bands settings. We are still looking for reasons for this problem.

For wheat CCC estimation, results with six bands (Figure 40C, RMSE = 53.94 µg/m^2 and Bias = 14.25 µg/m^2) or three bands (Figure 42C, RMSE = 53.21 µg/m^2 and Bias = 16.24 µg/m^2) using 1D model provide similar accuracy. Overestimation occurs when wheat CCC is larger than 200 µg/m^2. For 3D wheat model, the best estimation is achieved using six bands with smallest bias (Figure 41C, RMSE = 43.39 µg/m^2 and Bias = -1.36 µg/m^2). For maize CCC, estimates with three 10m bands using 1D model has the smallest RMSE (Figure 42F, RMSE = 63.47 µg/m^2 and Bias = 47.50 µg/m^2), while estimates with 8 bands using 3D maize model performs best (Figure 39F, RMSE = 51.49 µg/m^2 and Bias = 26.88 µg/m^2). However, for both 1D and 3D inversion, the overestimation always exist, which might inherit from the overestimates of maize C_{ab}. Compared with estimation of GAI and C_{ab}, more uncertainties might be included for CCC estimation since it is the combination of two other results (GAI and C_{ab}). In addition, errors from two filed measurement instruments would also result in inaccuracy in validation.

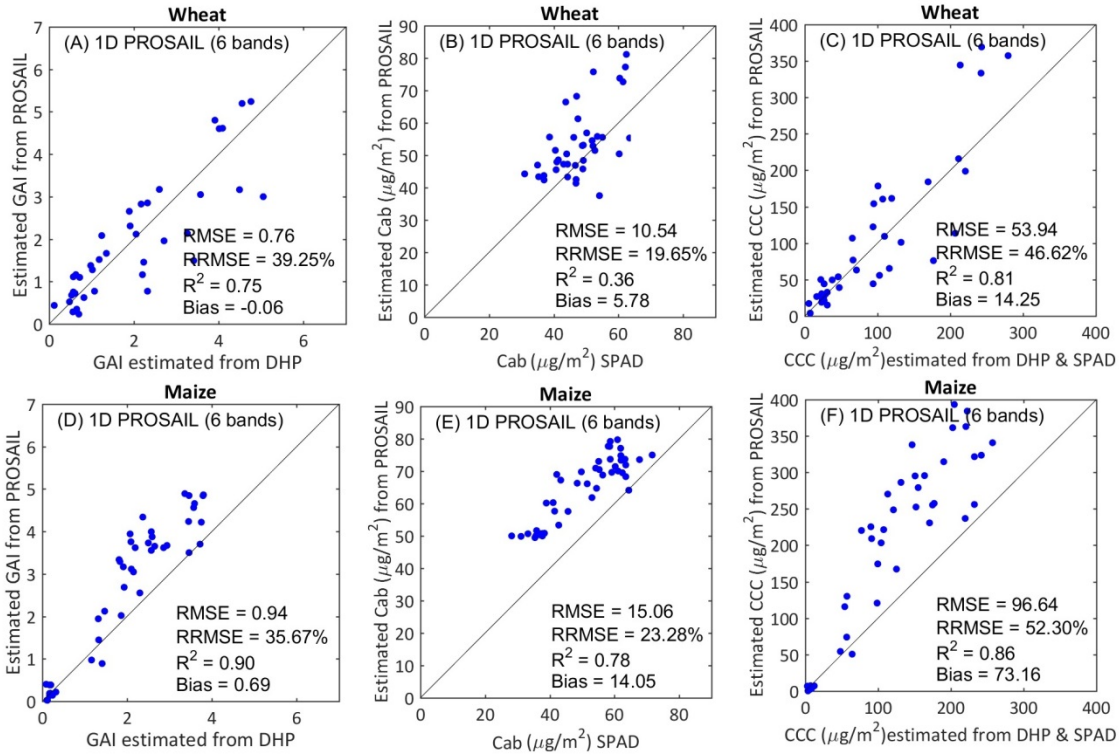

Figure 40 Accuracy of the GAI, C_{ab} and CCC retrieved from S2 images for the bands set (B3, B4, B5, B6, B7 and B8a) of wheat (A, B and C) and maize (D, E and F) using 1D PROSAIL model. The black solid line is the 1:1 line.

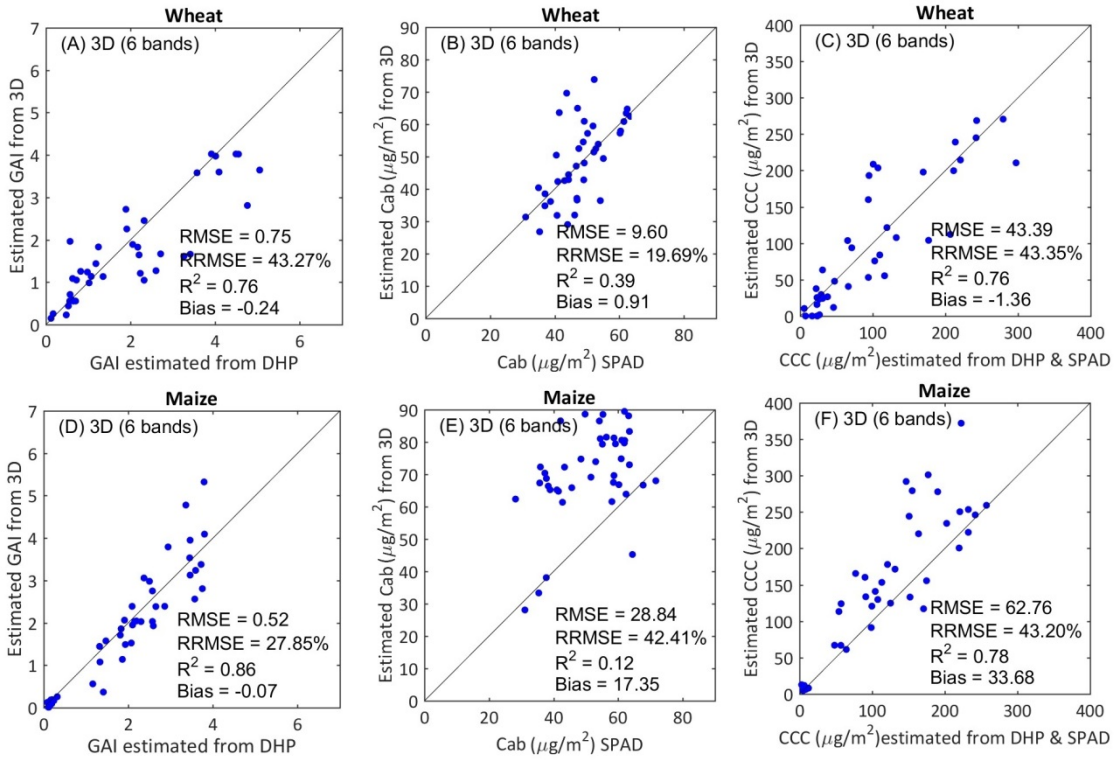

Figure 41 Accuracy of the GAI, C_{ab} and CCC retrieved from S2 images for the bands set (B3, B4, B5, B6, B7 and B8a) of wheat (A, B and C) and maize (D, E and F) using 3D wheat and maize model. The black solid line is the 1:1 line.

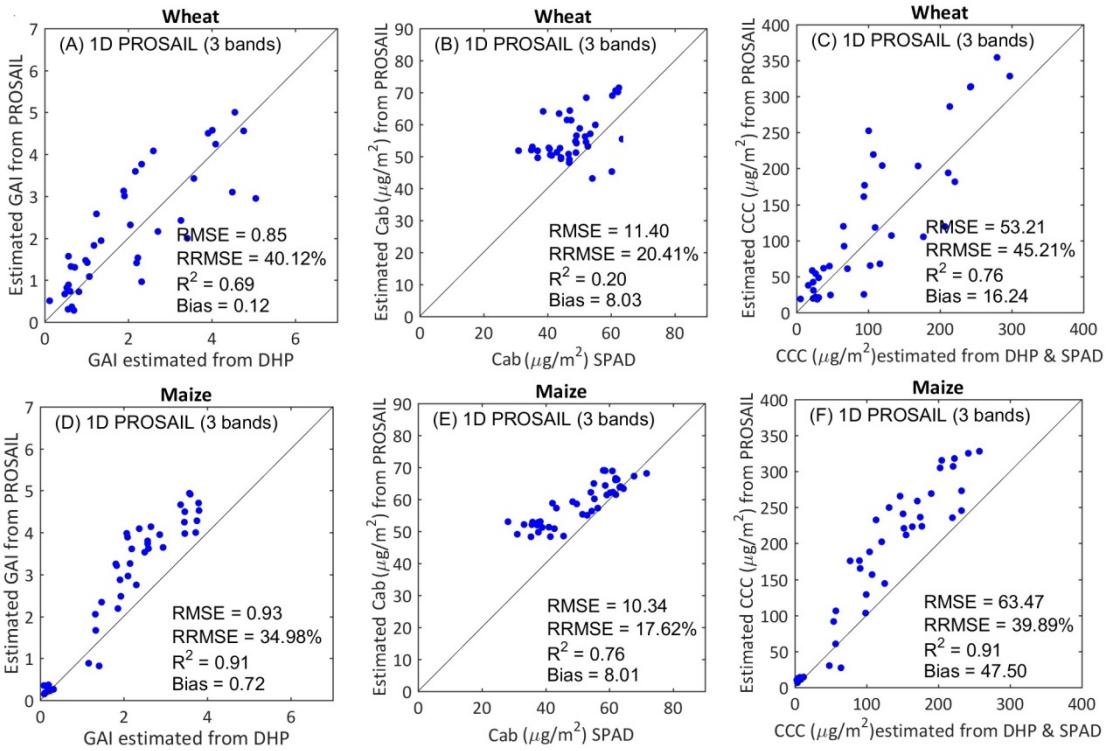

Figure 42 Accuracy of the GAI, C_{ab} and CCC retrieved from S2 images for the bands set (B3, B4 and B8) of wheat (A, B and C) and maize (D, E and F) using 3D wheat and maize model. The black solid line is the 1:1 line.

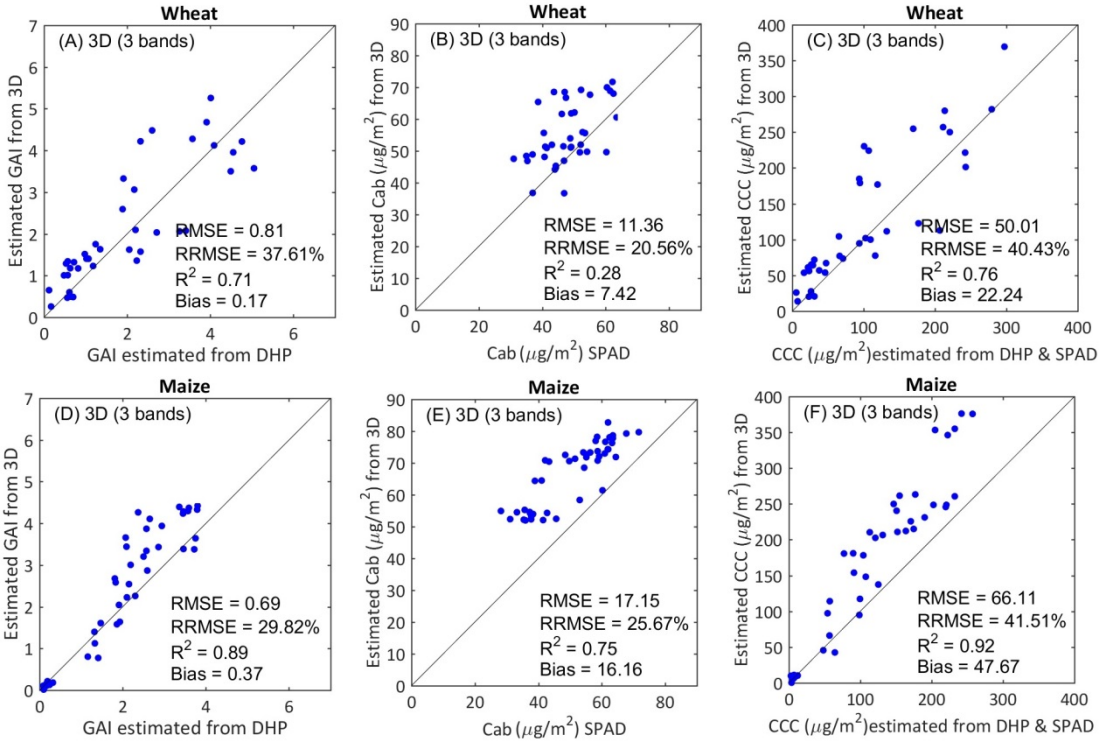

Figure 43 Accuracy of the GAI, C_{ab} and CCC retrieved from S2 images for the bands set (B3, B4 and B8) of wheat (A, B and C) and maize (D, E and F) using 3D wheat and maize model. The black solid line is the 1:1 line.

Simulated reflectance from training database of 3D wheat and maize model are compared with reflectance from 1D PROSAIL model as well as reflectance from S2 (Figure 44). Three red-edge bands (B5, B6 and B7) are compared with the green band (B3). For both wheat and maize, reflectance from 1D model has the larger ranges compared with 3D specific model. However, different distribution of reflectance is showed for reflectance from 3D simulations because of the different crop architectures and canopy structures. When compared with reflectance from S2, most bands are within the changing ranges of 3D reflectance. But for B5 (705 nm) of maize canopy, bias is observed with some overestimation. These would largely impact on the estimated value of chlorophyll content since it is close to the pigment absorption region and might be the reason of the poor estimation of maize C_{ab}.

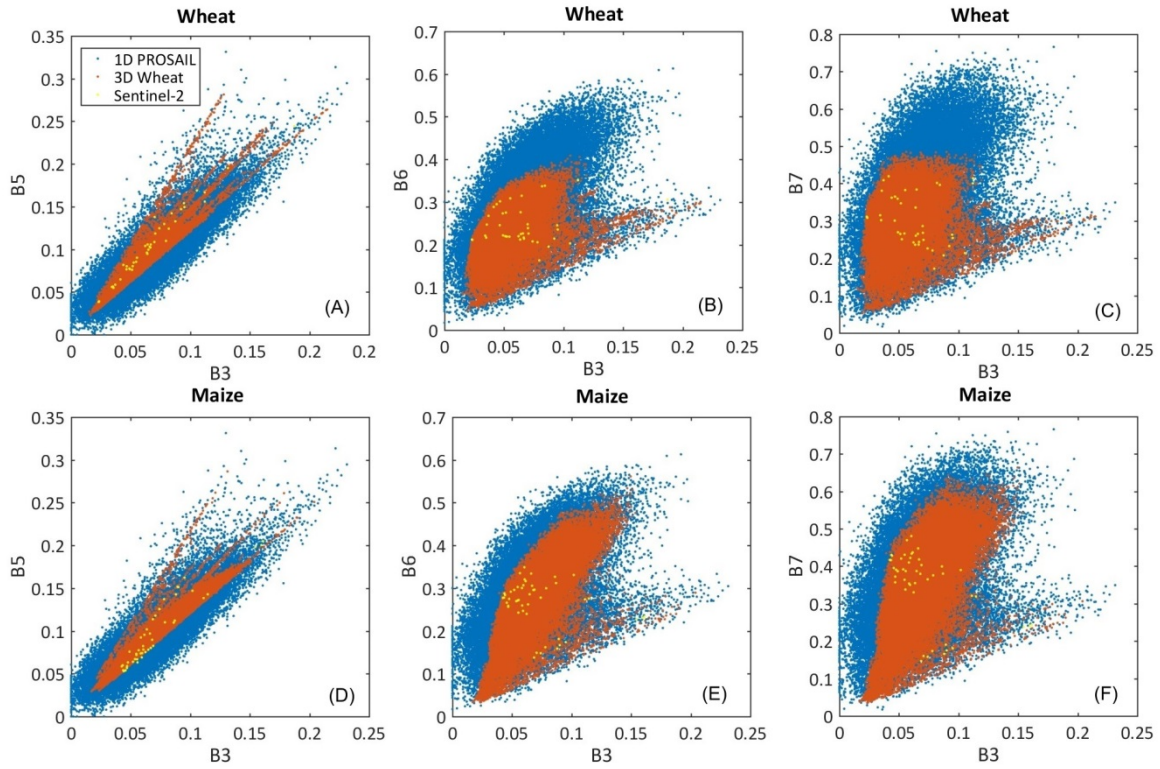

Figure 44 Comparison between reflectance from training dataset (blue points: 1D PROSAIL; orange points: 3D specific model) and S2 reflectance of ESUs (yellow points) of wheat (A, B and C) and maize (D, E and F).

4 Conclusion

The estimation of GAI and chlorophyll from 1D and 3D RTM with NN are compared in the case of wheat and maize crops in this study. NN with single output has better performance compared with NN with multiple outputs especially for 3D specific model. Compared with 1D generic model, 3D specific model could provide more accurate estimation through comparison with field measurements using S2 observations. For GAI, estimation with eight bands provides the best estimation because of the more added information. Compared with wheat, more gain in accuracy is achieved for maize with RMSE reduced by half. For wheat C_{ab}, adding bands in red-edge region improves the estimation. Even though overestimation always exists from 1D model when wheat C_{ab} is larger than 50 µg/m^2, it is reduced by 3D wheat model with bias smaller than 1 µg/m^2. For estimation of CCC, performance of band setting changes with species and RTM. The application of 3D model reduces the RMSE by around 10 µg/m^2 with smaller bias for both wheat and maize.

Problems still exist for the estimation of maize C_{ab} which is might because of the settings of maize leaf optical properties. For further studies, more simulations with intensive sun angles are needed to generate the generic NN with mixed sun angles. Since earring and flowers would impact on crop canopy reflectance largely, including more phenological stages after earring is also necessary.

3D RTM inversion has been utilized to estimate biophysical variables with several studies including adding gap fraction from 3D simulation to PROSAIL inversion (Casa et al. 2010) or complied with LUT (Banskota et al. 2015; Gascon et al. 2004; Hernández-Clemente et al. 2017). Even though improved performances were achieved when accounting for canopy structures, the former one did not truly consider the radiative transfer process within the canopy and the latter ones include a serious of

simplifications with limited changing variables which limited the extension of the method. In this study, 3D wheat and maize models are applied with broader conditions through including different soil backgrounds, vegetation optical properties and crop structures at different phenological stages. Through the comparison of estimated result with PROSAIL model, improvements in GAI and CCC estimation are achieved especially for maize which is more different from turbid medium canopy as a row crop. Therefore, 3D specific model could be an effective way to estimate biophysical variables with remote sensing observations. But for more heterogeneous 3D structures, more validation of the method is needed before further applications.

Reference

Bacour, C., Baret, F., Béal, D., Weiss, M., & Pavageau, K. (2006). Neural network estimation of LAI, fAPAR, fCover and LAI× C ab, from top of canopy MERIS reflectance data: Principles and validation. *Remote Sensing of Environment, 105*, 313-325

Baetens, L., Desjardins, C., & Hagolle, O. (2019). Validation of Copernicus Sentinel-2 Cloud Masks Obtained from MAJA, Sen2Cor, and FMask Processors Using Reference Cloud Masks Generated with a Supervised Active Learning Procedure. *Remote Sensing, 11*, 433

Banskota, A., Serbin, S.P., Wynne, R.H., Thomas, V.A., Falkowski, M.J., Kayastha, N., Gastellu-Etchegorry, J.-P., & Townsend, P.A. (2015). An LUT-based inversion of DART model to estimate forest LAI from hyperspectral data. *IEEE Journal of Selected Topics in Applied Earth Observations and Remote Sensing, 8*, 3147-3160

Baret, F., & Buis, S. (2008). Estimating canopy characteristics from remote sensing observations: Review of methods and associated problems. *Advances in land remote Sensing* (pp. 173-201): Springer

Baret, F., De Solan, B., Lopez-Lozano, R., Ma, K., & Weiss, M. (2010). GAI estimates of row crops from downward looking digital photos taken perpendicular to rows at 57.5 zenith angle: Theoretical considerations based on 3D architecture models and application to wheat crops. *Agricultural and Forest meteorology, 150*, 1393-1401

Baret, F., Hagolle, O., Geiger, B., Bicheron, P., Miras, B., Huc, M., Berthelot, B., Niño, F., Weiss, M., & Samain, O. (2007a). LAI, fAPAR and fCover CYCLOPES global products derived from VEGETATION: Part 1: Principles of the algorithm. *Remote Sensing of Environment, 110*, 275-286

Baret, F., Houles, V., & Guérif, M. (2007b). Quantification of plant stress using remote sensing observations and crop models: the case of nitrogen management. *Journal of Experimental Botany, 58*, 869-880

Baret, F., Weiss, M., Lacaze, R., Camacho, F., Makhmara, H., Pacholcyzk, P., & Smets, B. (2013). GEOV1: LAI and FAPAR essential climate variables and FCOVER global time series capitalizing over existing products. Part1: Principles of development and production. *Remote Sensing of Environment, 137*, 299-309

Broge, N.H., & Leblanc, E. (2001). Comparing prediction power and stability of broadband and hyperspectral vegetation indices for estimation of green leaf area index and canopy chlorophyll density. *Remote Sensing of Environment, 76*, 156-172

Casa, R., Baret, F., Buis, S., Lopez-Lozano, R., Pascucci, S., Palombo, A., & Jones, H.G. (2010). Estimation of maize canopy properties from remote sensing by inversion of 1-D and 4-D models. *Precision agriculture, 11*, 319-334

Cerovic, Z.G., Masdoumier, G., Ghozlen, N.B., & Latouche, G. (2012). A new optical leaf-clip meter for simultaneous non-destructive assessment of leaf chlorophyll and epidermal flavonoids. *Physiologia Plantarum, 146*, 251-260

Chen, J.M., & Black, T. (1992). Defining leaf area index for non-flat leaves. *Plant, Cell & Environment, 15*, 421-429

Clevers, J.G., & Gitelson, A.A. (2013). Remote estimation of crop and grass chlorophyll and nitrogen content using red-edge bands on Sentinel-2 and-3. *International Journal of Applied Earth Observation and Geoinformation, 23*, 344-351
Croft, H., & Chen, J. (2017). Leaf pigment content. In: Elsevier Canada
Delegido, J., Verrelst, J., Alonso, L., & Moreno, J. (2011). Evaluation of sentinel-2 red-edge bands for empirical estimation of green LAI and chlorophyll content. *Sensors, 11*, 7063-7081
Delloye, C., Weiss, M., & Defourny, P. (2018). Retrieval of the canopy chlorophyll content from Sentinel-2 spectral bands to estimate nitrogen uptake in intensive winter wheat cropping systems. *Remote Sensing of Environment, 216*, 245-261
Drusch, M., Del Bello, U., Carlier, S., Colin, O., Fernandez, V., Gascon, F., Hoersch, B., Isola, C., Laberinti, P., & Martimort, P. (2012). Sentinel-2: ESA's optical high-resolution mission for GMES operational services. *Remote Sensing of Environment, 120*, 25-36
Duveiller, G., Weiss, M., Baret, F., & Defourny, P. (2011). Retrieving wheat Green Area Index during the growing season from optical time series measurements based on neural network radiative transfer inversion. *Remote Sensing of Environment, 115*, 887-896
Fernandes, R., Plummer, S., & Nightingale, J. (2014). Global Leaf Area Index Product Validation Good Practices. CEOS Working Group on Calibration and Validation-Land Product Validation Sub-Group. *Version 2.0: Public version made available on LPV website*
Fournier, C., Andrieu, B., Ljutovac, S., & Saint-Jean, S. (2003). ADEL-wheat: a 3D architectural model of wheat development. In: Springer Verlag
Gascon, F., Gastellu-Etchegorry, J.-P., Lefevre-Fonollosa, M.-J., & Dufrene, E. (2004). Retrieval of forest biophysical variables by inverting a 3-D radiative transfer model and using high and very high resolution imagery. *International Journal of Remote Sensing, 25*, 5601-5616
Gastellu-Etchegorry, J., Martin, E., & Gascon, F. (2004). DART: a 3D model for simulating satellite images and studying surface radiation budget. *International Journal of Remote Sensing, 25*, 73-96
Hernández-Clemente, R., North, P., Hornero, A., & Zarco-Tejada, P. (2017). Assessing the effects of forest health on sun-induced chlorophyll fluorescence using the FluorFLIGHT 3-D radiative transfer model to account for forest structure. *Remote Sensing of Environment, 193*, 165-179
Houles, V., Guerif, M., & Mary, B. (2007). Elaboration of a nitrogen nutrition indicator for winter wheat based on leaf area index and chlorophyll content for making nitrogen recommendations. *European Journal of Agronomy, 27*, 1-11
Jacquemoud, S., & Baret, F. (1990). PROSPECT : A model of leaf optical properties spectra. *Remote Sensing of Environment, 34*, 75-91
Jacquemoud, S., Verhoef, W., Baret, F., Bacour, C., Zarco-Tejada, P.J., Asner, G.P., François, C., & Ustin, S.L. (2009). PROSPECT + SAIL models: A review of use for vegetation characterization. *Remote Sensing of Environment, 113*, S56-S66
Jay, S., Gorretta, N., Morel, J., Maupas, F., Bendoula, R., Rabatel, G., Dutartre, D., Comar, A., & Baret, F. (2017). Estimating leaf chlorophyll content in sugar beet canopies using millimeter-to centimeter-scale reflectance imagery. *Remote Sensing of Environment, 198*, 173-186
Jiang, J., Weiss, M., Liu, S., & Baret, F. (2019a). The importance of LAI definition when deriving it from reflectance observations. *Remote Sensing of Environment, will be submitted*
Jiang, J., Weiss, M., Liu, S., Rochdi, N., & Baret, F. (2019b). Speeding up 3D radiative transfer simulations: a physically based approximation of canopy reflectance dependency on wavelength, leaf biochemical composition and soil reflectance. *Remote Sensing of Environment, Under revision*
Kimes, D., Nelson, R., Manry, M., & Fung, A. (1998). Attributes of neural networks for extracting continuous vegetation variables from optical and radar measurements. *International Journal of Remote Sensing, 19*, 2639-2663
Kuusk, A. (1994). A multispectral canopy reflectance model. *Remote Sensing of Environment, 50*, 75-82
Li, W., Weiss, M., Waldner, F., Defourny, P., Demarez, V., Morin, D., Hagolle, O., & Baret, F. (2015). A generic algorithm to estimate LAI, FAPAR and FCOVER variables from SPOT4_HRVIR and landsat

sensors: evaluation of the consistency and comparison with ground measurements. *Remote Sensing, 7*, 15494-15516
Liu, J., Pattey, E., & Jégo, G. (2012). Assessment of vegetation indices for regional crop green LAI estimation from Landsat images over multiple growing seasons. *Remote Sensing of Environment, 123*, 347-358
López-Lozano, R., Baret, F., Chelle, M., Rochdi, N., & Espana, M. (2007). Sensitivity of gap fraction to maize architectural characteristics based on 4D model simulations. *Agricultural and Forest meteorology, 143*, 217-229
Lunagaria, M.M., & Patel, H.R. (2018). Evaluation of PROSAIL inversion for retrieval of chlorophyll, leaf dry matter, leaf angle, and leaf area index of wheat using spectrodirectional measurements. *International Journal of Remote Sensing*, 1-21
LuxCoreRender (2018). LuxCoreRender Wiki. https://wiki.luxcorerender.org/LuxCoreRender_Wiki. In
Miller, J. (1967). A formula for average foliage density. *Australian Journal of Botany, 15*, 141-144
Minolta (1989). SPAD-502 owner's manual. Industrial Meter. In. Ramsey: Minolta Corp
North, P.R. (1996). Three-dimensional forest light interaction model using a Monte Carlo method. *IEEE transactions on Geoscience and Remote Sensing, 34*, 946-956
Pharr, M., Jakob, W., & Humphreys, G. (2016). *Physically based rendering: From theory to implementation*. Morgan Kaufmann
POV-team (2013). Introduction to POV-Ray for POV-Ray version 3.7.http://www.povray.org
Rouquié, B., Hagolle, O., Bréon, F.-M., Boucher, O., Desjardins, C., & Rémy, S. (2017). Using copernicus atmosphere monitoring service products to constrain the aerosol type in the atmospheric correction processor MAJA. *Remote Sensing, 9*, 1230
Schlerf, M., & Atzberger, C. (2006). Inversion of a forest reflectance model to estimate structural canopy variables from hyperspectral remote sensing data. *Remote Sensing of Environment, 100*, 281-294
Segl, K., Richter, R., Küster, T., & Kaufmann, H. (2012). End-to-end sensor simulation for spectral band selection and optimization with application to the Sentinel-2 mission. *Applied Optics, 51*, 439-449
Sola, I., García-Martín, A., Sandonís-Pozo, L., Álvarez-Mozos, J., Pérez-Cabello, F., González-Audícana, M., & Llovería, R.M. (2018). Assessment of atmospheric correction methods for Sentinel-2 images in Mediterranean landscapes. *International Journal of Applied Earth Observation and Geoinformation, 73*, 63-76
Stuckens, J., Somers, B., Delalieux, S., Verstraeten, W., & Coppin, P. (2009). The impact of common assumptions on canopy radiative transfer simulations: A case study in Citrus orchards. *Journal of Quantitative Spectroscopy and Radiative Transfer, 110*, 1-21
Van der Meer, F., Van der Werff, H., & Van Ruitenbeek, F. (2014). Potential of ESA's Sentinel-2 for geological applications. *Remote Sensing of Environment, 148*, 124-133
Veloso, A., Demarez, V., & Ceschia, E. (2012). Retrieving crops Green Area Index from high temporal and spatial resolution remote sensing data. In, *First Sentinel-2 Preparatory Symposium*
Verger, A., Baret, F., & Camacho, F. (2011). Optimal modalities for radiative transfer-neural network estimation of canopy biophysical characteristics: Evaluation over an agricultural area with CHRIS/PROBA observations. *Remote Sensing of Environment, 115*, 415-426
Verhoef, W. (1984). Light scattering by leaf layers with application to canopy reflectance modeling: the SAIL model. *Remote Sensing of Environment, 16*, 125-141
Verrelst, J., Malenovský, Z., Van der Tol, C., Camps-Valls, G., Gastellu-Etchegorry, J.-P., Lewis, P., North, P., & Moreno, J. (2018). Quantifying vegetation biophysical variables from imaging spectroscopy data: A review on retrieval methods. *Surveys in Geophysics*, 1-41
Verrelst, J., Muñoz, J., Alonso, L., Delegido, J., Rivera, J.P., Camps-Valls, G., & Moreno, J. (2012). Machine learning regression algorithms for biophysical parameter retrieval: Opportunities for Sentinel-2 and-3. *Remote Sensing of Environment, 118*, 127-139

Verrelst, J., Rivera, J.P., Moreno, J., & Camps-Valls, G. (2013). Gaussian processes uncertainty estimates in experimental Sentinel-2 LAI and leaf chlorophyll content retrieval. *ISPRS journal of photogrammetry and remote sensing, 86*, 157-167
Weiss, M., & Baret, F. (2016). S2ToolBox Level 2 products: LAI, FAPAR, FCOVER
Weiss, M., Baret, F., Leroy, M., Hautecoeur, O., Bacour, C., Prevol, L., & Bruguier, N. (2002). Validation of neural net techniques to estimate canopy biophysical variables from remote sensing data. *Agronomie-Sciences des Productions Vegetales et de l'Environnement, 22*, 547-554
Widlowski, J.-L., Robustelli, M., Disney, M., Gastellu-Etchegorry, J.-P., Lavergne, T., Lewis, P., North, P., Pinty, B., Thompson, R., & Verstraete, M. (2008). The RAMI On-line Model Checker (ROMC): A web-based benchmarking facility for canopy reflectance models. *Remote Sensing of Environment, 112*, 1144-1150
Zhou, X., Huang, W., Kong, W., Ye, H., Luo, J., & Chen, P. (2016). Remote estimation of canopy nitrogen content in winter wheat using airborne hyperspectral reflectance measurements. *Advances in Space Research, 58*, 1627-1637

3.4 Conclusion of the chapter

In this chapter, we used the ray-tracing model LuxCoreRender to simulate the 3D radiative transfer process within wheat and maize canopies based on realistic 3D description of the canopy structure. A speeding up method, which describes the dependency of canopy reflectance from the wavelength, leaf and soil properties, was first proposed. This allowed simulating a training database by considering a large range of simulations. Then, we applied machine learning inversion algorithm to retrieve canopy state variables including different definitions of LAI, C_{ab} and CCC.

LuxCoreRender was validated against other reference radiative transfer models applied both to homogeneous and heterogeneous canopies. Results show very good agreement between LuxCoreRender simulations and the reference values. Since simulating a sufficient number of 3D scenes to train the machine learning algorithm is time consuming, a specific speeding up procedure to reduce the number of simulations from the 3D model is implemented. The four stream approximation is used to couple the vegetation and the soil layers. This allows estimating the canopy reflectance of a given scene with any soil background by running only two simulations with two different soil backgrounds. For a given canopy structure and observational configuration, the three terms describing the vegetation layer in the four stream approximation vary smoothly and monotonically with the leaf total absorption coefficient value K, for a given value of leaf mesophyll structure parameter and leaf refractive index. Therefore, only 12 (linear approximation) to 18 (four stream approximation) simulations of a reference model are needed to describe the full canopy reflectance dependency to wavelength, leaf and soil properties with RMSE = 0.0017 for the four stream approximation and RMSE = 0.0022 for the linear approximation. The proposed approach provides an efficient way to reduce the computation time required to generate large training datasets used to invert radiative transfer models and retrieve some canopy characteristics. Even though, we showed results LuxCoreRender simulations for maize canopies, it is applicable to any canopy architecture and any reference 3D RTM.

Based on the proposed speeding up method, canopy reflectance of wheat and maize under different conditions were simulated at nadir with LuxCoreRender using 3D crop mock-up of maize and wheat canopies. 33750 cases were generated for each geometry configuration and crop type. According to the estimation results from neural networks trained with 3D simulations, we showed that the effective GAI was better estimated than LAI, PAI or the true value of GAI. To compare the theoretical performances of different inversion methods including VIs, 1D RTM PROSAIL and 3D RTM LuxCoreRender, we simulated an independent validation database of 3D simulations. Compared to VIs which is sensitive to the large range of canopy parameters and neural networks trained on 1D RTM PROSAIL simulations, the 3D model inversion provides the best estimation of effective GAI with RMSE = 0.33 for wheat and RMSE= 0.47 for maize.

According to the generated learning database from 3D simulation, GAI and chlorophyll at leaf and canopy level of wheat and maize are estimated based on NN inversion with Sentinel 2 observations and are compared with in-suit measurements. Results show that 3D model improves the estimation of GAI, C_{ab} and CCC when compared with PROSAIL estimation with slight improvement for wheat (RMSE of GAI = 0.72, RMSE of C_{ab} = 9.6 $\mu g/m^2$ and RMSE of CCC = 43.39 $\mu g/m^2$) and larger improvement for maize (RMSE of GAI = 0.37 and RMSE of CCC = 51.49 $\mu g/m^2$). NN with single output has better performance compared with NN with multiple outputs especially for 3D specific model. When different band settings are applied, the inclusion of bands in SWIR and red-edge region improve the accuracy of GAI estimation and bands in red-edge region is important for the estimation of C_{ab}.

4 Conclusion and perspectives

In this study, complex RTMs at both leaf and canopy levels were developed to retrieve leaf and canopy characteristics from close and remote sensing observations. At the leaf level, FASPECT is able to simulate reflectance and transmittance by considering differences between the upper and lower faces. Compared with PROSPECT-5 and PROSPECT-D, higher accuracy is achieved for reflectance and transmittance simulation of the upper leaf face for most of the spectrum. When inverting the models to estimate the leaf biochemical content, even though FASPECT shows similar performance as PROSPECT-D for chlorophyll, there is a significant improvement for the dry matter content. At the canopy level, we designed a 3D RTM by combining the LuxCoreRender engine with 3D specific crop architecture models. We simulated a training database that includes a large number of wheat and maize canopy cases thanks to a speeding up method, which allows simulating the canopy reflectance at any wavelength, and for any leaf biochemical composition and soil background reflectance from 3D simulations over a limited number of soil and leaf properties. Based on both an independent simulated validation database and *in situ* measurements acquired with SENTINEL-2 images, we conclude that the 3D model inversion allows getting the most accurate estimates of effective GAI and CCC and unbiased results for both wheat and maize canopy. The gain in accuracy is larger for maize canopy which departs more than wheat from the 1D model assumption.

Although we demonstrated an increase in accuracy both in forward and inverse modes, and at the leaf and canopy levels, a more detailed description of the structure is made at the cost of an increase in the number of parameters. This implies to investigate more on the distribution of each of these parameters to better apprehend their effect on the simulated radiative transfer or the variable retrieval in inverse mode. For FASPECT, we introduced six parameters, four of them describing the two leaf surfaces, and two of them describing the chlorophyll and water distributions between the palisade and spongy mesophylls. We recalibrated the absorption coefficients of the biochemical content. However, the calibration database only included reflectance and transmittance from the upper leaf face, which might result in uncertainties in the calibrated specific absorption coefficients, especially for chlorophyll and carotenoids. This, indeed, might be one reason that no significant improvement was achieved for these pigment estimation. Furthermore, for the same reason, we only provided a partial FASPECT validation due to limited available measurements. Only one over the eight databases contained measured optical properties of the upper and lower leaf faces with no associated leaf biochemical content while the remaining ones provide the upper leaf reflectance and transmittance as well as biochemical contents. Therefore, further investigations should focus (i) on the acquisition of a more complete measured database to complement the calibration and validation of the FASPECT model (ii) on the range and distribution of the model parameters for the different kind of leaves, depending on their constitution (monocotyledons versus dicotyledons) or on the differences between faces (colour, hair, wax,…). Finally, we suggest that hyperspectral measurements could be used in place of destructive measurements regarding the delicate protocol required for destructive leaf chlorophyll assessment. Furthermore, this could provide relatively high throughput for both precision farming and phenotyping applications.

For the 3D RTM model simulations, we preferred using PROSPECT for leaf optical properties for two main reasons: first, both wheat and maize are monocotyledon plants which do not show obvious differences in leaf optical properties between faces, and second is a lack of knowledge of the distribution of FASPECT parameters for the two considered crops as well as for senescent leaves.
The objective of this study was to provide ways of estimating crop state variables in relation to nitrogen fertilization applications. We therefore focused on two crop types with relatively simple 3D architecture. However, we relied on functional plant structural models, each model being specific to a given species and requiring significant developments and measurements to be designed adequately. For example, we limited the simulations to stages before the flowering/earing stage, since very few information is available about ear and flowers optical properties.

We first evaluated the 3DRTM simulation performances against few reference scenes from the RAMI exercise that correspond as well to rather simple canopy architectures. Furthermore, to speed up the simulations, we proposed a method based on the four stream theory that considers scattering between homogeneous scattering layers. We successfully validated this methodology over a maize crop, which corresponds to a relatively simple row structure, with only two type of elements (green leaves and stems). This result should be further confirmed for other canopies such as the ones proposed in the RAMI exercise, including forests characterized by more heterogeneous structure and more contrasted optical properties of the constituents (trunks, leaves).

We capitalized on this 3DRTM simulations to develop a crop specific algorithm to estimate different definition of leaf area index, CCC and LCC from satellite remote sensing measurements. We showed increased performances as compared to a generic algorithm based on 1D simulation for all variables. However, for both methods, as expected, the best estimates were obtained for the variables that are the most closely linked to the radiative transfer, e.g effective GAI (including all green elements) and CCC. The best improvement concerns the chlorophyll content estimation. Note that to save computational time, we limited the simulations to nadir viewing directions, with varying sun positions.

Considering satellite remote sensing applications, crop specific algorithms can only be applied with a priori information on land cover. If implemented in an operational way, a land cover map should also be generated in near real time, with accurate discrimination between crops, and the impact of misclassification when using the crop specific estimation should be evaluated as well. The increased accuracy in GAI and chlorophyll estimation should consequently improve the estimation of canopy nitrogen content (CNC) through the relationship between CCC and CNC, which also requires further investigations.